

DISS. ETH NO. 16065

FINITE ELEMENT SIMULATION OF A CARVING SNOW SKI

A dissertation submitted to the

SWISS FEDERAL INSTITUTE OF TECHNOLOGY ZURICH

for the degree of

Doctor of Technical Sciences

presented by

PETER ANDREAS FEDEROLF

diploma physicist, ETHZ

born 18.01.1974

citizen of

Federal Republic of GERMANY

accepted on the recommendation of

Prof. Jürg Dual, examiner

Dr. Walter Ammann, co-examiner

Dr. Anton Lüthi, co-examiner

2005

Abstract

Winter sports have developed tremendously during the last century. This increased popularity has not only generated significant industrial activities, but has also boosted tourism in many mountainous regions. The design of new skiing equipment has to date always been the work of expert craftsmen, who improved the existing equipment in expensive and time-consuming prototyping and testing cycles. Nowadays, advanced numerical simulation tools offer new ways to assist ski manufacturers in the development of new equipment designs and shorten the required prototyping and testing cycles. Furthermore, numerical simulation methods offer new ways to analyse the interaction between skier, skiing equipment, and snow, and they offer the opportunity to analyse the impact of single parameters on the turn characteristics.

The primary objective of this thesis is to develop a finite element simulation of the ski-binding system in the situation of a carved turn, specifically taking into account the ski-snow interaction. A quasi-static equilibrium of the external forces and moments is assumed, which allows to determine the boundary conditions on the model. These boundary conditions depend on the one hand on the forces and moments exerted by the skier onto the binding, on the other hand on the snow resistance pressure to the penetrating and sliding ski. Additionally the impact of the skis' weight and of inertia forces, which are brought about by accelerations of the system, was analysed. Via a detailed kinematic analysis of selected turns a consistent set of coordinates describing both the motion of the skis, and of the skier's centre of mass was obtained. Simultaneously, the forces and moments transferred from the skier onto the binding were measured, which constitute the first part of the boundary conditions to the simulation. The second part was determined by an extensive investigation of the ski-snow interaction process. In the regime of snow penetrating speeds typical for skiing, snow deformation is dominated by brittle fracture processes. To characterise the impact of the snow on a penetrating ski, the snow resistance pressure was measured in several penetration tests using two newly developed measurement devices. The results were summarised in an empirical equation describing the snow resistance pressure as a function of the penetration depth and of the edging angle. The penetration speed has a negligible effect on the resistance pressure. The snow type is characterized in the empirical equation by three coefficients. Due to the multifaceted characteristics of snow these three coefficients scatter strongly when measured on actual ski pistes and it was not possible to correlate them to other physical snow properties. In order to evaluate the impact of varying snow types on the simulation results, mean values for soft, medium, and hard snow conditions on the examined ski pistes were determined.

The numerical model of the ski and binding consists of shell and volume elements, respectively. The two blocks are coupled via constraints. The ski model represents the actual structure and geometry of the ski in detail, whereas the binding model represents all the important mechanical properties but does not model the numerous individual binding parts in detail. The mechanical properties of the numerical model were verified by comparison to static bending and torsion tests. Additionally, the force distribution under a loaded ski was calculated and compared to measurements.

The simulation of the ski-binding system in a turn was in a first step implemented for the static case, in which the ski-binding system is loaded with a given force and penetrates snow of a given resistance strength. The calculated shape of the lower ski edge was compared to the shape of the ski's trace obtained by measurements in a corresponding measurement set-up. Small deviations in the form of the measured and the calculated traces arise from

inhomogenities of the snow but the results still agree within the measurement accuracy. In a second step a circle was fitted to the calculated shape of the lower ski edge and its radius was compared to the instantaneous radius of the trace of an actually carved turn. To represent a moving ski two dynamical effects were included in the boundary conditions modelling the ski-snow interaction: the penetration of the ski into the snow is a non-reversible process generating a trace in the snow. This trace interacts with the ski's rear end instead of the undisturbed snow surface. Therefore, a hysteresis was implemented in the boundary condition representing the snow's penetration resistance. Moreover, the ski's side cut causes a lateral displacement of the trace, which is also included in the implemented boundary condition. The boundary conditions for the model obtained by the kinematic and kinetic analysis, and empiric snow resistance function, which were discussed in the first part of this work, were then used to calculate the ski radii for several discrete situations. These radii were compared to actual turn radii determined from the traces of the skis remaining in the snow. In the steering phase of the turns, in which the skis in fact carve, the simulated ski radii agree well with the instantaneous radii determined from the skis' traces. Small deviations arise on the one hand from errors in the large number of necessary input data of the simulation and on the other hand from uncertainties in the determination of instantaneous radius of the traces. Finally, the implemented simulation tool was used to investigate the interrelations between the turn radius and the edging angle, the load on the ski binding, and the snow type.

The simulation tool developed in this thesis was designed to allow an easy adaptation of new ski and binding designs in order to assist ski and binding manufacturers in the evaluation of new skiing equipment. It could also assist athletes and coaches in the selection of skiing equipment best suited to the athlete's body characteristics and skill. Finally, this research allows further investigation into the interrelationship of turn parameters and physical processes in skiing.

Zusammenfassung

Seit seiner Entstehung erfuhr der Skisport einen nahezu kontinuierlichen Aufschwung, wodurch nicht nur ein bedeutender Wirtschaftszweig sondern auch der Wintertourismus in den alpinen Regionen entstand. Die Entwicklung von Skisportgeräten war bisher immer die Arbeit von erfahrenen Handwerkern, die in zeitaufwendigen Versuchsreihen die Sportgeräte weiterentwickelten. Moderne Simulationsmethoden bieten heute die Möglichkeit Skihersteller bei der Weiterentwicklung ihrer Produkte zu unterstützen, da sie den Kreislauf des Bauens und Austestens neuer Prototypen verkürzen können. Ausserdem erlauben numerische Simulationen das Zusammenspiel von Skifahrer, Sportgerät und Schnee mit neuartigen Methoden zu analysieren und sie erlauben die Bedeutung einzelner Parameter für den Schwungverlauf zu untersuchen.

Das Hauptziel dieser Arbeit ist die Entwicklung einer Simulationsmethode für das System Ski-Bindung in einem gecarvten Schwung mit Hilfe der Finiten Elemente Methode unter besonderer Berücksichtigung der Ski-Schnee Interaktion. Dazu wurde ein quasistatischer Gleichgewichtszustand der äusseren, am System angreifenden Kräfte und Momente angenommen, wodurch die Randbedingungen des Skimodells bestimmt werden können. Diese Randbedingungen hängen einerseits davon ab, welche Kräfte und Momente vom Skifahrer auf die Bindung übertragen werden, andererseits hängen sie ab vom Widerstandsdruck den der Schnee dem Ski an der Kontaktfläche entgegensetzt. Auch der Einfluss des Eigengewichts des Skis und der Inertialkräfte, die durch Beschleunigungen des Systems hervorgerufen werden, wurde untersucht. Durch eine detaillierte kinematische Analyse ausgewählter Schwünge wurde ein konsistentes Set von Koordinaten bestimmt, welche sowohl die Bewegung der beiden Skier, als auch die Bewegung des Schwerpunkts des Skifahrers beschreiben. Gleichzeitig wurden die Kräfte und Momente gemessen, welche vom Skifahrer während der Fahrt auf die Bindung übertragen werden, um sie als Randbedingungen in der Simulation einzusetzen. Um die zweite Randbedingung, welche an der Kontaktfläche zwischen Ski und Schnee wirkt zu bestimmen, wurde eine umfangreiche Untersuchung der Ski-Schnee-Wechselwirkungen durchgeführt. Bei hohen Deformationsgeschwindigkeiten des Schnees, welche beim Skifahren typischerweise auftreten, bestimmen im wesentlichen Sprödrbrüche das Deformationsverhalten des Schnees. Um den Widerstand des Schnees auf einen eindringenden Ski zu untersuchen, wurde der Widerstandsdruck des Schnees auf eine eindringende Platte mit zwei neuentwickelten Messgeräten charakterisiert. Die Messergebnisse wurden in einer empirischen Gleichung zusammengefasst, welche den Schneewiderstandsdruck als Funktion der Eindringtiefe und des Aufkantwinkels angibt. Die Eindringgeschwindigkeit hat dabei nur einen geringen Einfluss auf den Widerstandsdruck. Die Schneeart wurde in der empirischen Gleichung durch drei Parameter charakterisiert, welche aufgrund der vielfältigen Erscheinungsformen des Schnees so stark variieren, dass sie bei Feldmessungen auf verschiedenen Skipisten nicht mit anderen physikalischen Schneeeigenschaften korreliert werden konnten. Um den Einfluss der Schneeeigenschaften auf die Resultate der Simulation zu untersuchen, wurden Mittelwerte für weiche, mittlere und harte Schneebedingungen auf den Skipisten berechnet.

Im numerischen Modell wurde der Ski durch Schalenelemente, die Bindung durch Volumenelemente dargestellt. Diese beiden Blöcke wurden durch Zwangsbedingungen („constraints“) miteinander verbunden. Das numerische Skimodell bildet den Ski in Geometrie und innerem Aufbau detailgetreu ab. Das Bindungsmodell dagegen enthält alle mechanisch relevanten Eigenschaften, jedoch nicht jedes der zahlreichen einzelnen Bauteile. Die

mechanischen Eigenschaften dieses numerischen Ski-Bindungsmodells wurden durch Biege- und Torsionstests überprüft. Zusätzlich wurde die Druckverteilung unter einem belasteten Ski berechnet und mit Messergebnissen verglichen.

In einem ersten Schritt wurde dann eine statische Kurvensituation für das Ski-Bindungsmodell implementiert, bei der das Modell auf einer bekannten Schneeunterlage mit einer vorgegebenen Kraft belastet wird. Die berechnete Verformung des Skis wurde anhand der Form der unteren Kantenlinie mit Messergebnissen aus einem entsprechenden Messaufbau überprüft. Kleinere Abweichungen zwischen berechneter und gemessener Kantenlinie werden durch Inhomogenitäten der Schneeoberfläche verursacht, dennoch stimmen die Ergebnisse im Rahmen der Messgenauigkeit miteinander überein. In einem zweiten Schritt wurde dann der Skiradius durch einen Kreisfit an die Skikante bestimmt und mit dem momentanen Radius, der aus der Spur eines gecarvten Schwungs bestimmt wurde, verglichen. Dabei zeigte sich, dass zwei Effekte berücksichtigt werden müssen, damit die Randbedingungen für einen fahrenden Ski gültig sind: das Eindringen des Skis in den Schnee ist ein nicht-reversibler Vorgang, wodurch eine bleibende Spur in der Schneeoberfläche erzeugt wird. In der Fortbewegung interagiert das Skiende deswegen nicht mit einer unberührten Schneeoberfläche, sondern mit der Spur, die vorher erzeugt wurde. Deswegen ist es notwendig, eine Hysterese in der Funktion, welche den Schneewiderstandsdruck beschreibt, zu berücksichtigen. Ausserdem wird durch die Taillierung des Skis eine seitliche Verschiebung der Spur verursacht, welche in der Implementierung der Ski-Schnee Randbedingung ebenfalls berücksichtigt werden muss. Mit den Ergebnissen aus der kinematischen und kinetischen Schwunganalyse, welche anfangs beschrieben wurde, konnten die Randbedingungen der Kurvensimulation für verschiedene konkrete Kurvensituationen implementiert und die Skiradien berechnet werden. Diese Radien wurden dann verglichen mit dem momentanen Kurvenradius, welcher für den simulierten Zeitpunkt aus der im Schnee zurückgebliebenen Spur des Skis bestimmt wurde. Vor allem in der Steuerphase des Schwungs, in der die Annahme eines gecarvten Schwungs am besten erfüllt ist, stimmen gemessener Kurvenradius und berechneter Skiradius gut überein. Anschliessend wurde die Simulation verwendet um die Zusammenhänge zwischen dem Skiradius und dem Aufkantwinkel, der Last auf der Bindung und der Eigenschaft des Schnees zu untersuchen.

Die empirische Gleichung für den Schneewiderstandsdruck, welche in dieser Doktorarbeit aufgestellt wurde, erlaubt es, die Ski-Schnee Interaktion genau zu berechnen, kann aber auch für andere Interaktionsprozesse mit Schnee verwendet werden. Das Simulationsprogramm, welches in dieser Arbeit erstellt wurde, kann von Ski und Bindungsherstellern für die Weiterentwicklung ihrer Produkte eingesetzt werden. Ausserdem eignet es sich für Athleten oder Skitrainer um Sportgeräte auszuwählen, welche den Körpereigenschaften eines Sportlers am besten angepasst sind. Auch für eine weitere Analyse der Beziehungen zwischen verschiedenen Kurvenparametern kann das Programm verwendet werden.

Acknowledgements

First I would like to thank Professor Jürg Dual of the Institute of Mechanical Systems at the Swiss Federal Institute of Technology (ETH), Zürich for accepting me as a PhD student and for his time, advise, and support.

I also gratefully acknowledge the support of Professor Markus Roos, who introduced me to the simulation tool SESES and greatly supported me in the implementation of the ski model and the appropriate boundary conditions.

This thesis would not have been possible without the infrastructure of the Swiss Federal Institute for Snow and Avalanche Research Davos (SLF) under the guidance of Dr. Walter Ammann. I highly value the excellent team spirit in the Team Snow Sports at the SLF, lead by Hansueli Rhyner. Especially, I would like to thank Dr. Anton Lüthi for supervising and supporting me during my studies, and Mathieu Fauve with whom I enjoyed to share my office with. I am also grateful to the other present and former members of our Team: Mirco Auer, Lukas Bäurle, Sven Bethke, Dr. Daniel Buhl, and Dr. Dénes Szabó.

I would also like to thank Bernhard Zingg, Martin Hiller and the staff of the mechanical workshop of the SLF, who helped in the construction of measurement devices for the snow characterisation, Daniela Kasbauer and Katja Oberhofer who helped in the analysis of the kinematic data obtained from video recordings, Florian JeanRichard, Timo Bulling, and Jan-Moritz Gwinner, who conducted many measurement series on skiing slopes and in the cold laboratory at the SLF. I am grateful to George Krüsi and Daniela Schmid for providing planar sections and microtomographical images of snow samples. First parameter studies with the simulation tool developed during my studies were carried out by Timo Bulling, Jan-Moritz Gwinner and Florian Hellberg. An advanced user interface for this simulation tool is being implemented with the help of David Lüthi.

Finally I would like to thank our industrial partners in this project, Stöckli Skis and Fritschi Swiss Bindings, for the good collaboration. The Swiss innovation promotion agency KTI/CTI provided financial support for this project.

Content

List of Variables.....	v
1. Introduction	1
1.1 Review of Historic Developments of Skiing Equipment	1
1.2 Design of Modern Skiing Equipment.....	1
1.2.1 Construction and Geometry of Modern Skis.....	1
1.2.2 Design Issues of Modern Bindings	3
1.3 Science and the Development of New Skiing Equipment.....	3
1.4 Objectives of this Thesis.....	6
1.5 Basic Mechanics of a Turning Ski.....	6
1.5.1 Coordinate Systems.....	6
1.5.2 Basic Kinematics and Dynamics of the Turning Ski as a Rigid Body...	8
1.5.3 Assumption of a Quasi-Static Situation	11
1.5.4 Deformations of the Ski-Binding System	12
1.6 The Finite Element Method for the Calculation of the Ski Deformation.....	15
2. Measurement of the Turn Parameters	17
2.1 Description of the Analysed Test Run	17
2.2 Kinematic Analysis of Two Selected Turns	18
2.2.1 Review of Available Measurement Methods	18
2.2.2 Employed 3D-Video System and its Calibration	19
2.2.3 Analysis of the Collected Video Data	20
2.2.4 Results of the Video Analysis	24
2.3 Forces and Moments Acting on the Ski-Binding System.....	33
2.3.1 Gravitational and Inertia Force.....	33
2.3.2 Forces and Moments Transferred from the Skier onto the Binding.....	35
2.3.3 The Ski-Snow Interaction Force.....	41
3. Determination of Snow Resistance to the Ski	43
3.1 General Mechanical Properties of Snow	43
3.2 The Interaction of Ski and Snow	44
3.2.1 Friction at the Ski-Snow Interface.....	44
3.2.2 Deformation of the Snow Surface by a Turning Ski	45
3.2.3 Summary and Conclusions of the Literature Review.....	46
3.3 Measurement Devices for the Snow Characterization	47
3.3.1 Agervis.....	48
3.3.2 Fast Snowdeformer	51
3.3.3 Snow Sample Analysis.....	53
3.3.4 Measurement of General Snow Properties.....	53

3.4	The Mean Snow Resistance Pressure on a Penetrating Plate	54
3.4.1	Mean Snow Resistance Pressure as a Function of Penetration Depth ..	54
3.4.2	Snow Resistance as a Function of Process Parameters	56
3.4.3	Mechanical Snow Resistance as a Function of Physical Snow Properties.....	61
3.5	Summary and Conclusions for the Implementation of the Ski-Snow Interaction in the Simulation.....	63
4.	Implementation of a FEM-Model of a Ski-Binding System	65
4.1	FEM Software and Employed Finite Element Types	65
4.2	Boundary Conditions	67
4.3	Implementation of the Ski	68
4.3.1	Composition and Shape of a Ski in the Numerical Model	68
4.3.2	Assigning Material Properties to the Ski in the Numerical Model	69
4.3.3	Ski Types Implemented in this Thesis.....	70
4.4	Implementation of the Ski Binding	70
4.4.1	The Fritschi „Rave PowerRide“ Binding in a Simplified FEM-Model	71
4.5	Experimental Verification Methods and Results	72
4.5.1	Bending and Torsion Stiffness of the Ski	72
4.5.2	Force Distribution between Ski and a Flat Surface	73
4.5.3	Summary of the Model Verification	75
5.	Simulation of the Ski in a Static Experiment.....	77
5.1	Boundary Conditions and Solving Algorithm in the FEM-Model	78
5.1.1	Implementation of the External Forces Acting on the Ski	78
5.1.2	Determination of the Snow Resistance Pressure in the Simulation	79
5.1.3	The Solving Algorithm.....	82
5.2	Comparison of Experimental and Numerical Results	83
5.2.1	Verification of the Calculated Snow Resistance Force	83
5.2.2	Comparison of the Calculated and the Actual Shape of the Ski	84
5.3	Application Areas for Static Ski Simulations	85
5.3.1	Advantages and Limitations of the Static Simulation	85
5.3.2	Application Example: Development of an Adjustable Binding Plate..	86
6.	Calculation of a Turning Ski	91
6.1	Boundary Conditions and Solving Algorithm	91
6.1.1	Required Assumptions for the Simulation of a Turning Ski	91
6.1.2	Incorporation of Plasticity of the Snow Deformation	92
6.1.3	The Shape of a Ski in Motion.....	95
6.1.4	Implementation of the Side Cut Effect.....	98
6.1.5	Convergence Behaviour of the Simulation	100
6.1.6	Simulation Output	100

6.2	Comparison of Experimental and Numerical Results	101
6.2.1	Method of an Experimental Verification for the Simulation Results .	101
6.2.2	Determination of the Turn Radius	102
6.2.3	Comparison of the Calculated Ski Radius and the Measured Trace's Radius	104
6.3	Results obtained with the Simulation	106
6.3.1	Influence of Different Turn Parameters on the Actual Ski Radius.....	106
6.3.2	The Pressure Distribution between Ski and Snow	109
7.	Conclusions and Outlook.....	111
7.1	Summary.....	111
7.2	Conclusions	112
7.3	Outlook	113
8.	References	115
9.	Glossary.....	125
	Curriculum Vitae	127

List of Variables

The following Table lists the more important variables in this thesis. It is not a complete list.

Notation convention: in this thesis parameters are generally printed as *italic* letters, vector and tensor quantities are printed **bold** (or in case of Greek letters they are explicitly indicated as vectors). For better distinction tensor equations will usually be written in terms of the tensor components.

variable	unit	description	defined on page/ by equation
α	°	inclination angle of the ski slope	Figure 4 on page 7
X	m	coordinates of the fixed external coordinate system	Figure 4 on page 7
Y	m		
Z	m		
v_X	m/s	velocity components as measured in the fixed external coordinate system	
v_Y	m/s		
v_Z	m/s		
a_X	m/s ²	acceleration components as measured in the fixed external coordinate system	
a_Y	m/s ²		
a_Z	m/s ²		
x	m	coordinates of the (accelerated) coordinate system used for the simulation. This system is rotated by the orientation angle β with respect to XYZ.	Figure 4 on page 7
y	m		
z	m		
v_x	m/s	velocity components observed in the coordinate system of the simulation	
v_y	m/s		
v_z	m/s		
a_x	m/s ²	acceleration components observed in the coordinate system of the simulation	
a_y	m/s ²		
a_z	m/s ²		
\bar{x}	m	coordinates of the (accelerated) coordinate system which is attached to the ski. This system is rotated by the edging angle θ with respect to xyz.	Figure 4 on page 7
\bar{y}	m		
\bar{z}	m		
β	°	orientation angle of the ski in the external coordinate system	equation 1, Figure 4 on page 7
θ	°	edging angle of the ski on the ski slope	Figure 4 on page 7, equation 38 on page 23
ϕ	°	blade angle of the ski. In ideally carved turns ϕ is close to zero.	Figure 4 on page 7,

variable	unit	description	defined on page/ by equation
ψ	$^{\circ}$	downtilt angle of the ski, which depends on the ski's penetration depth into the snow ($\psi \sim 0^{\circ}$ - 1.5°). In this work ψ is considered to be zero.	Figure 4 on page 7
$\omega = \omega\beta$	$^{\circ}/s$	angular velocity of the ski's turn	page 9
$\dot{\omega}$	$^{\circ}/s^2$	angular velocity of the ski's turn	page 9
$\omega\theta$	$^{\circ}/s$	angular velocity of the ski's edging motion	page 9
$\dot{\omega}_{\theta}$	$^{\circ}/s^2$	angular acceleration of the ski's edging motion	page 9
r	m	distance to the coordinate origin. The corresponding coordinate system is either indicated as index or explained in the text	e.g. page 9
e_x, e_y, e_z		unit vector in direction of the given index	page 9
F	N	force - the most important forces are the following four:	
$F_{athlete}$	N	force transferred from the athlete onto the ski-binding system	page 12
F_{SSI}	N	force transferred from the snow onto the ski-binding system	page 12
G_{ski}	N	gravitational force acting on the ski-binding system	page 12
$F_{inertia}$	N	inertia force acting on the ski-binding system in the reference frame of the simulation coordinate system xyz.	page 12
M	Nm	moment of force w.r.t. the coordinate origin the most important moments are	equation 12 on page 10
$M_{athlete}$	Nm	moment of force transferred from the athlete onto the ski-binding system	equation 12 on page 10, equation 46 on page 39
M_{SSI}	Nm	moment of force transferred from the snow onto the ski-binding system	equation 12 on page 10
$M_{G_{ski}}$	Nm	gravitational moment of force acting on the ski-binding system (if the coordinate origin is not in the centre of mass, then $M_{G_{ski}} \neq \mathbf{0}$)	equation 12 on page 10
$M_{inertia}$	Nm	inertia moment of force acting on the ski-binding system in the reference frame of the simulation coordinate system xyz.	equation 12 on page 10
L	$kg\ m^2/s$	angular momentum	page 10
J	$kg\ m^2$	tensor of the moment of inertia	equation 16 on page 10

variable	unit	description	defined on page/ by equation
d	m	penetration distance of a device (plate, stamp or a ski) into the snow	Figure 39 on page 49
D	m	penetration depth of a device into the snow: measured perpendicular to the snow surface	Figure 39 on page 49
p_{Snow}	Pa	<p>snow resistance pressure to a penetrating device.</p> <p>Note:</p> <p>In chapter 3 the <i>mean resistance pressure</i> on a penetrating device is measured experimentally: p_{Snow}</p> <p>In chapter 5 and 6 the <i>actual snow pressure</i> on a point of the boundary surface of the FEM model is needed: $p(D)$</p>	<p>page 49</p> <p>see equation 66 on page 80</p>
A, B, C	Pa/m, Pa, Pa/m	coefficients characterising the snow resistance pressure as a function of the penetration depth D	equation 49 on page 63
s	Pa	stress tensor	
e		strain tensor	equation 52 on page 65
u	m	displacement vector (degree of freedom field in the FEM model for shell as well as for volume elements)	page 65
$\vec{\varphi}$	rad	rotation vector (degree of freedom field in the FEM model for shell elements)	equation 54 on page 66
n		unit normal to a boundary surface	
C	Pa	tensor of elasticity (4x4 tensor)	equation 59 on page 69
E	Pa	Young's modulus	
ν		Poisson's ratio	
L	m	lateral displacement of the trace due to the ski's side cut	equation 81 on page 96

variable	unit	description	defined on page/ by equation
$s(x)$	m	sidecut of the ski at position x	equation 84 on page 97
R	m	radius Note: In this thesis two radii are distinguished: The <i>turn radius</i> refers to the (instantaneous) radius of the ski's trajectory (which can be determined from the ski's trace in the snow) The <i>ski radius</i> refers to the radius of the lower ski edge, which depends on the ski's side cut, its bending and its torsional deformations (calculated by the simulation) In case of ideal carving these two radii are equal.	see section 6.2.2 and section 6.2.3

1. Introduction

Skiing has grown continuously during the last century putting forth not only important industry activities, but also boosting tourism in many mountainous regions of the industrialised countries. Nowadays thousands of people economically depend on the skiing sport. The continuous growth of skiing was accompanied by numerous changes and improvements of the skiing equipment. This chapter starts with a short review of the historic developments of skiing equipment (section 1.1). Then the design characteristics of skis and bindings are discussed (section 1.2). The development of new ski and binding designs has so far always been the work of expert craftsmen, but during the 70ies different branches of science started to investigate and to some extent influence the development of skiing equipment (section 1.3). After reviewing previous research the objectives of this thesis are defined (section 1.4). Then the basic mechanics describing the ski in the situation of a turn are discussed (section 1.5). This discussion leads to the outline of the work presented in this thesis (section 1.6).

1.1 Review of Historic Developments of Skiing Equipment

There are historical and even prehistorical evidences of early forms of skiing [1] as a means of travelling and transportation in snowy areas. Modern skiing originates from Norway [2], where Sondre Nordheim developed first a toe and a heel strap, which allowed steering a turn and even jumping without the skis going off. This strap may be considered to be a first type of binding with which the first skiing techniques, the „telemark turn“ and the „Christiania skidded stop turn“ could be performed. In 1870, he also introduced the first side-cut ski, which became the prototype of all modern skis. The alpine skiing technique was developed by two Austrians, Mathias Zdarsky and Johannes Schneider. Up to 1930, skis had consisted purely of wood, when Rudolph Lettner invented the first steel edge, which was originally intended to reduce wear, but also significantly improved the grip in turning on hard snow. In 1933 the laminated ski construction was patented simultaneously in Norway and in the United States. The first useful release binding was invented in 1939 by Hjalmar Hvam. In 1949 the first commercially successful aluminium reinforced skis were sold. In 1952 fibreglass reinforced skis were tested, in 1955 polyethylene base was introduced, and in 1959 the first plastic fibreglass ski was invented. Since then, many more additive materials have been tested in order to improve the ski properties. However, it was not until 1990 that the classical telemark geometry of the skis were replaced by deep-side cut shaped skis, which allowed to significantly change - and in many aspects simplify - modern skiing techniques. Thus the emerging carving skis were able to revitalize the whole skiing sport, which had started to experience a decline in the early 1990s.

1.2 Design of Modern Skiing Equipment

1.2.1 Construction and Geometry of Modern Skis

Present day skis are still laminates of several material layers. The bottom layer usually consists of sintered or extruded polyethylene enframed by steel edges. Above the base layer a sandwich structure of a wood or plastic core enclosed by two metal face layers follows. This sandwich structure determines the bending and torsional stiffness of the ski. The thickness of the core

material varies along the ski axis. Thus the stiffness distribution of the ski can be adjusted. Typical metal layers consist of aluminium or titalal. Additionally layers of fibreglass laminates (often embedded in polyurethane) increase the torsional stiffness of a ski. On top of these layers a surface layer with the decoration of the ski, but usually without constructional relevance, completes the ski structure. Figure 1 displays a simplified example of a typical composition of a modern ski. Additional to this basic structure a lot of modern skis are equipped with accessory features which are intended for example to further increase the torsional stiffness or to enhance damping properties.

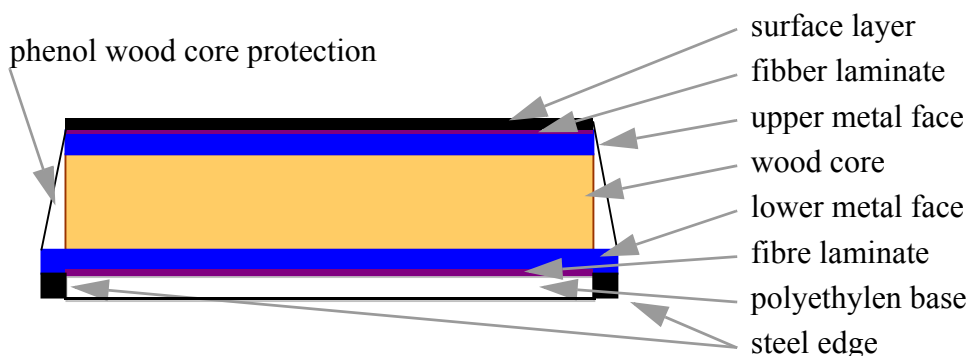


Figure 1. Simplified example of a sandwich structure of a modern ski.

The material layers are glued together with a special epoxy resin by press sizing. The form of the press induces a deformation and thus prestresses the sandwich structure of the ski when the layers are glued together. These prestresses cause the ski to camber (see Figure 2, side view). If the ski is loaded in the middle section, the camber transfers pressure to the ski end and the shovel, which improves the snow grip of the ski edges at shovel and tail and facilities turning.

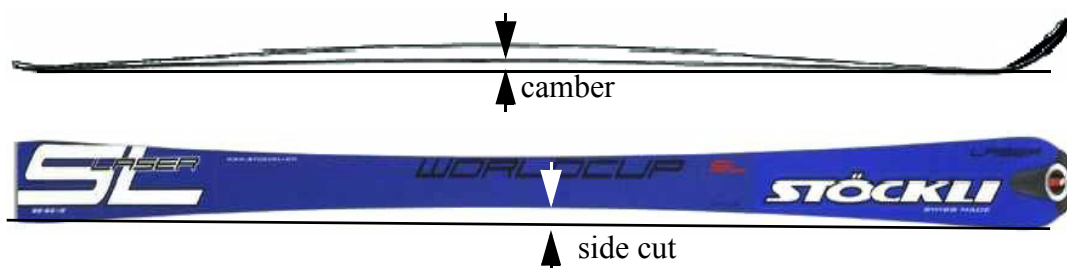


Figure 2. Ski in side view and top view, displaying the ski's camber and side-cut. (photos: www.stoeckli.ch.)

The variable width of the ski along its length (see Figure 2, top view) defines the ski's side cut. In a turn the edged ski is bent until the middle section of the ski comes into contact with the snow. The side cut of the ski thereby determines how much the ski will be bent. The shape of the ski is chosen such that the ski edge will in a good approximation assume a circular shape. Therefore, the ski's side cut is a measure of the radius of a ski. (Note: the „FIS radius“ of a ski is a reference value, which is calculated for an undeformed ski according to regulations defined by The Federal Skiing Federation (FIS) [3]. Thus it does not correspond to an actual turn radius.)

1.2.2 Design Issues of Modern Bindings

Modern ski bindings have to meet two basic requirements:

1. They have to firmly hold the ski to the skier's ski boot.
2. In case of extreme strain they have to release the ski boot to prevent injuries of the skier.

In addition to these basic functions, a binding has to adapt to the ski such that the interaction between athlete, ski, and snow is enhanced and not interfered. This requires that the ski's bending characteristics are largely preserved, but at the same time it has to be sturdy enough to bear up the high forces generated during a turn. Binding manufacturers solve this problem by different designs. Usually the binding consists of separate toe and heel parts, which comprise the clamps holding the ski boot and the release mechanism. The connection between these two parts is usually flexible, such that the bending of the ski is not significantly interfered. The whole system is screwed onto the ski or onto a damping plate, which is frequently mounted on carving skis.

The carving binding of the manufacturer Fritschi (Figure 3), which will be particularly considered in the present study, uses a different design which renders the use of an additional binding plate unnecessary and thus reduces the weight of the whole ski-binding system: The toe and heel part are mounted on a stiff rail, which is connected to the ski via a joint under the toe part of the binding, but can slide freely back and forth in the heel plate if the ski is bent. The binding is described in more detail in chapter 4.



Figure 3. Rave Powerride Binding by Fritschi (photo: www.fritschi.ch).

Recently some ski manufacturers have developed skis, which are already equipped with a fixed binding system. This allows a better adaptation of the single components and thus a better tuning of the overall properties of the ski-binding-system.

1.3 Science and the Development of New Skiing Equipment

From the beginning, many craftsmen and engineers have contributed to the major advancements of the skiing sport in general and the development of the skiing equipment in particular. Along with the growth of this sport, scientific interest in the design and manufacturing of skiing equipment started to emerge. A very important contribution to the safety of skiing was due to extensive analysis of injuries occurring in skiing, which strongly influenced today's regulations for the safety of skis and bindings. Since 1974 conferences on

„Skiing Trauma and Safety“ have been held [4], and address the design of skiing equipment, among other predominantly therapy-related topics. In 1996 the First International Conference on Skiing and Science was held in Austria, which addressed a broad range of scientific topics related to skiing and recurred since then quadrennially. Also in 1996 the first conference on sports engineering was held in Sheffield, UK, on which some studies related to the design of skiing equipment were published [5].

As early as 1977 Schultes [6] had published a very comprehensive book addressing the correlations of the mechanical properties and the riding quality of skiing equipment. More recent books on this topic were written by Howe [7],[8] (1983 and a revised second edition in 2001), and in 1996 by Lind & Sanders [1]. Lind & Sanders, as well as many other later studies relate to the descriptions of skiing by Howe. Biomechanics of skiing was discussed in many scientific papers, for example in Glenne & VonAllmen [9], Fetz & Müller [10], or Schöllhorn et al. [11]. Carving emerged in the 90s as a new technique and it was specifically investigated in the studies of Mössner et al. [12], Niessen & Müller [13], and Johnson et al. [14]. Comparative studies of the new carving technique in relation to the „classical“ skiing technique were published by Raschner et al. [15], Yoneyama et al. [16], and Burtscher et al. [17]. Most of these publications investigating the new carving technique focused on the implications of the new skiing equipment on the skiing technique and the implications for the skiers body (with the exception of Howe’s revised book [8]).

Since Schulte’s book about ski design [6] the significance of the mechanical properties of a ski for its turning characteristics has been known. However, the number of published scientific studies addressing this issue is quite small. Most research in this area is done directly by the ski manufacturing companies, which do not publish their results. Some studies on the general mechanical properties of skis have been published by Glenne et al. [18],[19],[20]. In some cases new materials were suggested for the use as additional layers in skis, for example, by Gibson & Ashby [21], who reviewed polyurethane foam as a means to lighten the ski, or by Scherrer et al. [22], who used Shape Memory Alloys to improve the damping properties of a ski. (The vibration characteristics of the skiing equipment is one of its key parameters and was investigated in more studies, which will be quoted later.) In 2001 Casey [23] reviewed the development of ski materials and ski designs up to the modern ski types. The author predicts that new materials will continue to create new ski designs and more diverse types of skis. He also expects that new simulation technologies are likely to have a distinct influence on this development.

The mechanical properties of binding plates and ski bindings and their impact on the mechanical properties of the ski-binding system is also an issue, which manufacturers investigate, but rarely publish results. Studies addressing the position of the binding on the ski and the impact on the biomechanics of a turn as well as on the comfort of the skier were published by Nigg et al. [24] and Schwameder et al. [25]. Neuwirth et al. [26] studied the differences of several designs of a specific binding model, while Müller [27] investigated in his diploma thesis the influence of different binding systems on the pressure distribution under a flat ski. Comprehensive studies characterising ski-binding systems in the interaction with the skier on the one side and the snow on the other have never been published so far.

The mechanical properties of a ski-binding system determine its vibration characteristics. Vibrations of the ski-binding system are frequently incited as the skier descends on the slope. The typical speed in skiing is comparably high and increased further with the emerging carving technique. At high speeds, vibrations of the ski interfere with the

ski-snow interaction on the one hand and increase the load on the motoric system of the skier's body on the other (see Mester et al. [28], or Schwarzer et al. [29]). In 1997 Niessen et al. [30] showed that the so called „chattering“ of skis is most likely a resonance effect of the ski-binding system. They used an wavelet analysis method by Schwameder & Tscharnner [31]. The dynamic properties of skis had already been described in 1972 by Piziali & Mote [32] and in 1994 by Glenne et al. [33]. The determination of a ski's resonance frequencies was one of the first ski-related problems which were solved by numerical methods: already in 1980 Devaux & Trompette [34], and later Ulrich et al. [35] calculated the dynamic properties of a ski.

It was already pointed out by Casey [23] that numerical simulations offer many new and promising possibilities to investigate the interaction between snow, skiing equipment and skier. Kitazawa et al. [36] suggested in 2000 a procedure for the design and construction of alpine skis using computer aided engineering, however, the first computer models designed for this purpose had already been published 18 years earlier. In 1982 Lieu presented in his thesis [37],[38] the first analytical model of a turning ski, which was solved by a FORTRAN encoded computer simulation. The ski-snow interaction was approximated by empirical data, which was obtained from extensive ice-cutting experiments [39]. In 1989 Clerc et al. [40] presented the first finite element simulation of a turning alpine ski. In this model the ski was represented by beam elements and the ski-snow interaction was approximated by non-linear springs. Renshaw & Mote [41] calculated the efficiency in performing a constant-radius turn with different skis by assuming an equilibrium of dynamic forces. Hirano & Tada simulated the ski-snow interaction in 1994 using a water jet analogy [42]. Later they replaced this approach by an empirical equation determined from ice-cutting experiments [39], and in 2002 they presented the first simulation, which used data obtained from experiments on snow. In 1997 Casolo et al. [45] presented a simulation model, which included a very detailed body model representing the skier. Later (2000) they introduced a detailed model for the ski, which calculated the ski's radius and the pressure distribution under the ski in an iterative solving algorithm [46]. The most comprehensive simulation program published so far was described by Nordt et al. [47] in 1999. In seven sub-models the different force components on the whole ski-skier system were calculated for a turn of constant radius. The simulation result, the time necessary to complete a turn with a given initial velocity, was compared to measured times and good agreement was found. In 2000 Glitsch [48] investigated the dynamic equilibrium of forces during a ski turn with simulations and experiments. Also in 2000, Kaps et al. [49] published a study on the pressure distribution under an edged alpine ski, for which they used a static simulation model.

The reason why so many different simulation tools have been developed is that skiing is a complicated dynamical process, which is not yet thoroughly understood. All of the simulations listed above use assumptions appropriate to their specific aims, giving leeway to other studies with a different focus area. Basic assumptions, which many of the above simulations rely on, are, for example, a constant turn radius, negligence of non-static effects, or a rough estimation of the ski-snow interaction. None of the simulations reviewed considers the binding in their model.

1.4 Objectives of this Thesis

The primary objective of this thesis is the development of a finite element simulation of the ski-binding system in the situation of a carved turn. This simulation is primarily intended to be used on the one hand to assist in the development of new ski and binding designs and on the other hand to allow a systematic analysis of turn parameters and their interrelationship. The specific requirements of this model were specified as follows:

- The design and the mechanical properties of the ski and binding should be implemented as detailed as possible.
- A detailed model of the interaction between ski and snow has to be included in the model.
- A realistic interaction of ski and binding with the athlete has to be implemented.
- The simulation results have to be verified by comparison to experimental results.
- Ski and binding should be implemented such that small modifications of the model for parameter studies, as well as a substitution of the whole ski or binding model is possible with little effort.

The output of the simulation should particularly include the deformed shape of the ski-binding system and the pressure distribution at the ski-snow interface. The ski's shape determines the turn radius, while the pressure distribution is considered to be an important indicator of the ski-snow interaction.

1.5 Basic Mechanics of a Turning Ski

1.5.1 Coordinate Systems

Determination of the turn parameters on the one side and the simulation of the ski-binding system on the other side suggest the use of three different coordinate systems [37]. In this thesis only turns on a slope of constant inclination α are considered. Process parameters as position, velocity, and acceleration will be measured in an external system attached to the slope (see Figure 4). The coordinate axis of this system are denoted with capital letters X , Y , Z . The origin of this system is chosen on the plane of the snow surface. The X -axis is directed downhill along the fall line, the Y -axis lies within the plane of the snow surface, perpendicular to the X -axis. The Z -axis is perpendicular to the other two coordinate axis and points upwards, such that a right-handed coordinate system is defined.

For the simulation of the ski-binding system a separate coordinate system is defined (see Figure 4). The coordinates of this system are denoted with small letters x , y , z . This system is adapted to the motion of the ski on the snow surface (but not to the ski) and is accelerated relative to the global system XYZ . The origin of the xyz -system is also located on the plane of the snow surface at the normal projection of the point on the ski axis, which is marked as the middle position of the ski boot. The x -axis points along the projection of the ski's velocity onto the plane of the snow surface. The z -axis points upwards, perpendicular to the plane of the snow surface (parallel to Z). The y -axis lies within the plane of the snow surface such that a right-handed coordinate system is set up. Thus, the x and y -axis are rotated in relation to X and Y by an orientation angle β , which is defined by the velocity of the ski:

$$\tan\beta = \frac{v_Y}{v_X}. \quad (1)$$

This system is determined for each ski separately. If both skis during a turn are simulated, then two coordinate systems, one for each ski, are determined.

The third coordinate system used in this study is a system, which is attached to the ski (Figure 4). The coordinates of this system are denoted as \bar{x} , \bar{y} , and \bar{z} . The origin of the \bar{xyz} -system was chosen on the ski axis at the position marked as middle of the ski boot on the top surface of the ski. Thus this origin is elevated by a distance z_0 compared to the origin of xyz . For better clarity, Figure 4 displays the system \bar{xyz} in relation to the system xyz for the special case of $z_0 = 0$. The \bar{x} axis is directed along the ski axis, the \bar{z} -axis is perpendicular to the upper surface of the ski and \bar{y} perpendicular to \bar{x} and \bar{z} .

The reason why the simulation is implemented in the xyz -frame of reference is that the ski-snow interaction depends on the penetration depth D of the ski into the snow (see chapter 3). In the xyz -coordinate system this penetration depth D coincides with the negative z -axis. Thus the implementation of the boundary condition describing the ski-snow interaction (see chapter 5) is significantly simplified if the xyz -coordinates are used instead of the \bar{xyz} - or the XYZ -coordinates.

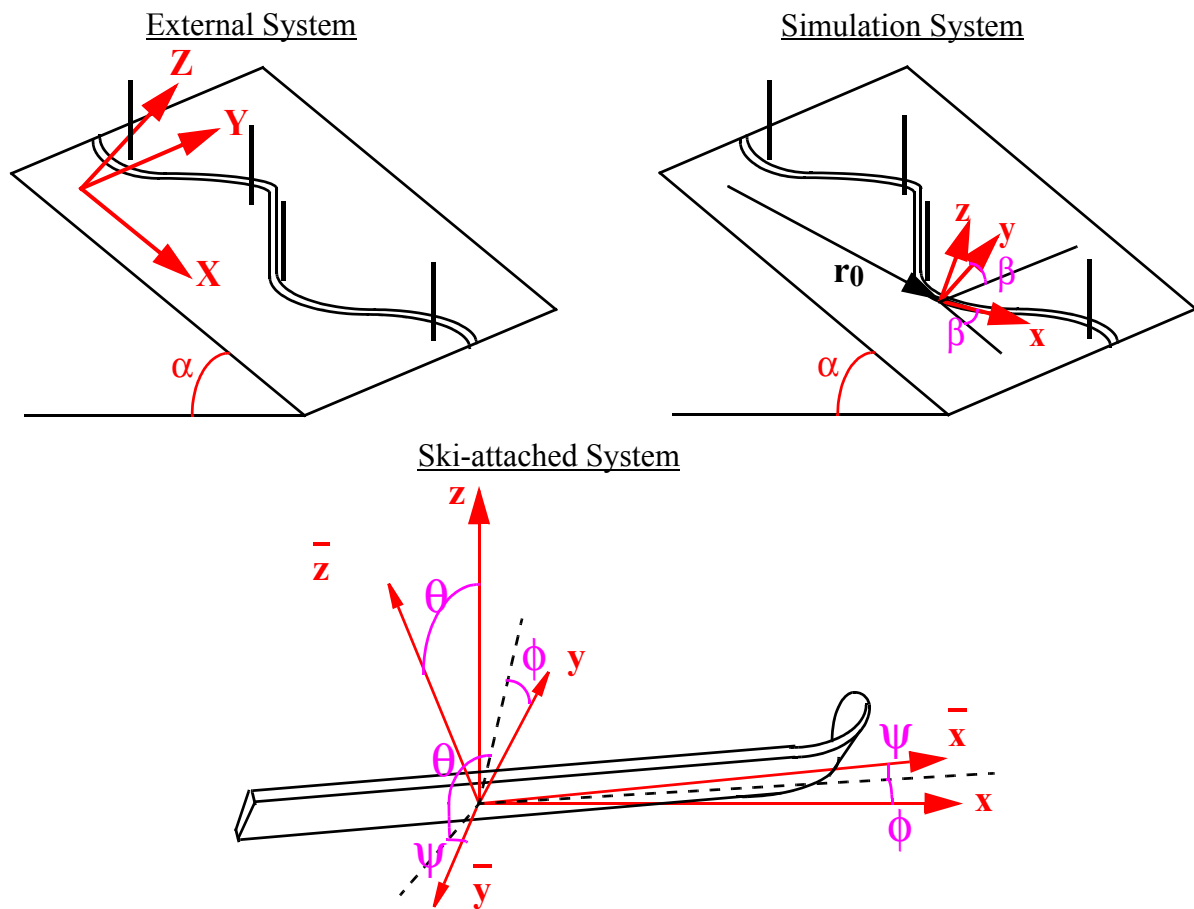


Figure 4. Coordinate systems used in this thesis.

To describe the state of the ski as a solid body the ski position $\mathbf{r}_0 = (X_0, Y_0, Z_0)$ and the orientation angles (Euler angles, see [51]) ϕ , θ , ψ of the ski have to be determined. It is convenient to define these angles in the system xyz : the blade angle ϕ denotes a rotation of the ski around the z -axis, the edging angle θ a rotation around the rotated x -axis and the downtilt angle ψ is defined as the rotation around the rotated z -axis ($=\bar{z}$ -axis). Note that the order of rotations is not commutative. ϕ can be identified as an angle observed when the ski skids, θ denotes the angle between ski underside and snow surface, and ψ depends on how much the ski's rear part penetrates the snow surface.

The transformation of XYZ -coordinates into xyz -coordinates, or the transformation of the \bar{xyz} -coordinates into xyz -coordinates are executed by a rotation, followed by a translation:

$$\begin{bmatrix} x \\ y \\ z \end{bmatrix} = \begin{bmatrix} \cos\beta & \sin\beta & 0 \\ -\sin\beta & \cos\beta & 0 \\ 0 & 0 & 1 \end{bmatrix} \cdot \begin{bmatrix} X \\ Y \\ Z \end{bmatrix} - \begin{bmatrix} X_0 \\ Y_0 \\ Z_0 \end{bmatrix}, \quad (2)$$

$$\begin{bmatrix} x \\ y \\ z \end{bmatrix} = \mathbf{T} \cdot \begin{bmatrix} \bar{x} \\ \bar{y} \\ \bar{z} \end{bmatrix} - \begin{bmatrix} 0 \\ 0 \\ z_0 \end{bmatrix}. \quad (3)$$

The rotation matrix \mathbf{T} in equation 3 is, in general, a complicated function of the angles ϕ , θ , and ψ (for an explicit notation see [51]). In this thesis, however, only carved turns are studied. In carved turns it is appropriate to assume that the ski axis is parallel to the velocity vector of the ski, which implies that $\phi = 0$. Moreover, ψ is also small enough to be neglected in a first approximation. This simplifies the rotation matrix \mathbf{T} in equation 3 to

$$\mathbf{T} = \begin{bmatrix} 1 & 0 & 0 \\ 0 & \cos\theta & -\sin\theta \\ 0 & \sin\theta & \cos\theta \end{bmatrix}. \quad (4)$$

1.5.2 Basic Kinematics and Dynamics of the Turning Ski as a Rigid Body

With the assumptions made in the previous section the ski-binding system has five degrees of freedom with respect to the external XYZ coordinate system: three degrees of translation, and two rotational degrees. The rotational degrees of freedom are a rotation with the orientation angle β around the z -axis and the rotation with the edging angle θ around the x -axis. In order to describe the ski-binding system's translatory motion the position $\mathbf{r}_{ski}(t)$ of the ski-binding system has to be determined in the external reference system. The velocity $\mathbf{v}_{ski}(t)$ and the acceleration $\mathbf{a}_{ski}(t)$ in the external frame of reference can then be determined by differentiation. The acceleration of the ski is a function of the external forces, $\mathbf{F}_i^{ext}(t)$, acting on the ski-binding system of mass m :

$$m\mathbf{a}_{ski}(t) = \sum_i \mathbf{F}_i^{ext}(t) \quad (5)$$

During skiing, the three main external forces acting on the system are: the forces transferred from the athlete onto the binding, $\mathbf{F}_{athlet}(t)$, the forces acting at the ski-snow interface, $\mathbf{F}_{SSI}(t)$,

and the gravitational forces $\mathbf{G}_{ski}(t)$. All other forces acting on the ski-binding system, for example air resistance, are small enough to be neglected:

$$\sum_i \mathbf{F}_i^{\text{ext}}(t) = \mathbf{F}_{\text{athlete}}(t) + \mathbf{F}_{\text{SSI}}(t) + \mathbf{G}_{ski}(t) \quad (6)$$

For the simulation the forces and the acceleration have to be expressed in the frame of reference of the xyz-coordinate system. This system is accelerated and rotates with the angular velocity $\boldsymbol{\omega} = d/dt \beta$ around the z-axis with respect to the external XYZ-reference frame. Therefore, any point P at position \mathbf{r} , with a velocity \mathbf{v}_r and an acceleration \mathbf{a}_r relative to the origin o of system xyz experiences additional accelerations due to the rotation of the system:

$$\begin{aligned} \mathbf{a}_p &= \mathbf{a}_o + \boldsymbol{\omega} \mathbf{e}_z \times (\boldsymbol{\omega} \mathbf{e}_z \times \mathbf{r}) + (\dot{\boldsymbol{\omega}} \mathbf{e}_z + \boldsymbol{\omega} \dot{\mathbf{e}}_z) \times \mathbf{r} + \mathbf{a}_r + 2\boldsymbol{\omega} \mathbf{e}_z \times \mathbf{v}_r \\ &= \mathbf{a}_o - \omega^2 r_{xy} \mathbf{e}_r + \dot{\omega} r_{xy} \mathbf{e}_\beta + \mathbf{a}_r + 2\boldsymbol{\omega} \mathbf{e}_z \times \mathbf{v}_r \end{aligned} \quad (7)$$

where \mathbf{a}_o is the acceleration of the origin o , \mathbf{e}_z is the unit vector in direction of the rotation axis, which is the z-direction, $\dot{\boldsymbol{\omega}}$ is the time derivative of the angular velocity, i.e. the angular acceleration, $\dot{\mathbf{e}}_z$ the time derivative of the unit vector \mathbf{e}_z on the rotation axis, which is zero if the inclination of the skiing slope is assumed constant. The scalar r_z denotes the distance between P and the rotation axis:

$$r_{xy} = \sqrt{r_x^2 + r_y^2} \quad (8)$$

\mathbf{e}_r is the unit vector from the rotation axis to the position of P , and \mathbf{e}_β is the unit vector in the direction of P 's motion:

$$\mathbf{e}_r = \frac{1}{r_{xy}} \begin{pmatrix} r_x \\ r_y \\ 0 \end{pmatrix} \quad \text{and} \quad \mathbf{e}_\beta = \frac{1}{r_{xy}} \begin{pmatrix} r_y \\ -r_x \\ 0 \end{pmatrix} \quad (9)$$

Within the reference frame of the xyz-coordinate system the ski-binding system still has one degree of freedom: a rotation around the x-axis in order to increase the ski's edging angle in the course of the turn. This rotation with the angular velocity $\boldsymbol{\omega}_\theta = d/dt \theta$ causes the relative velocity \mathbf{v}_r and the relative acceleration \mathbf{a}_r of point P in the frame of reference of the xyz-coordinate system, which affect the last two coefficients of equation 7.

In the frame of reference of the xyz-coordinate system the acceleration components in equation 7, which occur due to the system's rotation can be considered as inertia forces $\mathbf{F}_{inertia}(t)$, which additionally act on ski and binding (D'Alembert's principle). Hence, equation 5 can be expressed in the frame of reference of the xyz-coordinate system as

$$\int_V \rho \mathbf{a}_r(t) dV = \sum_i \mathbf{F}_i^{\text{ext}}(t) + \mathbf{F}_{inertia}(t) \quad (10)$$

where ρ is the density of the material in the volume dV , and \mathbf{a}_r is the acceleration measured in the frame of reference of the xyz-coordinate system. The inertia forces of the ski may be calculated using the remaining components in equation 7:

$$\mathbf{F}_{\text{inertia}}(t) = -\int_V \rho(\mathbf{a}_o - \omega^2 \mathbf{r}_{xy} \mathbf{e}_r + \dot{\omega} \mathbf{r}_{xy} \mathbf{e}_\beta + 2\omega \mathbf{e}_z \times \mathbf{v}_r) dV \quad (11)$$

All inertia components depend on the time t . In chapter 2 the magnitude of the components of the inertia force will be estimated (section 2.3.1) using actual measurements of the acceleration, angular velocity and angular acceleration (section 2.2.4) of the skis in a carved turn.

As discussed in the beginning of this section the ski-binding system has two rotational degrees of freedom during the turn. Within the external coordinate system XYZ the general rotational motion is described by the angular momentum equation:

$$\mathbf{M}^{\text{ext}}(t) = \frac{d}{dt} \mathbf{L}(t) = \frac{d}{dt} \int (\mathbf{r}(t) \times \mathbf{v}(t)) dm \quad (12)$$

where $\mathbf{L}(t)$ is the angular momentum of the ski-binding system, and $\mathbf{M}^{\text{ext}}(t)$ is the moment of force generated by the external forces acting in point \mathbf{r}_i on the ski-binding system, with

$$\mathbf{M}^{\text{ext}}(t) = \sum_i \mathbf{r}_i(t) \times \mathbf{F}_i^{\text{ext}}(t) . \quad (13)$$

Equations 12 and 13 are valid within the external XYZ-coordinate system or the xyz-coordinate system since its origin is located on the rotation axes. Within the rotating xyz-coordinate system the external moments of force acting on the ski-binding system are

$$\mathbf{M}^{\text{ext}}(t) = \mathbf{M}_{\text{athlete}}(t) + \mathbf{M}_{\text{SSI}}(t) + \mathbf{M}_{\text{Gski}}(t) + \mathbf{M}_{\text{inertia}}(t) \quad (14)$$

The angular momentum \mathbf{L} can be calculated by multiplication of the angular velocity components with the constant moment of inertia tensor \mathbf{J} . The rotational degrees of freedom are a rotation with $\omega_\theta = \omega_x$ around the x-axis and a rotation with $\omega_\beta = \omega_z$ around the z-axis. The rotation around the y-axis ω_y is zero because the downtilt angle ψ is assumed to be constant: $\psi(t) = 0$. Thus, the angular momentum of the ski-binding system in the xyz-system can then be calculated by

$$\begin{aligned} \mathbf{L} = & (\omega_\theta J_{xx} - 0 \cdot J_{xy} - \omega_\beta J_{xz}) \mathbf{e}_x \\ & + (0 \cdot J_{yy} - \omega_\theta J_{xy} - \omega_\beta J_{yz}) \mathbf{e}_y \\ & + (\omega_\beta J_{zz} - \omega_\theta J_{xz} - 0 \cdot J_{yz}) \mathbf{e}_z \end{aligned} \quad (15)$$

The components of the moment of inertia \mathbf{J} can be calculated by

$$J_{xx} = \iiint \rho(y^2 + z^2) dx dy dz \quad (16)$$

$$J_{xy} = \iiint (\rho \cdot xy) dx dy dz \quad (17)$$

where ρ is the density. The other components are obtained with similar equations but exchanged indices between x, y, and z.

Within the rotating frame of reference of the xyz-coordinate system the time derivative of the vector \mathbf{L} is

$$\left. \frac{d}{dt} \mathbf{L} \right|_{xyz} = \frac{d}{dt} \mathbf{L} - \omega_\beta \mathbf{e}_z \times \mathbf{L} \quad (18)$$

thus

$$\begin{aligned} \left. \frac{d}{dt} \mathbf{L} \right|_{xyz} = & (\dot{\omega}_\theta J_{xx} - \dot{\omega}_\beta J_{xz} + \omega_\beta (-\omega_\theta J_{xy} - \omega_\beta J_{yz})) \mathbf{e}_x \\ & + (-\dot{\omega}_\theta J_{xy} - \dot{\omega}_\beta J_{yz} - \omega_\beta (\omega_\theta J_{xx} - \omega_\beta J_{xz})) \mathbf{e}_y \\ & + (\dot{\omega}_\beta J_{zz} - \dot{\omega}_\theta J_{xz}) \mathbf{e}_z \end{aligned} \quad (19)$$

The rigid body motion of the ski-binding system is determined by equation 10 and by equation 12. In order to solve these equations the external forces and moments acting on the ski-binding system have to be determined. However, the ski-snow interaction force $\mathbf{F}_{SSI}(t)$ and the associated moment $\mathbf{M}_{SSI}(t)$ are very difficult to be experimentally determined. They depend obviously on the penetration depth of the ski into the snow and the contact area between snow and ski. Both of these parameters depend on the bending properties of the ski, on the snow strength, and on the applied forces.

1.5.3 Assumption of a Quasi-Static Situation

The main objectives of this thesis are to calculate the deformation state of the ski and the pressure distribution between ski and snow. For this purpose it is not necessary to solve the equations of the ski's motion (equation 10 and equation 12). In fact, the force and the moment of force needed to accelerate and rotate the ski are significantly smaller than the forces, which cause the deformation of the ski:

The velocity \mathbf{v}_r and acceleration \mathbf{a}_r observed within the frame of reference of the xyz-coordinate system are caused by the rotation ω_θ ¹:

$$\mathbf{v}_r = \omega_\theta \mathbf{e}_x \times \mathbf{r}, \quad (20)$$

$$\mathbf{a}_r = \frac{d}{dt}(\omega_\theta \mathbf{e}_x \times \mathbf{r}) = \dot{\omega}_\theta \mathbf{e}_x \times \mathbf{r} + \omega_\theta \mathbf{e}_x \times (\omega_\theta \mathbf{e}_x \times \mathbf{r}), \quad (21)$$

with an absolute value of

$$|\mathbf{a}_r| = \sqrt{r_y^2 + r_z^2} \cdot |\dot{\omega}_\theta| + \sqrt{r_y^2 + r_z^2} |\omega_\theta|^2. \quad (22)$$

The distance $\sqrt{r_y^2 + r_z^2}$ from the x-axis is smaller than 0.1 m for all parts of the ski binding system. In chapter 2 measurements of the angular velocity and the angular acceleration will be presented. The extreme values for the angular acceleration are in the order of 25 rad/s² and for the angular velocity 6 rad/s. The highest accelerations experienced by the outermost parts of the system are in the order of 6 m/s². The overall acceleration experienced by the whole ski-binding system can thus be estimated to be about 3 m/s², which is significantly less than the gravitational acceleration of the ski and can thus be neglected. For the purpose of this study it is therefore possible to calculate the deformation of the ski-binding system by assuming an

1. Additional relative velocities and accelerations arise from deformations of the ski-binding system, which are not considered in this section.

equilibrium of forces in the frame of reference of the xyz-coordinate system instead of Newton's law of motion (equation 10):

$$\mathbf{F}_{\text{athlete}}(t) + \mathbf{F}_{\text{SSI}}(t) + \mathbf{G}_{\text{ski}}(t) + \mathbf{F}_{\text{inertia}}(t) = 0 \quad (23)$$

In order to estimate the moment necessary to generate a rotation of the ski-binding system the time derivative of the angular momentum (equation 19) has to be estimated. Thereto the ski-binding system was approximated by a homogeneous cuboid of density ρ extending between $x = -0.8$ m and $x = +1.2$ m, $y = -0.05$ m and $+0.05$ m, and $z = 0$ m and 0.02 m. In this case the tensor of the moment of inertia becomes:

$$\mathbf{J} = \rho \cdot \begin{pmatrix} 4 \cdot 10^{-6} \text{m}^5 & 0 \text{m}^5 & 8 \cdot 10^{-6} \text{m}^5 \\ 0 \text{m}^5 & 1.5 \cdot 10^{-3} \text{m}^5 & 0 \text{m}^5 \\ 8 \cdot 10^{-6} \text{m}^5 & 0 \text{m}^5 & 1.5 \cdot 10^{-3} \text{m}^5 \end{pmatrix} \quad (24)$$

Only the J_{yy} and J_{zz} components are non-negligible. Typical angular accelerations and angular moments of the rotation around the x-axis (causing the edging angle θ) and the rotation around the z-axis (determining the orientation angle β) can be found in chapter 2. If a mean density of 700 kg/m^3 for the ski-binding system is assumed then typical moments of force necessary to change the ski-binding system's angular momentum are in the range of 5 Nm or smaller. These moments are so small that they insignificantly affect the deformation of the system and thus it is possible to simulate the ski-binding system during a carved turn by assuming an equilibrium of the external moments acting on the ski-binding system:

$$\mathbf{M}_{\text{athlete}}(t) + \mathbf{M}_{\text{SSI}}(t) + \mathbf{M}_{\text{Gski}}(t) + \mathbf{M}_{\text{inertia}}(t) = 0 \quad (25)$$

The quasi-static approach expressed by equations 23 and 25 allows to calculate the unknown ski-snow interaction force $\mathbf{F}_{\text{SSI}}(t)$ and the associated moment $\mathbf{M}_{\text{SSI}}(t)$ if the other external forces and moments and the inertia terms in equations 23 and 25 have been determined.

1.5.4 Deformations of the Ski-Binding System

The forces and moments acting on a ski-binding system during a turn cause bending and torsional deformations. In the situation of a turn bending in \bar{z} -direction (i.e. around the \bar{y} -axis) and torsion around the \bar{x} -axis have significant impact on the system properties. Bending in \bar{x} or \bar{y} -direction and torsion of the system around the \bar{y} or \bar{z} -axis are negligible². In order to calculate the ski radius and the pressure distribution between ski and snow, it is necessary to precisely determine the deformation of the ski, whereas not the deformations of the binding are of immediate interest, but rather the contribution of the binding to the system stiffness and the load transmission onto the ski.

2. Forces and moments on a ski were experimentally determined in this study and are discussed in chapter 2.3 of this thesis. The measured components of the force acting from the athlete onto the ski, which are displayed in Figure 34 on page 41 show that the transverse force for bending in x- or y-direction is a order of magnitude smaller. Moreover, the ski's bending stiffness in these directions is significantly higher.

1.5.4.1 Bending of the ski

Figure 5 displays a simplified model of the ski as a homogeneous beam of varying width and thickness. In this example the edging angle is considered to be zero, i.e. the ski rests flat on the snow surface. The ski is loaded by forces and moments transferred at position $\bar{x}_{B,rear}$ and $\bar{x}_{B,front}$, a line force $q_{z,snow}(\bar{x})$ exerted by the snow, and a line force $q_{z,acc}(\bar{x})$ due to accelerations experienced by the ski, i.e. the gravitational acceleration and the acceleration terms of the inertia force (see equation 11).

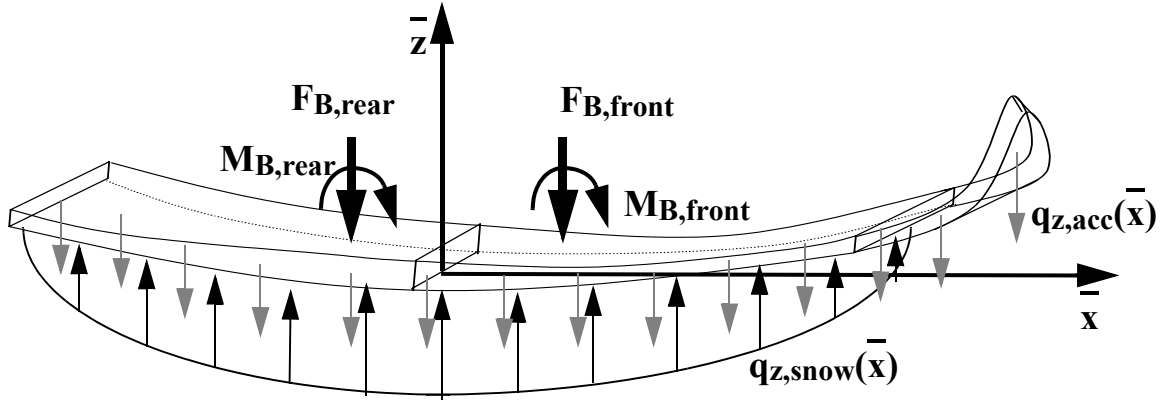


Figure 5. Types of load on a ski causing bending deformation.

If shear stresses in the beam are neglected and only small bending is assumed, then a differential equation can be derived for the deflection line $w(\bar{x})$ [52]:

$$\frac{d^2}{d\bar{x}^2} w(\bar{x}) = -\frac{M_b(\bar{x})}{EI_y(\bar{x})}, \quad (26)$$

where $M_b(\bar{x})$ denotes the bending moment acting on the beam and $EI_y(\bar{x})$ the bending stiffness. Both are a function of the position \bar{x} along the ski axis. The bending stiffness $EI_y(\bar{x})$ of a beam with a rectangular cross section depends on its width $W(\bar{x})$ and height $H(\bar{x})$ [52]:

$$EI_y(\bar{x}) = E \cdot \frac{W(\bar{x})H(\bar{x})^3}{12} \quad (27)$$

The bending moment $M_b(\bar{x})$ of a transverse force $F_Q(\bar{x})$ or a transverse line force $q_z(\bar{x})$ can be calculated from

$$M_b(\bar{x}) = \int F_Q(\bar{x}) d\bar{x} = -\int_{\bar{x}_{min}}^{\bar{x}_{max}} \int q_z(\xi) d\xi d\bar{x} \quad (28)$$

The bending moment acting at position \bar{x} of the ski has to be determined for three separate zones: zone (I) from the ski end, \bar{x}_{end} , to position $\bar{x}_{B,rear}$, where the forces and the moments of the rear part of the binding are transferred onto the ski, zone (II) between $\bar{x}_{B,rear}$ and $\bar{x}_{B,front}$, and zone (III) between $\bar{x}_{B,front}$ and the ski shovel at \bar{x}_{shovel} .

$$M_{b,(I)}(\bar{x}) = \int \int_{\bar{x}_{end}}^{\bar{x}} (q_{z, snow}(\xi) - q_{z, acc}(\xi)) d\xi d\bar{x} \quad (29)$$

$$M_{b,(II)}(\bar{x}) = M_{B, rear} - F_{B, rear}(\bar{x} - \bar{x}_{B, rear}) + \int \int_{\bar{x}_{end}}^{\bar{x}} (q_{z, snow}(\xi) - q_{z, acc}(\xi)) d\xi d\bar{x} \quad (30)$$

$$\begin{aligned} M_{b,(III)}(\bar{x}) &= M_{B, rear} + M_{B, front} - F_{B, rear}(\bar{x} - \bar{x}_{B, rear}) \\ &\quad - F_{B, front}(\bar{x} - \bar{x}_{B, front}) + \int \int_{\bar{x}_{end}}^{\bar{x}} (q_{z, snow}(\xi) - q_{z, acc}(\xi)) d\xi d\bar{x} \\ &= - \int \int_{\bar{x}}^{\bar{x}_{shovel}} (q_{z, snow}(\xi) - q_{z, acc}(\xi)) d\xi d\bar{x} \end{aligned} \quad (31)$$

The line force $q_{z, acc}(\bar{x})$ due to the accelerations experienced by the system can be calculated by

$$q_{z, acc}(\bar{x}) = \rho(\bar{x})W(\bar{x})H(\bar{x}) \cdot (g + a_z(\bar{x})) \quad (32)$$

where $\rho(\bar{x})$ is the mean density, $W(\bar{x})$ the width and $H(\bar{x})$ the height of the beam at position \bar{x} , g is the gravitational acceleration, and $a_z(\bar{x})$ is the z-component of the acceleration experienced at position \bar{x} on the ski (see equation 7). The line force $q_{z, snow}(\bar{x})$ depends on the mean pressure p_{snow} on the ski-snow interface at position \bar{x} :

$$q_{z, snow}(\bar{x}) = p_{snow}(\bar{x}) \cdot W(\bar{x}) \quad (33)$$

Equation 26 can be solved after all components in equations 27 and 29 - 33 have been determined³ and suitable boundary conditions have been supplied.

1.5.4.2 Torsion of the ski

If the edging angle θ between ski and snow surface is not zero, then torsion occurs at the ski shovel and the rear part of the ski (see Figure 6).

In order to calculate the torsional deformation, the ski is assumed to be clamped in the middle of the ski binding ($\bar{x} = 0$). The torsion angle $\Delta\theta(\bar{x})$, which decreases the actual edging angle θ of the ski, increases with the distance $|\bar{x}|$ from the clamping at $\bar{x} = 0$. The torsion angle $\Delta\theta(\bar{x})$ can be calculated by [52]:

$$\Delta\theta(\bar{x}) = \frac{M_t(\bar{x}) \cdot |\bar{x}|}{GI_t(\bar{x})} \quad (34)$$

where $M_t(\bar{x})$ is the torque at position \bar{x} and $GI_t(\bar{x})$ is the shear stiffness, with $I_t(\bar{x})$ the torsional moment of inertia.

3. Chapter 3 of this thesis will show, that the pressure at the ski-snow interface p_{snow} (equation 33) depends on the penetration depth D of the ski into the snow, which is a function of the deflection line $w(\bar{x})$. Thus, the actual differential equation, which has to be solved is of the form $w''(\bar{x}) = f(w(\bar{x}))$.

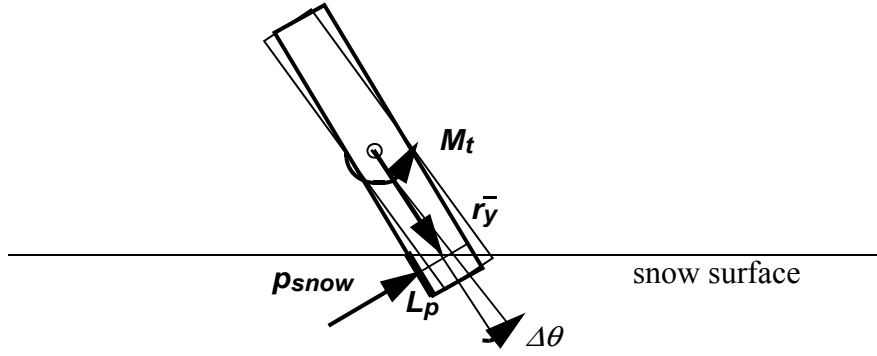


Figure 6. Torsion of the ski.

If the ski is approximated by a homogeneous beam of rectangular cross section, then the torsional moment of inertia $I_t(\bar{x})$ is of the form [52]:

$$I_t(\bar{x}) = c W(\bar{x}) H(\bar{x})^3 \quad (35)$$

where c is a constant factor, which depends on the ratio of W/H . For a ski c is in the range between $c = 0.28$ (near the position of the ski binding) and 0.32 (towards the ski shovel or the ski end). The torque $M_t(\bar{x})$ at position \bar{x} can be calculated by

$$M_t(\bar{x}) = \int_0^{\bar{x}} p_{\text{snow}}(\bar{x}) L_p(\bar{x}) r_{\bar{y}} d\bar{x} \quad (36)$$

where $p_{\text{snow}}(\bar{x})$ is the mean pressure on the ski-snow interface, $L_p(\bar{x})$ is the contact length of the interface, and $r_{\bar{y}}(\bar{x})$ is the distance from the centre of rotation to the ski snow interface (see Figure 6):

$$r_{\bar{y}} = \frac{W(\bar{x}) - L_p(\bar{x})}{2} \quad (37)$$

Equation 34 can be solved after all components in equations 35 - 37 have been determined and suitable boundary conditions have been supplied.

1.6 The Finite Element Method for the Calculation of the Ski Deformation

In the last section analytical equations were introduced, which allow to calculate the bending displacement $w(x)$ and the torsion angle $\Delta\theta(x)$ of the ski in simplified cases. In actual turns the loading conditions are more complicated and the layered structure of actual skis additionally complicates the situation. Therefore, the finite element method is more suitable to calculate the deformation of the ski-binding system. The ski and binding designs can be taken into account in more detail, and different loading cases can be solved in less time.

The finite element simulation as well as analytical calculation methods need appropriate boundary conditions in order to calculate the deformation of the ski-binding model for a given

situation. There to, all forces and moments, which act on the ski binding system in the used quasi-static approach defined by the equations 23 and 25, have to be determined. Figure 7 shows an overview of all input parameters, which are necessary to specify the numerical model of ski and binding, and the boundary conditions, which define the loading situation at a given point of time during the turn.

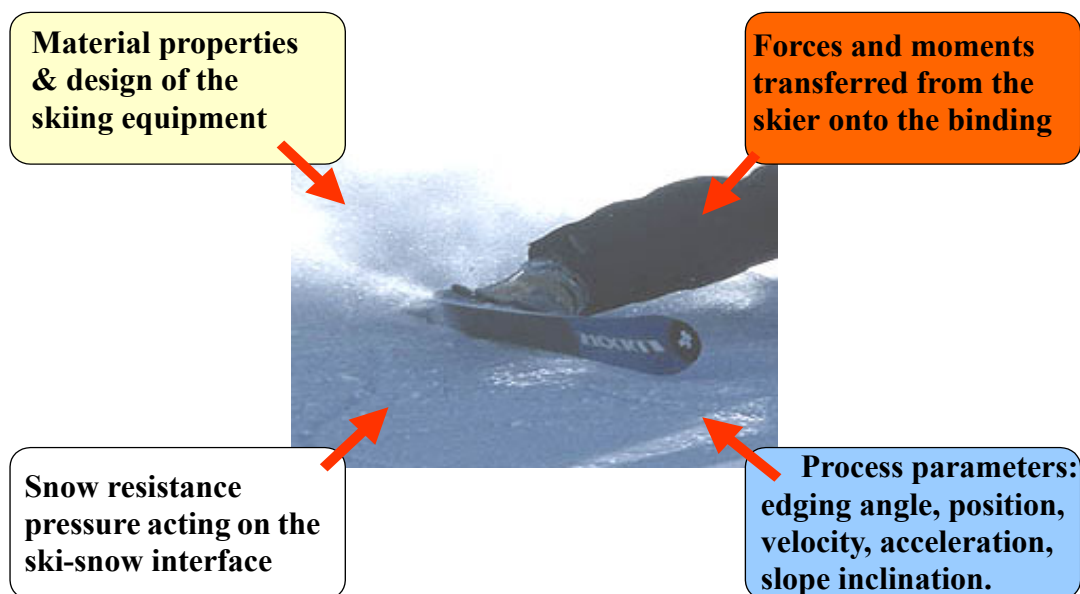


Figure 7. Grouped parameters determining the performance of a ski in a carved turn.

With the exception of the design properties of ski and binding, all other input parameters to the simulation depend upon the snow conditions on the slope and how the skier actually performs a turn. Therefore, this study comprises three major steps:

In the first step measurement methods are established, which allow to determine the process parameters and the forces and moments acting on the ski-binding system during a turn. A full kinematic and kinetic analysis of two selected turns is presented in chapter 2. With these results typical input parameters for the simulation are obtained. Moreover, the trajectories of the skis recorded in these measurements allow to calculate the instantaneous turn radius which can be compared to the ski radius calculated by the simulation for the loading condition at a given point in time. This comparison constitutes a verification method for the simulation results (see chapter 6).

In a second step, discussed in chapter 3, the ski-snow interaction in a carved turn is investigated. New measurement devices are introduced and the dependence of the snow resistance strength on the process parameters edging angle and deformation speed are analysed. Thus, a full set of all input parameters to the simulation is completed.

The third step comprises the actual implementation of the simulation for the ski-binding system. In chapter 4 the governing equations and the implementation of the ski and binding models are discussed. Chapter 5 presents the implementation and the simulation results for the limiting case of a static situation. In chapter 6 boundary conditions to simulate a moving ski are discussed and the results are compared to measured reference values.

2. Measurement of the Turn Parameters

In the previous chapter the coordinates defining the position and orientation of the turning ski-binding system as well as the forces and moments, which govern the deformation of the system have been introduced. In this chapter measurement methods and the results of a full kinematic and kinetic turn analysis are presented. In the first section of this chapter, section 2.1, the analysed test run is described. The kinematic measurement methods and results are presented in section 2.2. Forces and moments acting on the ski-binding system are discussed in section 2.3. The parameters presented in this chapter provide the necessary input data for the simulation of the ski during the turn, as well as data used for a verification of the simulation results.

2.1 Description of the Analysed Test Run

The kinematic and kinetic analysis presented in this chapter is based on measurements conducted on the 19. November 2003 in the ski dome in Neuss, Germany. In the ski dome the measurements were independent on weather conditions and the snow on the slope did not change significantly during the course of the day. Figure 8 displays the conditions in the ski dome prior to the measurements.



Figure 8. Ski dome in Neuss, Germany where the analysed test runs were recorded. The left side of the slope was closed off for the measurements.

A short course of three left and two right turns was marked on the slope. A high level ski racer performed this run several times and was filmed with a system of two high speed digital cameras, which will be described in section 2.2.2. Most of the test runs were additionally recorded with a second video system consisting of three analog cameras operated by members of the Department of Sports Sciences of the University of Salzburg. Comparison of the analysis results of these two independent systems were used for an error estimation. Two turns were selected for a detailed analysis in this thesis. The inclination of the slope near these

selected turns was measured with a water level and found to be approximately constant with an inclination angle of $\alpha = 11.8^\circ$. Prior and between the test runs the snow of the slope was characterised with the measurement methods discussed in chapter 3.

The tested ski-binding system consisted of Stöckli Spirit Fun 170 cm skis equipped with a Fritschi Rave Powerride binding. The mass of this system was $m = 2.8$ kg. They were additionally equipped with *Kistler*TM force sensor plates, which will be described in section 2.4. Subsequent to the run which will be analysed in this thesis, the position of the ski's trace in the snow was determined in 30 points by a professional geometer.

2.2 Kinematic Analysis of Two Selected Turns

2.2.1 Review of Available Measurement Methods

Table 1 lists the coordinates required to describe the position and the orientation of a ski in an external coordinate system. Also included are the velocity, the acceleration, the angular velocity, and the angular acceleration. For each parameter considered measurement methods are compiled. If similar measurements were found in the reviewed literature focusing on the characterisation of ski turns, then the references are quoted as well.

Table 1. Coordinates and process parameters determining the motion of the ski in an external system XYZ. All parameters have to be determined in function of time.

Parameter	Symbol	Available Measurement Methods
position of the ski (expressed in the coordinates of the external system)	$\mathbf{r}(t) = (X(t), Y(t), Z(t))$	video analysis [55][56][57], geometrical measurement (only for reference measurements), combined systems of differential global positioning system (DGPS), inertia system and acceleration sensors [58][59][60][61][62].
velocity of the ski (expressed in the coordinates of the external system)	$\mathbf{v}(t) = (v_X(t), v_Y(t), v_Z(t))$	differentiation of video analysis or DGPS data / integration of data of inertia systems or acceleration sensors [55][56][58].
acceleration of the ski (expressed in the coordinates of the external system)	$\mathbf{a}(t) = (a_X(t), a_Y(t), a_Z(t))$	acceleration sensors [no references for an application to characterise skiing movements were found] differentiation of video analysis or DGPS data [55][56][58].
orientation angle of the ski in the external coordinate system	$\beta(t)$	photo [53] and video analysis [55][56].

Table 1. Coordinates and process parameters determining the motion of the ski in an external system XYZ. All parameters have to be determined in function of time.

Parameter	Symbol	Available Measurement Methods
angular velocity of the rotation around the z-axis	$\omega(t) = \omega_{\beta}(t)$	differentiation of video analysis data / integration of data of inertia systems or acceleration sensors [no references for an application to characterise skiing movements were found]
angular acceleration of the rotation around the z-axis	$\dot{\omega}(t) = \dot{\omega}_{\beta}(t)$	differentiation of video analysis data [no references found]
edging angle	$\theta(t)$	photo [53][54] and video analysis [55][56].
angular velocity of the rotation around the x-axis	$\omega_{\theta}(t)$	differentiation of video analysis data / integration of data of inertia systems or acceleration sensors [no references for an application to characterise skiing movements were found]
angular acceleration of the rotation around the x-axis	$\dot{\omega}_{\theta}(t)$	differentiation of video analysis data / integration of data of inertia systems or acceleration sensors [no references for an application to characterise skiing movements were found]
blade angle	$\phi(t)$ Within this thesis $\phi(t) = 0$ is assumed.	In skidded turns this angle can be determined by photo or video analysis [54], in carved turns it is probably too small to be observed.
downtilt angle	$\psi(t)$ Within this thesis $\psi(t) = 0$ is assumed.	It could be estimated from the depth D of the ski track: if $D < 3\text{cm}$ then $\psi < 1^{\circ}$.

After reviewing and testing available measurement techniques [63],[64] a 3D video analysis system was selected for the kinematic measurements, since it allows the highest resolution for the analysis of single turns.

2.2.2 Employed 3D-Video System and its Calibration

In order to determine the trajectory of the skis two high speed digital cameras manufactured by Redlake [71] and a 3D-video analysis software, called „WINanalyse“, by Mikromak Service K. Brinkmann [72] were used. The frame rate of the cameras is adjustable between 50 and 250 frames per second, while the corresponding recording duration is restricted to 10 s and 2 s, respectively. Both digital cameras are equipped with a circular buffer. A light barrier triggers both cameras simultaneously and thus synchronizes the film sequences of the two cameras.

For the determination of the skier's path it is necessary to calibrate the perspectives of each camera. This is done by recording a 3D calibration model with both cameras, as displayed in Figure 9. The position of each of the calibration points was determined by a professional geometer with an accuracy of 2 mm. This calibration defines the XYZ-coordinate system on the slope (as defined in section 1.5.1).

After the coordinates of the reference points have been identified as shown in Figure 9 (the so called „ground truth information“) the software calculates for each camera view eleven projection parameters. These permit to calculate the real-world-coordinates of each point visible simultaneously in both camera images. The calculated parameters are the rotation matrix \mathbf{R} (3 parameters) and the translation matrix \mathbf{T} (3 parameters) which transform the real world coordinates into camera view coordinates. Additionally, camera specific parameters are calculated, namely the focal length f (1 parameter), the radial lens distortion coefficient κ (1 parameter), the image scale uncertainty factor s_x (1 parameter) and the image plane origin C_x , C_y (2 parameters). Tangential lens distortion is neglected. This calibration method was developed by R. Y. Tsai [73]. A more detailed description of the camera calibration is found in the manual of WINanalyse [74].

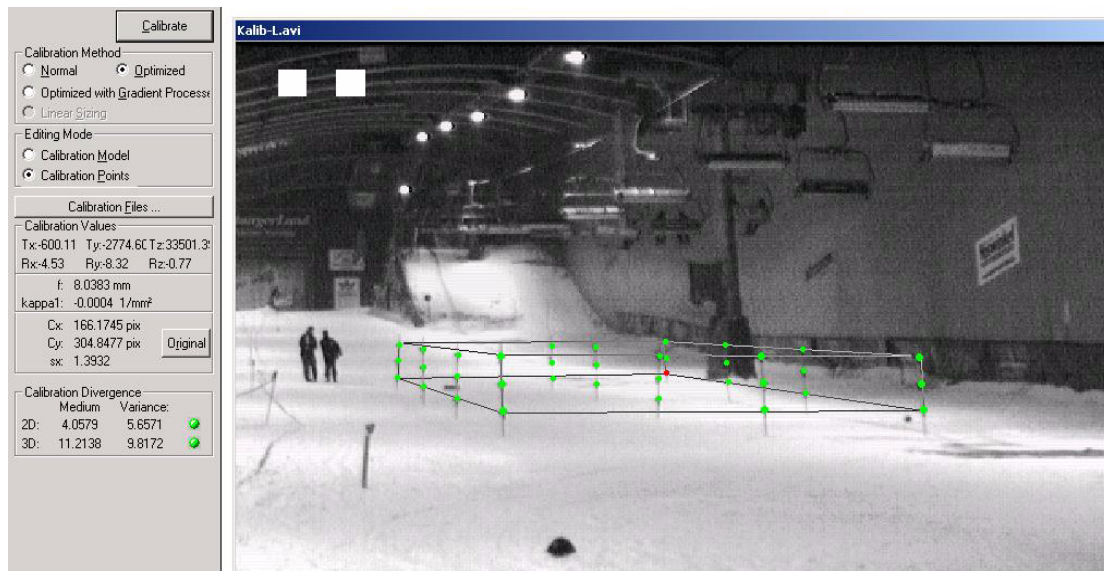


Figure 9. Calibration of the perspective of one of the digital cameras with a 3D-model. For each reference point the 3D coordinates in the XYZ-coordinate system („ground truth information“) are allocated.

2.2.3 Analysis of the Collected Video Data

After calibrating the video sequences, the 3D-position of markers can be calculated, which are assigned to objects visible in both video frames of the two synchronised video sequences. For the motion analysis the skier's body shape was identified by assigning 18 markers to body joints, head and torso of the skier (see Figure 10).

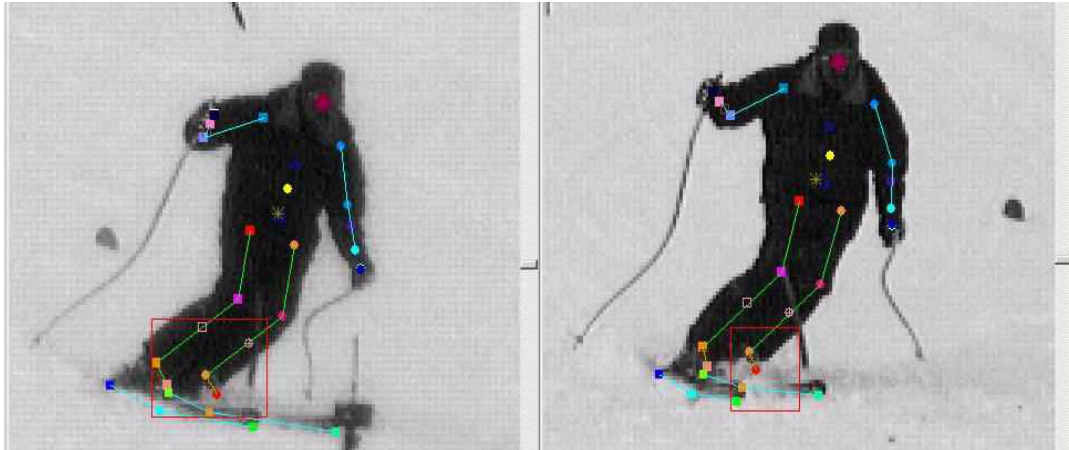


Figure 10. Identification of the shape of the skier's body in the video sequences of the two synchronized cameras by 18 markers. This example shows an athlete performing short turns.

2.2.3.1 Skier's Centre of Mass

The path of the skier's centre of mass (CM) in the external XYZ-coordinate system was determined as a reference value. Thereto, the body model according to Hanavan was used [76]. This model comprises 15 body segments, which were identified in the video sequences by assigning the 18 markers to the body joints, to the skier's head, and to the middle of torso (Figure 10). The relative weight distribution of the 15 body segments is shown in Table 2. It is based on data for a male proband according to Dempster [75].

Table 2. Body segments and their relative weight in the calculation of the CM according to Dempster.

body segment	relative weight	body segment	relative weight
left foot	0.014	right foot	0.014
left shank	0.045	right shank	0.045
left thigh	0.097	right thigh	0.097
left forearm	0.016	right forearm	0.016
left upper arm	0.027	right upper arm	0.027
left hand	0.006	right hand	0.006
upper torso	0.2555	lower torso	0.2555
head	0.079		
total relative weight	1		

The used video analysis software WINanalyse™ incorporates the body model of Hanavan and automatically calculates the skiers CM after assigning the necessary reference points.

2.2.3.2 Position of the Skis

The position of the skis was marked with three additional reference points (see Figure 10), however, during the analysis of the video data it turned out that the markers on the ski are

unsuitable to obtain a reliable position and orientation of the ski. During the devolution of the turn the skis are often hooded behind the other ski, spraying snow, or the skiers legs and the position of the markers could only be guessed. Therefore, the position of the skis were approximated by the position of the skiers ankle, which could be clearly identified in most of the video frames.

2.2.3.3 Numerical Differentiation of the Position Data

To obtain the velocity \mathbf{v} and acceleration \mathbf{a} numerical differentiation of the position data is necessary. Numerical differentiation is a badly conditioned problem, which always amplifies the data error [77]. Therefore several differentiation methods have been tested. The most suitable method is the best trade-off between strong data smoothing, in which high frequency characteristics of the specific turn are lost but the differentiation error is small, and little data smoothing, which preserves the curve characteristics but generates strong error amplification by the differentiation. Specifically tested were differentiation of a fit-curve to the whole data set [63], differentiation of linear or cubic splines [56], and differentiation using a Woltring filter. The obtained accelerations were used to approximate the forces acting between the skier and the skis, which were then compared to direct force measurements in the skis' binding plates [78]. The riser plates with integrated force sensors employed for the direct force measurements are introduced in section 2.3.2 of this thesis. Of the tested differentiation methods the best agreement was obtained for the differentiation of a piecewise linear fit to nine neighbouring data points [78]. For the employed measurement frequency of 50 Hz this corresponds to an averaged slope value for the data points of a period of 0.18 s. The acceleration values were obtained by a second differentiation with the same method using nine velocity values.

2.2.3.4 Orientation Angle of the Skis

The orientation angle β of the skis in the external coordinate system was calculated from equation 1. The velocity components v_X and v_Y were obtained from differentiation of the position data as described above.

2.2.3.5 Edging Angle of the Skis

A direct observation of the ski's edging angles in the video sequences is nearly impossible since the skis are barely visible on many frames. With the use of two assumptions, which restrict this analysis to the case of carved turns, the edging angle can be determined from the position of the skiers lower leg. These two assumptions are

1. The ski axis is parallel to the projection of the ski's tangential velocity \mathbf{v}_τ onto the plane of the snow surface. This assumption is equivalent with the assumption that the blade angle ϕ of the ski is zero. (This assumption has already been introduced when defining the transformation of the XYZ-coordinate system into the xyz-system in section 1.5.1).
2. The skiers lower leg is firmly attached to the ski leaving only one degree of freedom, namely a forward kneeling parallel to the ski axis. Geometrically this means that the lower leg of the skier is a part of the plane defined by the ski axis and the normal vector \mathbf{e}_z to the bottom side of the ski.

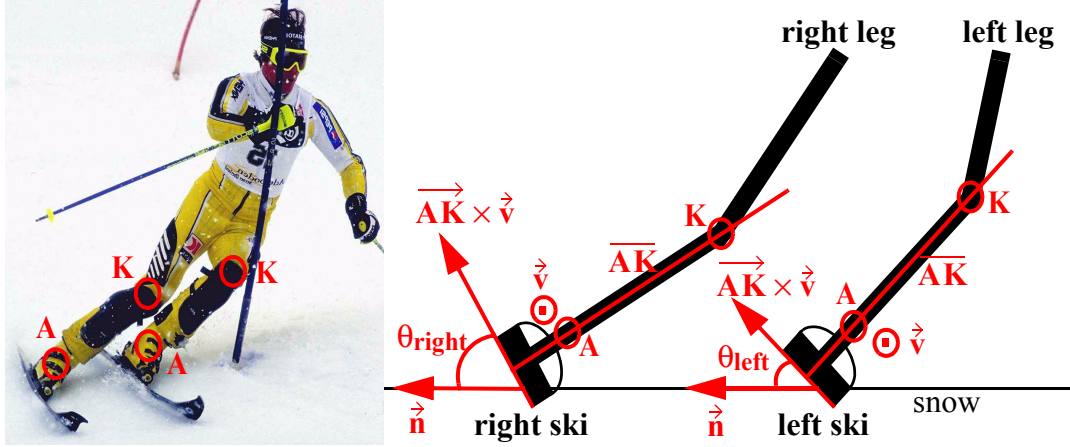


Figure 11. Reference points for the ankle A and knee K on the photo of a skier (left). Schematic diagram displaying the vectors used to calculate the skis' edging angles (right).

The position of the lower leg is determined by the straight line between the skier's ankle A and the skier's knee K . Both of these points have been marked in the video frames and thus their positions can be determined by the analysis software. The cross product of the straight line \overline{AK} , defined by the knee and ankle positions, with the skier's trajectory \vec{v} is a vector perpendicular to the ski axis and parallel to the undersurface of the ski. The edging angle of the ski can then be identified as the angle between $(\overline{AK} \times \vec{v})$ and the projection of the normal vector on the trajectory onto the plane of the snow surface \vec{n} (see Figure 11). Thus the edging angle θ can be calculated by

$$\cos \theta = \frac{\vec{n} \cdot (\overline{AK} \times \vec{v})}{|\vec{n}| \cdot |(\overline{AK} \times \vec{v})|} \quad (38)$$

the projection of the normal vector on the ski's trajectory onto the snow surface is

$$\vec{n} = \left(\frac{-v_Y}{\sqrt{v_X^2 + v_Y^2}}, \frac{v_X}{\sqrt{v_X^2 + v_Y^2}}, 0 \right). \quad (39)$$

2.2.3.6 Error Estimation

The spatial error calculated by the image calibration routine in the 3D analysis software is in the range of 10 cm. However several additional error sources contribute to the total error of the 3D measurement data, such as the error due to mispositioning of the markers on the video sequences and the time synchronization error. These later error sources are not statistically distributed, but lead to a non-avoidable systematic error. Thus the total error of the data obtained by 3D video analysis is very difficult to calculate or estimate⁴. In order to quantify the

4. Video analysis is a common measurement method in biomechanical studies. However, an analysis of the total measurement error, taking into uncertainties of the calculated 3D coordinates as well as the error amplification due to numerical differentiation, has not been found in corresponding literature. To my knowledge, the studies of Oberhofer [56] and of Luethi et al. [78] are the first to compare the results of two independent analysis systems.

error one test run of a skier was recorded and analysed by two independent camera and analysis systems. The average difference in the obtained data found in this comparison gives a measure of the absolute measurement error that has to be assumed in the video analysis. Due to the camera perspectives the absolute errors differ for the three position coordinates. Both cameras were positioned on the slope below the recorded turns. Therefore, the X-component of the trajectory data exhibits the largest measurement errors (see Table 3). The calculation method for the position of the skier's CM is a weighted average of the position of several body parts, which levels out the stochastic scattering in the data. Thus, the error in the CM data is significantly reduced. The velocity and acceleration components were obtained by differentiation of a piecewise linear fit to the data points (see previous subsection). The data error is significantly amplified by this differentiation method, but characteristics of the data curves are still preserved. A more detailed analysis of error sources and values in this 3D video analysis method applied for the determination of a skiers trajectory was published in [78]. Table 3 summarises the data error estimated for each position, velocity and acceleration component averaged over the two turns.

Table 3. Estimated data error in the results of the video analysis [56][78].

vector component	X	Y	Z	X_{CM}	Y_{CM}	Z_{CM}
position	0.18 m	0.08 m	0.06 m	0.12 m	0.06 m	0.03 m
velocity	0.9 m/s	0.3 m/s	0.3 m/s	0.5 m/s	0.17 m/s	0.12 m/s
acceleration	9 m/s ²	3 m/s ²	3 m/s ²	5.7 m/s ²	1.9 m/s ²	1.4 m/s ²

The measurement uncertainty of the employed calculation method for the edging angle θ and the orientation angle β of the skis was also analysed by comparison of the results of two independent video analysis systems [56]. The mean difference of the edging angles determined by these two systems is 5° , the mean difference in the orientation angles is 2.6° . The mean difference in the angular velocity values are $\Delta\omega_\theta = 0.5 \text{ rad/s}$ and $\Delta\omega_\beta = 0.4 \text{ rad/s}$, and in the angular acceleration values $\Delta\dot{\omega}_\theta = 6 \text{ rad/s}^2$ and $\Delta\dot{\omega}_\beta = 5 \text{ rad/s}^2$.

2.2.4 Results of the Video Analysis

2.2.4.1 Trajectory of the Skis and the Skier's Centre of Mass

The X-, Y- and Z coordinates of the position of the skier's CM are displayed in the next three figures as a function of time for two consecutive turns. The position of the skis is approximated by the position of the skier's ankles, as explained in section 2.2.3. The error bars indicate the measurement error, which was discussed in section 2.2.3.6. For the first two position components, however, the absolute error is so small compared to the coordinate range, that it is hardly visible in the figures.

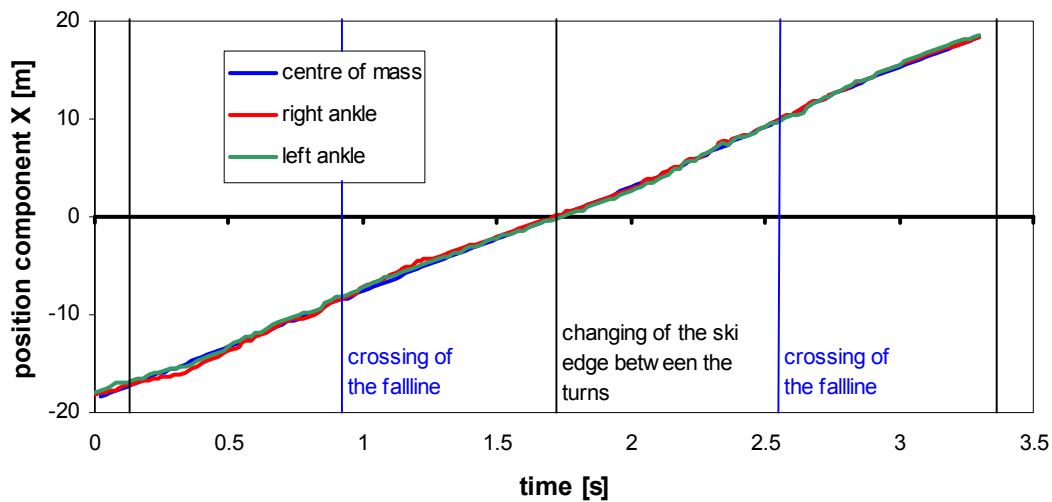


Figure 12. Position of the skis and the skier's CM in the X-coordinate as a function of time.

Figure 12 shows that the motion of the skier along the fall line is nearly linear, which indicates that the skier had already assumed a velocity in which the gravitational energy gain and the energy losses are balanced over the period of one turn. The fact that the initiation phase and the steering phase of the turn are hardly recognisable indicates that the energy loss due to the ski-snow interaction during the steering phase is minimized - which is typical for a carved turn.

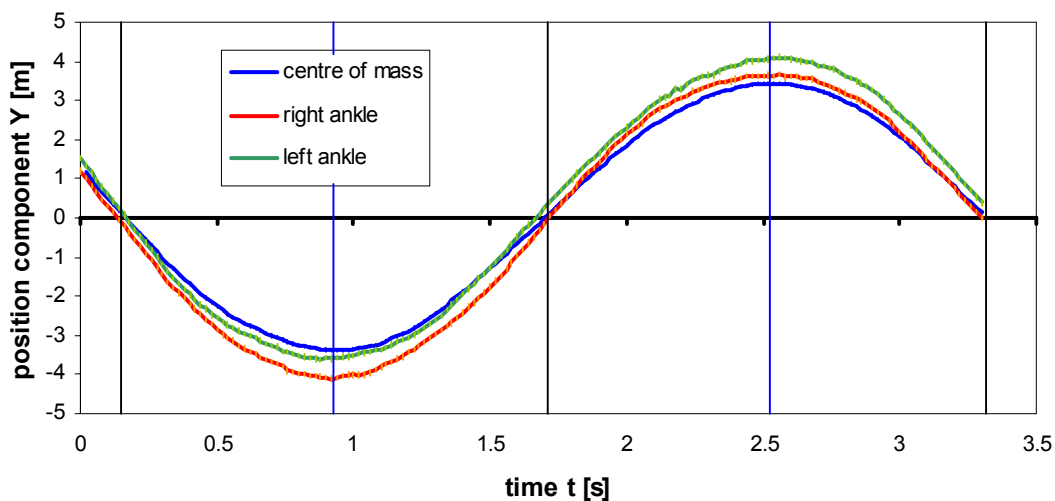


Figure 13. Position of the skis and the skier's CM in the Y-coordinate as a function of time.

The curves of the Y-component of the skis' and skier's positions (Figure 13) are in a good approximation sinusoidal. An inward-leaning of the skier during the turns is evident.

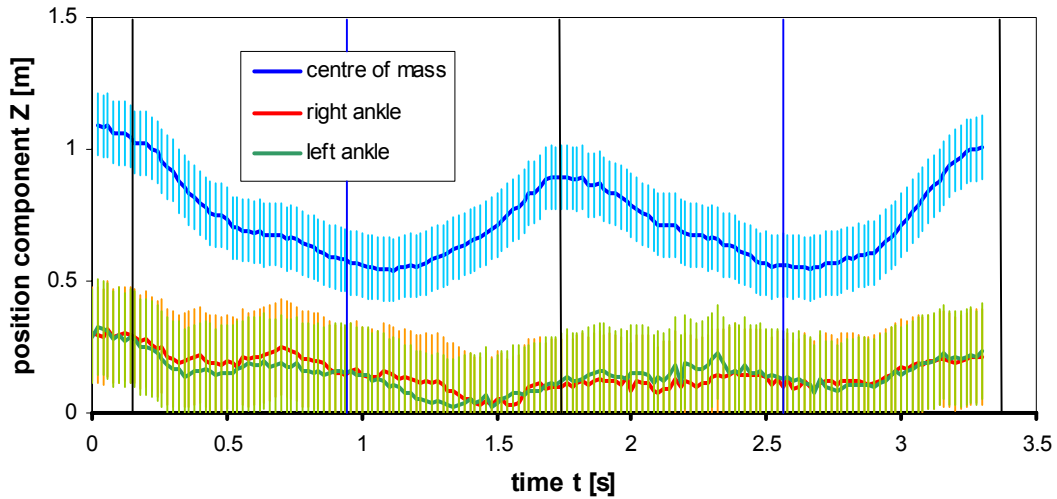


Figure 14. Position of the skis and the skier's CM in the Z-coordinate as a function of time.

The Z-component of the skier's ankles, which are used to approximate the skis' position, are nearly constant during the two turns. The ski slope in the first turn was slightly more inclined than in the second turn. The motion of the skier's CM displays a lifting and lowering during a turn, which is caused by two processes: on the one hand an active vertical movement of the skier (lifting during the change of the ski edge, lowering during the steering phase), and on the other hand an inward leaning of the skier in the turning position. This motion is roughly sinusoidal but with twice the frequency of the turn.

2.2.4.2 Velocity of the Skis and the Skier's Centre of Mass

The velocity data was obtained from differentiation of the position data, as discussed in section 2.2.3.3.

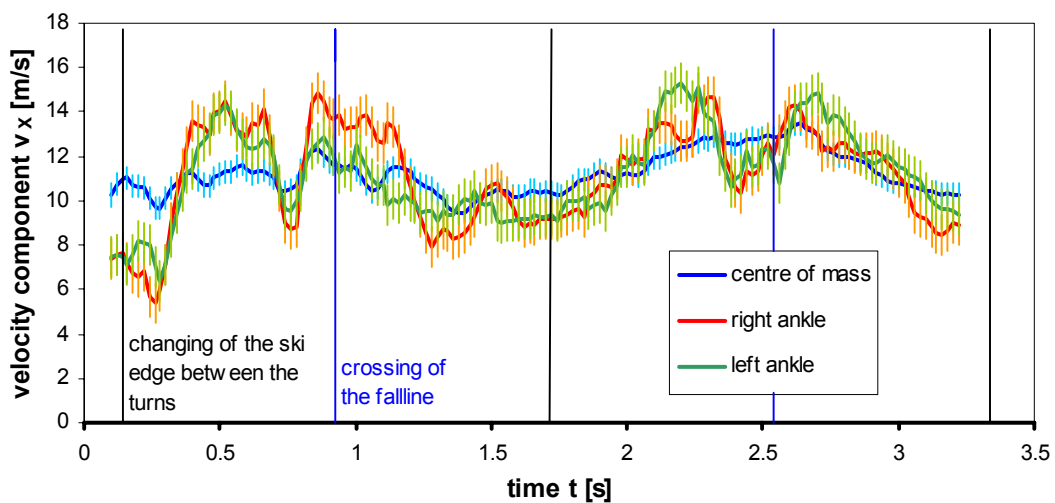


Figure 15. Velocity of the skis and the skier's CM in the X-coordinate as a function of time.

The velocity component parallel to the fall line, v_x , is on average slightly increasing during the two turns (Figure 15). As the skier turns towards the fall line the speed increases slightly, after the fall line has been crossed the speed begins to decrease.

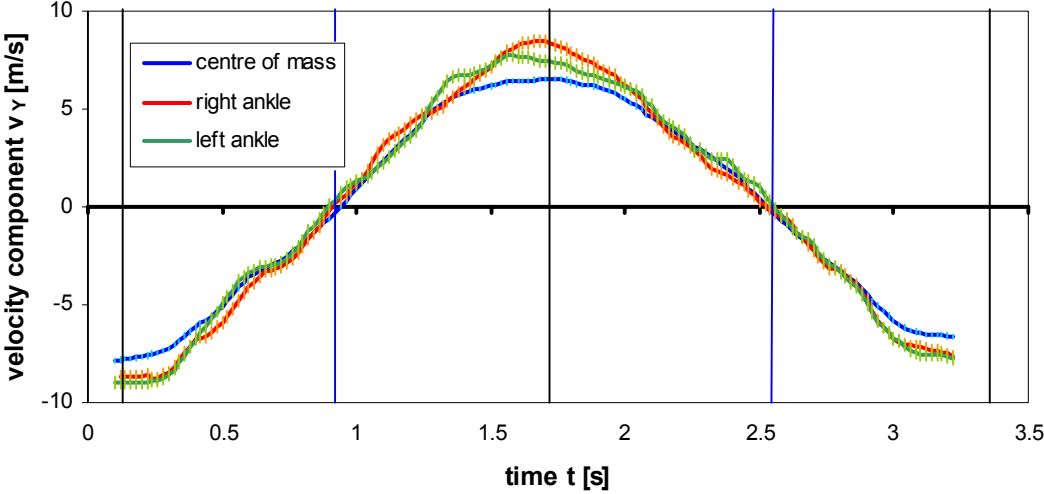


Figure 16. Velocity of the skis and the skier’s CM in the Y-coordinate as a function of time.

The progression of the turn is also clearly visible in the Y-component of the velocity (Figure 16). As the skier changes from one turn to the next his centre of mass is slower in this velocity component than his ankles: due to the inward leaning during the turn the centre of mass has to cover less distance in the Y-direction.

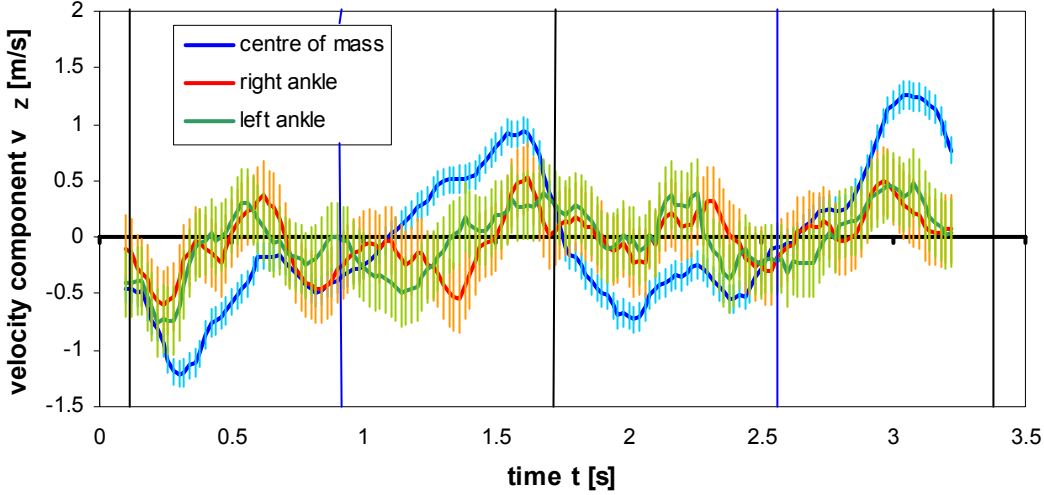


Figure 17. Velocity of the skis and the skier’s CM in the Z-coordinate as a function of time.

The Z-component of the ankles’ velocity is in a good approximation zero. The up and down motion of the skier’s CM takes place at velocities of up to 1.2 m/s.

2.2.4.3 Acceleration of the Skis and the Skier's Centre of Mass

The acceleration data was obtained from differentiation of the velocity data, as discussed in section 2.2.3.3.

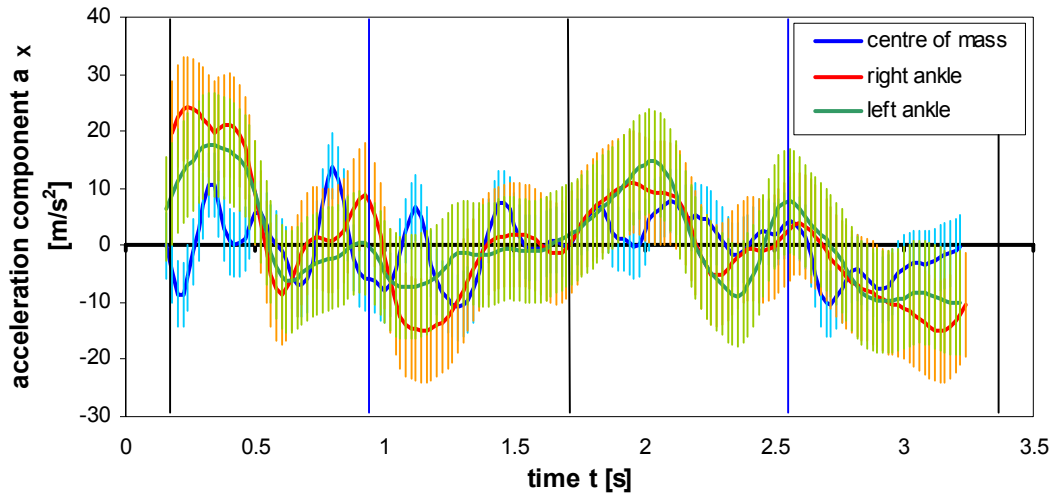


Figure 18. Acceleration of the skis and the skier's CM in the X-coordinate a function of time.

The accelerations observed for the skier's CM stay predominantly in the range of about $\pm 10 \text{ m/s}^2$. The fluctuations are probably error dominated. The small changes in the downhill velocity observed in Figure 15 cannot be detected in the acceleration data. The acceleration data of the skier's ankles fluctuates strongly. The high amplitude of these accelerations are probably caused by corrections of the reference marks in the video analysis and are thus no real physical phenomena. Therefore, the data was smoothed by averaging about the same number of points used for the numerical differentiation of the position data.

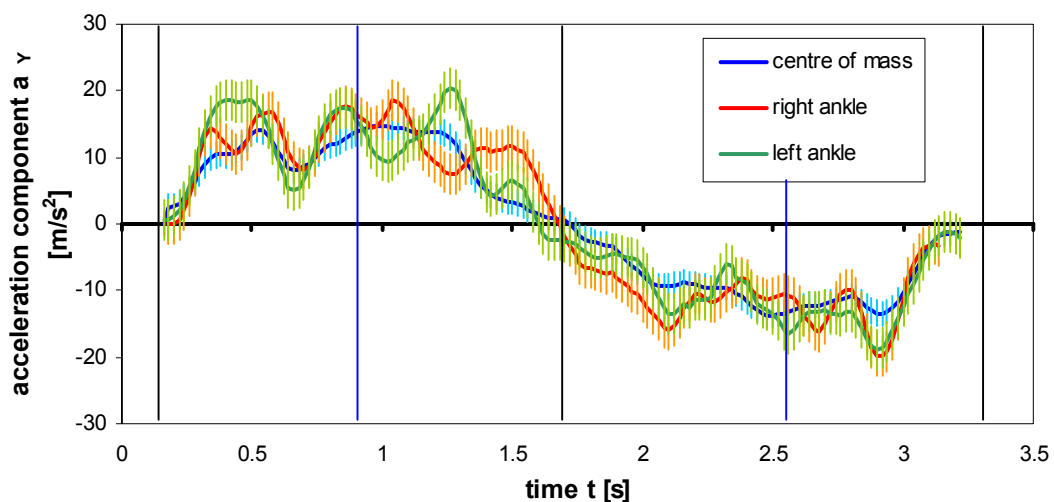


Figure 19. Acceleration of the skis and the skier's CM in the Y-coordinates a function of time.

The Y-component of the acceleration is generated by the turning forces. Thus the characteristics of the two turns are still clearly visible. The acceleration curves determined for the skier's ankles fluctuate around the smoother acceleration curve calculated for the skier's CM. These fluctuations are probably error induced, however, the relative data error is in comparison to the other acceleration components still low. Therefore no additional data smoothing was conducted.

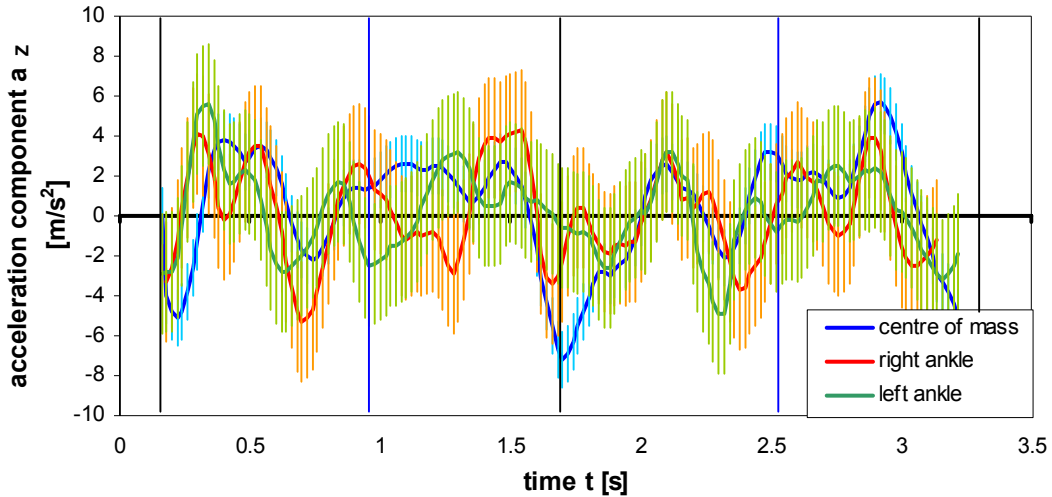


Figure 20. Acceleration of the skis and the skier's CM in the Z-coordinates a function of time.

The Z-components of the acceleration scatter between $\pm 6 \text{ m/s}^2$ with an estimated error of 3 m/s^2 . The acceleration in this component is therefore insignificant.

2.2.4.4 Orientation Angle, Angular Velocity and Angular Acceleration

Figure 21 displays the orientation angle calculated using equation 1 from the velocity data of the left and right ankle, β_{left} and β_{right} , respectively, and β_{CM} of the skier's centre of mass. The three data sets were smoothed by averaging over seven neighbouring data points.

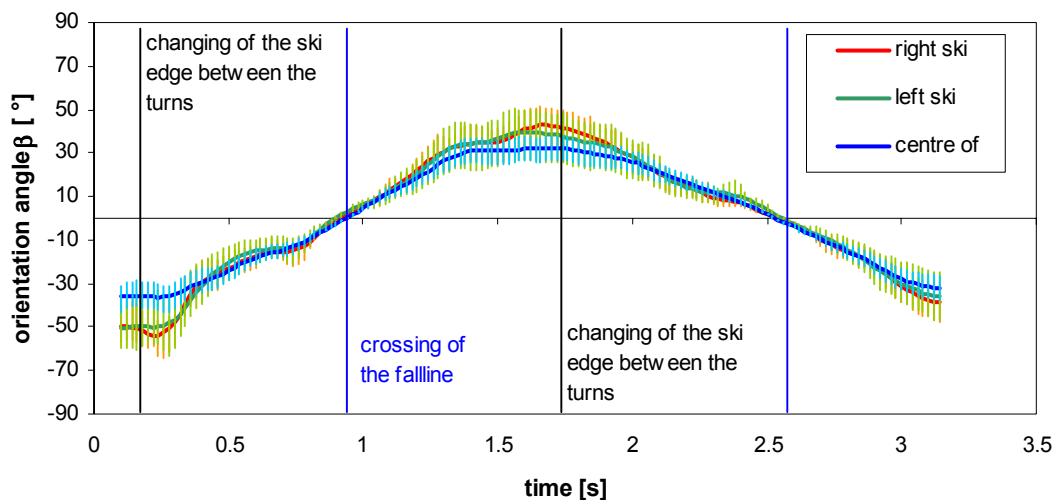


Figure 21. The orientation angles, β_{left} and β_{right} of the two skis and of the skier's CM, β_{CM} .

The orientation angles calculated for the skis exhibit a higher maximum value in between the turns compared to the orientation angle calculated for the motion of the skier's centre of mass. This can be explained by the shift of the skier's CM from one inward-leaning position to the other. The orientation angle determined for the two skis match well taking into account the estimated error.

The angular velocity for the rotation around the z-axis was determined for each of the three reference points indicating the skis' and the skier's motion. It is obtained by the same differentiation method described in section 2.2.3 observed. Figure 22 shows the angular velocity ω_β in radian units.

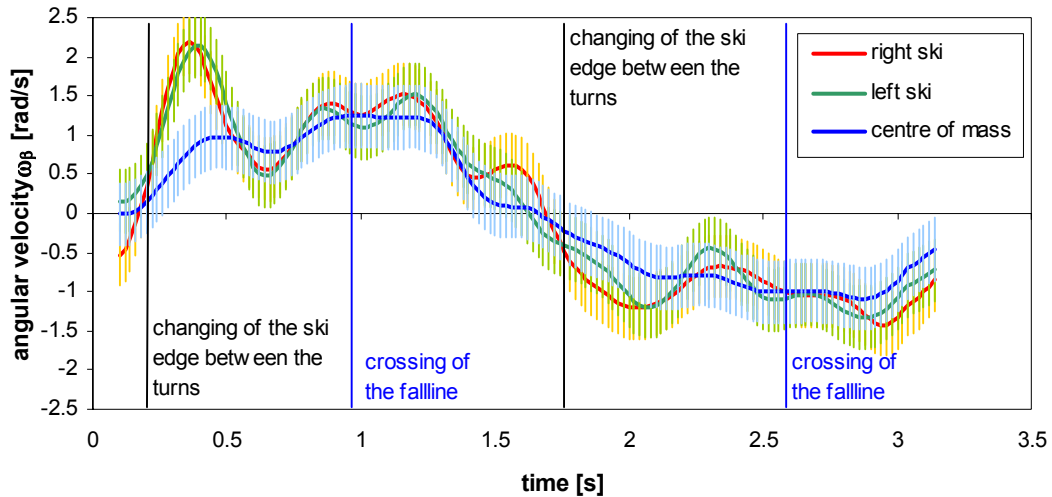


Figure 22. The angular velocities of the skis' and the skier's motion.

The angular velocities, ω_β , determined for the left and right ski match within the error bounds. During the steering phase of the carved turn the angular velocity of the skier's centre is equal to the angular velocity of the skis. During the initiation phase of the turn (after the skier has changed the ski edges) the angular velocity of the skier's centre of mass is slightly smaller than that of the skis. This decrease of the centre of mass's angular velocity is caused by an active inward-shifting of the skier's body during the turn initiation.

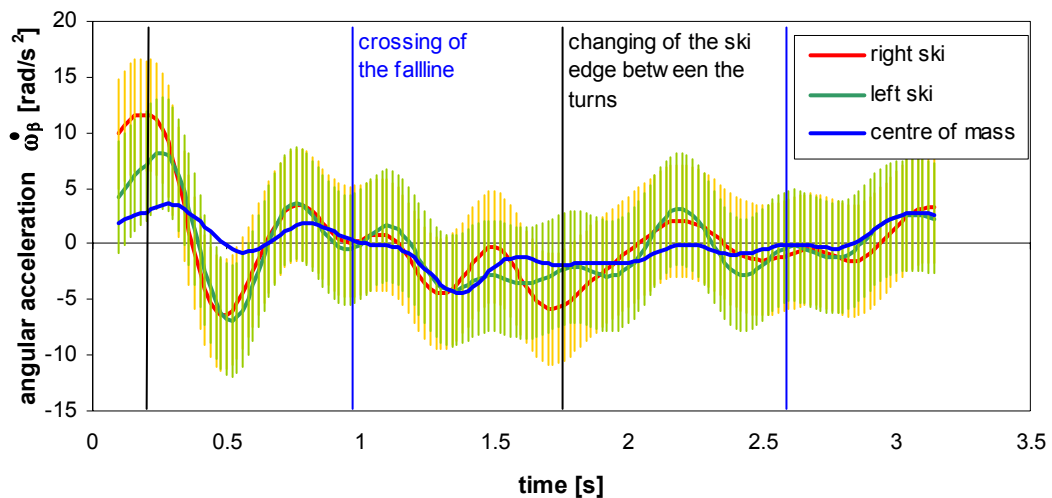


Figure 23. The angular accelerations of the skis' and the skier's motion.

The angular acceleration $\dot{\omega}_\beta$ is obtained by a second differentiation of the orientation angle data. Figure 23 shows the angular acceleration in radian units. As a general trend, the angular acceleration $\dot{\omega}_\beta$ changes its algebraic sign when the skier crosses the fall line, but not in between the turns. In Figure 23 a significant acceleration is visible in the first 0.5 s. The high amplitude of this acceleration is probably error dominated. For the rest of the two turns the angular acceleration ranges between -5 and 5 rad/s².

2.2.4.5 Edging Angles, Angular Velocity and Angular Acceleration

Figure 24 displays the edging angle θ of left and right ski during the two analysed turns calculated according to equation 38. The two data sets were smoothed by averaging over seven neighbouring data points.

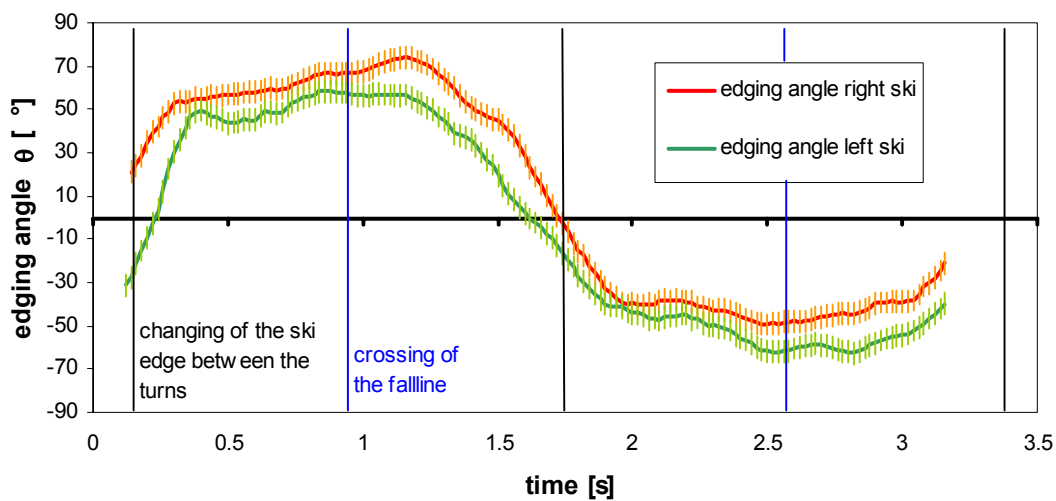


Figure 24. The edging angles θ_{left} and θ_{right} of the two skis.

Even though the velocity was not very high and the turns were not very tight for a giant slalom course edging angles above 60° were measured. The change of edges is conducted during a period of about 0.7 s. In the progression of the turn the edging angles continue to increase due to the slope's inclination.

The angular velocity ω_θ of the skis' rotation around the x-axis was obtained by the differentiation of the edging angle-time data sets. It is displayed in the units rad/s.

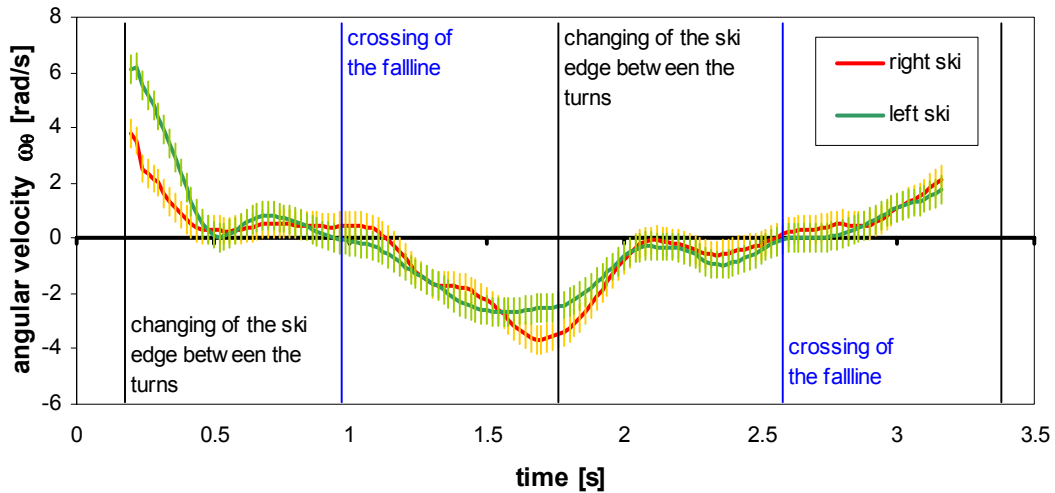


Figure 25. The angular velocity of the edging motion of the skis.

After the turn initiation is completed the skis' edging angle stays nearly constant and the angular velocity is therefore close to zero. Already at the end of the steering phase the skier reduces the edging angles of the skis with an angular velocity of approximately 2-3 rad/s (absolute value). The change of the ski edges in between the turns is conducted at higher angular velocities between 4 and 6 rad/s.

The angular acceleration $\dot{\omega}_\theta$ of the rotation around the x-axis is displayed in Figure 26:

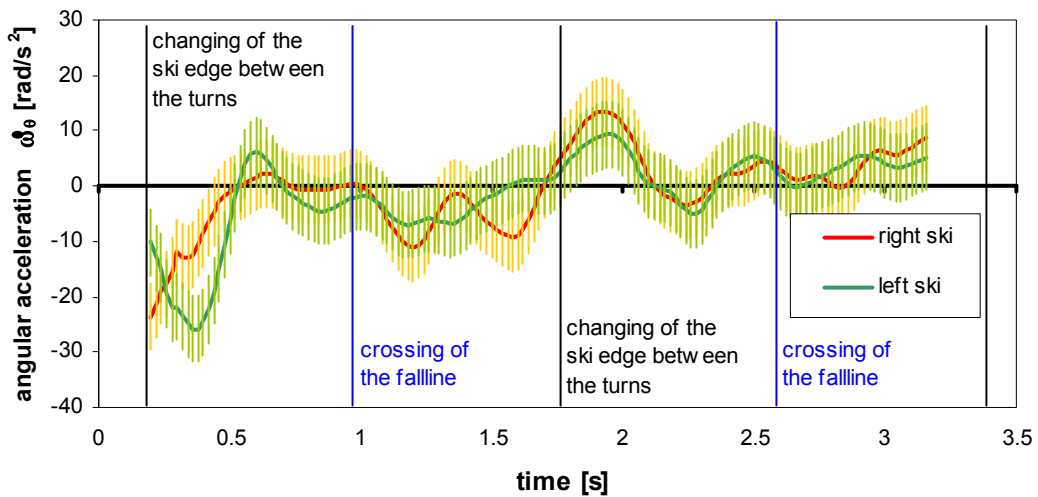


Figure 26. The angular acceleration of the edging motion of the skis.

At the end of the steering phase the skier slowly decreases the edging angles of his skis. The angular accelerations during this turn phase stay in the range between -10 and +10 rad/s².

2.3 Forces and Moments Acting on the Ski-Binding System

The main forces acting on the ski-binding system are the force transferred from the athlete onto the binding $F_{athlete}(t)$, the force of the ski-snow interaction $F_{SSI}(t)$, the gravitational force G , and the inertia force $F_{inertia}(t)$, which is generated by the acceleration of the ski-binding system (see section 1.5 of the introduction). The ski's motion in the external frame of reference, for which the coordinates XYZ were introduced, is determined by Newton's law (equation 5). Using a quasi-static approach (see section 1.5.3) this equation may be reduced to a balance of the external forces and the inertia forces experienced by the ski in the accelerated and rotating system of xyz (equation 23). The moments of force acting on ski and binding cause a rotation (equation 12), which is also reduced to a balance of moments (equation 25) in the quasi-static approach. In this section the components of the these two quasi-static equations will be discussed in detail.

2.3.1 Gravitational and Inertia Force

The gravitational force G acting on the ski-binding system were not directly measured in this thesis. In the external coordinate system the gravitational force G can be calculated from the mass $m = 2.8$ kg of the ski-binding system, the inclination $\alpha = 11.8^\circ$ of the slope, and the constant gravitational acceleration $g = 9.81$ m/s² by

$$\mathbf{G} = m\mathbf{g} = m \begin{bmatrix} g \sin \alpha \\ 0 \\ -g \cos \alpha \end{bmatrix} \quad (40)$$

In the simulation the gravitational force acts on any volume dV with density ρ of the ski-binding system:

$$\mathbf{G}(t) = \int \rho \mathbf{g} dV \quad (41)$$

The inertia force $F_{inertia}(t)$ acting on the ski-binding system were calculated in equation 11:

$$\mathbf{F}_{inertia}(t) = - \int_V \rho (\mathbf{a}_o - \omega^2 r_{xy} \mathbf{e}_r + \dot{\omega} r_{xy} \mathbf{e}_\beta + 2\omega \mathbf{e}_z \times \mathbf{v}_r) dV \quad (42)$$

The results of the kinematic analysis presented in the last section of this chapter allow to determine the five acceleration components:

- The vector components of the acceleration \mathbf{a}_o of the reference points for the skis' position are displayed in Figure 18, Figure 19, and Figure 20. During the turns the absolute value of the reference points' accelerations range between 20-25 m/s². In between the turns the y-component, which acts as a centripetal acceleration decreases to zero and the absolute value decreases to less than 10 m/s².
- The second contribution to the acceleration in equation 42, $\omega^2 r_{xy} \mathbf{e}_r$, is a centrifugal acceleration due to the ski's rotation around the z-axis. The centrifugal acceleration experienced by point P on the ski depends on its distance r_z to the z-axis. Thus the centrifugal acceleration affects predominately the ski sections near the shovel, where r_z assumes a maximum value of about 1 m, and near the ski end, where r_z increases up to

0.8 m. The angular velocity determined for the rotation about the x-axis is displayed in Figure 22. During the turns the absolute value of ω_β is in the range of 1.5 rad/s (with some outliers at the beginning of the first turn). The maximum centrifugal acceleration acting on the ski's shovel evaluated for the ski shovel is thus 2.3 m/s², which was omitted for the purpose of the simulation.

- The third contribution, $\dot{\omega}_{r_{xy}}e_\beta$, arises from an angular acceleration $\dot{\omega}_\beta$ of the rotation around the z-axis. Its absolute value of the acceleration experienced by point P depends again on its distance r_z to the z-axis. An evaluation of Figure 23 shows that the maximum value of this contribution is in the order of 5 m/s² and acts mainly in a short period of time in between the analysed two turns. For the simulation of the ski's deformations in the turn this term was also omitted.
- The last term on the right side of equation 42 depends on a relative motion v_r of the ski within the xyz-coordinate system. In this system the ski has only one degree of freedom, namely the rotation about the x-axis necessary to edge the ski. The velocity v_r can be calculated by equation 20, which have been introduced in section 1.5.3. The vector product of $e_x \times r$ has maximum values of about 0.05 m on the ski's side faces. Comparing this value with the angular velocity of the ski's edging motion displayed in Figure 25, shows that the last contribution in equation 42 is negligible even compared to the previously discusses acceleration terms.

These approximations show that the inertia acceleration of the ski-binding system is dominated by the acceleration a_0 determined for the ski's reference point in the external frame of reference. All contributions arising from the ski's rotary motions are small enough to be neglected for the purpose of this study.

It is assumed that the ski-binding system does not vibrate during the two turns. Vibrations of the system would lead to additional acceleration terms $a_0(t) = a_0(\bar{x}, \bar{y}, \bar{z}, t)$ depending on the position of point P on the ski-binding system. Therefore, it was important to make sure that during the analysed turns no significant vibrations of the ski-binding system occurred. Equation 42, which calculates the inertia force $F_{inertia}(t)$ acting on the ski, can then be reduced to the integral

$$\mathbf{F}_{inertia}(t) = \int_V -\rho \mathbf{a}_0(t) dV, \quad (43)$$

where ρ is the density in volume dV of the ski. Figure 18, Figure 19, and Figure 20 display the measured components of the acceleration a_0 as a function of time.

Both of the two forces $F_{inertia}(t)$ and G acting on a volume dV of the ski-binding system generate a moment of force with respect to the origin of the xyz-coordinate system (as discussed in section 1.5.2):

$$\mathbf{M}_{GSki}(t) = \int_V -\rho \cdot \mathbf{r} \times \mathbf{g}(t) dV \quad (44)$$

$$\mathbf{M}_{inertia}(t) = \int_V -\rho \cdot \mathbf{r} \times \mathbf{a}_0(t) dV \quad (45)$$

2.3.2 Forces and Moments Transferred from the Skier onto the Binding

2.3.2.1 Evaluation of Measurement Systems

The forces $F_{athlete}(t)$ and moments $M_{athlete}(t)$ acting on the binding have to be directly measured. For the direct measurement two commercially available measurement methods, pressure insoles and sensor plates, were evaluated. Pressure insoles are placed within the ski boot and determine a one dimensional force transferred on the ski [64][65]. Sensor plates [66][67][68][69][70] are mounted between the ski and the binding and thus alter the tested system, however, they are the only measurement method, which allows an accurate determination of the moments acting between ski and binding [56][64].

2.3.2.2 Employed Force Sensor Plates

The data presented in this thesis was obtained from measurements with force sensor plates manufactured by Kistler Instrumente AG [79]. Each of the plates consists of two riser plates, which are placed between the ski and the binding. This method of mounting has two disadvantages:

- Accelerations of the own weight of the binding contribute to the forces measured by the force plates.
- The plates are comparably high, which alters the ski-binding system and thus the force distribution within the system.

Both of these disadvantages have to be taken into account when using the obtained forces and moments as input for the simulation. On the other hand, the force sensor plates are the only measurement device, which allow a precise measurement of forces as well as moments in the ski-binding system.

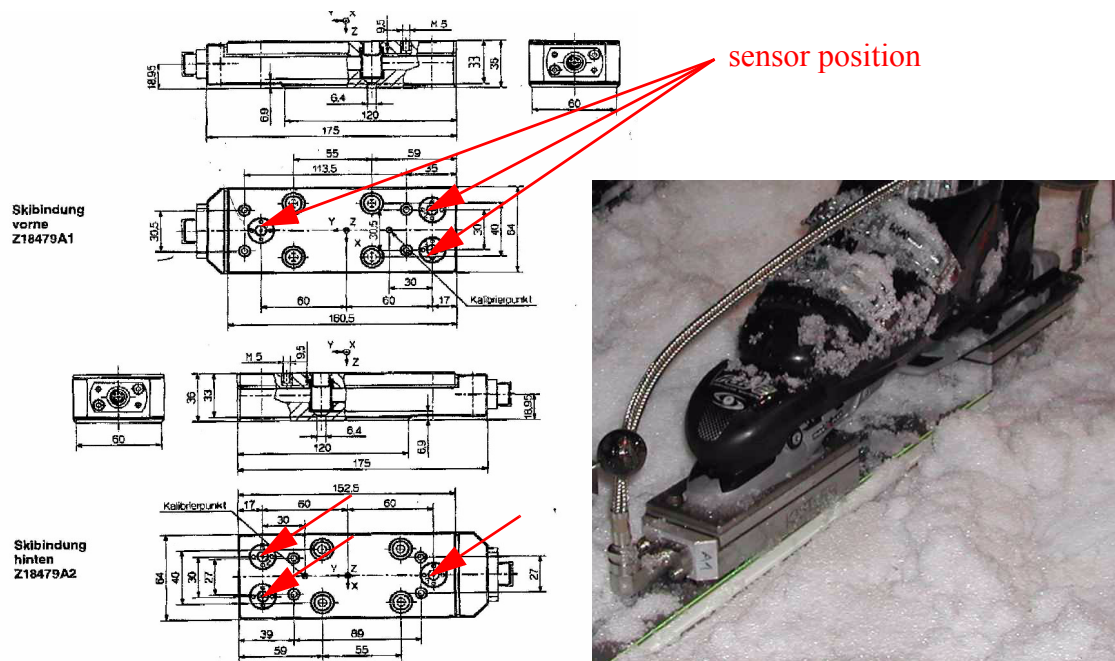


Figure 27. Constructional drawing [79] of the ski dynamometer by Kistler™, which was designed to measure the forces and moments transferred from the binding to the ski. The photo on the right was taken during the measurement campaign in Neuss (D) in November 2002.

Each of the four riser plates, which are assembled below each front and backside part of the binding, consists of three 3-component-dynamometers (see Figure 27). Thus, the force components as well as resulting moments on each binding segment can be determined. The measurement ranges of the force sensors are +/- 1.0 kN, +/- 1.5 kN, and -1.5 / +4 kN for the force components along the ski axis (\bar{x} -component), perpendicular to the ski axis (\bar{y} -component), and perpendicular to the ski surface (\bar{z} -component), respectively. Linearity and hysteresis in each component are better than 1 %. The crosstalk of components is lower than 2%. The measurements were recorded with a frequency of 200 Hz. Figure 27 on the right shows the mounted force plates as they were used during the measurement campaign in Neuss in November 2002.

2.3.2.3 Forces Transferred from the Skier onto the Ski-Binding System

The forces, which are transferred from the skier onto the skis in a turn are generated by two main sources [1][8]: on the one hand the gravitational force acting on the skier is transferred vertically down onto the skis. On the other hand the skier experiences centrifugal forces when he performs a turn. The centrifugal force acts in a plane parallel to the snow surface (see Figure 28).

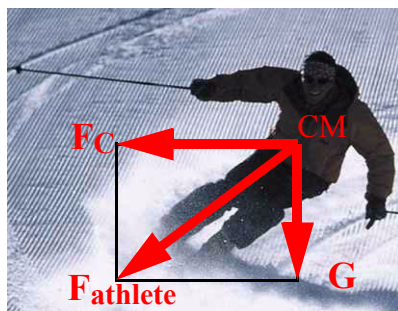


Figure 28. Main sources of the forces transferred from the skier on the skis.

The forces acting between ski and binding, which are recorded with the *Kistler*TM sensor plates, can be identified with the forces transferred from the athlete onto the ski-binding system, if the mass of the binding is neglected. On each ski the force measured on the six individual force sensors of the *Kistler*TM plate were added up. The following three graphs (Figure 29, Figure 30, Figure 31) show the three components of this totalised force. The forces acting on the left and the right ski are displayed separately. They have been transformed into the external XYZ-coordinate system, in which the results of the kinematic analysis have been presented. The transformation into the external coordinate system depends on the edging angle θ of each ski and the orientation angle β of the skis in the external coordinate system (refer to section 1.5.1, equation 2 and equation 3). Each of the graphics will be discussed briefly.

The X-components of the forces measured between skier and skis, which are displayed in Figure 29, are dominated by the centrifugal forces on the skier during a turn. The centrifugal force acts perpendicular to the ski axis, i.e. perpendicular to the x-coordinate axis. The transformation of the measured forces into the external XYZ-coordinate system maps the centrifugal force partly on the X-coordinate. This transformation depends on the orientation angle β . As the skier crosses the fall line β changes from negative to positive values (left turn) or vice versa (right turn), as shown in Figure 21. Therefore, the X-component of the observed force also changes its algebraic sign. In between the two turns, when the skier shifts his weight

from one side to the other, the orientation angle β assumes a maximum value. But during that phase of the turn the centrifugal force changes its direction, and the X-component of the force changes back to negative values.

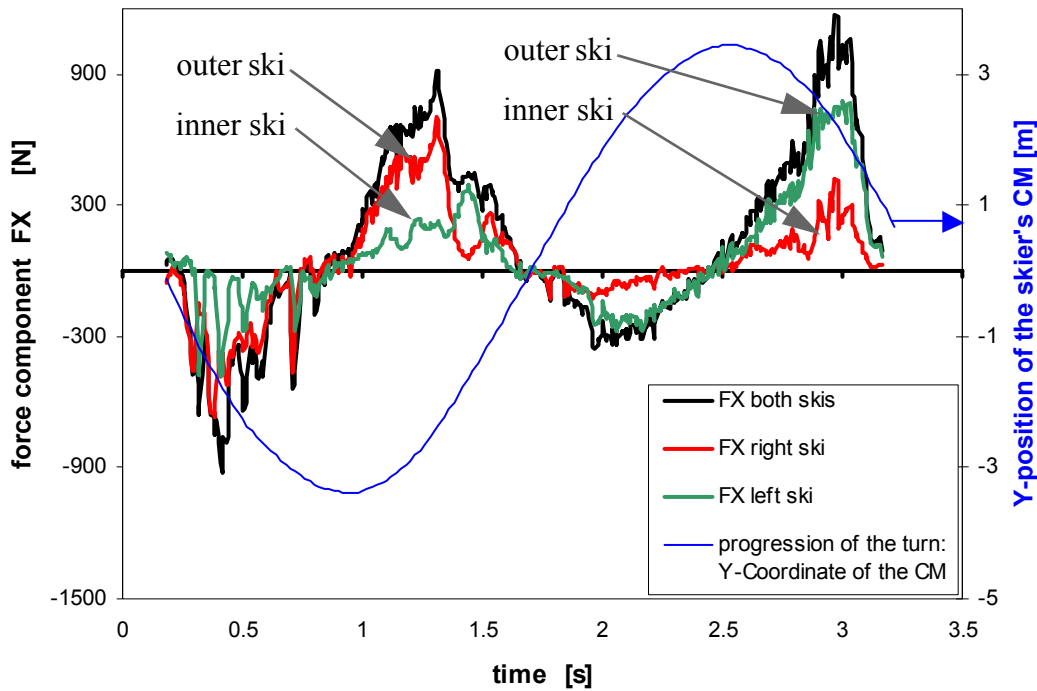


Figure 29. X-component of the force acting on the ski plate. The propagation of the turn is indicated in the graph (blue line).

Figure 30 shows the Y-components of the forces measured on the binding plate. The main contribution to the forces in Y-direction is also the centrifugal force on the skier. It is clearly visible that the highest load acts on the outer ski of each turn. During the turn the load on the skis continuously increases to about 1400 N on the outer ski. The maximum load is reached after the fall line has been passed. In this part of the turn the centrifugal force and the downhill-slope force component of the gravitational force act together [1][8].

The negative Z-component of the forces acting on the ski, displayed in Figure 31, corresponds to the forces which are perpendicularly transferred onto the snow surface. The skier's mass M is 88 kg. Therefore, the Z-component of the summarized force transferred from the skier onto the two skis oscillates around $Mg \cos \alpha = 845$ N. These oscillations are caused by motions of the skier, for example, in the phase between the two turns he rises his body, thus exerting an additional force onto the ground (visible in the graph between 1.2 to 1.5 s). This motion generates a short period of unloading of the skis (between 1.6 and 1.8 s), in which the skier shifts his weight and changes on the other ski edges. Smaller oscillations are visible, for example, in the total force between 2.0 and 2.5 s. These oscillations are characteristics of the skier or rather of the way he specifically carried out a turn. The oscillation mentioned here can be explained by a typical arm movement, which is very pronounced in the right turns of this test person.

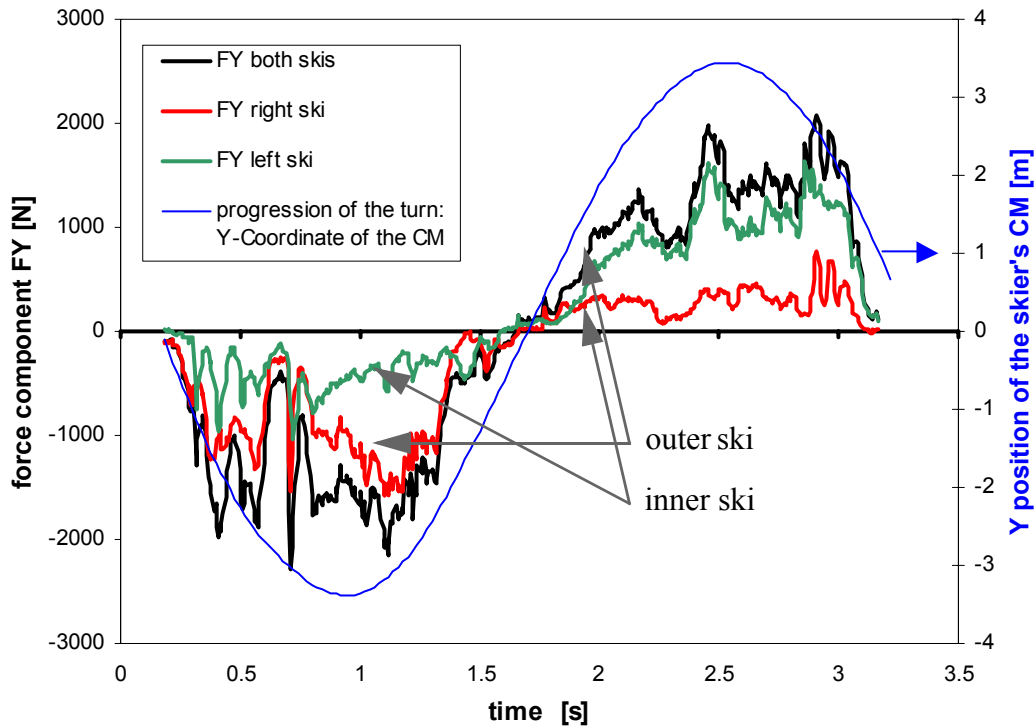


Figure 30. Y-component of the force acting on the ski plate. The propagation of the turn is indicated in the graph (blue line).

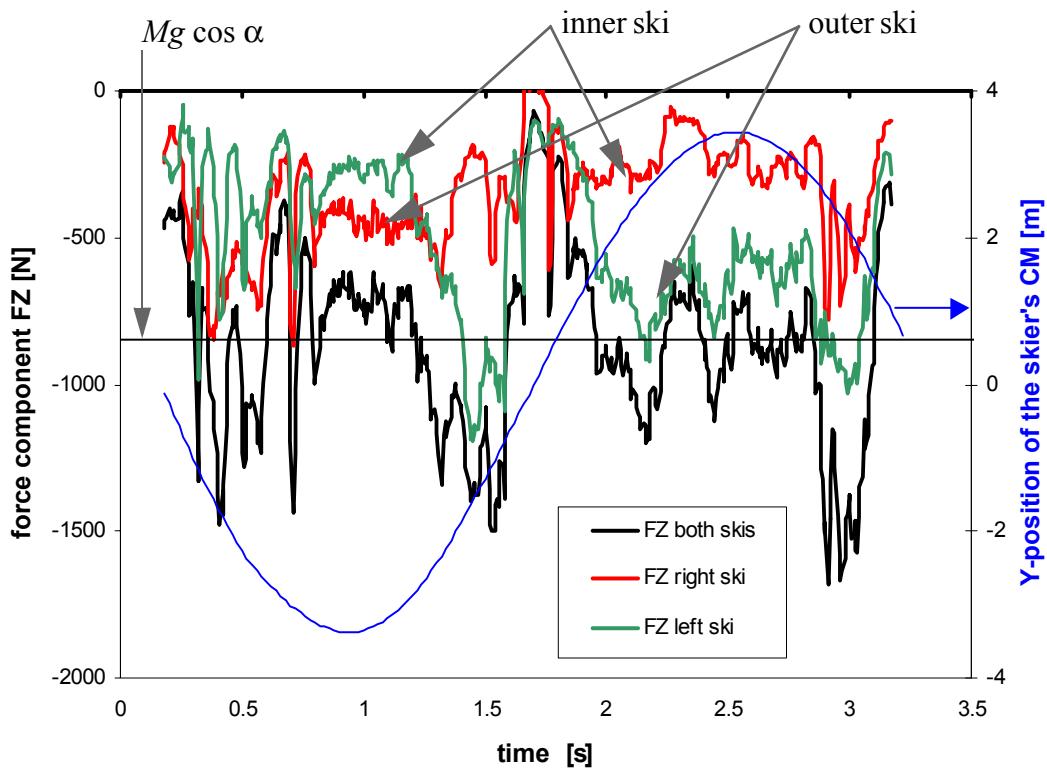


Figure 31. Z-component of the force acting on the ski plate. The propagation of the turn (motion of the skier's CM in the Y-component) is indicated in the graph (blue line).

The force distribution between left and right ski is expected to be as asymmetric as the force distribution in the X-component, however, in the first of the two turns the load is almost evenly divided on the left and the right ski most of the time. At the end of the turn the load even shifts to the inner ski. This is an unusual force distribution and indicates that the skier had to adjust small imbalances, which possibly resulted from the repeated snow impacts visible at the beginning of the first turn. In the video record a little bumpiness of the snow surface at the beginning of the first turn is visible, but no indication of an imbalance during the first turn is visible when observing the skier. The force distribution of the second turn exhibits the expected characteristics. The outer ski is loaded about twice as much as the inner ski and the increase of load on both skis as the skier stands up at the end of the turn is clearly visible in the data curves.

2.3.2.4 Moments of Force Acting between Binding and Ski

The arrangement of force sensors in the *Kistler*TM plates (see Figure 27) allows to calculate the moments acting on each ski. All components of the moment $\overline{M}_{athlete}$ acting on the ski binding system were determined in the \overline{xyz} -coordinate system by

$$\overline{M}_{athlete} = \sum_{i=1}^6 \overline{r}_i \times \overline{F}_i \quad (46)$$

where the index i denotes the sensor number, \overline{r}_i denotes the distance of sensor i to the origin of \overline{xyz} , and \overline{F}_i denotes the force measured by sensor i . For the simulation this moment had to be transferred into the simulation coordinate system xyz . However, the data will be displayed and discussed in the \overline{xyz} -coordinate system, because the interpretation of the moment represented in other coordinate systems is much more difficult: bumps on the snow surface and the impulses they transfer on the ski have a strong impact on the moment displayed. Such impacts can be observed for the outer ski in both turns, but especially in the beginning of the second turn. They cause strong amplitudes and strongly affect the characteristics of the moment of force in the \overline{y} -coordinate (see Figure 32). If the moment is transformed into another coordinate system the signals of these bumps strongly alter all other components.

Figure 32 shows the moment of force on the ski with respect to the \overline{y} -axis. The actual values of the moment observed in this component exceed the values observed in the other components by almost one order of magnitude. This moment is generated by the position of the skier's CM with respect to the origin of the \overline{xyz} -coordinate system. Fluctuations in the characteristics of this component of the moment of force can be caused by bumpiness of the snow surface or by vibrations of the ski. The characteristics of the moment of the right ski during the first turn is typical for the general behaviour of this component: During the initiation of the turn the skier shifts his weight towards the front of the skis, which facilitates the rotation into the new turn. In this situation the moment is positive. As the turn proceeds the skier shifts his weight backwards. In the steering phase, in which his main load is on the rear part of the ski, the observed moment is negative. The oscillation in this component of moment of about +/- 200 Nm corresponds to an approximate shift of +/- 23 cm of the skier's CM around the neutral position. The backward leaning of the skier in the steering phase is clearly visible in the video sequences. The characteristics of the moment acting on the outer ski are mirrored by a much smaller counter moment on the inner ski.

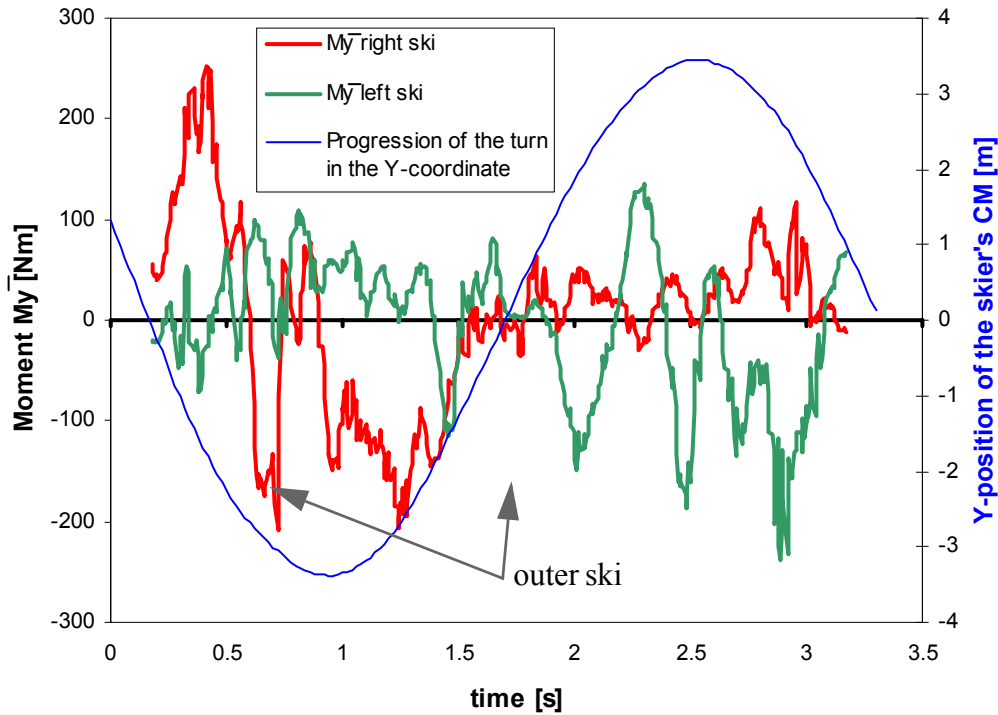


Figure 32. Moment on the skis around the \bar{y} -axis.

The moment along the ski axis, $M_{\bar{x}}$, is necessary to keep the ski on it's edge during the turn (see Figure 33 on the left side). The outer ski is more loaded and thus experiences higher moments. The maximum values of this moment of about 20 Nm are lower than expected, which indicates that a considerable fraction of pressure is exerted to the running surface of the ski.

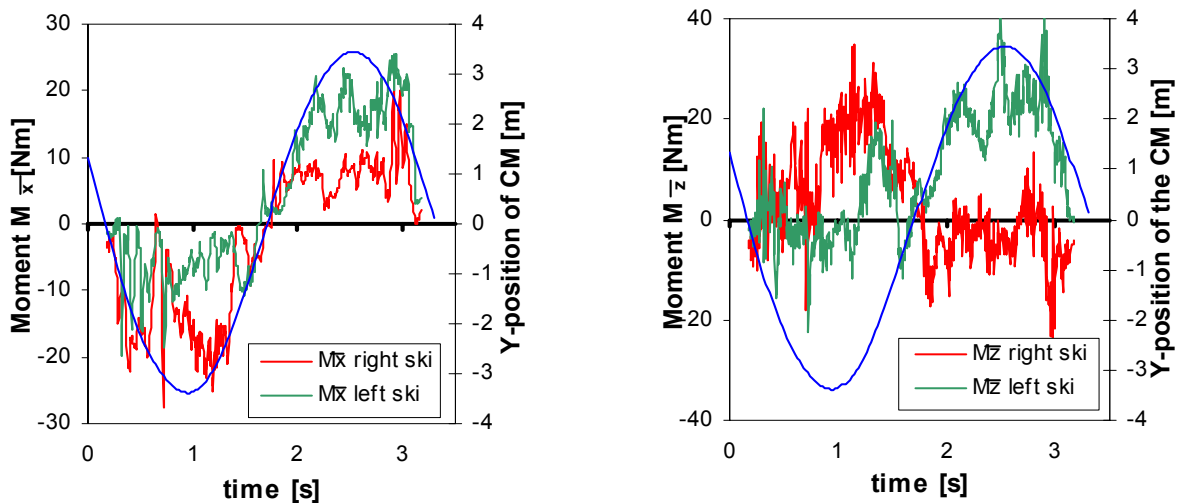


Figure 33. Moment on the skis around the \bar{x} -axis (left) and the \bar{z} -axis (right).

The component $M_{\bar{z}}$ of the moment of force shown in Figure 33 on the right side is again much lower than $M_{\bar{y}}$. The data of these two turns, but also for the other turns of this test run show an unexpected bias towards positive values. The reliability of this data is therefore questionable. The most probable explanation for this bias is a cross talk of force components within the

sensor plate. The manufacturer specified the crosstalk of force components by $< 2\%$, which would be sufficient to cause the bias observed in M_z . The other two components of the moment are insignificantly affected by cross talk effects.

The components M_x and M_z of the moment $M_{athlete}$ are so small, that they can be neglected in the simulation of the ski if the edging angle is defined as a fixed input parameter.

2.3.3 The Ski-Snow Interaction Force

The ski-snow interaction force $F_{SSI}(t)$ depends on the pressure at the ski-snow interface, which will be investigated in detail in the next chapter. The simulation of the ski-binding system in the turn determines ski-snow interaction force $F_{SSI}(t)$ and its corresponding moment $M_{SSI}(t)$ as the counterpoise of the other forces acting on the system. By far the largest contribution to the forces acting on the ski-binding system is the force transferred from the skier onto the binding. Figure 34 displays the three vector components of this force in the xyz -coordinate system as measured by the *KistlerTM* force plates. The largest component of these forces are the F_z components, which act perpendicular to the skis' surfaces. The other vector components, F_x and F_y , are insignificant in relation to F_z .

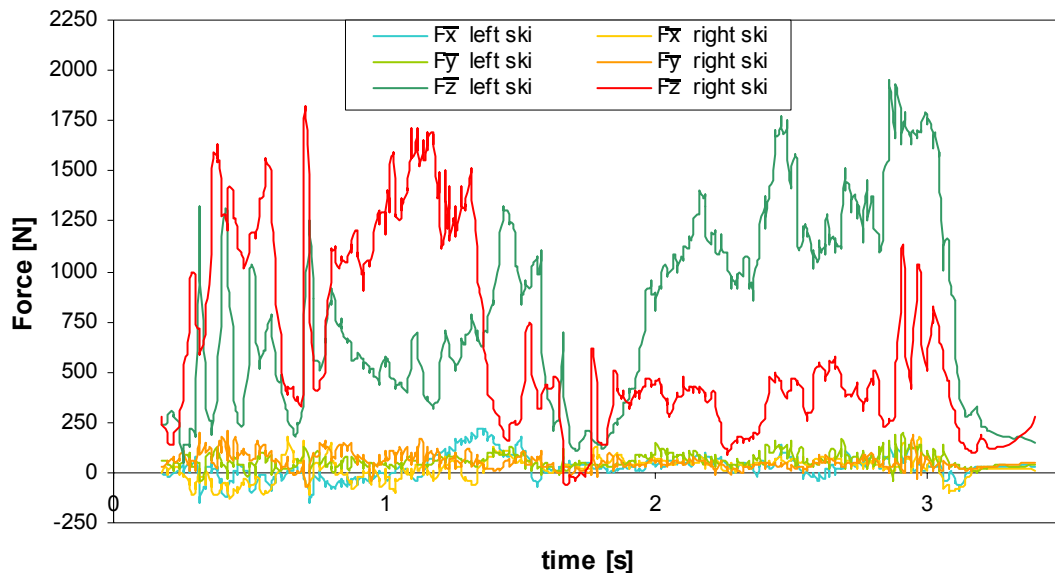


Figure 34. The three components of the forces acting on the binding.

From the proportions of these vector components it was concluded that the major fraction of the ski-snow interaction force acts on the running surface of the ski (see Figure 35). Snow forces acting on the side face of the ski are marginal and were neglected in the simulation.

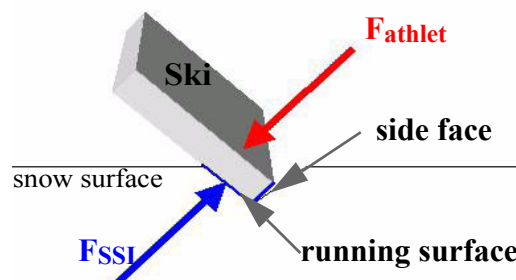


Figure 35. The two main forces acting on the Ski during a turn.

3. Determination of Snow Resistance to the Ski

When characterizing the turning behaviour of a ski-binding system it is necessary to take the snow conditions into account. The snow does not only support the skier, but it also enables the skier to generate the centripetal forces and moments needed for a turn. In fact, all of the forces and moments which enable the skier to turn, originate at the ski-snow interface. The other two major forces acting on the skier's body, air drag and gravity, are either only slowing him down or act unchangingly. Therefore, a thorough investigation of the ski-snow interaction is a prerequisite for the understanding of ski turns and the evaluation of a ski-binding system's performance.

Snow is one of the most multifaceted materials known. It consists predominantly of ice and air, but also contains liquid water and water vapour. It constantly undergoes a metamorphism process. The mechanical properties of snow change over a very large scale. In the first section of this chapter the general properties of snow are discussed shortly with a focus on its mechanical deformation characteristics. The second section of this chapter reviews existing literature relevant for modelling the interaction between a ski and the snow. In the third section suitable new testing devices for the characterization of the snow's resistance to a turning ski are introduced. Numerous measurements with these devices led to an empirical model of the ski-snow interaction, which is presented in section four.

3.1 General Mechanical Properties of Snow

Natural snow is formed in clouds, where it forms flakes of fragile snow crystals or compact grains of ice depending on temperature and humidity conditions [80]. As soon as it is deposited on the ground a metamorphism process starts, which transforms fragile ice crystals into snow grains. The snow metamorphism strongly depends on the temperature gradient within the snow, which arises from the various energy inputs to the snow cover, e.g. air temperature, geothermic heat, radiation (loss and gain of energy) and wind [81],[82]. The metamorphism of the snow cover is accompanied and affected by various physical sub-processes: the snow settles, the grains start to sinter [83] and in spring a daily melt-freeze cycle is initiated. Thus the type, size and shape of the snow grains present in a snow cover vary strongly and likewise do the inter-granular bonds which define the cohesive strength of the snow cover [84],[85].

The general mechanical properties of snow have been summarized, for example, by Bader [86], Mellor [87],[88] or Salm [89]. These publications include several models for the mechanical deformation characteristics of snow cover on a macroscopic scale. Those models proved to be valid under specific conditions, but disappoint if a broad range of conditions is regarded (e.g. a broad density range, a broad range of penetration speeds). More recent studies link their findings about the macroscopic snow characteristics to the micro scale properties of their samples (Shapiro et al. [90], Johnson & Schneebeli [91],[92]). Thus critical values, which indicate a transition to a different physical process on the micro scale within the snow sample, have been postulated and in part experimentally confirmed [114].

For the snow on ski pistes the material strength is the most important property in view of skiing sports, but also from an environmental viewpoint, since the snow cover protects the underlying alpine vegetation. Modern preparation methods aim at generating compact, robust

and durable pistes [93]. Machine-made snow is more and more employed in ski resorts, to ensure snow covered slopes over the whole winter season. Because of its high strength machine-made snow is also frequently used for alpine winter sports competitions. Advantages of machine made snow are not only the higher independence on the weather conditions, but also it's high material strength, which is caused by the enhanced sintering of the small rounded artificial grains [94].

3.2 The Interaction of Ski and Snow

In the characterization of the interaction between ski and snow two main physical processes can be distinguished:

- Friction at the ski-snow interface as the ski glides over the snow's surface.
- Deformation of the snow surface by a turning ski.

The former has been well studied and numerous publications have been produced, which will only be summarized here. The later is much more important for the turning of skis, since it provides the major part of the turning forces for the skier. The number of publications dealing with the snow deformation during skiing is rather small. The changeover to the new carving technique and the development of appropriate skis additionally limits the number of relevant publications, since the involved physical interaction processes have also changed.

3.2.1 Friction at the Ski-Snow Interface

As a ski glides over the snow surface different types of friction occur. In the latest model dry friction is supposed to dominate in the region of the ski shovel [95],[96]. The generated frictional heat [97],[98],[99] causes the uppermost snow surface, which is in contact to the ski [100], to melt and thus provide lubrication for the succeeding contact area. The gliding properties of skis are influenced by a high number of material properties and environmental parameters [101]: they include weather and snow conditions (most of all snow temperature [102], air temperature, humidity and the sun's radiation onto the snow surface [103],[104]), surface roughness of the ski [105] and the preparation of the skis running surface [95],[100].

All published studies address the situation of a flat ski gliding over the snow surface and focus on the friction between polyethylene and snow. There are no studies specifically concerned with friction between edged skis and the snow, which would be much better suited for any turning motion. The contact area between ski and snow for edged skis is in most cases much smaller than that of flat skis. Thus the contact pressure is much higher. Therefore, for cold snow one would have to assume a lower effective friction coefficient (due to an enhanced generation of a lubrication layer), for warm weather and warm snow a higher effective friction coefficient (due to an increased capillary suction effect) [106]. Friction at the steel ski edge is often neglected when considering friction of a flat ski, however, for inclined skis the friction coefficient of steel on snow becomes more important. The friction coefficient of steel on ice is comparable to the friction coefficient of polyethylen on ice, but for snow temperatures between -10° and 0° it is slightly lower [107].

3.2.2 Deformation of the Snow Surface by a Turning Ski

As mentioned above, the development of carving as a new technique of skiing has changed the physical processes involved in the ski-snow interaction. In the conventional skiing technique the turning forces are mainly generated by skidding over the snow's surface. The shape and bending properties of carving skis, however, are adjusted to typical turn radii. Thus skidding becomes obsolete. The ski still penetrates the snow's surface due to the mechanical load of the skier, but to generate the turning forces of ideally carved turns no additional skidding is necessary (see Figure 36).

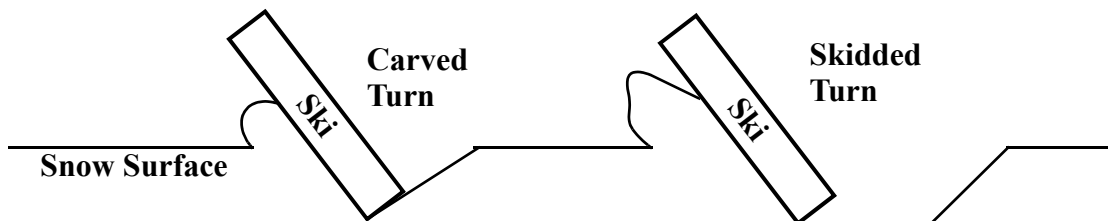


Figure 36. Different types of ski-snow interaction in carved and skidded turns.

The review of relevant literature about the snow deformation processes in the ski-snow interaction was divided into the sub-chapters „skidding“ and „carving“. The former concentrates on machining of snow, the later specifically reviews publications about the penetration resistance of snow.

3.2.2.1 Skidding

Skidding is a form of a cutting process - in many ways similar to the machining of metals or wood. Lieu was the first who viewed the skidding process as a form of machining. He conducted cutting tests on pure ice [37],[39] which he and Mote [38] and later Renshaw and Mote [41] used to develop a model for the turning snow ski. Brown & Outwater [108] were the first who conducted machining experiments on snow. They tried to find a critical edging angle at which skidding occurs. Hirano & Tada also published several studies in which they present simulations of turning skis. In their first publication in 1994 they developed a water jet analogy for the ski-snow interaction [42]. In 1999 they conducted measurements on amorphous ice samples [43] with a density of 902 kg/m^3 and only recently, in 2002, on snow samples of density 383 kg/m^3 [44]. However, their results neither quantitatively nor qualitatively agree with the findings of Lieu, Renshaw and Mote [39],[41].

Cutting processes on metals have been the subject of numerous studies, however, there are several distinct differences in the physical processes of metal cutting compared to the machining of the snow surface in skiing. Skidding of skis over the snow surface occurs at negative rake angles [39] (using the terminology of metal cutting), which is rather uncommon in the machining of metals [109]. All physical theories developed for metal cutting to describe the deformation processes within the machined material are based on the assumption of incompressibility for the machined material. Considering the machining of snow this assumption seems to be questionable.

3.2.2.2 Carving

The carving technique, in contrary to the traditional skiing technique, is characterised by minimized skidding during a turn. The ski merely cuts into the snow surface to a depth which allows the snow to support the load of the ski. There is only one study, published by Mössner et al. [111], which describes testing the snow resistance to a penetrating ski appropriately to the loading conditions during carving. It shows that the mean resistance pressure is a linear function of the penetration depth, depending on the edging angle of the ski.

The mean resistance pressure of snow on a penetrating plate or piston, however, has been studied in a number of laboratory experiments. The most comprehensive study was published 1979 by Fukue [112]. He concluded that during the deformation different processes occur depending on the penetration speed. At 0.097 mm/s ductile compression of the snow under the penetrating plate was observed. For a penetration speed of 0.98 mm/s the snow is deformed in brittle compression, in which a bulb of compressed snow forms under the plate. Other publications confirm that the penetration speed is a key parameter when investigating the ski-snow interaction because of the different deformation mechanisms during the process [113],[114]. By a simple estimation one can show that the expected penetration speeds of the ski-snow interaction in a carved turn range typically between 0.1 and 0.9 m/s depending on the penetration depth and the skier's speed. According to Fukue's results brittle fracture processes are expected to dominate the snow deformation during ski-snow interaction.

Several authors also measured stress-strain curves and their dependence on the density of the snow sample at several strain rates [115],[116]. However, in skiing as in most other technical applications it is not possible to determine the actual internal stresses, strains or the strain rate of the snow deformation, since it is not known what happens within the snow, or to which depth the snow is being deformed [117]. The snow's mean resistance pressure to the penetrating object, the penetration depth and the penetration speed are more suitable parameters to be considered when investigating the ski-snow interaction.

3.2.3 Summary and Conclusions of the Literature Review

The ski-snow interaction processes include friction, penetration of the ski into the snow and skidding. The most relevant figures which characterize these processes are:

- The effective sliding friction coefficient between polyethylen (surface material of the bottom side of the ski) and snow is between 0.03 and 0.3 [101]. It depends on snow and weather conditions, on the surface properties of the ski, as well as on the normal force applied. The friction coefficient of steel on snow (sliding) is between 0.02 and 0.15 [107]. Friction between an inclined ski and the snow has so far not been investigated.
- The skidding process is a form of a machining process with analogies to the thoroughly studied machining of metals. However, most models of the machining of metals rely on the assumption of an incompressible machining material, which is not applicable to describe the deformation of snow. In experiments of machining ice and snow the resultant cutting forces were found to act normal on the face of cutting tool (ski) [37]. The cutting forces were found to be independent of cutting speeds in the range between 0.01 and 1.0 m/s [37].
- For the carving technique the penetration process into the snow is considered more important than the machining process of snow at a constant penetration depth, which is better suited of describing skidded turns. There is only one study which tests the snow's penetration characteristics on actual skiing slopes [111]. It shows that the penetration

resistance pressure is a linear function of the penetration depth. The penetration resistance to an inclined ski increases with an increasing edging angle. The dependence of the resistance pressure on the penetration speed was not considered in this study.

- The compression of snow is governed by different physical deformation processes (e.g. ductile compression, brittle compression, which leads to pore collapse, deformation of snow grains, etc.) [112],[114], which strongly dependent on the strain rate and thus the penetration speed. In the interaction of skis with snow brittle processes are expected to dominate [112].
- The stress and strain during the deformation depend on the sample density and probably on other snow characteristics. Stress and strain are only measurable if well defined deformation lengths and sample sizes are known. In field measurements, however, it not possible to determine to which depth the snow is affected by the impact on its surface. Therefore, the mean resistance pressure to a penetrating device and the penetration depth into the snow are determined instead. This mean resistance pressure is in a good approximation linear dependent on the penetration depth [112].

For the simulation of a turning ski the ski-snow interaction can be implemented as a boundary condition on the ski's surface if the mean resistance pressure at the ski-snow interface is known. The resistance pressure depends on the one hand on interaction parameters (penetration depth, edging angle and speed of the snow deformation) and on the other hand on the characteristics of the snow type. There is not sufficient data or a convincing comprehensive model for the mean resistance pressure available from published literature. It is therefore necessary to quantify the snow resistance and its dependence on interaction parameters and snow properties. Then an empirical equation for the ski snow interaction can be formulated and implemented in the numerical model. From the literature review it follows that the experimental study of the resistive strength of snow should take into account the following important points:

- The penetration speed is a key parameter, which determines what kind of physical processes occur during the penetration of snow. Therefore, tests at several typical penetration speeds are necessary to quantify this effect.
- Most of the published results rely on data obtained in laboratory measurements. Snow of actual skiing slopes varies strongly and is less homogeneous. To ensure that results are valid for the simulation of actual skis on skiing slopes, field measurements are necessary.
- It was confirmed by the first comparable tests [111] that the mean resistance pressure of snow strongly depends on the edging angle of the ski. The edging angle in a carved turn varies between 0° and almost 70° (see chapter 2). A suitable test device should therefore also cover this range.
- The load on the penetrating test device and the load rate should correspond approximately to the load and the load rates occurring during skiing.

3.3 Measurement Devices for the Snow Characterization

In order to characterize the ski-snow interaction two new test devices were built. The first device, called „Agenvis“, deforms the snow at a constant rate. The second device, called „Fast Snowdeformer“, was designed to measure impact of the penetration speed on the mean resistance pressure to a penetrating piston. Additionally, several other devices were used to

characterize the snow and to analyse ski traces in the snow or indented snow samples. These devices were already presented and described in detail in other publications and will only be mentioned shortly with an appropriate reference.

3.3.1 Agenvis

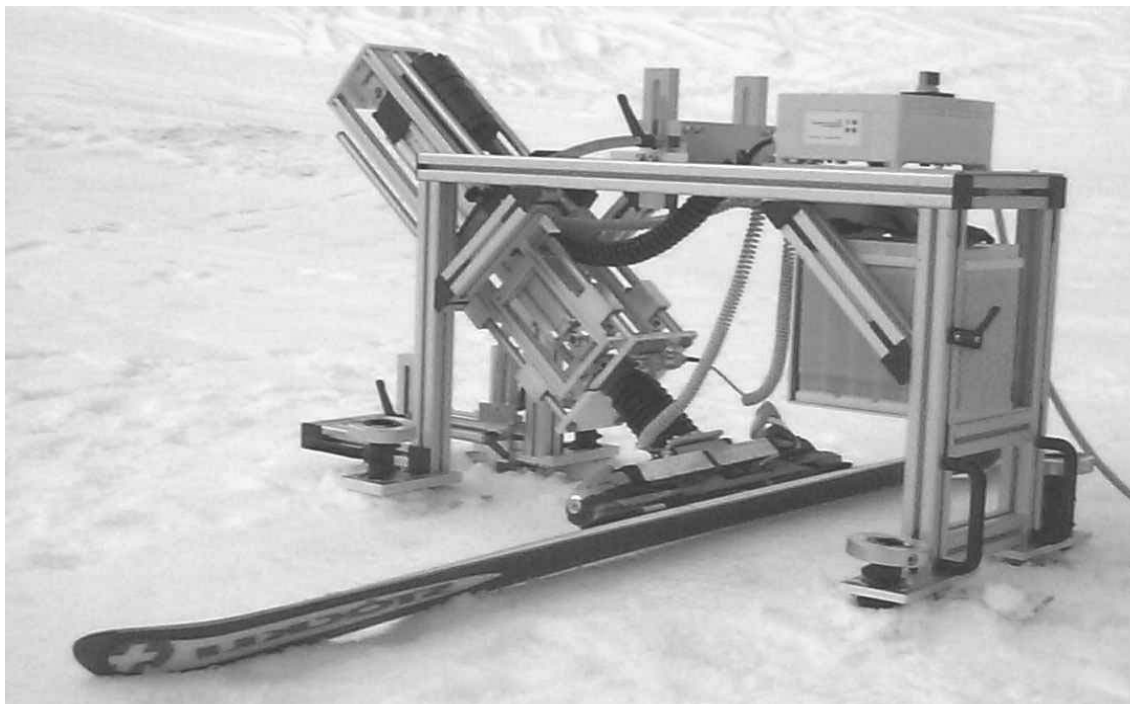


Figure 37. The test device „Agenvis“ equipped with a ski

The measurement device Agenvis (Figure 37) was built within the framework of a diploma thesis [118] at the polytechnic college „Interstaatliche Hochschule für Technik Buchs“ [119]. Agenvis was built for the use with actual skis and was also utilized to verify the ski simulation for the static case (see section 5.2). For the characterization of the mean resistance pressure the device was equipped with a rigid metal plate and modified by supplementing an optical displacement sensor.

3.3.1.1 Device Specifications

A schematic representation of the employed device configuration is displayed in Figure 38. The device consists of a robust aluminium frame, which supports an electric motor powered by a standard car battery. The motor drives a mounting, which supports either the ski or a rigid metal plate. The measurements described in this chapter were all conducted using the metal plate since it allows to determine more precisely the contact area with the snow. The metal plate can indent the snow at edging angles between 15° and 70° . Within the mounting of the plate an axial force sensor is integrated. The penetration speed is nearly constant at 30 mm/s. The penetration distance d into the snow is measured by an optical incremental encoder module with a resolution of 0.2 mm. Data acquisition is computer controlled. During the penetration the resistance force and the covered distance were sampled with a frequency of 50 Hz. The maximum force exerted by the electric motor is restricted to 3000 N. In order to exert such forces to the snow surface, it is necessary to fix the device to the snow with four tip-pole

screws. The attachment of the measurement set-up on the metal frame can be laterally displaced by 15 cm, thus several measurements can be conducted on comparably hard snow surfaces before the measurement device had to be unscrewed and relocated. On soft snow relocation of the device was necessary after each measurement. This time consuming procedure limited the number of measurements which could be conducted during one measurement campaign, but each measurement was repeated at least once to confirm the reproducibility of the result.

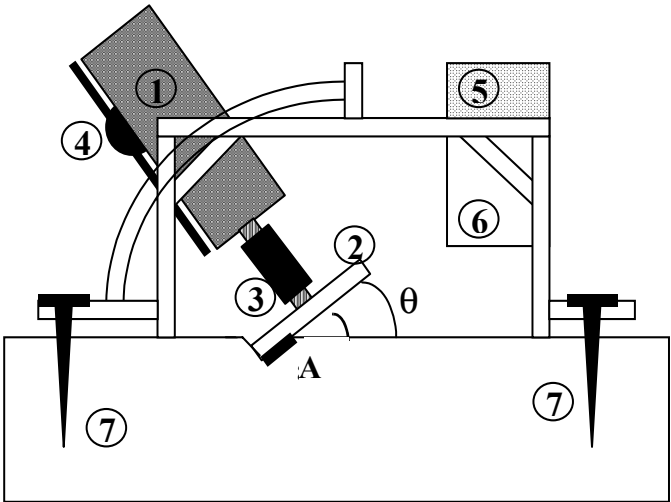


Figure 38. Schematic of the field-portable test device Agenvis for the snow resistance: (1) electric motor; (2) metal plate, (3) force sensor, (4) optical encoder and linear stripe, (5) box with electronic, (6) battery, (7) screws to fix the device on the ski piste. The edging angle θ and the contact area A between plate and snow are variable process parameters.

3.3.1.2 Collected Data and Data Analysis

From the measured penetration distance d and the inclination angle θ the effective penetration depth D was calculated by $D = d \cos\theta$ (see Figure 39). The mean snow pressure on the plate p_{Snow} was calculated by dividing the measured resistance force F by the contact area A between plate and snow: $p_{Snow} = F/A$. Usually not the whole plate's surface is in contact with the snow. Thus, the contact area A between snow and plate has to be calculated from the width b of the plate and the contact length $l = d / \tan\theta$: $A = b d / \tan(\theta)$.

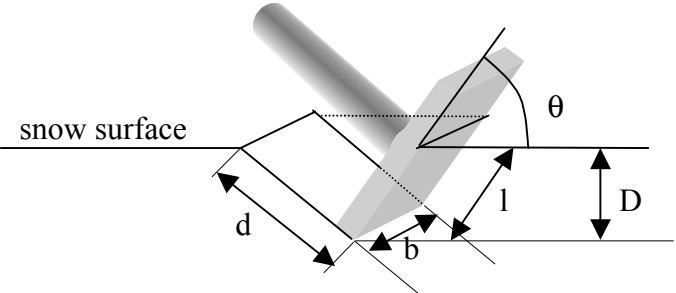


Figure 39. Schematic of the plate penetrating the snow. D denotes the penetration depth of the trace in the snow, d the penetration distance, l the contact length, b the width of the plate and θ the edging angle.

Snow which is removed from the indent during the penetration process piles up under the plate as indicated in Figure 38. The actual contact length therefore increases, however, this snow is usually considerably softer and in fast processes - like in downhill skiing - a significant fraction of the removed snow also sprays away. Therefore, the pile up was neither considered in the calculation of the contact length l , the contact area A , and the successive calculation of the mean snow resistance pressure p_{Snow} in the experiments, nor it was considered in the definition of the boundary condition describing the ski-snow interaction in the simulation (see chapter 5).

Figure 40 on the displays the results of six measurements on the same snow for edging angles of 30° and 55° . In the graph on the left the resistance force F is displayed versus the penetration distance d . Figure 40 on the right displays a graph of the mean snow resistance pressure p_{Snow} versus the penetration depth D for the same six measurements. The measured snow resistance forces scatter more for large edging angles than for small edging angles. The high variations in the force curves during penetration are a first indicator that fracture processes govern the deformation of snow. Due to the division in the calculation of the mean resistance pressure the curves of the calculated pressure approach to infinity for small penetration depths. This effect is caused by an amplification of the measurement error for small penetration distances. Therefore, the pressure-depth curves of inclined penetration test were only evaluated for penetration depths above 3 mm.

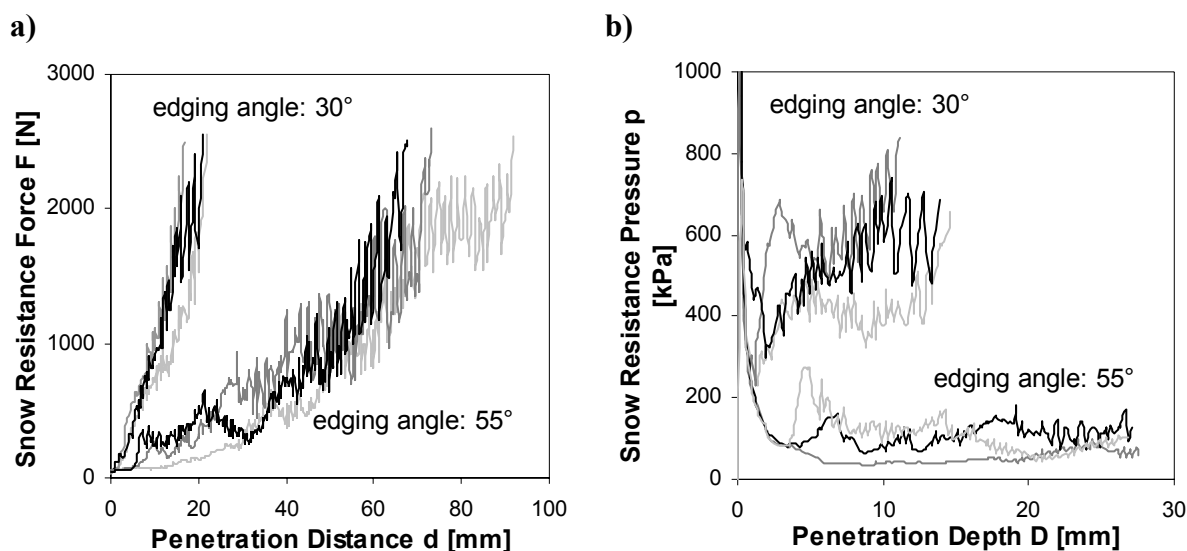


Figure 40. a) Six measurements of the resistance force F on a comparably hard snow piste the same snow during the penetration at two different edging angles. b) Mean snow resistance pressure p versus penetration depth D for the same measurements.

The measurement device Agennis was used for most field test in order to characterize the snow resistance pressure, however, this device operates at only one given penetration speed. In order to characterize the dependence of the mean snow resistance pressure on the deformation speed an additional device was needed.

3.3.2 Fast Snowdeformer

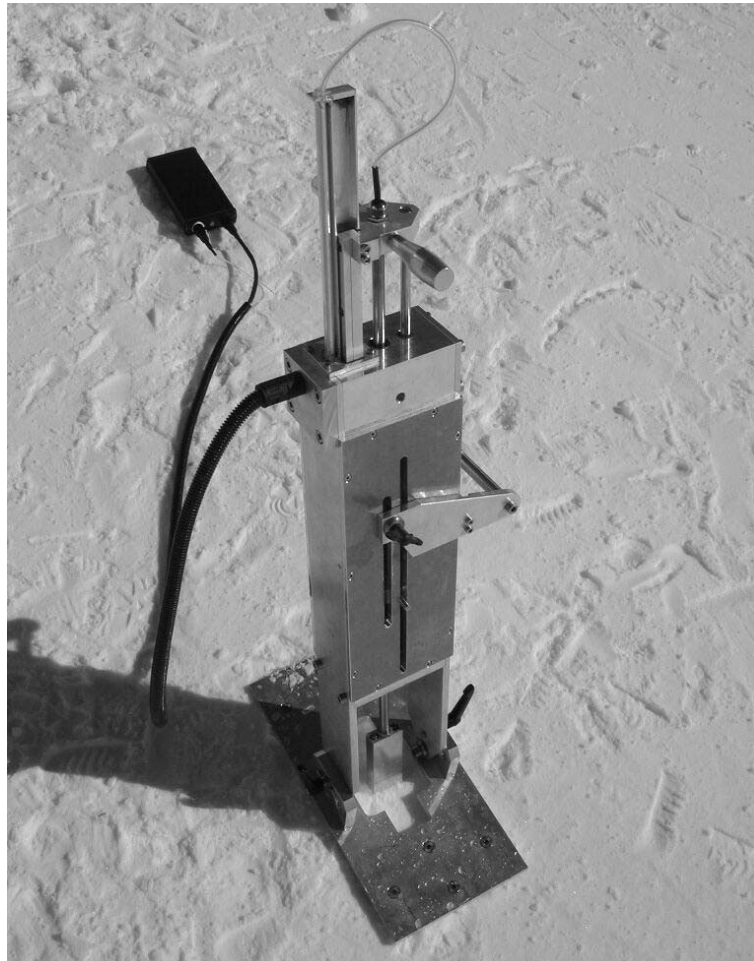


Figure 41. Measurement device „Fast Snowdeformer“.

The purpose of the Fast Snowdeformer is to investigate the snow resistance pressure on a penetrating piston as a function of different penetration speeds. It was designed as an impact test device in which a piston hits the snow surface under a given impact angle. The piston is first accelerated by a spring, but one centimetre before the impact the piston is released and impacts the snow as a free falling device. During the impact the snow decelerates the piston from the impact speed down to zero velocity. Forces on the piston and its displacement are measured and allow to calculate the contact pressure, the penetration depth and the piston's velocity.

3.3.2.1 Device Specifications

The Fast Snowdeformer consists of a quadratic metallic piston of 1 cm² area which indents the snow. The piston is mounted on a force sensor and is accelerated by a spring such that impact velocities up to 4.5 m/s are possible. The piston including force sensor and guidance has a mass of 2.0 kg. Impact angles can be adjusted between 30° and 90° relative to the snow surface. The distance covered by the piston during the impact is measured by an optical encoder with an accuracy of 0.2 mm. The data read-out of the force and displacement sensors are synchronized and recorded with a sample frequency of 20 kHz. Data collection is

controlled by a laptop using a control software written with Labview™. A graph of the measurement set-up is displayed in Figure 42.

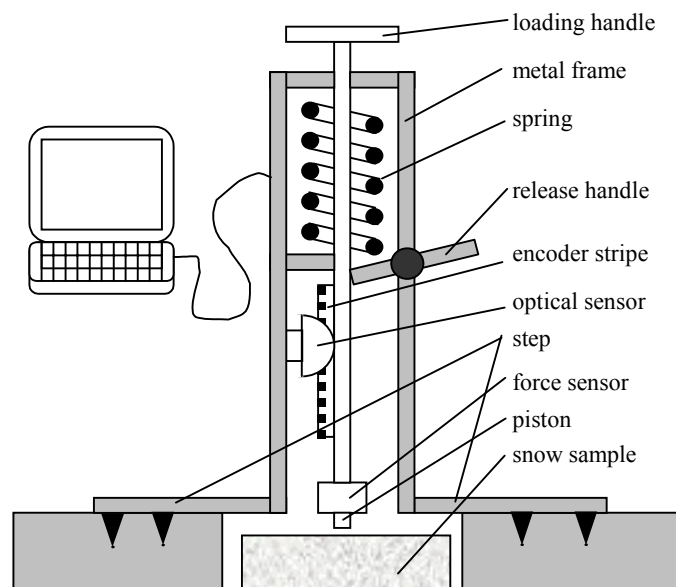


Figure 42. Schematic of the test device „Fast Snowdeformer“.

During the experiments the experimenter steps on two steps on the Fast Snowdeformer’s metal frame to secure the device on the ground. Four spikes of 3 cm length prevent the device from sliding. The measurement device is field portable, however, the measurement results in field tests vary much stronger compared to laboratory tests due to additional parameters which influence the measurement, e.g. inhomogeneities of density distribution, grain types, or layering of the snow on the studied skiing slopes.

3.3.2.2 Collected Data and Data Analysis

Figure 43 displays an example of a typical 90° impact measurement on a very dense, well sintered snow sample. In this case, a fraction of the impact energy is stored elastically in the system, which causes the piston to be repelled from the snow surface. Thus a damped oscillation is initiated. The distance measurement proves that a fraction of the elastic energy is stored within the snow, as the penetration depth in the second and the succeeding impacts are less than in the first impact in which forces are clearly higher. However, the accuracy of the test device does not allow to study the elastic effects in detail. Such an elastic behaviour is typical for dense, well sintered snow. On softer snow the oscillation is much more damped or no elastic response is visible.

For the investigations presented in this thesis only the first impacts were considered. The velocity and the deceleration of the piston during the impact were determined by differentiation of the time-distance data. The mean snow resistance pressure p_{snow} and the penetration depth D were calculated from the penetration distance d and the resistance force F analogue to the procedure explained in the discussion of the measurement device Agenvis (see Figure 39 and the discussion in section 3.3.1).

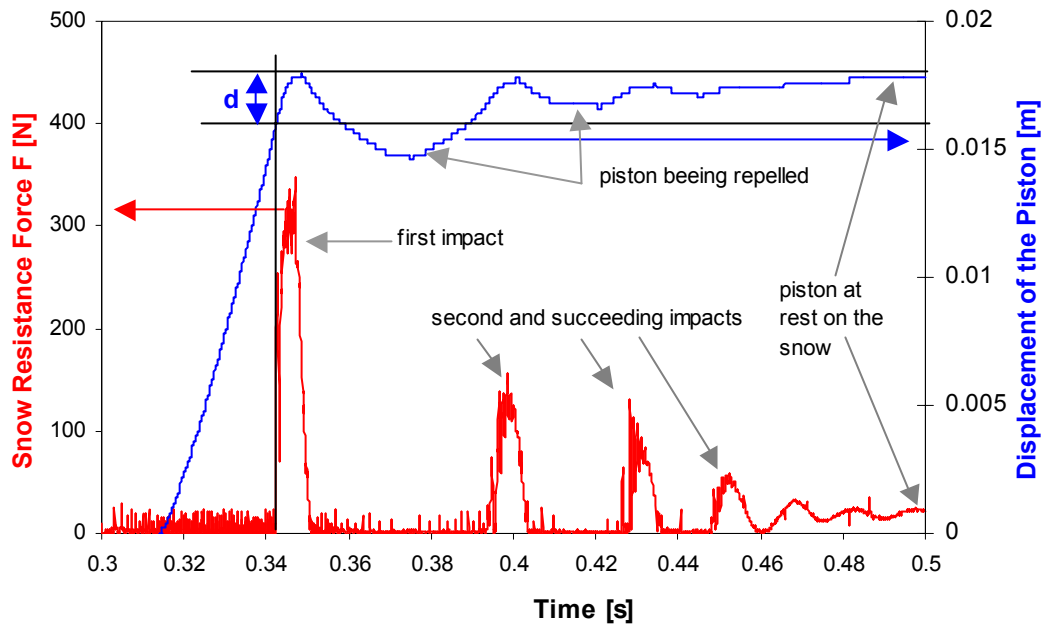


Figure 43. Force and displacement of the piston in a impact experiment normal to the snow surface.

3.3.3 Snow Sample Analysis

To qualitatively investigate the mechanical phenomena which occur during the deformation of a snow sample or in the ski snow interaction, images of cuts through the snow samples were analysed. These images were obtained using a microtomograph as a non-destructive method or by producing cut sections of a snow sample. For microtomographical recordings the „ μ CT 80“ manufactured by Scano Medical AG [120] was used. It allows to reconstruct 3D-images of the sample's snow structure. For producing sections of a snow sample, the air gaps in the snow are filled with dimethyl-phtalate, an acid which freezes at about $-4\text{ }^{\circ}\text{C}$. The samples are cut at about $-15\text{ }^{\circ}\text{C}$. Grey scale images of the cuts were taken with a camera. Detailed descriptions of this method can be found for example in Kronholm (2003) [121]. A series of such section images can also be reconstructed into a 3D image [122].

3.3.4 Measurement of General Snow Properties

The mechanical properties of snow depend strongly on its temperature and density. Temperature was measured with a standard commercial thermometer. The density of the snow was determined by weighing a well defined snow volume. Surface density was also measured with a capacitive measurement device developed by T. Achammer and A. Denoth [123]. To investigate cross-correlations, the ultimate shear strength was measured with a scissometer [124] and the penetration resistance was measured with an adapted version of the SnowMicroPenTM developed by Schneebeli and Johnson [92].

3.4 The Mean Snow Resistance Pressure on a Penetrating Plate

The measurement devices presented in the last section were used to characterise the mean resistance pressure on a plate penetrating the snow surface. First the dependence on the penetration depth was investigated. Then the influence of process parameters and correlations to other snow properties were examined.

3.4.1 Mean Snow Resistance Pressure as a Function of Penetration Depth

3.4.1.1 Mean Resistance Pressure on the Penetrating Plate

The snow's resistance pressure on the penetrating plate in the Agenvis measurements and on the Fast Snowdeformer's piston was determined in numerous measurement campaigns. Two measurement examples are shown in Figure 44:

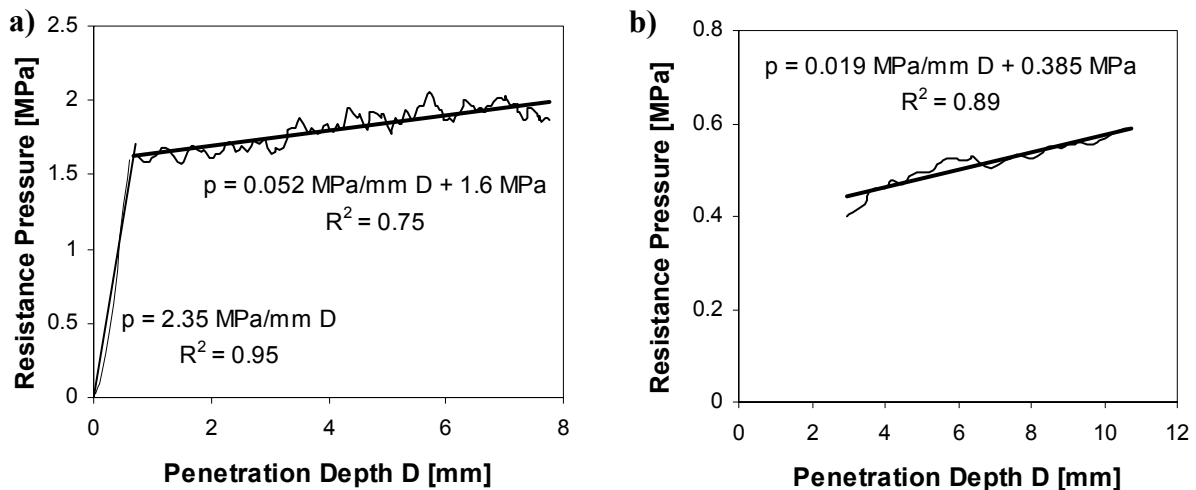


Figure 44. a) Mean resistance pressure (smoothed) of an 1.17 m/s impact on a artificially sintered snow sample of 505 kg/m^3 density measured with the Fast Snowdeformer. b) Mean resistance pressure to an inclined penetrating plate with an edging angle $\theta = 30^\circ$ on an actual skiing slope (density 440 kg/m^3) measured with Agenvis. Linear fits to the pressure data and their correlation coefficient are included in both graphs.

Figure 44a) displays the penetration resistance in a vertical (edging angle $\theta = 0^\circ$) impact experiment carried out with the Fast Snowdeformer. The linear increase in the first 0.5 mm is probably caused by an increasing contact area of snow and piston (the grain size of the snow sample was about 0.5 mm). Then brittle compression is initiated. The snow resistance during brittle compression fluctuates due to ongoing fracture events in the snow microstructure. Figure 44b) shows a penetration experiment with an inclined plate using the measurement device Agenvis. For inclined impacts the snow resistance for penetration depths below 3 mm cannot be determined, since the contact area between the plate and the snow is too small to be determined with sufficient accuracy (see Figure 39 and the discussion in section 3.3.1).

In both cases a linear approximation for the dependence of the mean resistance pressure p on the penetration depth D is an appropriate description (for vertical penetration a linear dependence has already been shown by Flukue [112]):

$$p(D) = A \cdot D + B \quad \text{for } D > 3 \text{ mm} \quad (47)$$

The coefficients A [MPa/mm] and B [MPa] of the snow resistance function are characteristics of the snow type, but depend also on the process parameters penetration speed v and edging angle θ (see next section). The correlation coefficient R^2 , of the fitted straight line is usually higher than 0.8 if the edging angle is smaller than 40° . For higher edging angle the correlation coefficient is sometimes much lower, however, a linearisation of the mean resistance pressure curves is still the most suitable choice (see section 3.4.3).

3.4.1.2 Mean Resistance Pressure on the Withdrawing Plate

When a ski passes over a snow surface the snow is first loaded and thus penetrated, but after the pressure maxima under the ski binding has passed, the snow is unloaded. If elastic energy has been stored in the snow it is then released as snow expands under the withdrawing plate. In this case the contact pressure does not drop instantly to zero, but decreases measurably. With the device Agenvis the snow pressure is also recorded as the penetrating plate is being withdrawn. Figure 45 shows such an example of an Agenvis measurement in the ski dome in Neuss, Germany.

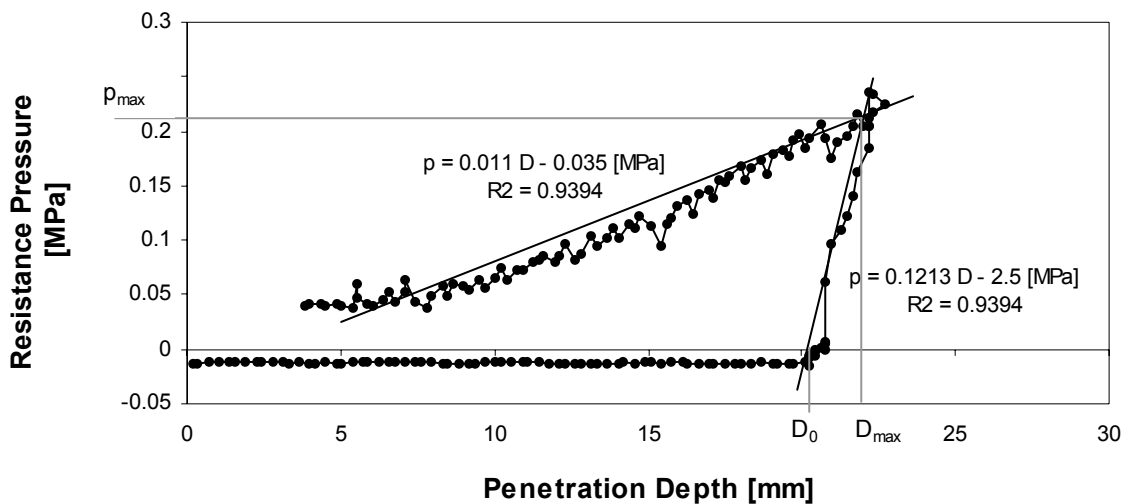


Figure 45. Measurement of the mean pressure on the penetrating plate during penetration and withdraw on machine-made snow during the measurement campaign in the ski dome in Neuss, Germany. The edging angle of the plate was 30° .

The linear equation for the measured mean snow pressure on the plate during penetration is displayed in the graph. The machine-made snow in the ski dome was very soft at the surface and its strength increased slowly with increasing depth. Therefore, the additive constant B in the equation for the general penetration resistance is negative (-0.035 MPa).

As expected for an elastic process, the pressure on the withdrawing plate decreases linearly with decreasing penetration depth. If the maximum penetration depth D_{max} and the maximum pressure p_{max} are known, the mean pressure $p(D)$ on the withdrawing plate can be described by the following equation:

$$p(D) = C \cdot (D - D_{\max}) + p_{\max} \quad \text{for } D_{\max} \geq D \geq D_0 \quad (48)$$

D_0 is the penetration depth at which all elastic stress in the snow is totally relieved and the plate loses its contact with the snow. The coefficient C [MPa/mm] in (48) depends similarly to the coefficients A and B in equation 47 on the process characteristics and the snow properties. However, C is determined only from a few measurement points and thus fracture events just before or during this short measurement period severely distort the measurement. Therefore, C could only be determined for edging angles lower than 40° and only a fraction of those measurements allowed to determine C .

3.4.2 Snow Resistance as a Function of Process Parameters

The literature review showed, that the coefficients A and B of the snow resistance function (equation 47) might depend on the penetration speed and on the edging angle. Therefore, testing series for each of these parameters were conducted.

3.4.2.1 Penetration Speed

The impact of the penetration speed on the snow's mean resistance pressure was tested with the Fast Snowdeformer. As the piston penetrates the snow it is continuously decelerated from the impact velocity to zero. If different impact velocities are chosen, then the mean resistance pressure of the snow can be characterized independently of the penetration depth. The resistance pressure depends also strongly on the snow properties. In order to minimize the influence of varying snow properties on the characterization of the mean resistance pressure as a function of penetration speed, the test series were not carried out on actual skiing slopes, but conducted in the cold laboratory at the SLF with snow samples, which were prepared from stored natural snow of winter 2002/2003. In a first step the snow was sieved using a sieve of 500 μm mesh size. Then the snow was densified at a velocity of 0.1 mm/min using a universal testing machine (Erichsen 490/20). At this speed the snow deformed mainly by creep and thus a relatively uniform density distribution within the snow samples was obtained. The densified snow samples had a diameter of 20 cm and a height of 8 cm. After densification the snow samples were stored for three days at -3°C to allow sintering of the snow grains. If further storage was necessary the samples were cooled down to a temperature of -40°C in order to slow down the sintering and metamorphism processes. All impact tests were carried out at temperatures of -10°C . Compared to natural snow on skiing slopes, the snow samples produced for these tests were much more homogeneous with respect to grain type and size, sintering, density, and temperature. Therefore, they exhibited a higher cohesive strength compared to most types of natural snow of comparable density.

Figure 46 displays the coefficients of the snow resistance function (equation 47) for six selected measurement series of vertical impacts on snow samples of different densities. These six measurement series have been selected for better clarity of the graphs. The omitted series fit well into the ones presented here. However, some outlier had to be neglected, which predominantly occurred at impact velocities smaller than 0.5 m/s. In these experiments the penetration depth into the snow was usually less than 1-2 mm (depending on the snow strength) and could thus not be reliably evaluated.

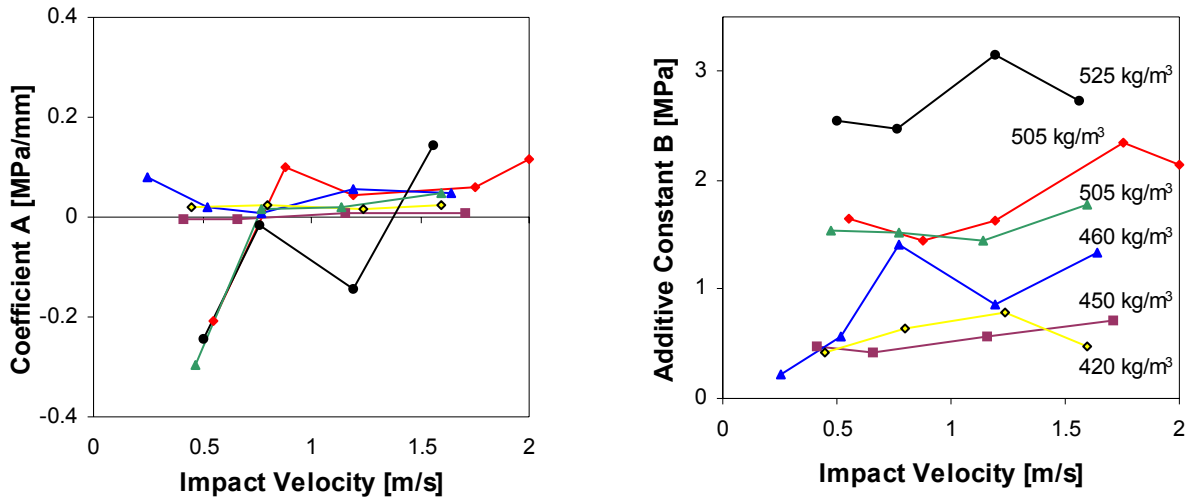


Figure 46. Slope A and additive constant B of the snow resistance function (equation 47) in dependence of impact velocity and snow density for an edging angle $\theta = 0$.

The coefficient A of the linear fit, which corresponds to the slope in equation 47, increases slightly with impact velocity. In contrary to the additive constant B , A does not depend on the snow density. The additive constant B of the linear fit, which corresponds to an initial resistance, also increases slightly with impact velocity, but in contrast to the slope A , a significant dependence on the sample's density is visible.

The indents in the snow samples were recorded with a microtomograph, such that 3D images of the indent could be obtained. Figure 47 on the left exhibits a cross section of the snow sample after a 90° impact. As the piston penetrates a bulb of densified snow forms under the piston. The formation of such a bulb is typical for brittle compression as described by Fukue [112]. The observed shape of the bulb varies between ball-shaped, cuboid-shaped or arrowhead-shaped, depending on the density distribution within the snow sample. The different bulb shapes are one of the reasons for variations in the coefficients A and B of the pressure function.

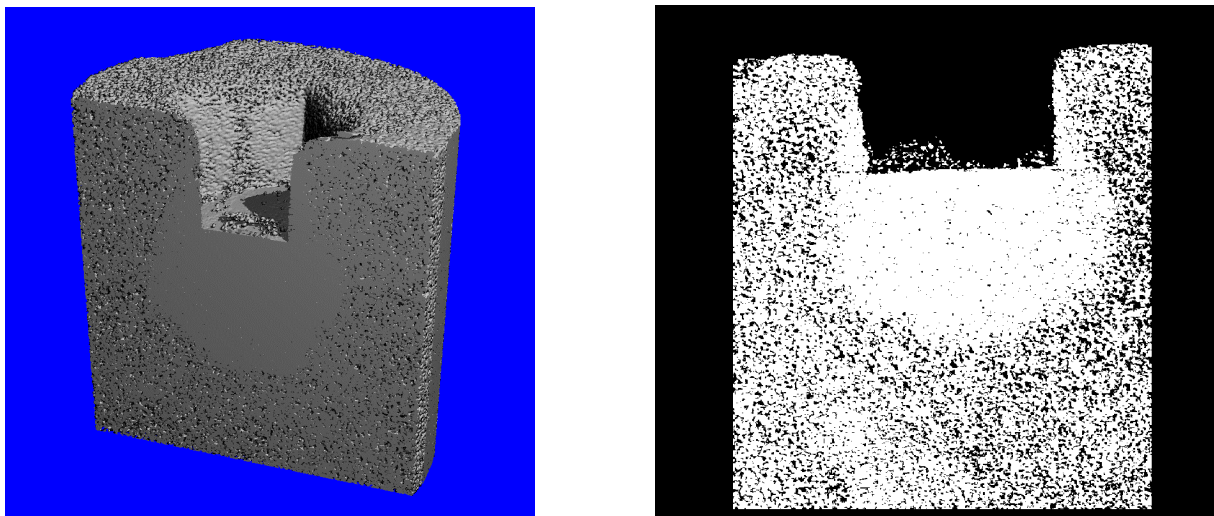


Figure 47. 3D reconstruction (left) and a cross section (right) of an imprinted snow sample of 505 kg/m^3 density reproduced from a microtomographical recording.

Determination of the density distribution within the bulb is difficult and was carried out only for one example. In this case the original snow sample of density 450 kg/m^3 was compressed to a density of 710 kg/m^3 in a depth of 0.5 mm below the piston and to a density of 690 kg/m^3 in a depth of 4.1 mm.

A distinct boundary between densified snow and undisturbed snow is visible. At this boundary the bonds between snow grains break and the fragments are pressed together. Within the bulb the compressed fragments seem to undergo a fast sintering process. Montmollin [126] investigated a fast metamorphism process with shear experiments in snow at deformation rates which did not cause brittle fracture. In compression of snow, the formation of new bonds between grains seems to be strongly enhanced and thus the sintering is very fast and does also occur after brittle fracture. In the few cases where the impact caused the whole sample to break into several pieces the compressed snow bulb always remained intact, often sticking out of one of the larger sample fragments.

The laboratory experiments summarized here show that the mean resistance pressure of snow in brittle compression is little influenced by the penetration speed within the tested range. Measurement results on actual skiing slopes vary much stronger (mainly because of inhomogeneities in the snow) but they also exhibit no distinct dependence on the impact velocity. In field tests on prepared skiing slopes the brittle compression and bulb formations are rarely observed. Particularly in inclined tests, shear fracture and a lateral (non-confined) displacement of the snow, is often a dominating effect (see next section). The impact of the penetration speed on ski-snow interaction for such processes was not characterized with these experiments. However, the experiments carried out by Lieu (1982) were dominated by shear fractures and chip formation. One of his results was also, that the snow resistance was independent of the penetration speed [37].

3.4.2.2 Edging Angle

In penetration tests with a plate which is inclined less than 40° the mean snow resistance pressure increases linearly in a good approximation (for an example see Figure 44). In penetration tests using edging angles above 40° the snow resistance initially increases rapidly, but is frequently reduced by pronounced fractures. Figure 48 displays two examples of Agennis measurements with a plate inclined with an edging angle of 60° on the same snow. The fracture events seem to occur randomly. So far no evident fracture criterion could be determined in the measurement series on skiing slopes. They seem to depend strongly on the local conditions within the snow at each measurement spot. Due to the fracture events, a linear function for the snow resistance is often not a good approximation (e.g. in the case of Figure 48b). However, the simulation of edged skis on the snow requires a formulation for the mean resistance pressure at edging angles higher than 40° in dependence of the penetration depth. The most suitable method seemed to be, also in this case, to describe the general behaviour of the snow resistance by applying a linear fit, but taking into account a higher margin of error.

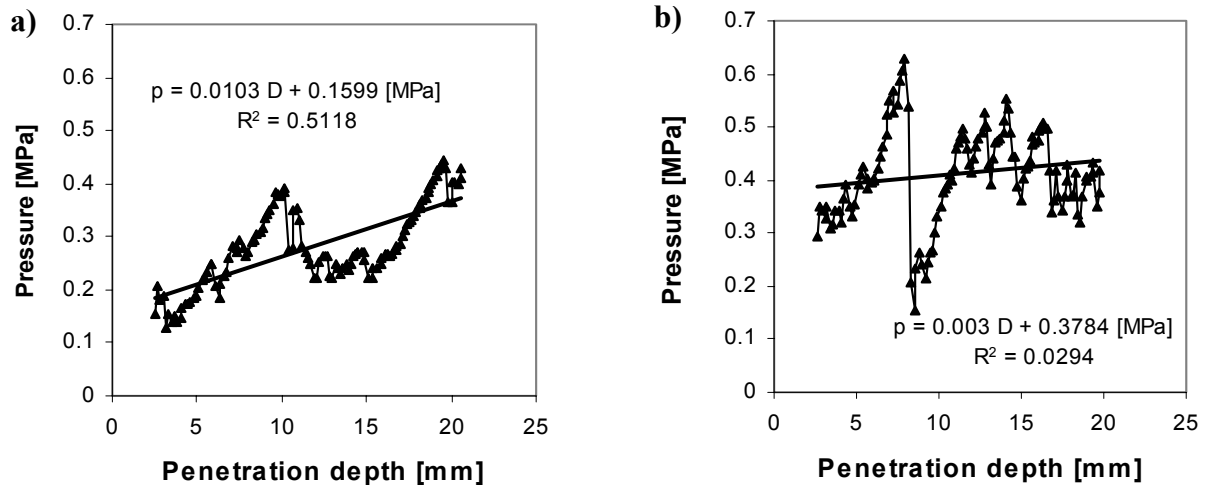


Figure 48. Mean resistance pressure vs. penetration depth for two measurement examples with an edging angle of 60° on the same snow (density 440 kg/m^3).

Figure 49 a) and b) show the slope A and the additive constant B of the snow resistance function determined in 19 measurements for 10 different edging angles on the same skiing slope measured at constant penetration speed with the measurement device Agenvis. In both graphs a transition from one type of snow deformation to another type is visible: In Figure 49 a) the inclination A remains between 0.015 and 0.35 MPa/mm for edging angles from 15° to 45° but drops to values between 0 and 0.015 MPa/mm for edging angles between 40° and 75° . The additive constant B of the resistance function first increases with the edging angle. In the experiments presented in Figure 49 b) the constant B increases from 0.08 up to 0.63 MPa. Mössner et al. [111] reported a quadratic correlation between the additive constant B and the edging angle. Figure 49 b) indicates such a relation, however, other measurement series with similar edging angles do not. As in coefficient A a transition to lower resistance pressures is visible at about 40° . For higher edging angles the coefficient B drops noticeably to values between 0.15 and 0.4 MPa.

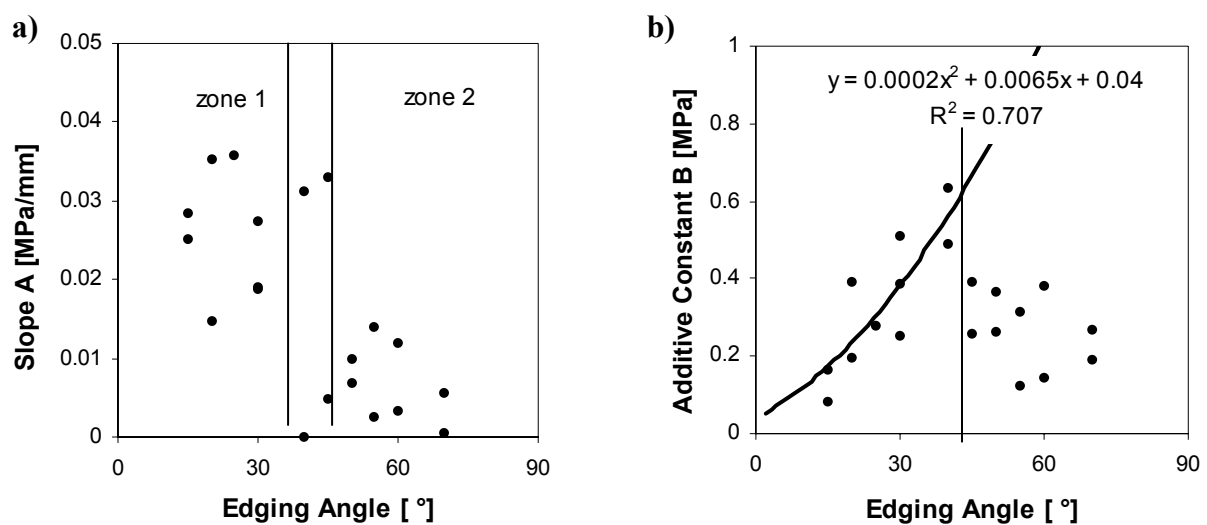


Figure 49. Slope A and additive constant B of the snow resistance function. Both graphs show a transition from one type of snow deformation (with higher resistance pressure) to another type of deformation (with lower resistance pressure).

The phenomenon of declining mean resistance pressure at high edging angles was not reported by Mössner et al. [111]. Probably due to the constructive restrictions of their measurement device, which always penetrates the snow vertically and not perpendicular to the surface of the penetrating plate.

When the indent of these experiments are examined it is obvious that the snow is not only compressed but also pressed out of the indent. A typical trace forms in the snow, which is comparable to a ski's trace (see Figure 50). During this penetration not only brittle compression, but also shear fractures of a larger scale occur in the snow. Small agglomerates of snow grains but also whole snow clods brake away.

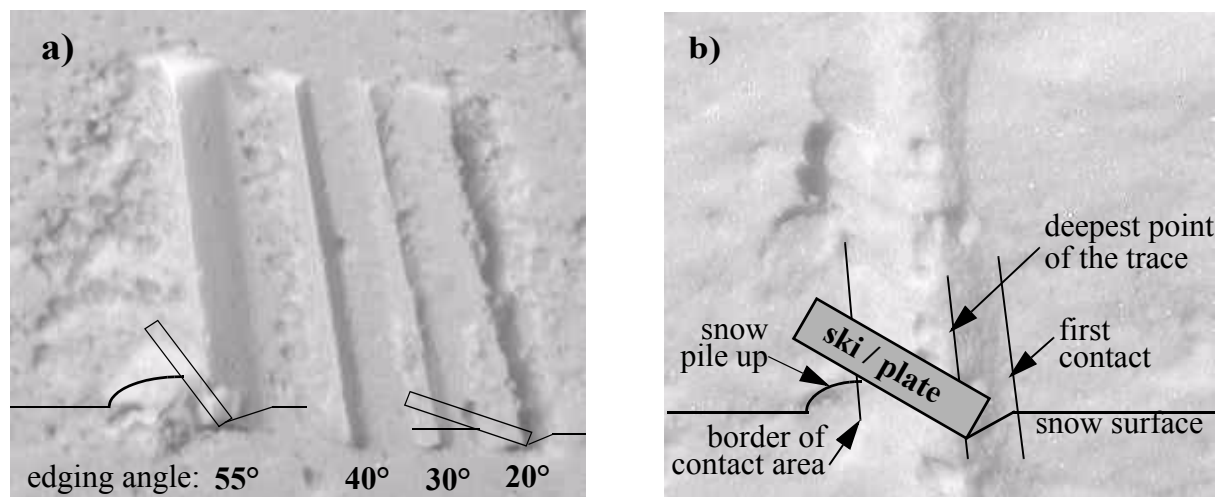


Figure 50. a) Photo of the traces after Agenvis measurements with edging angles of 55°, 40°, 30° and 20° (from the left). The orientation of the trace is indicated for the 55° and the 20° imprint. b) Trace of a skier on the same type of snow. The orientation of the ski and the main face characteristics are indicated in the picture.

Inclined measurements were also carried out with the device Fast Snowdeformer on artificially sintered snow samples (Figure 51). These samples had a much higher cohesive strength compared to natural snow of actual ski pistes.

The mean resistance pressure in these experiments exhibits a different behaviour compared to the findings with the device Agenvis: The pressure curves are not linear, but exhibit a step which can be identified as the point at which the upper piston edge enters the snow sample (Figure 51a). Microtomographical images show that the compressed bulb, which was observed in vertical impact experiments forms similarly in the inclined impacts (Figure 51b). During the deformation of this type of snow the densified bulb of snow, which forms below the piston, has to be sheared by the pistons edge [127].

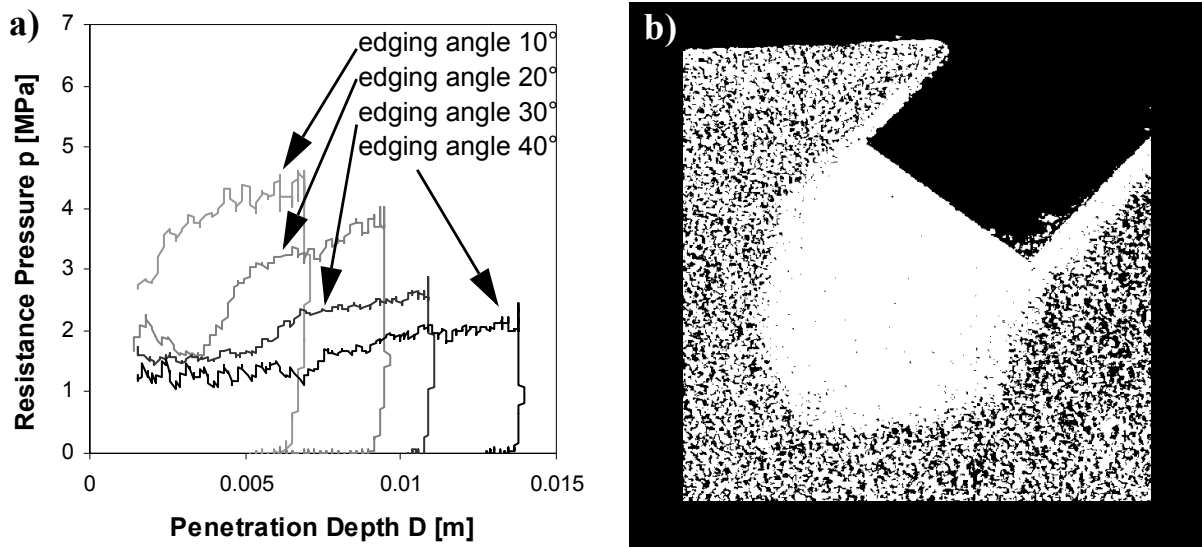


Figure 51. a) Measurement series with impact velocities of 1.55 m/s at edging angles between 10° and 40° on a well sintered snow sample of 515 kg/m³.
 b) Microtomographical image of the imprint with an edging angle of 40°.

The analysis of the previous graphs and field observations allow the following interpretation: At small edging angles compression of snow dominates the penetration process. During compression pressure builds up with increasing penetration depth. The inclination A of the linear regression line is therefore distinctively higher, compared to the results of measurements at large edging angles. During penetration with high edging angles repetitive shear fractures relieve the pressure. In the field chip formation or small clods of snow, which have been pressed out of the trace, are observable (compare with Figure 50). Therefore, the overall pressure remains constant and the inclination factor A is small. Between compaction dominated and shear fracture dominated processes a transition zone between 40 and 45° is found, in which either process may occur.

3.4.3 Mechanical Snow Resistance as a Function of Physical Snow Properties

In experiments with artificially sintered snow samples, which were carried out in the cold laboratory under controlled environmental conditions, the coefficient B of the snow resistance function showed a strong dependence on the sample's density (see Figure 46 on page 57), but coefficient A seemed to be independent. Figure 52 exhibits B as a function of the sample's density ρ . These results fit well to an exponential function.

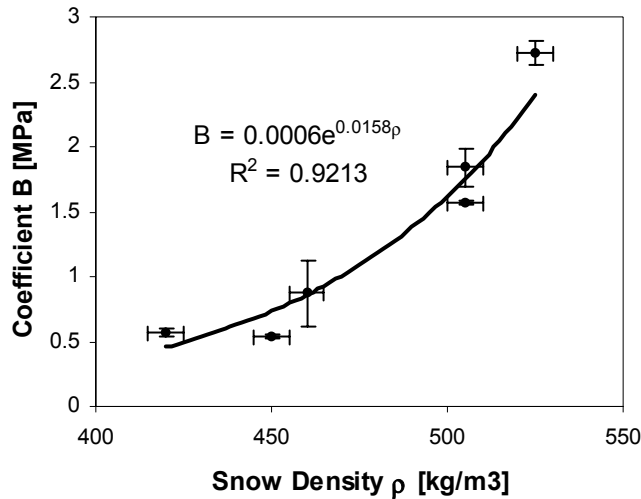


Figure 52. Coefficient B of the snow resistance function in dependence of the snow density.

On actual skiing slopes numerous tests were carried out by F. JeanRichard [125] in order to determine which snow properties have the highest influence on the snow mean resistance pressure. He focused on the snow temperature, density and ultimate shear strength. In contrary to the laboratory experiments the test on actual skiing slopes did not confirm a clear correlation between the coefficients A or B and the snow density or any of the other examined snow parameters. The snow strength obviously depends more on the conditions of the metamorphism and the snow sintering process and on specific conditions of the testing locations, e.g. impurities in the snow, density variations or presence of fractures within the snow structure. The variability of natural snow is too high to be able to determine the exact dependence of the snow resistance pressure on a single parameter. This confirms predictions of Shapiro et al. [90] who suggested that snow density is not a reliable indicator for snow properties. For statistically significant correlations, a much higher number of tests would be necessary, yet the time consuming handling of the field portable measurement devices limits the number of measurements.

During winter 2002/2003 the measurements with a modified version of the SnowMicroPen™ [92], equipped with either a conical or a cylindrical tip of a 5 mm cross section, were compared with the resistance pressure measurements. The aim was to determine if SnowMicroPen™ measurements are a suitable and fast means to classify the snow with respect to its capacity to exert mean resistance pressure. However, results exhibited a very high spatial variability. The SnowMicroPen™ was designed to test a snow cover for critical layers [121]. Therefore, it is very sensitive to the local cohesive strength between a small number of grains. On skiing slopes the snow cover is permanently mechanically processed by grooming machines and by the skier traffic. Therefore, the spatial variability of the snow strength is so high that even on very close measurement spots totally different penetration strength characteristics and corresponding penetration energies were found. In the current version the SnowMicroPen™ is not a suitable device to classify the snow with respect to the resistance on a passing ski [125].

3.5 Summary and Conclusions for the Implementation of the Ski-Snow Interaction in the Simulation

The mean resistance pressure p in the ski-snow interaction is a function of the penetration depth D and the edging angle θ . The penetration speed has a negligible influence on the snow resistance pressure. Since the penetration resistance arises from fractures in the microstructure of the snow the penetration resistance curve exhibits a very strong hysteresis between loading and unloading (see Figure 53):

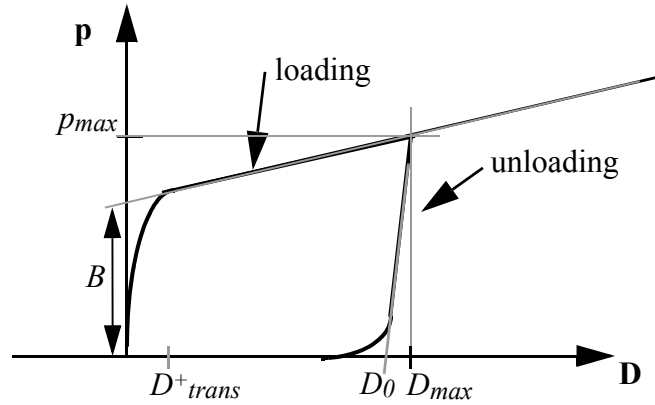


Figure 53. The penetration resistance of snow as a function of penetration depth, which exhibits a hysteresis between loading and unloading.

In relation to the whole ski-snow interaction the transition zones between $D = 0$ and D^+_{trans} during loading and for $D < D_0$ during unloading have negligible influence and can be omitted in the simulation. Thus the snow resistance function can be formulated by

$$p_{\text{load}}(D) = \begin{cases} A(\theta) \cdot D + B & D > 0 \\ 0 & D \leq 0 \end{cases} \quad (49a)$$

$$p_{\text{unload}}(D) = \begin{cases} C \cdot (D - D_{\text{max}}) + p_{\text{max}} & D_{\text{max}} \geq D > D_0 \\ 0 & D \leq D_0 \end{cases} \quad (49b)$$

The parameters D_{max} and p_{max} in the unloading function depend on the preceding loading process. In the ski-snow interaction of a moving ski they correspond to the maximum penetration depth D_{max} and the maximum contact pressure p_{max} . Figure 54 illustrates the loading and unloading zones of the snow under a moving ski. In the simulation D_{max} and p_{max} will be calculated in each time step.

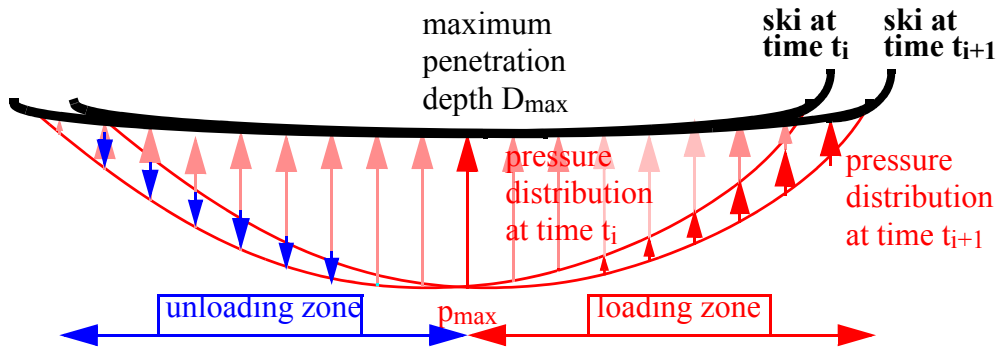


Figure 54. Schematic pressure distribution under a loaded ski during turn. The contact areas under which the snow experiences loading or unloading are indicated.

The coefficients $A(\theta)$, B , and C in equation 49a) and equation 49b) are characteristics of the snow type. They can be measured directly on the skiing slope by the testing device Agenvis. In laboratory experiments the mean resistance pressure could be empirically described by an exponential function of the snow density, however, in field experiments many other parameters influence the mean resistance pressure and thus no clear correlation to any single snow parameter could be found. $A(\theta)$, B , and C were found to be independent of the penetration speed and thus independent on the velocity of the skier, but they strongly depend on the edging angle θ of the ski. At edging angles of $\theta \sim 40^\circ$ a transition to different snow deformation processes can be observed. Thus the edging angle of 40° poses a critical angle at which the parameter $A(\theta)$ drops to distinctively smaller values.

During winter 2002-2003 fifteen measurement campaigns on prepared ski slopes in the ski resort Davos, Switzerland, and on a reference test field were carried out with the measurement device Agenvis. Approximately 250 single measurements were obtained. Mean coefficients of each parameter $A(\theta)$, B , and C were calculated for each measurement campaign. The snow conditions on each ski slope were subjectively classified as soft, average, or hard snow. For each of those snow types the mean values were determined to obtain typical parameters as input for the simulation. Table 4 lists these parameters. Note that this classification was only applied for normally prepared ski pistes. Specially prepared pistes for ski races or unprepared powder snow were not considered.

snow type	coefficient A for edging angles $\leq 40^\circ$	coefficient A for edging angles $> 40^\circ$	coefficient B [MPa]	coefficient C [MPa/mm]
	[MPa/mm]	[MPa/mm]		
soft snow	0.005	0.002	0	0.15
average snow	0.025	0.015	0.2	0.50
hard snow	0.04	0.02	0.4	1.15

Table 4. Coefficients of the snow resistance function for three typical snow conditions.

4. Implementation of a FEM-Model of a Ski-Binding System

This chapter describes the basic features of the implemented FEM models of ski and binding. First, feasible element types and their governing equations are introduced as well as the standard boundary conditions, which are provided by the employed FEM software. Then the actual ski and binding models are discussed in detail. In the last section, numerical results of the ski-binding model simulating standard mechanical tests are compared to experimental results.

4.1 FEM Software and Employed Finite Element Types

Ski and binding are modelled with the commercial FEM-software package SESESTTM distributed by the Numerical Modelling GmbH. [128]. For mechanical deformations SESESTTM solves the linearized partial differential equation

$$-\partial_i(s_{ij} - s_{ij}^{ini}) = f_j \quad (50)$$

where s is the stress tensor of linear elasticity, s^{ini} an initial stress and f the applied body force per unit of volume [129]. The internal stresses described by the stress tensor s are linked with the displacement $\mathbf{u} = (u_x, u_y, u_z)^T$ via the linearized strain tensor e and the material stiffness tensor C_{ijkl} :

$$s_{ij} = C_{ijkl}(e_{kl} - e_{kl}^{ini}) \quad (51)$$

$$e_{kl} = \frac{1}{2}(\partial_k u_l + \partial_l u_k) \quad (52)$$

Further background in the theory of elasticity may be found in [130]. The basic methods for the computation of solutions by finite element methods are described for example in [131]. For elastic deformations SESESTTM incorporates two types of finite elements: volume elements and shell elements.

Volume Elements

SESESTTM offers two types of volume elements: 8 knot and 20 knot elements. For both element types SESESTTM solves equation 50, equation 51, and equation 52 for the displacement $\mathbf{u} = (u_x, u_y, u_z)^T$.

Shell Elements

Bending deformations of shallow structures like beams, cantilevers, shells - or skis - are poorly described by common discretization methods [129]. In shell elements the mechanical deformation is described in terms of the displacement $\mathbf{u} = (u_x, u_y, u_z)^T$ and the rotation vector $\vec{\phi}$ (see Figure 55). The governing equations of the SESESTTM shell elements are based on the classical Kirchhoff plate theory [132], which requires the following conditions [129]:

- Shell particles lying on a normal with respect to the (tangential) plane of the undeformed shell remain on a straight line during the deformation, moreover,

- for thin shells transverse shear effects can be neglected, i.e. particles on a normal to the tangential plane remain normal during the deformation.
- Components of the stress tensor perpendicular to the (tangential) plane of the shell, σ_{xz} , σ_{yz} , and σ_{zz} , can be neglected⁵.

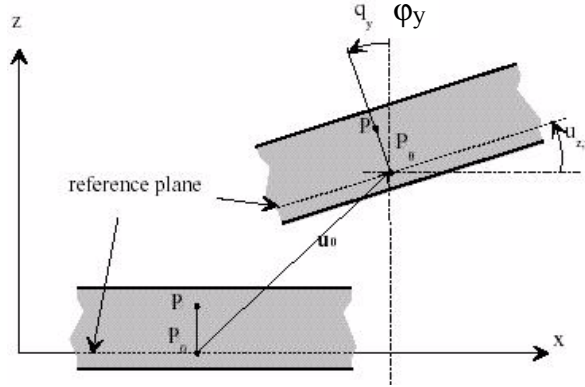


Figure 55. Degrees of freedom of the shell elements in SESESTTM[129].

The displacement \mathbf{u} of any point $P(\mathbf{x})$ can then be described as a displacement \mathbf{u}^0 of the associated point $P_0(\mathbf{x})$ on the reference plane of the shell and a rotation $\vec{\phi}$. With z the distance between P and P_0 and \mathbf{n} the vector normal on the reference plane [129]:

$$\begin{aligned} u_x(\mathbf{x}) &= u_x^0(x, y) + z\phi_y(x, y) \\ u_y(\mathbf{x}) &= u_y^0(x, y) - z\phi_x(x, y) \\ u_z(\mathbf{x}) &= u_z^0(x, y) \end{aligned} \quad (53)$$

In absence of transverse shear (Kirchhoff condition 3) the rotations ϕ_x and ϕ_y are given by [129]:

$$\begin{aligned} \phi_x(x, y) &= \frac{\partial}{\partial y} u_z \\ \phi_y(x, y) &= -\frac{\partial}{\partial x} u_z \end{aligned} \quad (54)$$

i.e. they correspond to the rotations (in radians) of the normals with respect to the undeformed shell in the y-z- and the x-z- plane, respectively [129].

The linearized strain field within the shell can be expressed with these relations and inserted into the local mechanical equilibrium equation 50 (see [129]). SESESTTM uses the so called free formulation shell elements [133] to calculate the element stiffness matrices [129], which allow very accurate simulations of bending states [134]. Bending and in-plane stretching deformations are taken into account. The geometry of the shells are specified three dimensionally in SESESTTM. If the shell consists of several layers SESESTTM calculates the

5. This assumption is discussed in [130], p. 48-49 for bending deformations of thin shells, which is a suitable assumption for the ski. For torsional deformations, however, the neglect of σ_{xz} is problematic and suggests the use of 20 knots-volumetric elements if torsion is considered an important issue.

corresponding compound bending and stretching elasticity matrix from the given 3D-elasticity tensors C_{ijkl} [129].

For a complete problem description sufficient boundary conditions and the elasticity tensors C_{ijkl} for each material have to be provided.

4.2 Boundary Conditions

The boundary conditions (BC) serve two purposes: on the one hand they restrict the rigid body degrees of freedom (dof) of the FEM model. This is a prerequisite for the simulation to find a solution. On the other hand, the external loads (forces or moments of force) are applied to the numerical model via the BCs. In this section the standard BCs provided by the software tool SESESTTM will be explained. The mathematical description of the BCs follows the definitions and descriptions presented in the user manual of SESESTTM [129], for the special case of elastic deformations.

- The „Natural Basic BC“ is a homogeneous Neumann condition, where the component of the force F_{ext} normal to the surface $\partial\Omega$ is zero for the calculated displacement \mathbf{u} :

$$(F_{ext})_1 = \int_{\partial\Omega} \mathbf{n}_k s_{1k} dA = 0, \text{ i.e. } \mathbf{n}_k s_{1k} = 0 \text{ for the displacement component } u_1 \quad (55)$$

where s denotes the stress tensor, \mathbf{n} the outward unit normal of the surface. The BC Natural Basic applies to all open surfaces of the ski-binding system. It does not have to be defined explicitly in the program code.

- The BC „Floating Basic“ applies to surface areas $\partial\Omega$ where the external force components $(F_{ext})_1$ on the BC surface are prescribed to a given value F_l :

$$(F_{ext})_1 = \int_{\partial\Omega} \mathbf{n}_k s_{1k} dA = F_l, \text{ for the displacement component } u_1. \quad (56)$$

In the current implementation of the SESESTTM-code this boundary condition exhibits the side condition that all points on the boundary surface $\partial\Omega$ are displaced by the same displacement vector \mathbf{u} . On the ski-binding system the external load acting on the binding is usually applied by a „Floating BC“.

- The BC „Dirichlet Basic“ is used to prescribe the displacement component u_1 on the boundary area to a given value C_{const} .

$$u_1 = C_{const} \quad (57)$$

This BCs are defined e.g. where the ski is supported or clamped in laboratory experiments (section 4.5).

- In SESESTTM the „generalized Neumann BC“ allows to prescribe the normal component of an external force F_{ext} as a function $f(u_1)$ of the displacement u_1 :

$$(F_{ext})_1 = \int_{\partial\Omega} \mathbf{n}_k s_{1k} dA = f(u_1), \text{ for the displacement component } u_1. \quad (58)$$

The generalized Neumann BC is necessary for the implementation of the ski-snow interaction, which will be described in more detail in section 5.1 and in section 6.1.

4.3 Implementation of the Ski

4.3.1 Composition and Shape of a Ski in the Numerical Model

All modern skis are composed of several functional layers of different materials [6],[8],[9]. The construction and geometry of modern skis has already been described in the introduction (section 1.2.1). In the implemented FEM model of a ski all material layers actually present are included (see Figure 56). These layers are defined by the side-cut of the ski and the thickness of each individual layer. All layers are separated by a glue layer. Unfortunately the thickness of the glue layers is highly variable not only from ski to ski, but it also varies within each glue layer itself [135]. Therefore, the average glue thickness was estimated from the total thickness of the ski [64] or determined by multiple microscopic measurements at several cuts of a ski [135].

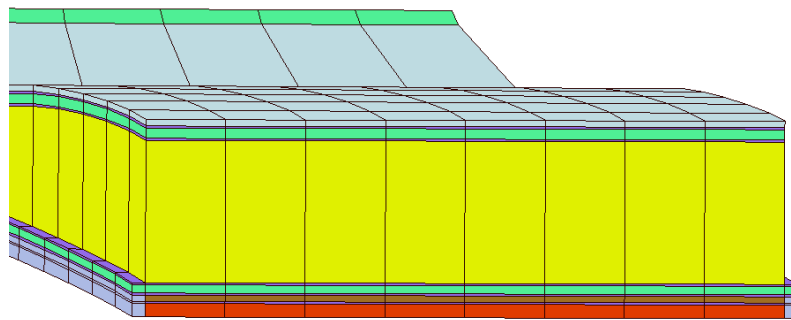


Figure 56. Cut through the FEM model of a ski. Element boundaries, the different material layers and the variable thickness of the wood core are visible.

SESES does not include a mesh generator. Thus all material layers have to be defined manually. Each material layer (including the thin glue layers) is represented as one element layer, except the wood core, which is sometimes divided into two element layers. The element discretization along the ski axis (\bar{x} -axis) is chosen such that each element had an approximate length between 50 and 80 mm. This element size allows reasonable calculation times. Parameter studies confirmed that the numerical solution is independent of the element length if the element length is smaller than 150 mm [139]. The discretization level along the y -axis depends on the interface areas of ski and binding, which are required to have the same refinement level.

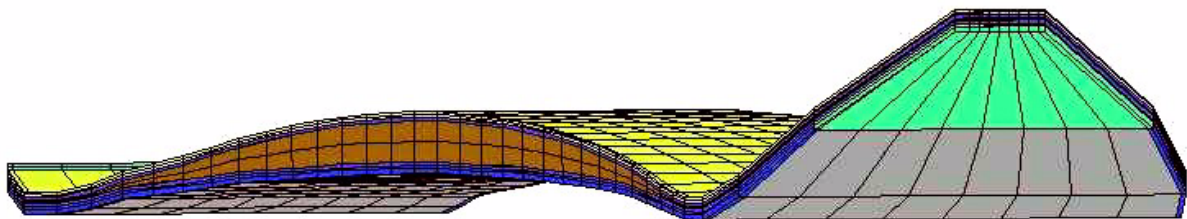


Figure 57. FEM-model of a ski without specified boundary conditions. The camber of the ski is incorporated in the model.

Another issue in the implementation of a ski model is the representation of the ski's camber (see Figure 57). The camber results on the one hand from plastic deformations of ski materials during press sizing and in the after treatment of the ski (e.g. glue layers, polyethylen layer). On the other hand the ski's shape represents an state in which the internal stresses imposed on the

material layers, which have been glued together while being elastically deformed during press sizing, are equilibrate over the ski's cross section (this refers for example to the metal layers) [64],[135]. It is not possible to determine the exact state of internal stresses within the various material layers of the ski, especially if considering that most of the skis have been attuned individually by plastic bending in the after treatment. Therefore, the FEM model of the skis described here considers the ski's camber as free of internal stresses in the initial state. It should be noted that as long as only quasi static elastic deformations are calculated there is no difference in the numerical results whether internal stresses are considered or not. However, if further studies need to investigate vibrations of a ski the internal stresses might have to be taken into account [23],[34],[35],[136]. Therefore, an optional function which could assign internal stress states to the layers was included in the code of the ski model. The shape of the ski, as well as the type of deformation during the carved turn suggests the use of shell elements in the simulation. The shell elements used are very well suited for bending deformations, while the results for torsion of the structure are less accurate (see also section 4.5). However, the Kirchhoff bending theory, which is a requisite for the application of shell elements requires three important restrictions, which have been mentioned in section 4.1. Since the ski consists of a sandwich structure of stiff and smooth materials the second and third restrictions, which require that „particles lying on a normal with respect to the (tangential) plane of the undeformed shell remain on a straight and normal line during the transformation“ i.e. that „transverse shear effects can be neglected“, might cause inaccurate results. In the case of strong bending transverse shearing of the smooth materials might be present, which would result in a relative displacement of the stiff material layers, i.e. the restrictions for the deformation of the shell would be violated. Therefore, shell elements are only applicable if such effects are negligible for the combination of the material layers within simulated the ski. To test this, strong bending of skis was calculated, firstly using 20-knot volume elements, which allow transverse shear, and secondly, using shell elements, which prevent transverse shear. This test was repeated for glue layers of different thicknesses, because they are the most likely layer to undergo transverse shear during the deformation. The numerical results of these tests showed, that provision for transverse shear does not significantly change the numerical results even for states of strong bending of the ski. Thus, shell elements are applicable for the simulation if bending is the most important deformation.

4.3.2 Assigning Material Properties to the Ski in the Numerical Model

Most materials within the ski are isotropic. In this case Young's modulus E and the Poisson ratio ν are a sufficient characterization of the elastic properties. The components of the elasticity tensor C_{ijkl} are then calculated automatically by SESESTM according to [129]:

$$C_{ijkl} = \frac{E\nu}{(1+\nu)(1-2\nu)}\delta_{ij}\delta_{kl} + \frac{E}{2(1+\nu)}(\delta_{ik}\delta_{jl} + \delta_{il}\delta_{jk}) \quad (59)$$

Young's modulus and the Poisson ratio of most of the materials used were either provided by the ski company Stöckli, its component suppliers or for standard materials (e.g. the metal layers) they were taken from literature values [51]. The mechanical properties of the thin glue layers and the Poisson ratio of some other materials had to be estimated [137],[138]. However, comprehensive parameter studies showed that the significance of the estimated material properties on the mechanical properties of the ski as a whole were very small [139]. In fact, the mechanical properties of the ski's sandwich structure are mainly determined by the properties of the metal layers and the thickness of the wood core [139]. The wood core and the fibre

layers within the ski are non-isotropic materials. The most important components of the C_{ijkl} tensor were determined by tensile tests⁶ [135].

4.3.3 Ski Types Implemented in this Thesis

Simulation results and verification of the FEM model, which are presented in this thesis were conducted with two ski models, namely with the all-round carver ski „Stöckli Spirit“ of the winter season 2002 (Figure 58) and the race carver „Stöckli Laser GS“ of season 2002 (Figure 59). However, new ski models may be implemented with little effort by few modifications of the present FEM program. For each ski the Stöckli company provided side cut data as well as information about type and thickness of the individual layers which constitute the ski.

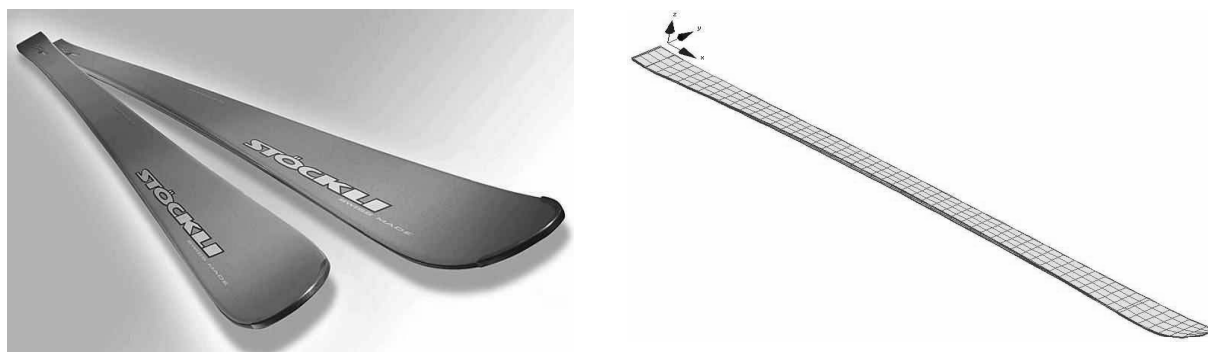


Figure 58. The Stöckli „Spirit“: photo and FEM-model (photo: www.stoeckli.ch).



Figure 59. The Stöckli „Laser GS“ (photo: www.stoeckli.ch).

4.4 Implementation of the Ski Binding

Apart from basic safety issues (mentioned in the introduction in section 1.2.2) one of the main functions of the ski binding is to transfer forces from the skier onto the ski and vice versa. The way the forces are transferred depends strongly on the type of binding. Modern bindings are complicated mechanical devices, which comprise a high number of different component parts.

6. The E-modules along and perpendicular to the fibres, $E_{||}$ and E_{\perp} , and the shear module G_{12} were measured. Values for the Poisson's ratios for lateral contraction due to stress along the fibres $\mu_{\perp||}$, for lateral contraction due to stress perpendicular to the fibres $\mu_{||\perp}$, and contraction along the fibres due to stress perpendicular to the fibres $\mu_{||\perp}$ were derived using the filling degree of the fibres, which is defined as the ratio between fibres and the embedding resin. These values were used to calculate the components of the S_{ij} tensor, which links the deformations with the stress components $\underline{\epsilon} = \underline{S} \cdot \underline{\sigma}$: $S_{11} = 1/E_{||}$, $S_{12} = -\mu_{\perp||}/E_{||}$,... (S_{ij} is the reduced engineering notation, where the rank 4 tensors are written as 6x6 matrices, while the rank 2 tensors, e.g. the stress tensor σ_{ij} , are expressed as 6 element vectors). The C_{ijkl} tensor was then obtained by inverting S_{ij} : $\underline{C} = \underline{S}^{-1}$.

However, relevant for the simulation of the ski-binding system are only the impact of the binding on the system stiffness and the force transfer onto the ski. For this purpose the mechanical functionality of the binding components (e.g. rails, joints, screws, etc.) are represented by the FEM model, but for the individual constructional components of the binding a rough representation is sufficient. The implementation of a comprehensive and detailed binding model (e.g. a detailed representation of the exact mechanism of the release system) would not significantly affect the turning characteristics of the system. Therefore, in the frame of the current thesis, all component parts of the binding were simplified and implemented as separate finite element blocks. Joints, screws and pressure transfer areas between those blocks and between the binding and the ski are represented by internal constraints. In the next section the concrete implementation of the Fritschi binding „Rave Powerride“ will be discussed.

4.4.1 The Fritschi „Rave PowerRide“ Binding in a Simplified FEM-Model

Figure 60a) shows the binding „Rave Powerride“: The binding features the „Max Flex° system“ [140] by Fritschi, which allows the ski to flex freely, while maintaining the same clamp pressure on the ski boot. The mechanical functionality of the „Max Flex° system is ascertained via three main components: A sturdy central rail, on which the toe piece and the automatic heel unit are mounted, a front and a rear plate. The central rail is affixed to the front plate of the binding with a joint but is only guided by a rear plate. Front and rear plate of the binding are screwed tightly onto the ski, but the central rail can slide back and forth, as the ski is bent.

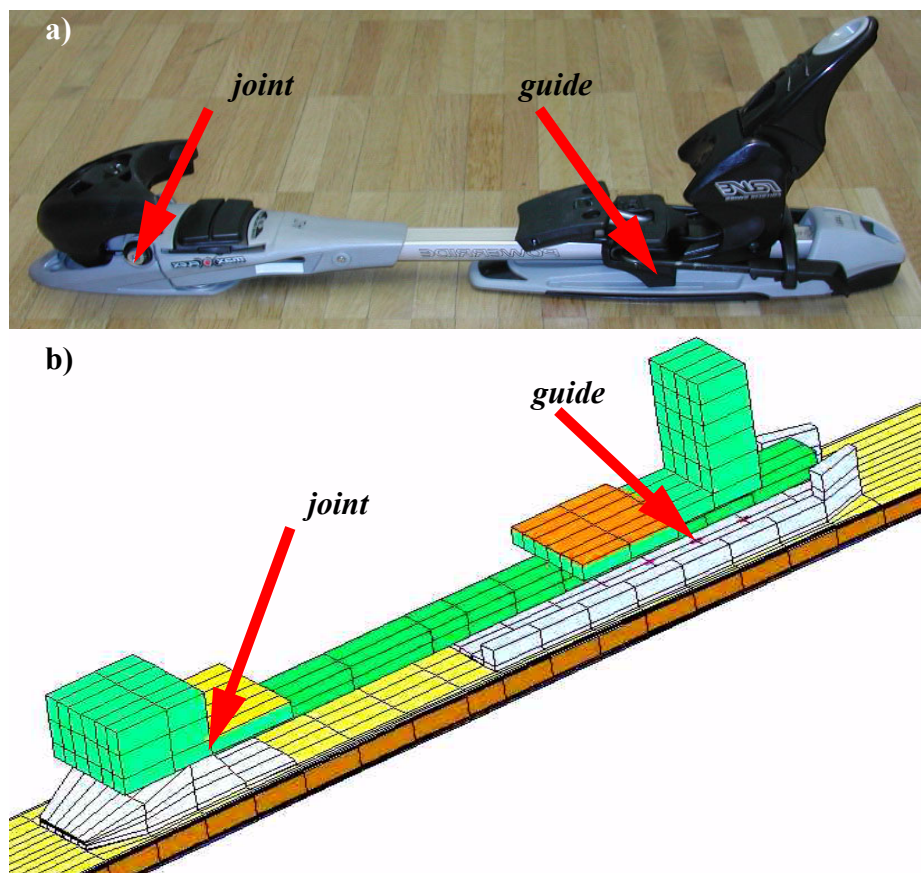


Figure 60. a) Photo of the binding model „Rave Powerride“ and b) its representation as FEM-Model. The joint and the guide which hold the central rail are indicated in both graphs.

The FEM model of the binding is displayed in Figure 60b). Like the real binding it consists of three cohesive blocks: the top block comprises the central rail, the toe piece and the automatic heel unit, which are coloured in different shades of green in the figure. The yellow and the brown surfaces indicate the boundary area on which forces are transferred from the ski boot onto the binding in the current model. The front plate bearing the joint, which connects to the central rail is a second independent block and coloured light blue in the figure. The rear binding plate bearing the guide for the central rail is a third independent block and coloured dark blue in the figure. The joint, the guide as well as other contact surfaces transferring pressure or forces between the above discussed binding blocks are represented by internal constraints, which were implemented as pointwise Floating BCs (as defined in section 4.2). The screws which attach the binding to the ski are represented by boundary conditions, defined as internal constraints using the Floating BC. Friction between parts of the binding is neglected.

The mechanical properties of the binding materials were provided by Fritschi, however, each of the blocks in the FEM-model represents a voluminous module. The real binding consists of thin, concave, structured component parts of different materials. Therefore the voluminous blocks of the current FEM-model can not be assigned to the given material properties of the main components, as this would stiffen the binding blocks improperly. Thus the material properties of the two blocks, which are directly attached to the ski (blue coloured in Figure 60) were adjusted such that the measured bending stiffness of the whole ski-binding system is calculated correctly by the ski-binding model. The necessary experimental test were carried out in the SLF-laboratory (refer to section 4.5). With the verified and adjusted bending properties of the model the FEM simulation is expected to generate reasonable results also for the case of a turning ski. Yet the specific stresses and deformations within the three binding blocks can not be predicted by this kind of binding implementation.

4.5 Experimental Verification Methods and Results

During a turn the ski is loaded by bending and torsional forces. Therefore a combined laboratory bending and torsion test rig was used to assure that bending and torsion properties are calculated correctly by the FEM simulation. Another key feature in the turning process of alpine skiing is the interaction between ski and snow. This interaction is governed by the way in which the ski-binding system transfers the turning forces into the snow. Therefore the force distribution under the bottom surface of a flat ski was measured and compared to simulation results.

4.5.1 Bending and Torsion Stiffness of the Ski

The bending and torsion test rig used (see Figure 61) was developed at the polytechnic college „Interstaatliche Hochschule für Technik Buchs“ [119] as a diploma thesis [141]. The bending stiffness of the ski or the ski-binding system are measured by determining the centre spring constant and the actual deflection line in a three point bending test. Torsion measurements were carried out by clamping the ski at the middle of the ski boot and applying a defined moment of force to its shovel or tail [64]. This methods for the characterization of elastic properties of ski and binding have been described in previous studies [6],[9].

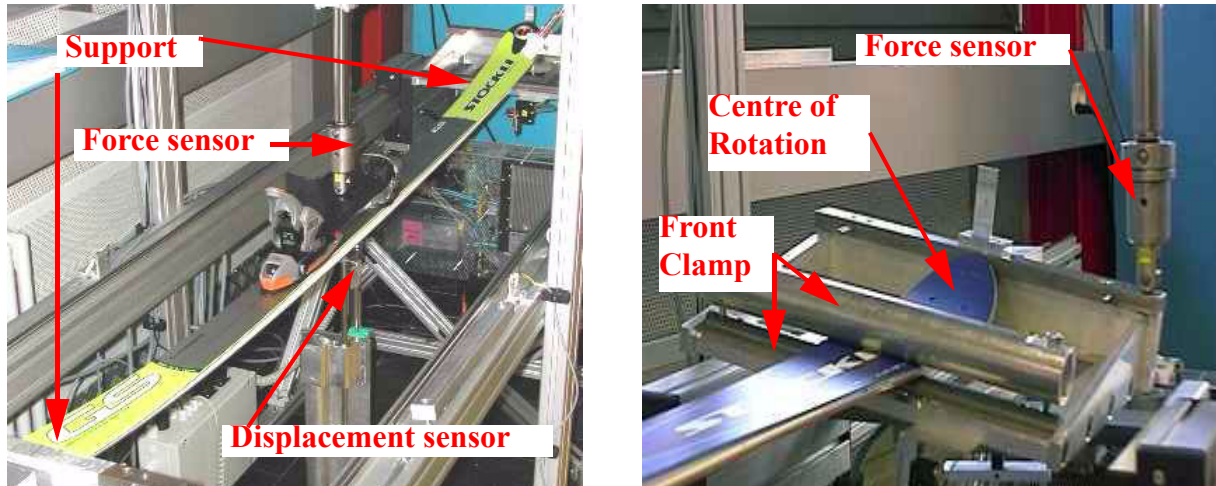


Figure 61. Bending and torsion tests on the laboratory test stand.

To calculate the ski's deformations with the finite element model, Dirichlet BC are defined on the surface of the ski where it is supported or clamped by the testing device. The mechanical loads are applied to the ski-binding model by a Floating BC (refer to section 4.2 for a detailed description of the definitions of the BCs).

The centre spring constant is calculated from the applied bending load divided by the effective deflection of the ski. Thus, it characterizes the overall elastic properties of the ski. For the Stöckli Spirit the simulated centre spring constant is 4.7 N/mm - 15% higher than the measured one [64]. In case of the Stöckli Laser GS the centre spring constant was measured to be 4.9 N/mm +/- 0.1 N/mm and calculated as 5.7 N/mm - 14% higher [64]. In the measurement results small deviations from a linear elastic behaviour are observable [64]. These deviations are probably caused by a slight inward sliding of the skis over the rounded support when the ski is loaded with the bending forces. In the FEM-simulation this situation can not be represented exactly by standard boundary conditions, which can explain part of the deviations between simulation and experimental results.

The deflection line, calculated as the difference of height of the unloaded and the loaded ski in the three point bending test described above, is a measure of the stiffness distribution of the ski-binding system. The difference between the absolute values obtained in the measurement or the simulation are again in the order of 15% of the respective values [64].

The torsional stiffness of the numerical model is about 20 % higher than the actual torsional stiffness found in laboratory tests [64]. The higher torsional stiffness of the numerical model arises from the Kirchhoff assumptions used for shell elements, which enforce that all points lying on a normal to the tangential plane of the shell remain on a normal and straight line during the deformation (see section 4.1).

4.5.2 Force Distribution between Ski and a Flat Surface

The pressure distribution between the ski and the snow was found to be a crucial criterion for the performance of a ski-binding system [142]. It is evident that the pressure distribution depends on several parameters such as the edging angle, the snow resistance pressure, the stiffness of the ski-binding system, and the forces acting on the binding. To verify the

numerical results for the pressure distribution a flat sensor panel consisting of 156 individual strain gauge force sensors, which were arrayed in 26 rows of 6 sensors, was employed [142][143]. The sensors were covered with a 1 mm thick rubber band and loaded with the test ski. The ski was then pressed down with a force of 400 N at the middle of the ski boot. The forces of the six sensors of each measurement row were then added up to determine the force distribution along the ski axis between ski and underlay (Figure 62).

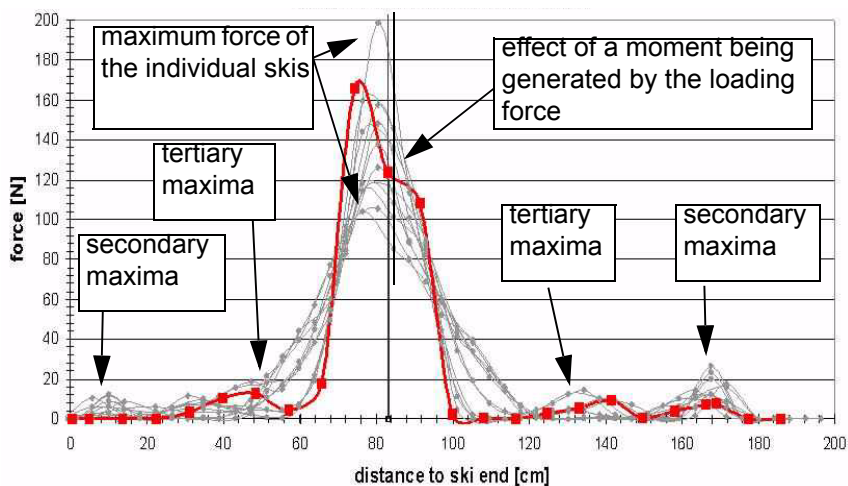


Figure 62. Calculated (red) and measured (grey) force distributions along the ski axis [64].

The grey shaded curves in Figure 62 represent twelve measurements with six individual skis of the Stöckli Laser GS series, i.e. with six skis, which are identical in construction. The obtained curves of each ski are reproducible, but vary strongly from ski to ski: The maximum force values found for each ski differ by about 100% [64].

All curves show a maximum force exerted on the underlying sensors, which is shifted by a few centimetres towards the ski end. This shifting might be explained by a moment of force, which is generated by the loading force, which acts on the slightly inclined upper ski surface. Secondary force maxima are found at the tip and the tail of the ski, which arise from the force necessary to press down the ski's camber. Again the magnitude of forces measured in these secondary maxima varies from ski to ski. Some skis exhibit a tertiary force maximum between ski shovel and the first pressure maxima.

In the simulation the ski was also loaded with 400 N, however, the underlying sensor panel was replaced by a flat surface, which exerts an adjustable resistance pressure to the ski, which is implemented as a function of the impression of the ski on the surface. The force distribution is then calculated by a piecewise integration of the calculated interface pressure over 8.3 cm long surface areas of the ski. This distance of 8.3 cm corresponds to the distance between the sensor rows in the measurement device. By this process the force values are re-normalised, which explains why the integral of the force distribution displayed in Figure 62 differs from the expected value of 420 N (loading force + weight of the ski), but the resultant force distribution is directly comparable to the measured force distribution:

The calculated force distribution blends easily into the array of measured curves (see Figure 62 red curve). However, there are some deviations: The displacement of the maximum force value towards the ski end is amplified, no secondary maxima is found at the ski end, and

the tertiary pressure maxima are more pronounced in the calculated force distribution compared to the measured one [64]. The simulation also shows, that the calculated force distribution strongly depends on the stiffness of the underlay, which indicates that a correct characterisation of the snow resistance pressure is crucial for the simulation of the ski-snow pressure in a ski turn.

4.5.3 Summary of the Model Verification

The comparison between experimental tests carried out with several test skis and the numerical simulation of the same ski models in similar loading conditions showed satisfactory agreement. However, there are a number of noteworthy deviations: Generally the numerical ski model was stiffer than the actual skis in the tests. For new skis the actual bending stiffness is about 15% lower than in the simulation. The torsional stiffness differs by about 20%, which may be explained by the restrictions of the employed shell elements. All tests were carried out with new ski models. Aging of the skis can be expected to further increase the differences to the numerical model.

The comparison of measured and simulated force distribution along the ski axis highlight the importance of the stiffness of the underlay under the ski as well as the variability of the properties of skis identical in construction. Taking this into considerations, the agreement between calculation and experiment is satisfactory.

5. Simulation of the Ski in a Static Experiment

As a first step towards the numerical simulation of a turning ski-binding system, the system was considered in a purely static situation. The implementation of the snow resistance and a suitable solving algorithm could thus be developed and tested in a simpler case, in which several numerically difficult problems do not appear. The simulation of a static case also simplifies the experimental verification procedures. Thus basic features of the simulation can be checked before the more complicated general case of a ski in motion is considered. This chapter focuses on the static simulation of a ski-binding system, the next chapter will then describe the general case of a moving ski-binding system. The first section of this chapter presents the theoretical background and necessary assumptions for the implementation of the turning simulation. The boundary condition for the ski-snow contact and a suitable solving algorithm are described in detail. For the verification of the static simulation results the measurement device Agervis, which was already introduced in subsection 3.3.1, was equipped with a complete ski-binding system. This is discussed in section 5.2. The last section of this chapter, section 5.3, discusses suitable applications of the static ski simulations and presents how static simulations aided in the development of a new prototype of an adjustable binding plate. Figure 63 exhibits an example of a static solution for the shape of a Stöckli Spirit ski under prescribed external force conditions.

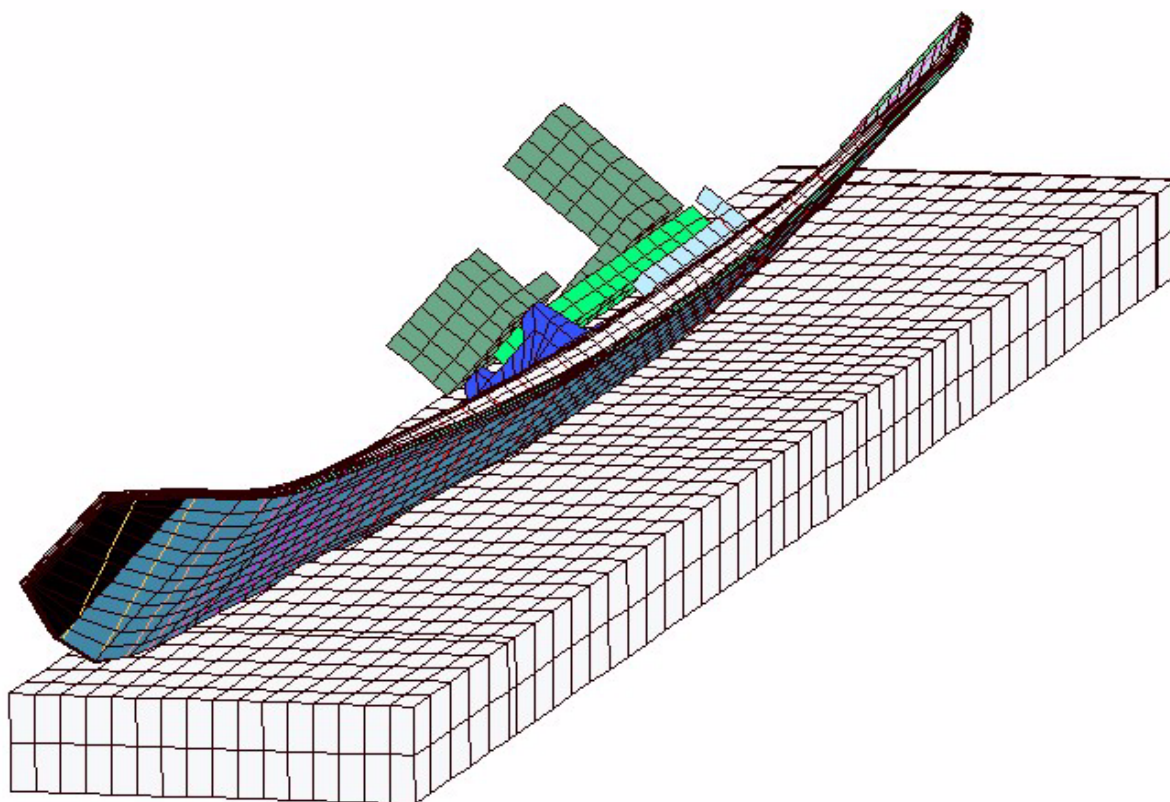


Figure 63. Simulated shape of a Stöckli Spirit ski on snow of medium strength, calculated for an edging angle of 50° and a loading force of 1500 N. The white block in the figure indicates the snow surface.

5.1 Boundary Conditions and Solving Algorithm in the FEM-Model

5.1.1 Implementation of the External Forces Acting on the Ski

The external forces and associated moments acting on a ski binding system during a turn were discussed in section 2.3. They comprise the forces and moments transferred from the athlete onto the binding of the ski, $F_{Athlet}(t)$ and $M_{Athlet}(t)$ (see section 2.3.2), the forces and moments acting in the ski-snow interaction, $F_{SSI}(t)$ and $M_{SSI}(t)$ (see section 2.3.3), gravitational forces acting on the ski, $G_{ski}(t)$ and $M_{G_{ski}}(t)$, and inertia forces $F_{inertia}(t)$ and $M_{inertia}(t)$ (see section 2.3.1). To simplify matters, the implementation of these forces into the numerical model is explained in this section already for the general case of a moving ski, although the ski-snow interaction needs some modifications, which will be explained in chapter 6.

1. The forces acting between ski binding and ski boot have been determined by measurements with Kistler™ force plates (as described in chapter 2). In these measurements the resulting total force $F_{Athlet}(t)$ and the resulting total moment $M_{Athlet}(t)$ with respect to the ski centre were determined. $F_{Athlet}(t)$ is implemented in the finite element model using the standard „Floating BC“ provided in SESEST™ (refer to section 4.2). It acts on the upper surface of the numerical binding model in a single point at the position $x = 0$ and $y = 0$, because the resultant moment of force was determined for the point on the ski surface at this position. The measurements have shown that only the \bar{y} -component of the moment vector $M_{Athlet}(t)$ contributes significantly to the system's deformation (see section 2.3.2). Therefore, only this vector component was implemented in the simulation as a „Floating BC“, which acts on the upper ski surface at the position $x = 0$ and $y = 0$. The other measured vector components of $M_{Athlet}(t)$ were omitted.
2. Forces acting between the bottom side of the ski and the snow, $F_{SSI}(t)$, which is composed of forces necessary to deform the snow surface and frictional forces

$$\mathbf{F}_{SSI}(t) = \mathbf{F}_{Snow}(t) + \mathbf{F}_{Friction}(t), \quad (60)$$

with

$$\mathbf{F}_{Snow}(t) = \int p_{Snow}(t, D) \mathbf{n}_A(t) dA_{Ski} \quad (61)$$

where \mathbf{n}_A is the local unit vector on the contact surface A and p_{Snow} the pressure distribution at the ski-snow interface, and

$$\mathbf{F}_{Friction}(t) = -\int \mu \vec{\tau}(t) p_{Snow}(t, D) dA_{Ski} \quad (62)$$

where μ denotes the coefficient of friction and τ the tangential unit vector on the ski's surface in the direction of the ski's motion. The coefficient of friction μ can be determined from literature values (relevant studies were discussed in section 3.2.1).

Chapter 3 showed that the interface pressure p_{Snow} is a function of the penetration depth D into the snow (see equation 49 on page 63) and thus a function of the displacement vector \mathbf{u} in the simulation. Therefore, the generalized Neumann BC has to be used for the implementation in the simulation model. The derivation of the interface pressure p_{Snow} in function of the displacement \mathbf{u} will be discussed separately in the next subsection.

3. Gravitational forces due to the skis own weight:

$$\mathbf{G}_{\text{ski}}(t) = \int \rho \mathbf{g} \, dV_{\text{ski}} \quad (63)$$

where ρ denotes the density of the ski or binding materials, \mathbf{g} the gravitational acceleration. The density of the ski materials is known from suppliers or has been estimated.

In the simulation the gravitation is implemented as volume force acting on each finite element. This volume force is specified as a function of the density which is assigned to each of the elements as one of the material properties. With this implementation the gravitational forces acting on each element automatically generate the moment $\mathbf{M}_{G\text{Ski}}(t)$, which therefore does not have to be implemented explicitly.

4. The inertia forces within the system of the ski depend on the acceleration and the density of the ski:

$$\mathbf{F}_{\text{inertia}}(t) = -\int \rho \mathbf{a}_{\text{Ski}}(t) \, dV_{\text{Ski}} \quad (64)$$

In the simulation it is also be implemented as volume force acting on each finite element. The accelerations of the turning ski were discussed in chapter 1. Note that vibrations of the ski-binding system would additionally generate strong accelerations, which are not considered in this study.

The forces discussed above determine the deformation state of a ski. However, none of the forces, and thus none of the boundary conditions discussed so far depends on the position of the ski in the simulation coordinate system xyz . As a result, any position of the ski on the $z = 0$ plane with the same result for the ski deformation would be an equivalently valid solution for the simulation. To ensure an unique solution an additional Dirichlet boundary condition was introduced, which fixes the ski-binding model in the $z = 0$ plane and thus eliminates the rigid body degrees of freedom. This Dirichlet boundary condition was defined at the point $x = 0$, $y = 0$ on the bottom surface of the ski. It is necessary to screen the forces occurring at this BC and ensure that they are small enough to be neglected considering the forces and moments which define the motion and the deformation state of the ski-binding model.

5.1.2 Determination of the Snow Resistance Pressure in the Simulation

When discussing the forces $\mathbf{F}_{SSI}(t)$ of the ski snow interaction in the last subsection it was pointed out that the snow resistance pressure p_{Snow} depends on the penetration depth D of the ski into the snow. For the simulation three assumptions were used for the implementation of the snow pressure in the simulation model:

- The snow resistance pressure p_{Snow} and thus the interaction force \mathbf{F}_{Snow} acts only on the undersurface and not on the side faces of the ski.
- \mathbf{F}_{Snow} acts perpendicular to the undersurface of the ski.
- A point on the undersurface experiences snow resistance only, if it has penetrated the snow surface (snow removed from the trace, which might build up under the edged ski is not considered).
- Friction at the ski-snow interface is neglected.

The coordinate system xyz for the simulation of the ski-binding system has been chosen such that the penetration depth D of any point $\mathbf{P} = (x, y, z)$ of the ski model can be determined by

the z -coordinate of its initial position $\mathbf{P}_0 = (x_0, y_0, z_0)$ and the displacement vector $\mathbf{u}(\mathbf{P}) = (u_x(P), u_y(P), u_z(P))$ by

$$D = -(z_0(P) + u_z(P)) \quad (65)$$

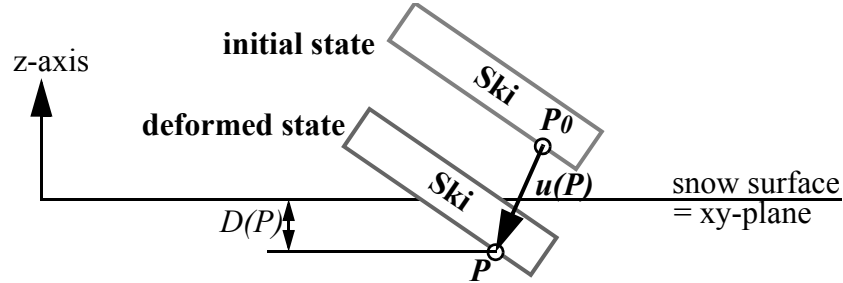


Figure 64. Calculation of the penetration depth $D(P)$ of point P in the simulation coordinate system.

In chapter 3 a relation of the mean resistance pressure of the snow as a function of the penetration depth was deduced from experimental data (equation 49). For the static case only loading of the snow has to be considered. This case is described by equation 49a), where the coefficients A and B are characteristics of the snow type. An important issue for the implementation of the snow pressure in the simulation is the fact that equation 49a) and b) describe the mean pressure measured at a penetrating plate. The simulation, however, requires the actual pressure $p_{Snow}(D)$ at a given point P of the boundary surface. With increasing values of the penetration depth D (for $D > 0$) the mean pressure increases linearly. Therefore, it is a likely assumption that the actual pressure on point P also increases linearly, but with a doubled slope coefficient:

$$p_{load}(D(P)) = \begin{cases} 2A \cdot D(P) + B & D(P) > 0 \\ 0 & D(P) \leq 0 \end{cases} \quad (66)$$

This function contains a non-differentiable point at the transition from positive penetration depths $D > 0$ to negative penetration depths $D < 0$. When calculating the numerical solution with this function assigned as boundary condition to the ski's undersurface the non-differentiable point will cause numeric divergence of the simulation. Therefore, this function has to be replaced by a smooth approximation function to ensure convergence to a valid solution. The partially linear function of the snow resistance is therefore expressed as a sum of a step function and a one-sided ramp, which are defined by:

$$\text{step}(D) = \frac{1}{2} \cdot \left(1 + \tanh\left(\frac{D - D_{off}}{\epsilon_{Step}}\right) \right) \quad (67)$$

$$\text{ramp}(D) = \frac{1}{2} \cdot \left(\sqrt{(D - D_{off})^2 + \epsilon_{Ramp}^2} + (D - D_{off}) \right) \quad (68)$$

An offset is included by the parameter D_{off} (for the loading case $D_{off} = 0$), and the parameters ϵ_{Step} and ϵ_{Ramp} determine the width of the transition zone between the two nearly linear parts (see Figure 65). In the simulation the two coefficients ϵ_{Step} and ϵ_{Ramp} were always chosen smaller than 0.5 mm. Thus the transition zone, which is necessary due to the numerical

implementation, is confined to penetration depths of ± 1 mm, which contributes insignificantly to the whole pressure distribution under the ski. Thus, the implemented function for the boundary condition for the penetration of the ski into the snow is

$$p_{\text{Snow}(\text{load})}(D) = 2A \cdot \text{step}(D) + B \cdot \text{ramp}(D) \quad (69)$$

This function is differentiable for all values of D and for $\varepsilon_{\text{Step}}$ and $\varepsilon_{\text{Ramp}} < 0.5$ mm describes the snow resistance pressure on any given point of the undersurface of the ski in a good approximation. Figure 65 displays an example of $p_{\text{Snow}(\text{load})}(D)$ for the arbitrarily chosen coefficients $A = 0.1$ and $B = 2$.

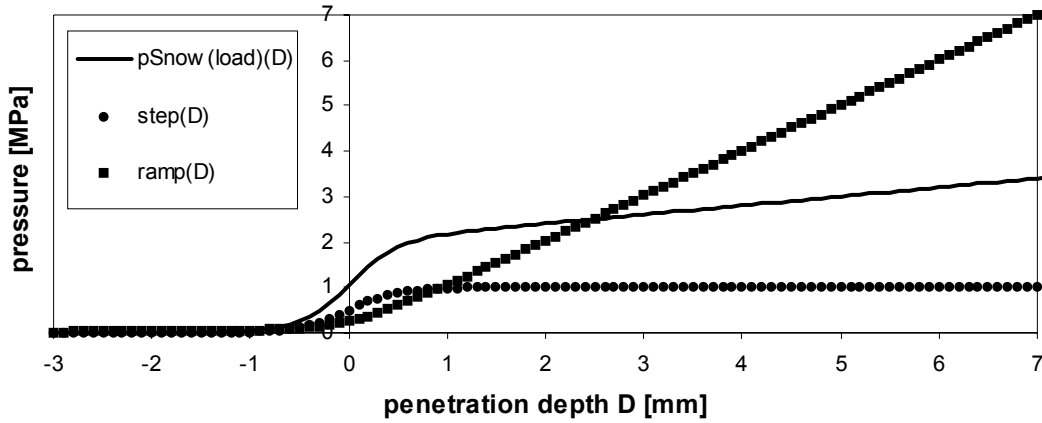


Figure 65. Example of the mathematical functions used for the implementation of the snow resistance pressure with the arbitrary parameters $A = 0.1$ MPa/mm, $B = 2$ MPa and $\varepsilon = 0.5$ mm.

After inserting equation 65 and equation 69 into equation 61 the snow resistance force $\mathbf{F}_{\text{Snow}}(t)$ can be defined as a boundary condition to the ski-binding model. However, $\mathbf{F}_{\text{Snow}}(t)$ is still not an independent quantity, since it depends on the displacement vector \mathbf{u} , and thus on the solution of the finite element simulation. Therefore, an iterative solving algorithm is implemented (see next subsection), which determines the shape of the ski (i.e. the displacement vector \mathbf{u}) and thus the pressure distribution $p_{\text{Snow}}(D)$ such that the equilibrium of forces (equation 23) and moments (equation 25) are satisfied:

$$\mathbf{F}_{\text{Snow}} = \int p_{\text{Snow}}(D) \mathbf{n}_A dA_{\text{Ski}} = -(\mathbf{F}_{\text{Athlet}} + \mathbf{G} + \mathbf{F}_{\text{inertia}}) \quad (70)$$

$$\mathbf{M}_{\text{SSI}} = \int p_{\text{Snow}}(D) \mathbf{n}_A \mathbf{r} dA_{\text{Ski}} = -(\mathbf{M}_{\text{athlete}} + \mathbf{M}_{\text{Gski}} + \mathbf{M}_{\text{inertia}}), \quad (71)$$

where \mathbf{r} denotes the position (x,y,z) on the boundary surface, and thus the distance to the origin for which the moment of force is calculated.

In the limiting case of a purely static problem (the ski is pressed into the snow but does not move) the inertia forces $\mathbf{F}_{\text{inertia}}(t)$ and corresponding moments $\mathbf{M}_{\text{inertia}}(t)$ are zero. Thus, for the static case equation 70 and equation 71 can be reduced to

$$\mathbf{F}_{\text{Snow}} = \int p_{\text{Snow}}(D) \mathbf{n}_A dA_{\text{Ski}} = -(\mathbf{F}_{\text{Athlet}} + \mathbf{G}) \quad (72)$$

$$\mathbf{M}_{\text{SSI}} = \int p_{\text{Snow}}(D) \mathbf{n}_A \mathbf{r} dA_{\text{Ski}} = -(\mathbf{M}_{\text{Athlet}} + \mathbf{M}_{\text{Gski}}) \quad (73)$$

5.1.3 The Solving Algorithm

SESESTTM contains a whole set of solvers for symmetric or non-symmetric problems [129]. The simulation of an edged ski leads to an stationary but non-symmetric problem [137], which is solved iteratively by a stabilized biconjugate gradient solver [129]. An iterative solver is necessary because the boundary for the ski-snow interaction depends on the calculated displacement vector: Starting from a suitable initial state SESESTTM calculates the pressure distribution on the ski undersurface for the given penetration depth of the ski into the snow. This completes the set of boundary conditions and allows SESESTTM to calculate the displacement vector of the ski-binding model. Thus a new shape of the ski, a new distribution of penetration depth into the snow, and a new pressure distribution on the undersurface of the ski are obtained. This new pressure distribution is then used for the next calculation step of the iteration. This procedure is repeated either until the difference of the calculated shapes of two consecutive iteration steps is smaller than a given stop criterion or until the simulation is aborted, after a given maximum number of iterations did not generate a stationary solution.

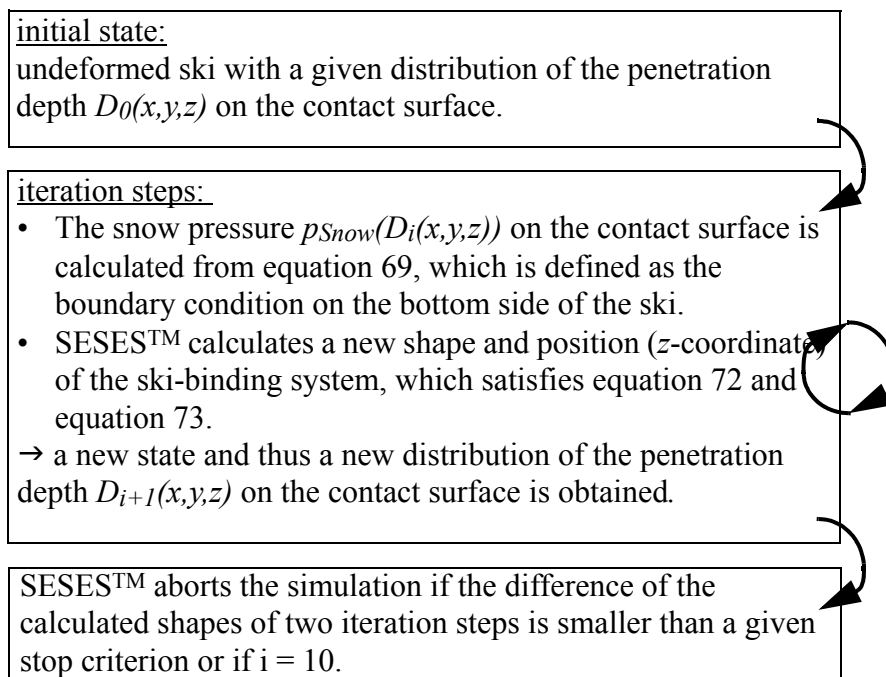


Figure 66. Flow chart of the iteration procedure carried out by the iterative solver in SESESTTM.

For the case of a static experiment in which only the penetration of the ski into the snow and no unloading is considered the iterative process usually converges to a stationary solution within ten iteration steps. The simulation is sensitive to the initial state of the ski model. If the number of necessary iterations exceeded 15 the initialisation was not optimal.

5.2 Comparison of Experimental and Numerical Results

5.2.1 Verification of the Calculated Snow Resistance Force

The snow resistance function was deduced from field experiments with the device Agenvis (see Figure 67 on the left), and implemented into the simulation according to equation 69. In order to verify that the implementation generates valid results, the Agenvis experiment with the metal plate was modelled by a simple SESES™ program as displayed in Figure 67 on the right.

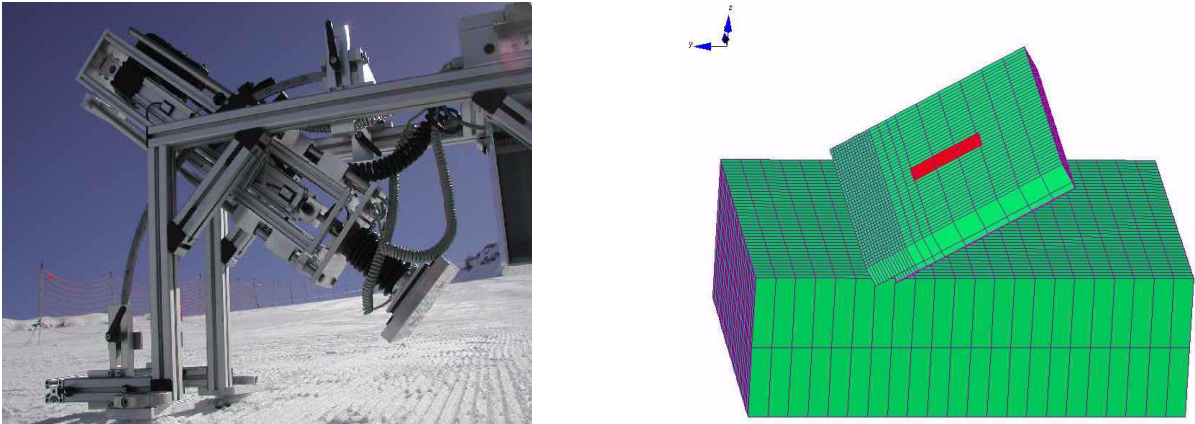


Figure 67. The Agenvis measurement device equipped with a metal plate (left) and a simple FEM model representing this measurement (right).

Figure 68 compares experimental and numerical results for the hard snow of a racing piste. For six different edging angles the resistance force on the penetrating plate was measured. Each of these measurements were repeated to ensure reproducibility. The force values of these measurements fluctuate, especially for larger edging angles. This is explained by the brittleness of the snow deformation (refer to chapter 3).

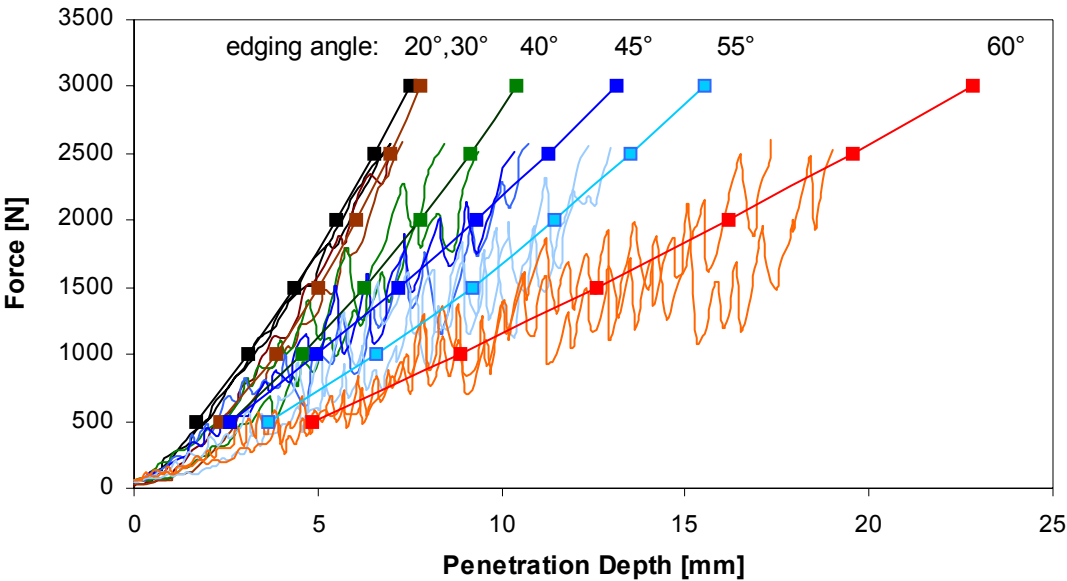


Figure 68. Measured and simulated snow resistance force in function of the penetration depth for six different edging angles.

For each of the edging angles six different loading forces were applied to the numerical model of the plate by a Floating BC. Then the penetration depth of this plate into the snow was calculated. The simulation results were added to the graph as small square dots. The calculated penetration depth agrees well with the experimental results. It is thus reasonable to assume that for a snow type characterized by the coefficients A and B , which have to be determined by Agenvis measurements, the implemented snow resistance function accurately describes the penetration process.

5.2.2 Comparison of the Calculated and the Actual Shape of the Ski

One main aim of the simulation is to predict the turn radius of a given ski-binding combination. Therefore the shape of the ski has to be calculated for the given loading situation of a turn. For the static case the loading conditions of a turn can be reproduced by the Agenvis test device equipped with a ski. Thus, the numerical results for the ski's shape can be verified by Agenvis measurements. Figure 69 shows a photo taken during an Agenvis measurement (on the left). In order to compare the actual and the calculated shape of the ski the position of the ski's lower edge in the snow was determined. This was repeated for two different edging angles. The snow resistance strength was characterized beforehand, close to the location of the ski measurements. The actual edging angle had to be double-checked with a water level, since the ski's mounting in Agenvis was not completely stiff.

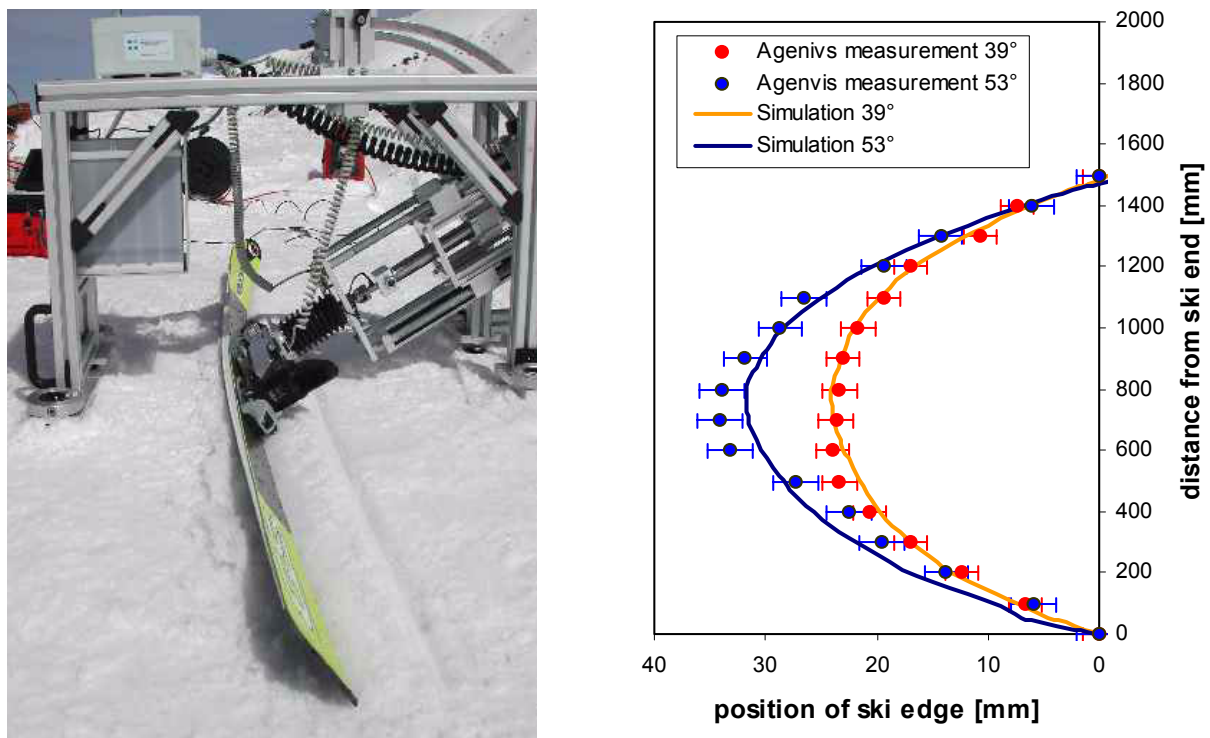


Figure 69. Agenvis measurements on a ski piste with a Stöckli LaserGS equipped with a Fritschi PowerRide (left). Position of the ski edge projected to the snow surface measured and simulated for the two edging angles 39 and 53° and a loading force of 3000 N (right).

Figure 69 on the right displays the measured positions projected to the plane of the snow surface, relative to an arbitrary line from the ski end to a point near the ski shovel. The

measurement accuracy is only about 3 mm because after pulling back the ski snow sometimes falls back into the ski trace and the exact position of the ski's edge in the snow is not always clearly visible. The continuous lines in Figure 69 on the right indicate the calculated positions of the ski edges. They were also projected to the snow surface and displayed relative to the same arbitrary line. For the smaller edging angle the measured and the calculated shape of the ski edge fit well. For higher edging angles some deviations are visible, which cannot be explained by the measurement inaccuracy alone. Yet, if considering that the snow deformation occurs by brittle fracture processes and that inhomogeneities are present in the snow, the agreement between the measured and the calculated edge positions is satisfactory.

5.3 Application Areas for Static Ski Simulations

One of the main purposes of the developed simulation tool is to compare the mechanical characteristics of different ski or binding designs. In the further development of existing ski types it is especially important to be able to analyse and adapt the overall ski properties after single layers of the sandwich structure have been altered or replaced. Common questions, which can be answered with static simulations, are for example:

- How thick should a new material layer be in order to replace a different material while maintaining the same ski stiffness?
- If there are deviations in the stiffness distribution along the ski axis after a ski property has been changed, how do they affect the ski-snow interaction?
- If the same ski is equipped with a different plate or a different binding, how does that affect the system's stiffness distribution or the pressure distribution between the ski and the snow for various snow types?

For such questions the static simulation of the ski is well suited because it offers some advantages compared to the more complex and more time consuming simulation of a ski-binding system in motion, which will be presented in chapter 6. Yet it is important to keep in mind the limitations of static simulation results.

5.3.1 Advantages and Limitations of the Static Simulation

Compared to the calculation of the ski radius in actually carved turns, which will be discussed in chapter 6, ski-binding simulations in the static case have a number of advantages:

- The necessary calculation time is short, i.e. the solution can be calculated on a standard personal computer within a few minutes. Thus static simulations are suitable if parameter studies for a broad range of input parameters are required.
- The simulation always converges to a physical solution if consistent, sensible boundary conditions have been specified.
- The results of the simulation can be double-checked with the measurement device Agenvis, whereas the shape of a moving ski cannot directly be determined. Only the radius of a ski's trace can be determined experimentally, but due to skidding the trace's radius and the ski's radius may not coincide.

- The boundary condition describing the ski-snow interaction is not disturbed by additional factors, which are necessary to describe the unloading of snow or geometrical effects of a moving ski (refer to the next chapters). The calculated pressure distribution is therefore smooth and does not exhibit numerical artefacts, which appear sometimes in the result of a moving ski.

The disadvantages of this simulation mode are that the calculated shape of the ski and the pressure distribution between ski and snow do not match the shape and the pressure distribution of a moving ski. Thus it is for example **not** possible to

- determine the exact radius of the ski for given situation.
- quantitatively evaluate how actions of the skier may influence the turn.
- study how the ski's geometry affects the turning characteristics.

In summary, static simulations are suitable to compare the mechanical properties of different systems of ski and binding or to qualitatively examine input parameters. They are not able to quantitatively evaluate the impact of an input parameter on the turning characteristics of a given ski-binding system.

5.3.2 Application Example: Development of an Adjustable Binding Plate

In all skiing disciplines skiers of different size and weight participate. Therefore, the ski manufacturers produce for each ski model several series of different lengths, so that each skier can select a suitable ski, which fits to his skill level and his body proportions. For each ski model four to five different ski lengths and shapes have to be developed, each of which requires its own production line. This leads to increased fixed development costs for each ski model. A reduction of the number of ski lengths would significantly reduce the development cost of the ski manufacturer. But a reduction of the number of ski lengths and shapes requires that the adjustment to different skiers is accomplished by a different method. One way to adjust the ski equipment to skiers of different weight is by stiffening the ski-binding system such that the effective ski radius of a heavier skier matches the one of the lighter skier.

In the years 2002 and 2003 the ski company Stöckli, the binding manufacturer Fritschi, and the Swiss Federal Institute for Snow and Avalanche Research (SLF) developed a binding plate of adjustable stiffness. The purpose of this study was to show, that an adjustment of the binding plate could change the properties of the whole ski system such, that it would be suitable for skiers of different sizes and weights [142]. During this project several design ideas were analysed with early versions of the FEM simulation program presented in this thesis. Some numerical findings will be summarized here as an example of application of the developed FEM tool.

In a first step binding plates were considered, which could be reinforced by exchangeable metal rods. In the simulation these rods were first implemented as stiffly attached to the binding plate. Figure 70 displays the FEM model of the ski equipped with a two-piece binding plate and a Fritschi binding. The exchangeable metal rods connect the two parts of the binding plate and are coloured in orange.

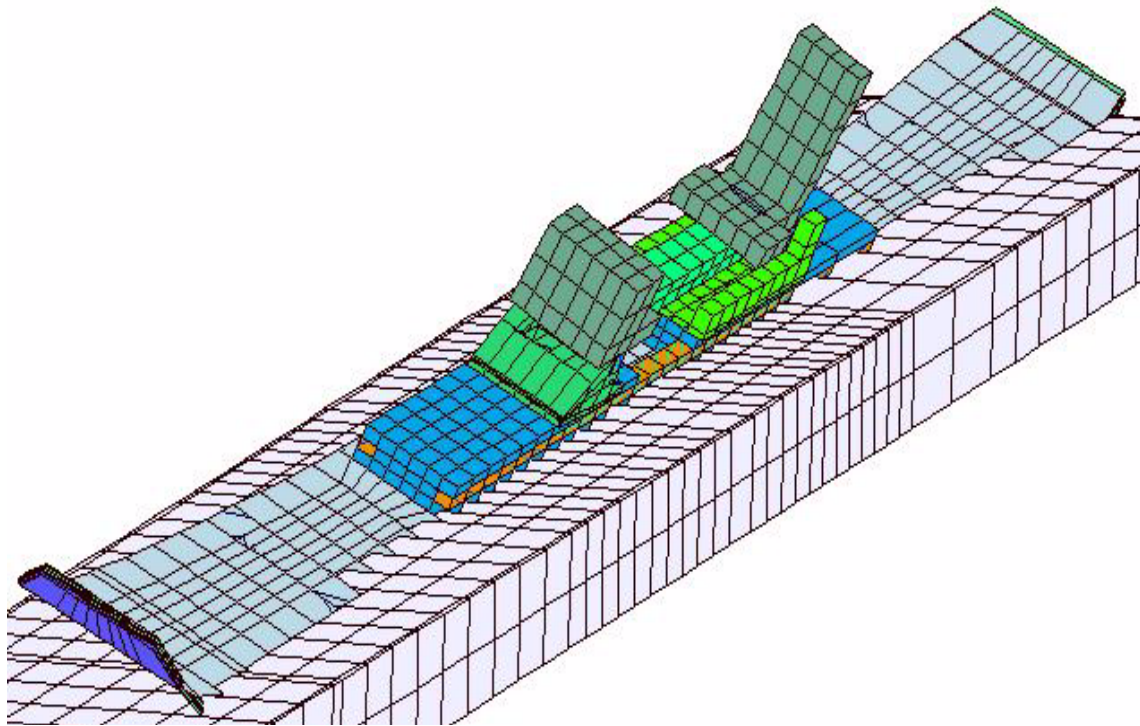


Figure 70. FEM model of a Stöckli ski equipped with a binding plate (blue), which can be reinforced by metal rods (orange), and a Fritschi binding (green).

The purpose of the static simulations of this first prototype was to get an idea of which parameters are capable of significantly changing the ski shape and the ski-snow interaction. Specifically the edging angle, the applied load, and the snow strength were examined for three different configurations of the binding plate, and compared to a ski equipped with only the binding. As an indicator of the ski shape the position of the lower ski edge, projected to the plane of the snow surface, was analysed. Figure 71 displays the projection of the ski's edge for three plate configurations compared to the ski equipped with only the binding without an additional plate (black line) on hard and soft snow types. The three configurations with of the plate are: binding plates without reinforcement (red); plates with aluminium reinforcement (green); plates with steal reinforcement (blue). The ski-snow interaction is characterized by the actual contact area between ski and snow and the pressure distribution on this area. As an characteristic indicator of the ski-snow interaction the snow pressure on the lower ski edge was examined. Figure 72 displays the pressure distribution on the edge line for the same input parameters as chosen in Figure 71.

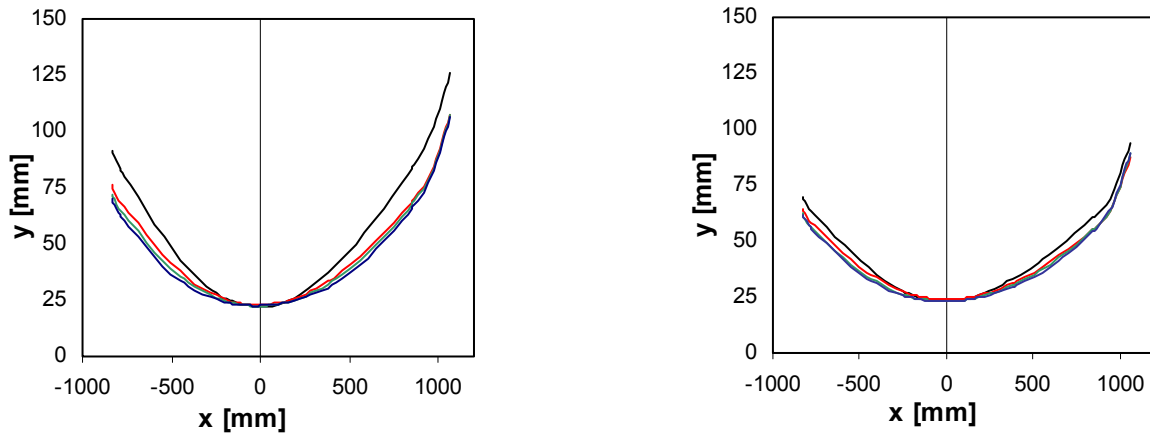


Figure 71. Position of the lower ski edge projected on the snow surface for various ski-plate-binding configurations edged with 60° and loaded with 1500 N. The ski deformation was calculated on soft (left) and hard (right) snow surfaces.

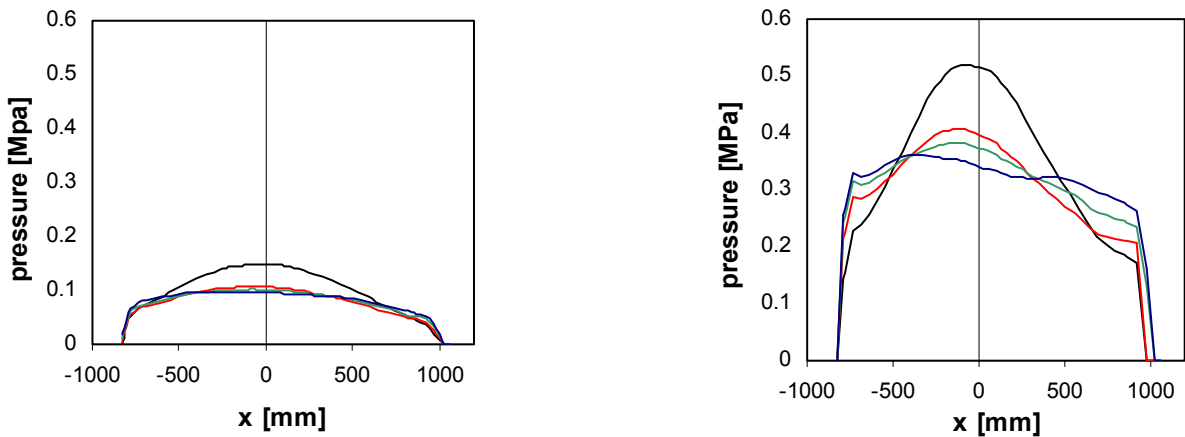


Figure 72. Snow pressure on the ski edge for the same ski-plate-binding configurations as above.

A detailed numerical analysis with the FE model of the prototype [144] lead to the following qualitative conclusions:

- The modification of the systems stiffness and modifications of the applied load affect the ski's shape much stronger if soft snow types are considered. On hard snow the ski shapes nearly coincided (see Figure 71).
- The distribution of the snow pressure along the ski edge differs strongly on hard snow types, but is much less affected on soft snow (see Figure 72).
- The shape of the ski as well as the pressure distribution are predominantly sensitive to the edging angle. The impact of the applied load, the system stiffness, or the snow resistance strength is low compared to the impact of a changing edging angle [144]. The larger the edging angle the more significant are differences due to different configurations of the binding plate [144].

- A stiffer binding plate leads to a more uniform pressure distribution as it reduces the pressure maximum below the binding and transfers pressure to the ski's shovel and rear end [144].

In the first numerical model of the binding plate the metal reinforcement rods were attached to the plate non-flexibly. In practice this turned out to be unsuitable, because the stresses at the fixations within the plates would be too high. In the following steps the reinforcement rods were mounted flexibly within the binding plates. Therefore, additional means to adjust the stiffness of this system were investigated numerically and experimentally. Particular attention was given to the fixation of the binding plates on the ski. Therefore, similar parameter studies were carried out to compare two types of screw fixations [145]: Fixed screws, which do not allow a relative movement of the two parts and screws guiding the binding plate such that a relative displacement between ski and plate was possible. Friction was neglected in the simulation.

Advanced prototypes of the binding plate were combined with the binding, but still embodied adaptability of the system stiffness (via different screw fixation and different reinforcement rods) as discussed above. By numerical and experimental investigations a combination of reinforcing metal inlays and fixation screws could be found, that allowed to adjust the mechanical properties of ski equipped with this prototype to either a light skier or a heavy skier [145]. The final system of ski and prototype binding was also tested in field studies by several skiers of different weight. For more details please refer to the final project report [142].

6. Calculation of a Turning Ski

The simulation of the turning ski is based on the same quasi-static approach, which has already been used for the static simulations. However, the boundary condition for the ski-snow interaction of an actually turning snow ski is in several aspects different from the condition of the static experiment, which was described in the last chapter. Section 6.1 first summarizes the necessary assumptions, which were used for the implementation of the simulation of a turning ski. Then the modifications in the ski-snow interaction model are discussed and adaptations to the solving algorithm are described. The experimental verification of the numerical results for a moving ski is discussed in section 6.2. Applications and results obtained with the simulation tool are presented in section 6.3.

6.1 Boundary Conditions and Solving Algorithm

6.1.1 Required Assumptions for the Simulation of a Turning Ski

The simulation of the turning ski is based on the quasi-static equilibrium of forces, which was discussed in the last chapter. Several assumptions and restrictions were made to simplify the model of the turning ski:

1. Ideally carved turns are assumed, which means that skidding is not considered.
2. Vibrations of the ski, which may be excited by the ski-snow interaction during an actual turn on a rough natural snow surface are not considered in the simulation. Accordingly, the effects, which the ski's vibrations might have on the forces acting on the ski, especially on the ski-snow interaction force $F_{Snow}(t)$ are not taken into account.
3. For simplicity the frictional forces $F_{Friction}(t)$ were neglected, since their absolute value is about one order of magnitude smaller than the absolute value of the snow deformation force $F_{Snow}(t)$.
4. As already mentioned in chapter 5, the snow deformation force $F_{Snow}(t)$ is implemented under the assumptions that the snow resistance pressure acts only at the ski undersurface, it acts perpendicular to the undersurface, and it differs from zero only on the part of the ski's undersurface, which lies below the snow surface.
5. A further necessary assumption is, that the turn parameters change slowly compared to the progress of the turn. Thus the remaining force components, particularly the snow resistance force $F_{Snow}(t)$, can be considered independent of the changes in other turn parameters. For example: if the edging angle changes very rapidly then the ski's trace, in which the rear part of the ski glides, differs from the trace being generated by the ski's shovel at the considered point of time (when the shovel formed the trace it was edged with a different angle). Thus, the snow resistance force would depend on the velocity and on the time dependency of the edging angle.

This assumption is well suited for the steering phase of a turn, but during the phase of the change of ski edges between two turns particularly the edging angle changes fast. As a matter of fact, in this phase of the turn the assumption of ideal carving is questionable.

With the these assumptions the FEM simulation solves the quasi-static equations 70 and 71, which were discussed for the static case in section 5.1.2 of the previous chapter. Now they are solved for the boundary conditions determined at time t :

$$\mathbf{F}_{\text{Snow}}(t) = \int p_{\text{Snow}}(D(t)) \mathbf{n}_A dA_{\text{Ski}} = -(\mathbf{F}_{\text{Athlete}}(t) + \mathbf{G}(t) + \mathbf{F}_{\text{inertia}}(t)) \quad (74)$$

$$\begin{aligned} \mathbf{M}_{\text{Snow}}(t) &= \int p_{\text{Snow}}(D(t)) \mathbf{n}_A \mathbf{r} dA_{\text{Ski}} \\ &= -(\mathbf{M}_{\text{athlete}}(t) + \mathbf{M}_{\text{Gski}}(t) + \mathbf{M}_{\text{inertia}}(t)) \end{aligned} \quad (75)$$

Determination of the forces $\mathbf{F}_{\text{Athlete}}(t)$, $\mathbf{G}(t)$, and $\mathbf{F}_{\text{inertia}}(t)$ and their corresponding moments $\mathbf{M}_{\text{Athlete}}(t)$, $\mathbf{M}_{\text{Gski}}(t)$, and $\mathbf{M}_{\text{inertia}}(t)$ has been discussed in chapter 2. Implementation of these parameters as boundary conditions in the numerical model was discussed in section 5.1.1 of chapter 5. As in the static case the snow reaction force $\mathbf{F}_{\text{Snow}}(t)$ and the moment it generates on the ski $\mathbf{M}_{\text{Snow}}(t)$ are determined in an iterative process, which calculates the pressure $p_{\text{snow}}(D(t))$ between ski and snow, which is a function of the ski's penetration depth into the snow, and thus depends on the ski's shape and position (see section 5.1.3). For the case of a moving ski function $p_{\text{snow}}(D)$ has to take into account that the snow at a given point on the interface surface generally does not interact with undisturbed snow, but with snow, which has already been deformed by the previous contact. It is assumed that the snow's resistance pressure exerted to a penetrating ski, which was characterised in chapter 2, does not change due to shearing of the snow surface, which might arise from frictional forces acting on the ski-snow interface. The adequate parameter describing the ski-snow interaction process of a ski in motion is still the ski's penetration depth D into the snow. However, there are two important differences in the ski-snow interaction for a moving ski compared to the static case described in the chapter 5: firstly, the ski does not only exert loading pressure on the snow, but after the pressure maximum has passed over a point on the snow surface, the snow experiences an effective unloading as the interface pressure decreases. Secondly, the ski's side cut affects the ski-snow interaction. Especially the second effect turned out to be a crucial issue for the correct calculation of the ski's shape in a turn. The next two sections describe these two effects in the implementation of the ski-snow interaction as boundary condition on the ski's gliding surface.

6.1.2 Incorporation of Plasticity of the Snow Deformation

The snow deformation during the ski-snow interaction is a brittle fracture process. This non-reversible deformation causes a strong hysteresis in the experimentally determined snow resistance function (equation 49, chapter 3). Figure 53 in chapter 3 displays the characteristic penetration resistance curves of the loading and unloading on snow.

Consider now a point on the snow surface as the ski passes over it. First the snow at this point experiences increasing pressure as the ski's front part passes over it. During this phase the ski penetrates the snow similarly to the plate penetration in the experiments described in chapter 3. When the maximum pressure is reached at a position under the binding, the penetration motion stops. As the ski's rear part crosses over the considered point the pressure exerted on the snow continuously decreases. The snow experiences an effective unloading. If elastic stresses are present within the snow, they are released as the load decreases. However, the main deformation energy has been consumed by plastic snow deformation and thus the penetration depth of the ski is reduced only slightly. The rear end of the ski thus glides within the trace, which had been generated during the earlier loading process.

In order to implement the snow deformation of a ski in motion into the FEM model the location of the maximum pressure between ski and snow has to be determined. Then the function for the snow resistance pressure during loading (equation 49a) can be assigned as

boundary condition for the interface area from shovel to the point of maximum pressure, the pressure function for the unloading process (equation 49b), can be assigned to the rear interface area (see Figure 73).

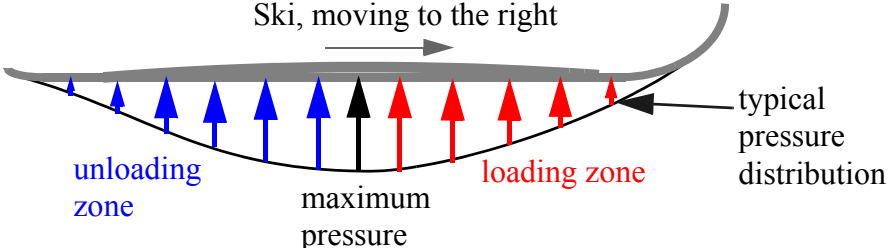


Figure 73. Schematic pressure distribution under a loaded ski during a turn. The contact areas under the ski, which experience loading or unloading are indicated.

The pressure distribution between ski and snow as well as the penetration depth of the ski into the snow are simulation outputs. Therefore, an outer iteration loop, in addition to the inner loop, which solves equations 74 and 75, was implemented. The iteration is initiated by calculating the pressure distribution of a ski for the case of pure loading of snow (equation 49a assigned for the whole boundary area of the ski-snow interface). Then the location of the maximum pressure is determined. From this point back to the ski end the pressure function for unloading of snow is assigned (equation 49b), replacing the pressure function of loading. With this modified boundary condition the calculation of the ski’s shape is repeated. The modification of the boundary conditions results in a new pressure distribution. Therefore, the determination of the maximum pressure, the modification of the boundary condition and the calculation of the new ski shape have to be repeated until a stable state is found. This is usually the case after six iterations of the second loop.

The pressure function describing the unloading process (equation 49b) contains three parameters, D_0 , D_{max} and p_{max} , which have to be determined by the simulation. D_{max} denotes the maximum penetration depth and p_{max} the maximum pressure at this point. D_0 is the penetration depth of the ski’s trace in the snow after the load and unload cycle has been completed (see Figure 53 in chapter 3). For an edged ski all three parameters actually depend on the traverse position y on the boundary surface:

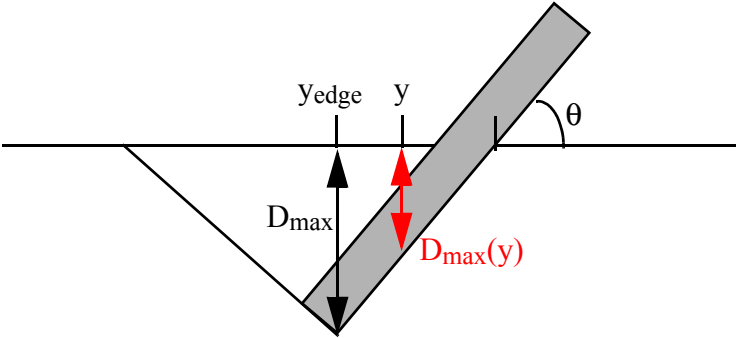


Figure 74. Schematic for the derivation of $D_{max}(x,y,z)$.

Figure 74 shows how $D_{max}(y)$ can be derived from D_{max} at the ski edge and the edging angle θ if the distance ($y_{edge}-y$) to the ski edge is known:

$$D_{\max}(y) = D_{\max} - \tan\theta \cdot (y_{\text{edge}} - y) \quad (76)$$

The maximum snow pressure at position y , $p_{\max}(y)$, can be calculated if the maximum penetration depth $D_{\max}(y)$ is known via equation 49a:

$$p_{\max}(y) = A \cdot D_{\max}(y) + B \quad (77)$$

Knowledge of $D_{\max}(y)$, $p_{\max}(y)$ and the inclination of the unloading pressure C finally allows to calculate $D_0(y)$ at position y :

$$D_0(y) = D_{\max}(y) - \frac{p_{\max}(y)}{C} \quad (78)$$

As regards the numerical implementation of the outer iteration loop in the solving algorithm, the buffering of data from one iteration step to the next is an important issue, since it severely affects the running time of the simulation. To reduce the amount of data passed from one iteration step to the next, only the position x of the maximum penetration depth and the actual penetration depth D_{\max} on the ski edge are transferred. All other necessary data can then be calculated from equations 76, 77, and 78. The evaluation of the penetration depth of the ski edge, which determines D_{\max} and the transfer to the next iteration step cannot be carried out by a standard function of the FEM software SESESTTM. Instead they were implemented in a external C-routine, which can be executed by SESESTTM.

After the unloading parameters D_0 , D_{\max} and p_{\max} have been determined the pressure function (equation 49b) can be implemented as boundary condition for the unloading zone of the ski-snow interface. As in the case of the load function (compare to section 5.1.2) non-differentiable points in the pressure function have to be avoided. Therefore, the smooth approximation functions $step(D)$ (equation 67) and $ramp(D)$ (equation 68), which were introduced in section 5.1.2 are again employed. In a first approach the snow function for the unloading process was implemented as

$$p_{\text{unload}}(D, y) = C \cdot \text{ramp}(D - D_0(y)) \quad (79)$$

But during the iterative determination of the pressure distribution on the ski-snow interface higher pressures and higher penetration depths than in the previous iteration may occur in the unloading zone. Therefore, equation 79 was modified such, that the calculated pressure $p_{\text{unload}}(D, y)$ will pass into the load function if penetration depths higher than the maximum penetration D_{\max} of the previous iteration step occur:

$$\begin{aligned} p_{\text{unload}}(D, y) = \\ C \cdot \text{ramp}(D - D_0(y)) - (C \cdot \text{ramp}(D - D_0(y)) - p_{\max}(y)) \cdot \text{step}(D - D_{\max}(y)) + \\ A \cdot (\text{ramp}(D) - D_{\max}(y)) \cdot \text{step}(D - D_{\max}(y)) \end{aligned} \quad (80)$$

An example for the pressure functions of equation 69, 79 and 80 is given in Figure 75.

7. The results presented in this thesis were calculated with an earlier version of the simulation, in which the edging angle θ was considered constant. The actual edging angle $\theta(x)$ is decreased due to torsion of the ski shovel or the ski end, and thus depends on the position x along the ski axis. First results of the calculated ski radius obtained by a new version, which allows for torsion, differ with 2-3%.

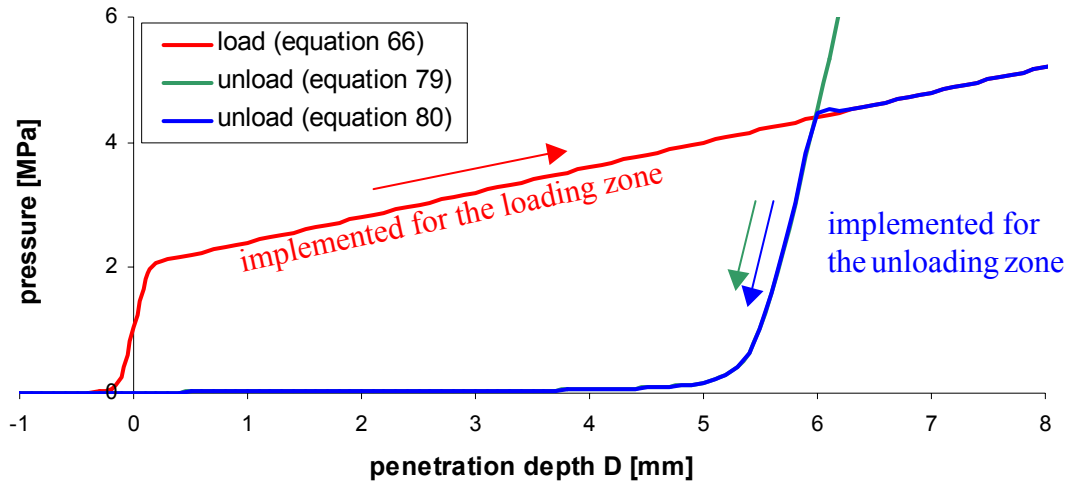


Figure 75. Example of the implemented mathematical functions for the loading and unloading snow pressure. The parameters used are $A = 0.4$, $B = 2$, $C = 8$, $d_{max} = 6$, $tr_{Step} = 0.1$ and $tr_{Ramp} = 0.2$.

6.1.3 The Shape of a Ski in Motion

The implementation of the hysteresis of the snow reaction function, which was described in the previous section of this chapter, ensures that the ski's tail will assume the correct penetration depth in the calculation. However, the lateral position of the ski's trace in the snow has not yet been taken into account. The ski only experiences snow resistance when in contact with the snow, but it has to be taken into account that a trace has been formed, by lateral removal of snow. The most difficult problem to solve, when simulating a moving ski in a quasi-static approach, is to determine where the ski's trace forms and thus to determine where the rear part of the ski experiences snow pressure.

The side cut of the ski has a high impact on the actual ski radius and the ski's trace. Howe [7],[8] calculated the actual turning radius of a carving ski from the side cut and the penetration depth of the ski into the snow. Casolo & Lorenzi [46] as well as Kaps et al. [49] revert to his description in their simulation methods for carving skis. The following model is also based on Howe's description, however, for the calculation of the ski's shape additional issues are taken into account.

The side cut of the ski denotes the fact that a ski's width is smallest at the position of the ski boot W_B , and increases continuously towards the ski shovel as well as towards the ski end. Usually the ski's width is maximum at the shovel, W_S , and the width near the ski end, W_T , is a few millimetres smaller. Figure 76 on the left displays a typical ski shape.

Considering an edged ski as it penetrates the snow surface during the turn (displayed in Figure 76 on the right as a projection to a plane perpendicular to the ski's velocity), the ski shovel is the first part of the ski to be in contact with the undisturbed snow. Little pressure is transferred to the snow at the shovel, thus it remains at the snow surface. This point is denoted y_S in the graph. The contact pressure between ski and snow continuously increases towards the mid-section of the ski until it reaches a maximum pressure near the ski's waist. In order to generate enough counter pressure in the snow, the ski has to penetrate the snow surface to a depth D . If the ski was cuboid shaped, then the ski's waist would reach the maximum

penetration depth at position y_W' , but since the ski's waist is narrower than the ski shovel, the position of the ski's waist is displaced to the position y_W . The projection of the contact area between ski and snow is indicated on Figure 76 as a blue triangle. As the ski moves forward, the snow within this triangle is pushed away. The trace formed by the ski is therefore not right-angled⁸. Towards the ski end the pressure at the ski-snow contact decreases, but the ski's width increases. Thus the ski's tail would rest somewhere between y_W and y_S , if the trace forming would not be considered. However, the trace has already been formed in the snow by the ski's shovel and waist, which is represented by the blue triangle. Within this triangle there is no snow, which could provide counter pressure for the ski's tail. Therefore, the ski's rear part remains at y_W .

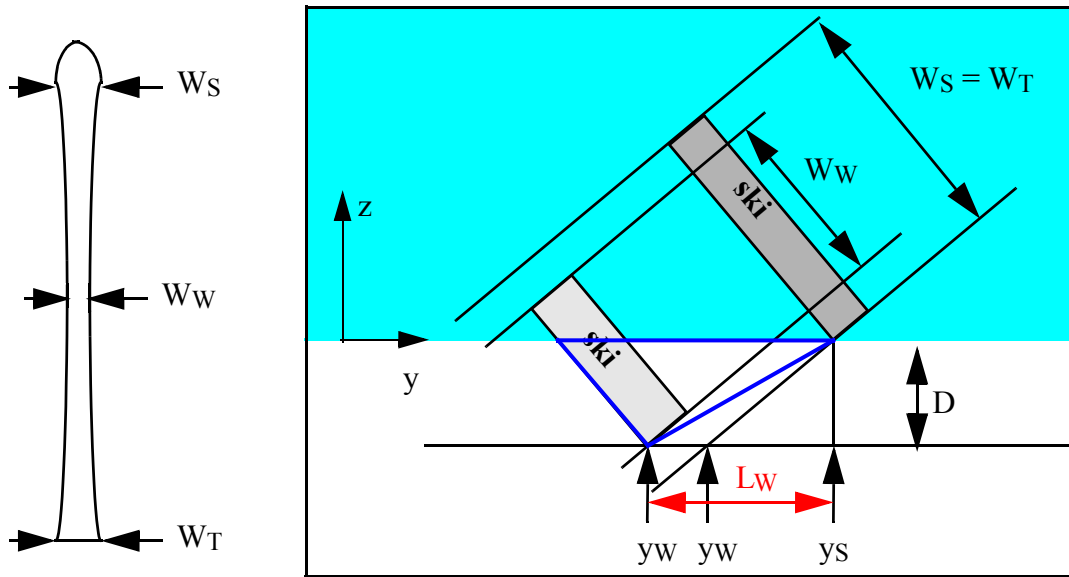


Figure 76. Illustration of the lateral displacement of the ski's waist due to the side cut effect, based on the description of Howe [8].

The total lateral displacement $L_W = y_S - y_W$ of the ski's waist can be estimated from the penetration depth $D(x_W)$ at the position of the ski's waist x_W multiplied with the tangent of the edging angle θ , and the side cut $s(x_W)$ divided by the cosine of the edging angle [8]:

$$L_W = D(x_W) \cdot \tan \theta + \frac{s(x_W)}{\cos \theta} \quad (81)$$

The side cut $s(x_W)$ of the ski is calculated by [8]:

$$s(x_W) = \frac{1}{2} \cdot ((W_S + W_T)/2 - W_W) \quad (82)$$

where W_i denotes the ski's width at the shovel ($i = S$), waist ($i = W$), or tail ($i = T$), respectively. Equation 81 is accurate if the contact of the ski edge with the snow starts exactly at x_S and ends exactly at x_T . Therefore, a new definition for W_S and W_T is here suggested,

8. This agrees well with field observation: For an example refer to Figure 50b on page 60, which displays a photo taken from an actual ski trace. The angle of the ski's trace, which formed in the snow, is clearly larger than 90° .

which differs from the definitions of Howe [8]: W_S denotes the ski width at the point where the snow contact starts, W_T the width where the contact ends.

Figure 77 depicts the projection of the ski's edge on the snow surface at an arbitrary time t_i . The ski bends until the integral of the pressure distribution between ski and snow counterbalances the other external forces applied to the ski.

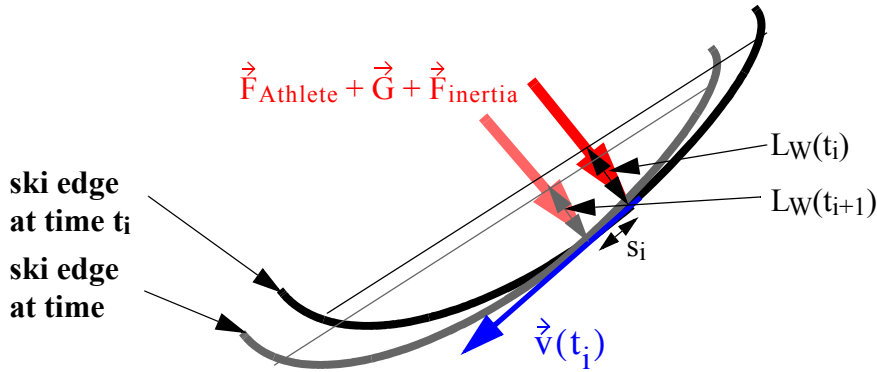


Figure 77. Bird's eye view of the ski's lower edge for two successive points of time.

The lateral displacement $L_0(x)$ of a point $P(x,y,z)$ on the front part of the ski's edge can be approximated by

$$L_0(x) = D(x) \cdot \tan\theta + \frac{s(x)}{\cos\theta} \quad x > x_W, \quad (83)$$

where

$$s(x) = \frac{1}{2} \cdot ((W_S + W_T)/2 - W(x)) \quad (84)$$

To determine the shape of a moving ski one has to consider the new position of the ski after a small time $\Delta t = t_{i+1} - t_i$. In a first approximation the new position (grey shape in Figure 77) can be calculated as a displacement s_i , which depends on the ski's tangential velocity $v(t_i)$: $s_i = v(t_i) \cdot \Delta t$. In this new position the whole rear part of the ski does not experience snow pressure since it lies within the trace generated by the ski in the earlier position. Therefore, the rear part of the ski is not bent as displayed, but retreats back to its earlier position at time t_i . If several such time steps are strung together it becomes clear that the lateral displacement of the ski's rear part may also be approximated by equation 81. This statement is equivalent with the postulation, that the ski's rear part should remain at y_w , which was proposed when discussing Figure 76. If the relaxation of the ski and snow due to unloading is also taken into account, the lateral displacement of the ski's rear part may be approximated by

$$L_{\text{trace}}(x) = D(x) \cdot \tan\theta + \frac{s(x_W)}{\cos\theta} \quad x \leq x_W \quad (85)$$

These considerations are only a first approximation in the description of a moving ski. What was not considered so far, is the fact that as the rear part of the ski retreats backwards the snow pressure at the ski shovel is unbalanced. Thus, an effective moment of force $M(t_{i+1})$ is generated, which causes a rotation $R(t_{i+1})$ of the ski as it moves forward. Figure 78 illustrates

this phenomenon. This moment of force, generated by the imbalance of the external forces, is also transferred to the skier and thus turns not only the ski, but the whole skier as he steers through the turn.

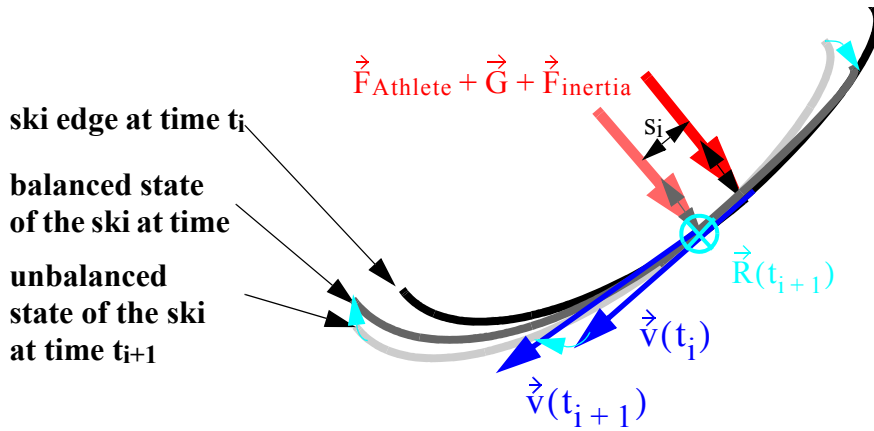


Figure 78. Rotation of the ski due to unbalanced external forces.

6.1.4 Implementation of the Side Cut Effect

The side cut effect, which was discussed in the last section, has to be implemented in the simulation by a modification of the ski-snow boundary condition. An iterative calculation of the ski's shape, starting from the case of pure loading, was already described when explaining the implementation of the snow function's hysteresis (section 6.1.2). For the implementation of the side cut effect this iteration is retained, but the calculation procedures of the ski-snow boundary condition need to be altered. In the first loop of the iteration the ski's position is determined assuming pure loading of the ski. The ski's tail is thus pressed back onto the surface of the snow and the motion has no effect on the ski's shape. In a second step the unloading function is applied and at the same time the necessary modification of the ski's lateral displacement due to the ski's motion is determined. An additional factor is introduced into the snow resistance function, which switches from one to zero if the calculated lateral position of the ski's rear part lies in the region, where it does not experience lateral snow pressure.

The key issue of this concept is to determine the position of the ski's trace in the snow. The lateral displacement of the ski's front part is given by equation 83. For the case of static loading of the ski, as calculated in the first loop of the above discussed iteration, equation 83 applies for the whole ski. The lateral displacement of a moving ski's rear part is given by equation 85. Unfortunately, both functions depend not only on the penetration depth, but also on the positions of the beginning and the end of the actual contact between ski and snow. These parameters are unknown prior to the simulation. However, if the lateral displacement of the moving ski is subtracted from the lateral displacement calculated for a static case, then the distance $\Delta L(x)$ between the position of the edge of the ski's rear part in case of a static loading, and the expected position of the trace of a moving ski can be determined:

$$\Delta L(x) = L_0(x) - L_{\text{trace}}(x) = \frac{s(x)}{\cos\theta} - \frac{s(x_W)}{\cos\theta} \quad x \leq x_W. \quad (86)$$

Inserting equation 82 and 84 gives:

$$\Delta L(x) = \frac{1}{2 \cos \theta} (W(x_W) - W(x)) \quad x \leq x_W. \quad (87)$$

This equation is independent of the penetration depth and the contact length between ski and snow. It can be used to determine the lateral displacement of the moving ski's rear part: in the first iteration step, where the ski's shape is calculated for the case of pure loading, the lateral displacement $L_0(x)$ is determined. The position of the ski's trace is then determined by adding the distance $\Delta L(x)$ to the calculated position of the edge of the ski's rear part ($x < 0$):

$$L_{\text{trace}}(x) = L_0(x) - \frac{1}{2 \cos \theta} (W(x_W) - W(x)) \quad (88)$$

In the succeeding iteration steps an additional factor is inserted in the ski-snow boundary condition, which switches from zero to one if the ski's rear part rests on the surface of the trace. As discussed in chapter 5, the ski-snow boundary may not be implemented as a non-differentiable function. Therefore, the step function introduced in section 5.1.2 as equation 67 was implemented as a function of the lateral ski displacement $L_n(x)$ at iteration step n :

$$L_n(x) = y_0(x) + u_y(x) \quad (89)$$

Thus, the implemented step function for the side cut effect is

$$\text{step}(L_n(x)) = \frac{1}{2} \cdot \left(1 + \tanh \left(\frac{L_n(x) - L_{\text{trace}}(x)}{\varepsilon_{\text{motion}}} \right) \right), \quad (90)$$

where $\varepsilon_{\text{motion}}$ is a transition factor, which has to be smaller than 0.5 mm. All lateral parameters depend on the position x along the ski axis. Particularly the determined position of the ski's trace, $L_{\text{trace}}(x)$ depends on x . $L_{\text{trace}}(x)$ is determined and saved in the first iteration step of the outer iteration loop, and has to be recalled in all succeeding steps. In view of the required calculation time it is not possible to save $L_{\text{trace}}(x)$ for every knot of the boundary surface. Instead $L_{\text{trace}}(x)$ is approximated by a circle function, so that only the quantities radius and position of the centre point have to be saved and recalled. This circle function is determined from three points on the rear part of the ski. With the exception of the ski end and the shovel the deviations between ski edge in the snow and the determined circle function are negligible. After the position of the ski trace has been determined for the ski edge the position of the ski trace for the inner points on the boundary area is determined using equation 76.

Figure 79 displays the calculated shape of a ski model after the first (left) and the tenth (right) iteration step. In the first step the side cut effect calculated by equation 90 is set to one and not displayed. In the second and all following iteration steps the side cut effect is evaluated on the whole model. The picture of the right hand visualizes this factor: on the yellow coloured surfaces it is one, on the black ones zero, between one and zero transition colours are used. Considering the shape of the ski one finds that the ski end after the tenth iteration stays within the snow and the rear part exhibits much less curvature than in the result of the first iteration step. A rotation of the whole ski model, as discussed in section 6.1.3 may also be recognized.

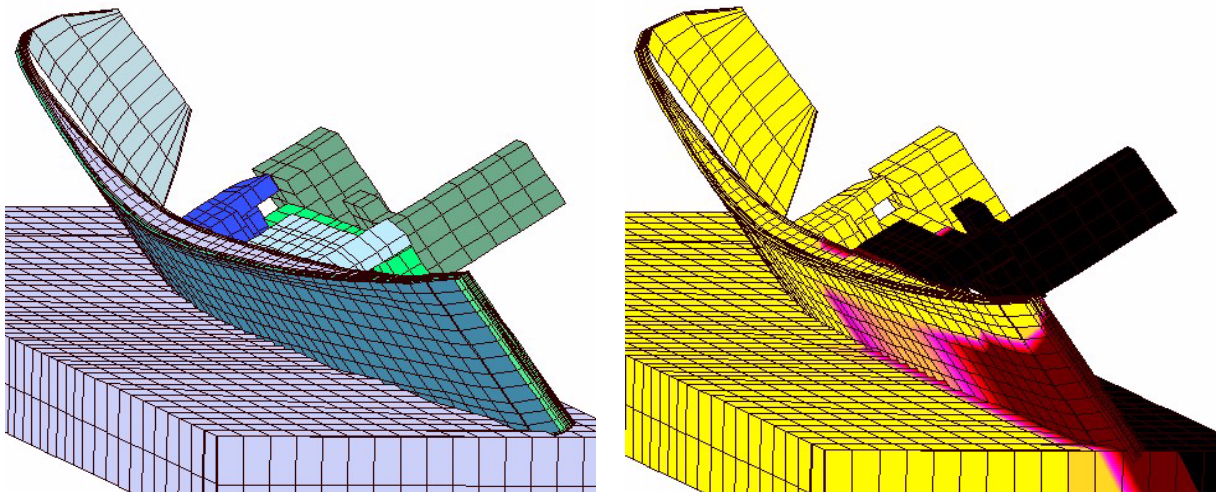


Figure 79. Shape of a turning ski in after the first and the tenth iteration step of the simulation.

6.1.5 Convergence Behaviour of the Simulation

The implementation of the side cut effect severely affects the convergence properties of the simulation. In the second iteration step, when the side cut effect affects the snow resistance function for the first time, a broad region of the ski's rear part does not experience snow resistance in its initial state. Therefore, it can happen that the simulation does not converge to a stable solution in the second iteration step. However, in succeeding steps a stable solution may still be found in spite of the ill-conditioned initial conditions. Nevertheless, the convergence behaviour of the simulation is still one of the main problems in the simulation tool presented here. Especially for very large edging angles ($> 70^\circ$) or for strong moments of force acting on the ski ($> 150 \text{ Nm}$) the simulation usually does not converge to a stable state.

Several modifications were tested in order to improve the convergence behaviour of the simulation. The following measures improved the convergence of the simulation:

- The factor determining if the ski has contact with the snow (equation 90) is implemented as an additional factor only in the x and y coordinates of the snow resistance function. This prevents the ski from sinking deeply into the snow in ill-conditioned intermediate states.
- The transition coefficient ϵ_{motion} in the step function (equation 90) is implemented variable, starting from a very large value of 0.1 m and is reduced in each iteration step down to 0.5 mm for the fifth and the following iteration steps.
- A suitable penetration depth for the initial state of the ski has to be chosen.

6.1.6 Simulation Output

The main output quantities of the simulation are the pressure distribution between ski and snow and the ski's radius. The pressure distribution between ski and snow can be graphically displayed by the SESESTM software. To evaluate the pressure distribution it is often practical to focus on the pressure at the ski edge (see section 6.3).

The ski radius is determined by the curvature of the ski's edge. The radius the ski actually carves corresponds to the radius of the ski's rear part, which glides in the trace generated by the front part of the ski. The ski shovel is more bent due to the snow deformation. Due to the penetration of the edge into the snow the curvature of the ski edge is a three dimensional quantity. However, the turn of the skier and the relevant motion of the skis are always described in the plane of the snow surface. Therefore, the ski radius, which is calculated by the simulation program, corresponds to the radius of the normal projection of the ski edge on the plane of the snow surface⁹. The ski radius was determined from three sample points on the ski edge: a first point at the position of the ski boot, a second point 5 cm in front of the ski end, and a third point in the middle between these two points. The actual shape of the ski edge deviates only slightly from this fit circle. Another possible method to determine the ski radius would be to calculate the curvature of the edge line from the three selected points. In fact, the radius calculated with this method differs from the radius of the fit circle only in the second decimal digit.

6.2 Comparison of Experimental and Numerical Results

6.2.1 Method of an Experimental Verification for the Simulation Results

The main feature of a carving turn is that the ski carves within its own trace, which minimises the energy losses due to the ski-snow interaction. Thus, the radius of the rear part of the ski should coincide with the radius of a circle fitted to the trace in the snow. Comparing the calculated radius of the ski's rear part with the radius of a circle fitted to the ski's trace in the snow allows not only to judge the basic assumptions, which were used to implement the simulation, but also to evaluate the accuracy of the simulation result.

In order to verify the result of the numerical simulation a comprehensive experimental test run was carried out, where all input parameters of the simulation were determined. The input parameters include all characteristics of ski and binding, as well as the external forces and moments acting on the ski. The test run was carried out by a high level ski racer in November 2002 in the ski-dome of Neuss, Germany. Several carving turns defined by gates were performed by a high-level ski racer. The used skis correspond to the ski and binding models described in chapter 4. These skis were additionally equipped with KistlerTM force plates, as described in chapter 2. Two plates were mounted on each ski, one placed between the toe part of the binding and the ski, the other one between the heel part of the binding and the ski. The KistlerTM plates recorded the forces acting between ski and binding. The measurement results are presented in chapter 2. At the same time the skier's motion was filmed with two digital high speed cameras with fixed camera perspectives. The cameras, the calibration methods, and the determined positions, velocities, and accelerations obtained from the video analysis of two turns of the test run are also presented in chapter 2. The trajectories of the skis were approximated by the positions of the skier's ankles, since they can be determined with higher precision in the video analysis¹⁰. The obtained positions are flawed with an estimated measurement error of up to 0.18 m (as discussed in section 2.2.3.6). Figure 80 displays the

9. Most other publications used the same projection when they define a ski radius, e.g. [46], [49].

10. The radii determined for the skier's ankles are a good approximation for the actual turn radii of the skis. The lateral difference between the position of the skier's ankle and his skis during the turn (due to the inclination of the skier) decreases the radius of the ski's trajectories by less than 10 cm.

measured trajectories of the skier's ankles projected to the plane of the snow surface. Additionally to the video analysis, the trace left behind by the two skis was determined in 30 sampling points in a high precision geometrical measurement. The positions of the sampling points was also projected to the plane of the snow surface and added to the graph in Figure 80.

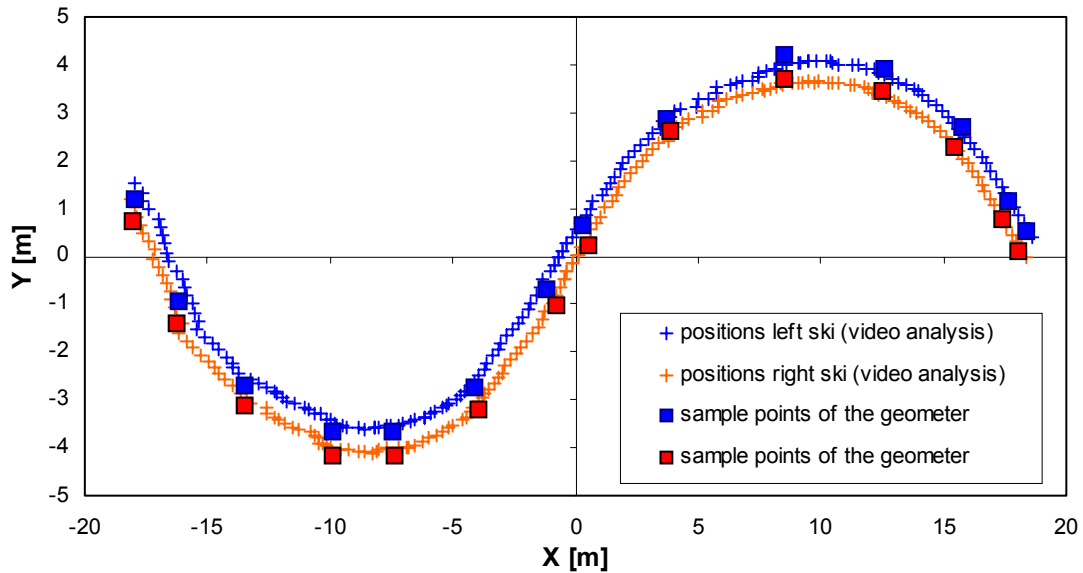


Figure 80. Trace of the ski projected to the plane of the snow surface. The dots indicate measurement points from video analysis (+) or from geometrical measurements (squares).

To complete the set of input parameters the snow properties were characterized with several Agenvis measurements. The characteristic parameters of the snow, the coefficients A , B , and C , were determined and are summarized in Tabelle 5, „Characteristic parameters of the snow resistance in the ski dome of Neuss, Germany in November 2002.“, auf Seite 102. Since the test runs were performed in an indoor snow dome the snow properties did not change significantly during the day. To prevent changes in the snow strength due to earlier runs a new course was marked for the run analysed here.

Table 5. Characteristic parameters of the snow resistance in the ski dome of Neuss, Germany in November 2002.

	A	B	C
edging angle < 40°	6.6 kPa/mm	65 kPa	150 kPa/mm
edging angle >= 40°	0.5 kPa/mm	65 kPa	150 kPa/mm

6.2.2 Determination of the Turn Radius

The projection of the path of the skis displayed Figure 80 coincides with the trace of the skis, which remained in the snow after the skier had completed his run. As a first characterisation of the two turns the overall turn radius was determined by fitting a circle function to the data points using an iterative non-linear least squares algorithm. The resulting mean turn radii are summarized in Table 1. The trajectories of left and right ski are in a very good approximation

circular during the two turns (see Figure 81). The coefficient of determination R^2 for a circular function was 0.98 or higher.

Table 6. Overall turn radii determined for the trace of the left and right ski.

	right turn	left turn
right ski	11.09 +/- 0.12 m	13.40 +/- 0.15 m
left ski	10.61 +/- 0.08 m	13.95 +/- 0.10 m

However, also a parabolic function fits equally well to the data ($R^2 > 0.98$). But the radius obtained from the curvature of the parabolic function obviously differs strongly from the constant radius obtained from the circular fit. In order to compare the simulated ski radius to the radius of the trace a more precise analysis is necessary. Therefore, the instantaneous radius of the skis' trace was determined. Several analysis methods were evaluated¹¹. In all reviewed methods the calculated instantaneous radius of the skis' path is very sensitive to any error source and strong smoothing of the data is necessary. In this thesis the instantaneous radius was calculated by the following procedure (also refer to Figure 81):

1. First the initial data points (indicated by crosses in Figure 81) were scrutinised to sort out deviant points, which disagreed with the general trend of the curves. Such deviations occur due to a slight mispositioning of markers in the video analysis procedure. The selected measurement points are marked by a small circle in Figure 81.

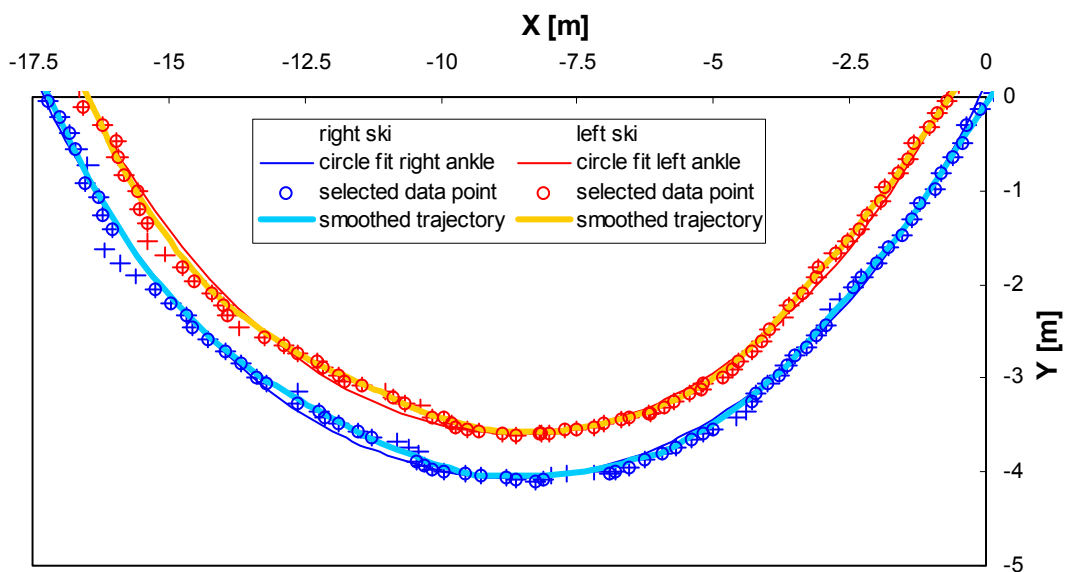


Figure 81. Measured (+) and selected (o) positions of the left and right ankle during the first turn. The overall turn radius determined for each trace is indicated as a thin line, the smoothed data curve, which was used to determine the instantaneous radius is indicated as a thick line.

11. For example, Mössner et al. [12] used the following equation, which could not be applied in this case due to the high error amplification in the numerical differentiation necessary to obtain the

velocity and acceleration values (as discussed in chapter 2):
$$R = \frac{(\dot{X}^2 + \dot{Y}^2)^{3/2}}{\dot{X}\ddot{Y} - \ddot{X}Y}$$

2. The curves were smoothed by averaging over nine neighbouring measurement points (thick line in Figure 81).
3. For each point on the smoothed data curve a circle function was determined using the third neighbouring points to the right and to the left. Thus, for each measurement point the mean radius was determined from a smoothed section of the trace of about 1.5 to 1.8 m length.

Figure 82 displays the instantaneous turn radius and the mean turn radius determined for the right and left ski during the two analysed turns. As expected, very high radii were obtained for transition phase between the two turns, in which the skier shifts his body and changes the ski edges (see chapter 2). The mean turn radius changes in the moment in which the ski is flat on the snow surface.

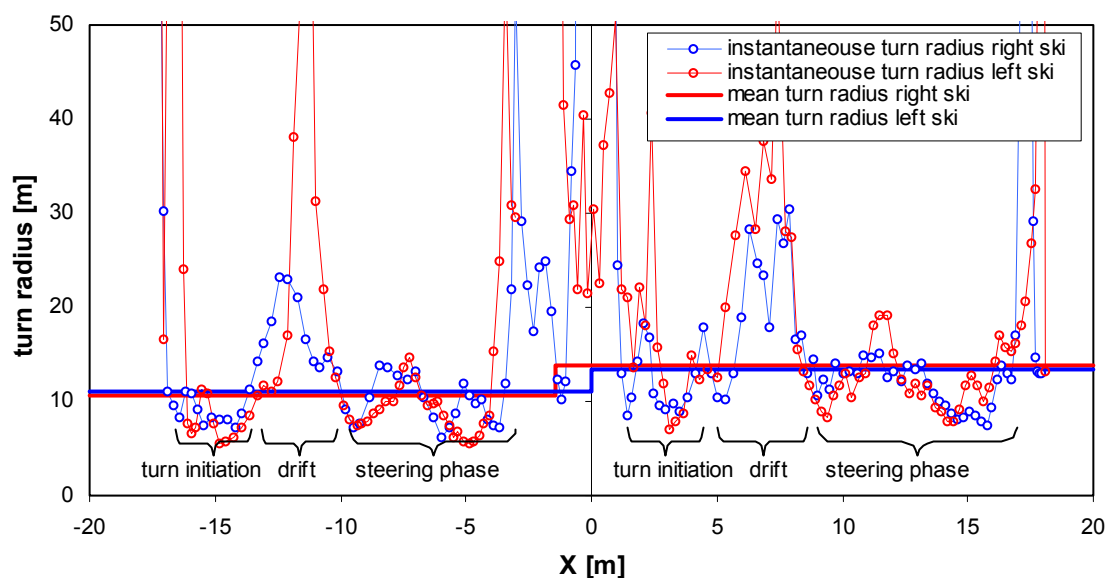


Figure 82. Comparison of the instantaneous and the mean turn radius.

The instantaneous turn radius indicates a turning characteristics of the skier, which was not noticed before: after the turn initiation the skier drifts a few meters before continuing the turn with true carving. This feature is visible in both analysed turns and was confirmed in a discussion of the video sequences with a former ski trainer on national level [146]. During the steering phase of the turn the skier carves with an instantaneous turn radius which is up to 45% lower than the mean turn radius determined for the overall turn.

6.2.3 Comparison of the Calculated Ski Radius and the Measured Trace's Radius

Since all input parameters of the simulation have been determined as a function of time it is possible to calculate the shape of the ski at a given point of time and compare it with the shape of the trace at that point. The employed numerical ski-binding model was implemented according to the specifications given by the ski and binding manufacturers. The Kistler™ measurement plates used in the tests also had to be included in the numerical model. The forces and especially the moments of force measured by the Kistler™ plates, which determine the boundary condition on the binding model, show strong fluctuations during the turn (see chapter 2). However, smoothing of the data before using it as input for the simulations rather

increased the differences between measured and calculated radii. Therefore, no data smoothing was used. Thus it becomes more obvious in which situations the simulation does not converge to a solution and when strong deviations between calculated ski shape and measured trace occur.

Figure 83 displays the instantaneous turn radius as calculated in the last section. For several points of time the ski radius was calculated by the simulation and the result added to the graph (blue and red squares). For most parts of the two turns the calculated ski radii fit well to the instantaneous turn radii. Strong deviations are visible for the phase of the turn where the skier drifted. In this phase, the assumption of ideal carving, which was used on several occasions in this thesis, e.g. the determination of the edging angle (see section 2.2.3), is not applicable. In the first turn some deviations are also visible in the initiation phase, In this phase the measured force on the binding fluctuates strongly (see Figure 31), which might explain the discrepancies. In the steering phase, in which the skis actually carve, the best agreement of simulation and turn radius is achieved.

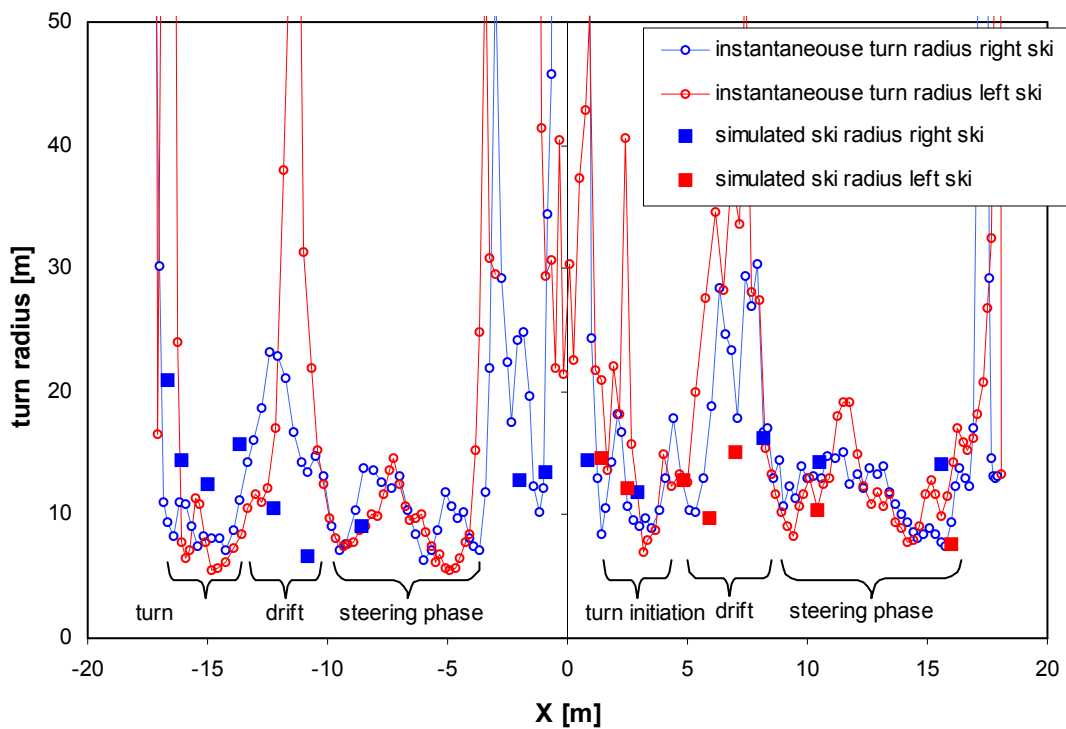


Figure 83. Simulated ski radii (squares) compared to the instantaneous turn radius determined from the skis' trajectories.

The calculation of the turn radius for several time steps in the considered turns showed some limitations of the implemented FEM simulation: Firstly, at large edging angles ($> 65^\circ$) the simulation does not converge to a stable solution. This occurs due to the strong shift of the ski between the first and second iteration step because of the side cut effect in the ski-snow boundary function as explained in section 6.1.4 and section 6.1.5. Therefore, no radii could be determined at X values between -7 and -3 m, and between 12 and 15 m. Secondly, strong moments of force (> 150 Nm) acting on the ski sometimes cause the simulation not to converge (as mentioned in section 6.1.5).

6.3 Results obtained with the Simulation

6.3.1 Influence of Different Turn Parameters on the Actual Ski Radius

The parameters, which are expected to have a distinct impact on the ski's turn radius are the ski's side-cut, its bending and torsional stiffness, the edging angle, the total load on the ski binding, the moment of force acting on the ski binding, the way of force transfer from the binding to the ski (i.e. the binding mechanism), and the snow strength. The simulation tool presented in this thesis allows to analyse and compare the impact of these parameters on the radius of a turning ski independently of other turn parameters. In actual turns all parameters change simultaneously (see chapter 2) and thus the impact of a single parameter on the turn radius is very difficult to quantify. The following study of how single turn parameters affect the turn radius of the ski was conducted using the FE model of a Stöckli Spirit ski equipped with a Fritschi Powerride binding, which was used for the verification in section 6.2.

6.3.1.1 Influence of the Edging angle on the Ski Radius

It is obvious that the edging angle θ of a ski has a pronounced impact on the turn radius. For a purely static approach the radius of a carving ski was estimated by Howe¹² [8]:

$$R_{\text{Howe}} = \frac{L^2}{8 \left[\frac{(W_S + W_T - 2W_W)}{4 \cdot \cos \theta} + d \cdot \sin \theta \right]} \quad (91)$$

where W_i denotes the ski's width at the shovel ($i=S$), tail ($i=T$), and waist ($i=W$). L denotes the length between ski shovel and ski tail. The investigated ski had the following properties: $L = 1.55$ m, $W_S = 11.7$ cm, $W_T = 9.97$ cm, and $W_W = 6.7$ cm. The coefficient d denotes the maximum penetration depth of the ski into the snow. Howe does not take into account, that usually d also depends on the edging angle θ .

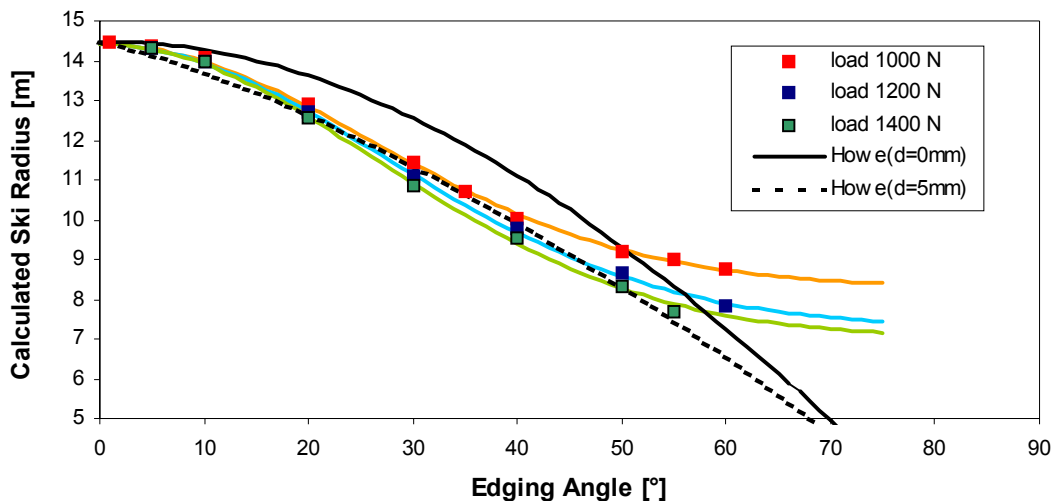


Figure 84. Calculated ski radius as a function of the edging angle of the ski for three different normal loads on the binding on a soft snow surface. For comparison Howe's approximation for the turn radius is added.

12. Several other publications rely on this equation, e.g. [46], [49].

Figure 84 displays the calculated ski radius for edging angles between 5° and 60° on soft snow for three different loading forces acting normal on the binding. The characteristics of the curves do not agree with Howe's function. For large edging angles the calculated turn radii level out and do not decrease as Howe predicts. The calculated ski radii fit very well to a Gauss curve, which has the form of

$$R = R_0 + H \cdot \exp\left(-2\left(\frac{\theta}{w}\right)^2\right). \quad (92)$$

where $(R_0 + H)$ corresponds to the maximum radius of the ski, which is determined by its side cut, and R_0 is a minimum radius to which the function converges for high edging angles. w indicates the width of the bell-shaped gauss curve. For the three curves displayed in Figure 84 the coefficients of the Gauss curve are summarized in Table 7.

Table 7. Coefficients of the Gauss fits on the ski radius as a function of the edging angle.

load	1000 N	1200 N	1400 N
R_0	8.31	7.29	7.03
H	6.10	7.12	7.39
w	51.58	54.01	52.92

Equation 92 for the turning radius in dependence of the edging angles fits much better with field observations: For the test run analysed for this study edging angles of more than 70° were found (Figure 24). For the skis used the approximated turn radius calculated according to Howe would be 4.95 m ($d = 0$ m), or 3.57 m if the penetration of the ski is taken into account ($d = 2.5$ cm). However, the minimum turn radius derived from the trace of the skis is in the order of 6 m (Figure 84). Especially for large edging angles Howe's static approximation does not give a good estimation of the actual turning radius of a ski in motion.

6.3.1.2 Influence of the Normal Load on the Ski Binding on the Ski Radius

The numerically calculated turn radius also depends on the load on the ski binding. Figure 85 displays the turning radius as a function of the normal load on the ski binding for four different edging angles on a soft snow surface. As the load increases the actual ski radius and the minimum radius determined by equation 92 decreases (see Tabelle 7, „Coefficients of the Gauss fits on the ski radius as a function of the edging angle.“, auf Seite 107). Within the range of loads, which are typical for skiing, the radius of a turning ski is in a good approximation a linear function of the loading force acting on its binding.

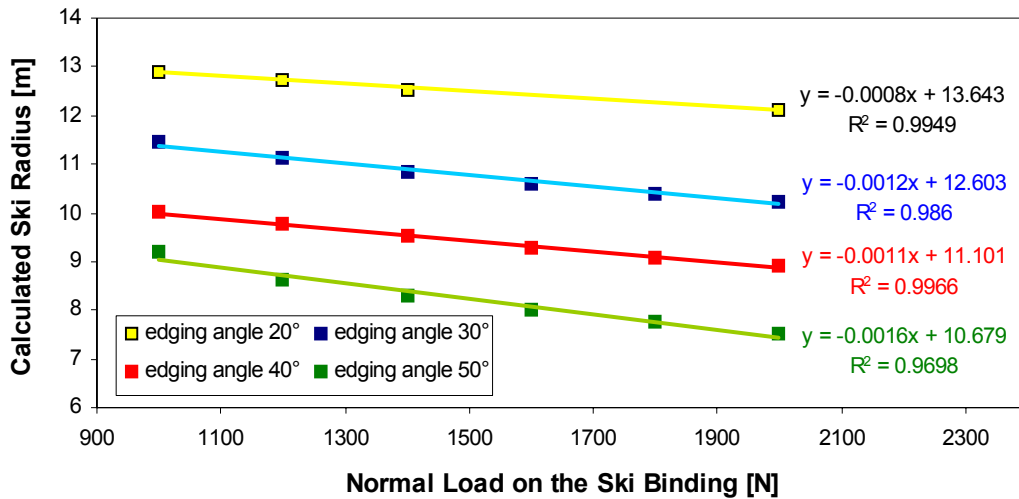


Figure 85. Calculated ski radius as a function of the normal load on the ski binding for edging angles of 20°, 30°, 40°, and 50° on a soft snow surface.

6.3.1.3 Influence of the Snow Resistance Strength on the Ski Radius

The snow investigated on the skiing slopes exhibits a broad range of resistance strengths. In section 3.5 typical coefficients of the snow resistance function for soft, average, and hard snow types were compiled (Tabelle 4, „Coefficients of the snow resistance function for three typical snow conditions.“, auf Seite 64). The previously presented examples in this section were all calculated for the soft snow type as specified in Tabelle 4, „Coefficients of the snow resistance function for three typical snow conditions.“, auf Seite 64. Figure 86 displays the turning radius of the ski as a function of the edging angle for the soft, average and hard snow types. For comparison the approximation by Howe (equation 91) is also included in the graph.

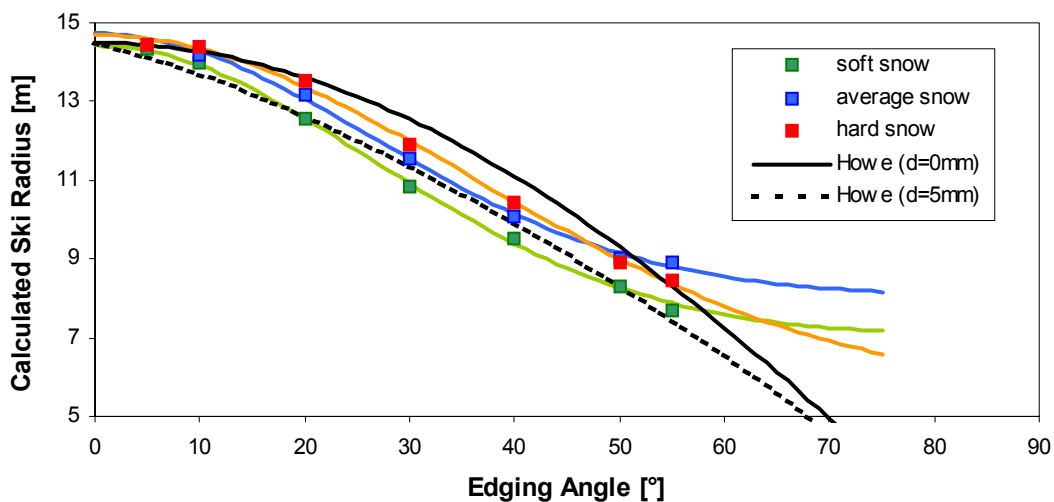


Figure 86. Turning radius of the ski as a function of the edging angle for three different snow strengths. The loading force on the binding was 1400 N, normal to the ski surface.

The ski radius as function of the edging angle can be fitted by a Gauss function for all three types of snow. It can be noted that on hard snow the characteristics of the curve changes compared to the soft and average snow types. For edging angles between 10° and 40° the

calculated ski radius exceeds the turn radii determined for the softer snow types. This effect is expected: the deeper the waist of the ski can penetrate the snow, the narrower the ski radius will be. For edging angles above 50° , however, a different mechanism governs the ski-snow interaction: For high edging angles a high minimum force is necessary just to bend the ski so far that the waist gets into contact with the snow. This force is transferred into the snow at the ski shovel and the ski end. If the snow strength is low, the snow will already yield at the ski's shovel and end before the ski's waist is even in contact with the snow. This yielding reduces the ski's bending and thus increases the turn radius. In the limiting case of an infinite hard snow surface the calculated ski radius would align with Howe's function for $d=0$ (equation 91).

6.3.2 The Pressure Distribution between Ski and Snow

The pressure distribution between ski and snow is the best indicator of the ski snow interaction. However, it is very difficult to measure experimentally. The simulation program presented in this thesis calculates the pressure distribution between ski and snow such that the integral of the pressure equals the sum of all other external forces acting on the ski (equation 70). The calculated pressure distribution on the undersurface of the ski is on the one hand governed by the experimentally determined snow resistance function, which depends on the penetration depth in the snow. On the other hand, it depends on the stiffness of the ski-binding system, which determines how much pressure is transferred to the front and rear parts of the ski.

Figure 87 displays the calculated pressure distribution on the undersurface of the ski for soft snow (on the left) and hard snow (on the right). The actual contact area between ski and snow is large on soft snow, while on hard snow basically only the ski edge is in contact with the snow. Due to the implementation of the hysteresis in the snow resistance function (section 6.1.2) and the side cut effect (section 6.1.3) the surface width of the contact area is nearly constant towards the ski end, even though the pressure is significantly reduced. Due to the larger contact area on soft snow slopes the observed pressures are much smaller than on hard snow. The maximum snow pressure calculated for the case of the ski in Figure 87 is 93 kPa for soft snow and 507 kPa for the hard snow slope.

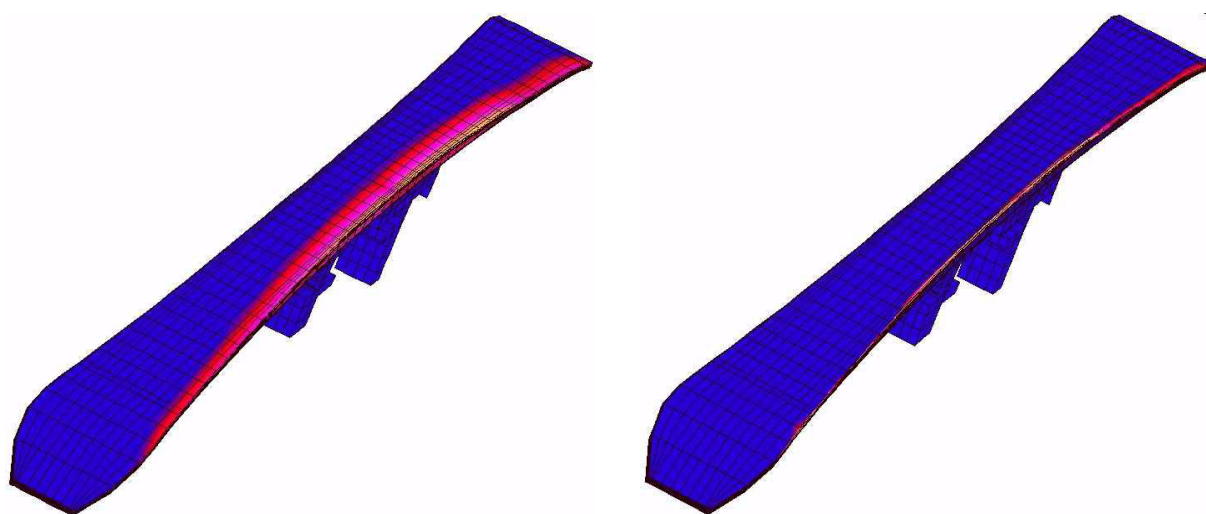


Figure 87. Pressure distribution on the undersurface of a turning ski for an edging angle of 50° and a normal loading force of 1400 N. On the left the simulation was calculated for soft snow, on the right for hard snow.

For a detailed analysis the pressure distribution on the lower ski edge is better suited. Figure 88 displays the snow pressure on the ski edge for a turning ski at edging angles of 30° (left) and 50° (right). In both cases the ski was loaded with a normal force of 1400 N on the binding. The pressure distribution is displayed for the three snow types, which were classified in Tabelle 4, „Coefficients of the snow resistance function for three typical snow conditions.“, auf Seite 64 of section 3.5.

For both edging angles the maximum pressures are found in the waist of the ski, where the binding is mounted. Secondary pressure maxima are visible at the ski shovel and the ski end. These pressure maxima arise from the ski's camber. As the edging angle is increased the pressure at the ski shovel and the ski end increases and the pressure distribution over the whole ski edge levels out.

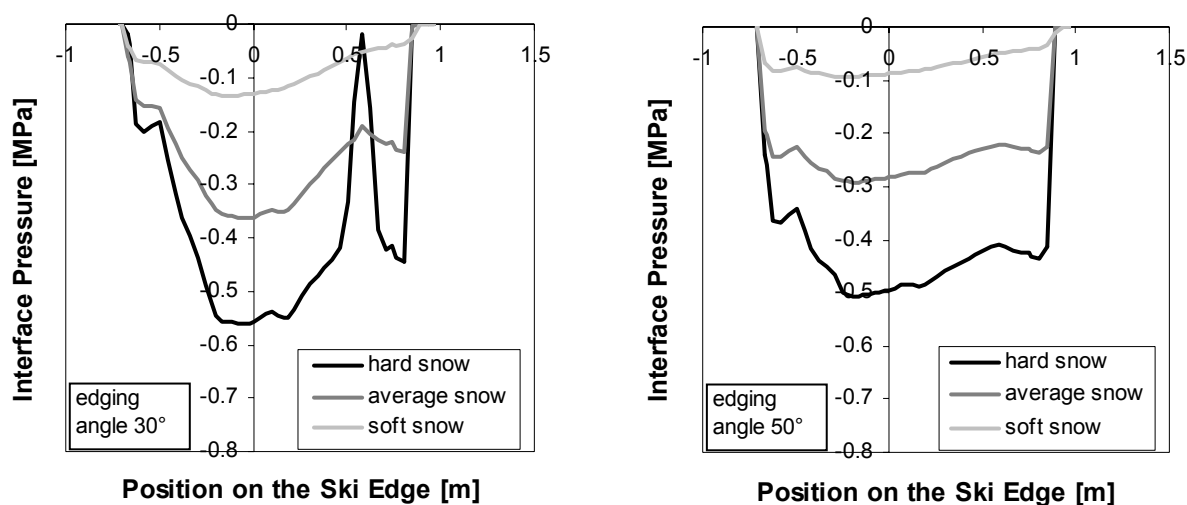


Figure 88. Pressure distribution on the ski edge for a turning ski with an edging angle of 30° (on the left) and 50° (on the right).

Considering the ski-snow interaction, which has been studied in chapter 3 an optimal pressure distribution on the ski edge may be postulated: The pressure maximum has to be in the mid-section of the ski, such that the load of the skier on the binding is directly supported by the snow. From ski shovel towards the binding the pressure should continuously increase: as the ski moves over the snow the trace within the snow has to be formed. If the trace is deep enough, the snow is able to support the load due to the skier as the mid-section of the ski passes over it. High gradients of pressure, which occur if sections of the ski have little or now snow contact (as visible in Figure 88 for a ski edged with 30° on a hard snow surface), should be avoided. Strong gradients of pressure will force the ski to penetrate rapidly into the snow, because only in a given depth enough snow resistance pressure is generated which is able to counter the loading pressure. The more rapid this penetration proceeds, the more likely a failure can occur on the snow side, which would lead to skidding, or in a worst case, to the fall of the skier.

Regarding the results of the calculated pressure distribution on the ski edge shown in Figure 88, the ski-binding system studied in this thesis (a Stöckli Spirit ski equipped with a Fritschi Powerride binding), which is intended for recreational skiers, is best suited for soft snow skiing conditions.

7. Conclusions and Outlook

7.1 Summary

This work presents the development of a simulation tool which calculates the shape of a ski in the situation of a carved turn. This was done in three main steps:

In the first step a comprehensive kinematic and kinetic analysis of two sample turns of a characteristic test run was performed. For the kinematic analysis of the turn a video analysis system was used, which allowed to trace 18 reference points of the skier's body. With the traced body segments the position of the skis and of the skier's centre of mass, as well as the skis' edging angles were determined. The kinetic analysis was carried out using force sensor plates placed between ski and binding. With these plates it was possible to determine the total force as well as the moment of force transferred from the bindings onto the skis. The comprehensive determination and analysis of the turn parameters provides the first part of the necessary input for the ski simulation.

In a second step the interaction between snow and ski was investigated. The interaction comprises two processes: friction and penetration into the snow. Friction between ski and snow has been analysed in several other studies, which are reviewed in chapter 3. In contrast to friction, the penetration process of a ski into the snow has so far only been investigated in very few publications. In order to experimentally study this penetration process two new measurement devices - „Agervis“ and „Fast Snowdeformer“ - were developed. With these devices the resistance pressure to a penetrating and then retrieving plate was measured, whereby an empirical function for the snow resistance pressure could be derived. This function contains three coefficients, which characterise the snow strength. The determination of the function for the snow resistance pressure completes the necessary input parameters needed for the simulation.

The third step comprised the implementation of the finite element model of a ski and the set up of boundary conditions for the situation of a carved turn. This step was split into three parts: First, the governing equations used in the finite element simulation software, SESETM, were summarized and the finite element models of ski and binding were described. In the second part, the boundary conditions for a turning ski were implemented for a static situation. In this case the ski is in a steady state. Thus boundary conditions are less complicated and the simulation results can be verified with simple static measurements. The third part covers the simulation of an actually moving ski. Thereto, an approach assuming a steady state, in which the external forces and the inertia forces of the ski are in equilibrium, was chosen. Due to the ski's motion the boundary condition describing the ski-snow interaction needs two major modifications: first, the snow experiences not only loading, but also unloading as the ski passes. This was incorporated in the model by the implementation of a hysteresis in the snow resistance function. Second, the rear part of a carving ski glides in the trace created by the ski shovel. This was incorporated in the ski-snow boundary condition as an additional factor, which causes the ski model to rotate into a position where the ski is in contact with the trace. For a verification of the simulation the measured radii of a ski trace were compared to the radii calculated with the ski's finite element model for the same turn. The turn parameters determined in step one and the snow reaction function derived in step two provided the necessary input data. Within the steering phase of the turn, in which the skis carved and a steady-state can be assumed, the calculated ski radii fit well to the instantaneous turn radii determined from the ski's trace. Finally, the simulation tool was used to analyse the impact of selected parameters on the turn radius of a moving ski.

7.2 Conclusions

Each of the three steps of the current thesis allows to draw separate conclusions:

1. Experimental Measurement of Turn Parameters

- For a full kinematic and kinetic evaluation of a carved turn two measurement devices are sufficient to obtain the necessary data, namely a video analysis system and force sensor plates.
- A video analysis system allows a full kinematic analysis, however, for differentiated values high measurement errors have to be accepted.
- For the measurement of the forces and moments transferred between ski and binding of each individual ski, force plates should be employed. Video analysis and pressure insoles are not capable of yielding all results with high enough precision.
- The ski's actual edging angles can be determined by video analysis with an accuracy of 5° .
- The turn parameters, determined for the test run analysed in this work, agree in general with the findings of previous studies.

2. Investigation of the Ski-Snow Interaction

- The mean resistance pressure of the snow on a penetrating plate varies linearly with the penetration distance.
- Since the snow deformation is a non-reversible process, the snow resistance function exhibits a strong hysteresis. The function can be parameterised using three coefficients A , B , and C .
- The three coefficients A , B , and C depend on the edging angle and the snow type. Within the range of deformation speeds typical for skiing, the dependence of the three coefficients on the deformation speed is negligible.
- On actual skiing slopes all three coefficients A , B , and C can be determined with the newly developed test device „Agenvis“.

3. Implementation of the Finite Element Model of a Carving Ski-Binding System

- The numerical results for mechanical deformations of the ski without binding were compared with experimental findings. In bending tests deviations in the order of 15%, in torsion test deviations of about 20% are found. Furthermore, the pressure distribution between a loaded ski model and a flat underlay was calculated. The numerical result fits well with the measured curves for actual skis.
- The ski-snow interaction can be implemented as a boundary condition on the numerical ski model. Then the pressure distribution between ski and snow and the deformation of the ski can be calculated with an iterative solving algorithm.
- The numerical results for the snow pressure on a penetrating plate and for a static ski deformation were verified by comparison to experimental findings.
- In order to simulate a carving ski in motion two effects have to be taken into account:
 1. If the pressure at the ski-snow interface decreases, the snow is effectively unloaded. Therefore, the hysteresis in the snow pressure function has to be incorporated in the boundary condition of the numerical ski model. This ensures that the correct snow penetration depth is calculated.

2. As the ski moves on the snow surface a trace in the snow is formed by removal of snow. When simulating a ski in motion it is necessary to ensure, that the ski's tail glides on this trace. Therefore, the boundary condition on the ski has to incorporate a factor, which determines if a point on the boundary surface is in contact with the snow, and thus experiences snow pressure, or if it rests above the trace, and thus does not experience snow resistance pressure.

- The simulation model which incorporates these two effects is able to predict the turn radius of a ski.
- The finite element simulation of a turning ski allows to study the influence of individual parameters on a carved turn. By studying the impact of the ski's edging angle on the turn radius, a disagreement with Howe's theory was uncovered: For a ski moving on a snow slope the calculated turn radius starts to level out at angles above 50° . Howe's theory predicted a continuous decrease. Only for the limiting case of an infinitely hard snow surface the calculated turn radius would align with Howe's theory. The dependence of the turn radius on the load applied to the ski binding is nearly linear.
- The pressure distribution at the ski snow interface is an indicator of the ski-snow interactions. For increasing edging angles the pressure along the ski edge increasingly levels out. A study of the pressure distribution on the ski edge offers a new evaluation method to assess the performance of ski-binding systems.

7.3 Outlook

The findings in this thesis for each of the three steps offer opportunities for applications, further developments, and further research:

1. Kinematic and Kinetic Analysis

The purpose of the kinematic and kinetic analysis of turn parameters was to obtain a consistent set of input parameters for the simulation in two sample turns. Starting from this valid set of parameters further studies can be carried out to investigate specific interrelationships of the input parameters, for example, by modifying the snow strength, or by assuming a different mass of the skier. The kinematic and kinetic analysis presented here was only carried out for two turns of a giant slalom run performed by a high level ski racer. The investigation of other types of turns as well as turns performed by skiers of different skill offers an interesting field for further studies.

2. Deformation Properties of Snow

The empiric function for the snow resistance pressure introduced in this thesis provides an accurate description for the penetration of skis into snow. It may also be used to describe other interaction processes with snow, for example, the interaction of other sports equipment, of snow boots, of winter tyres, or sledges with snow. The characterisation of the snow resistance was strongly orientated on the application for the numerical ski model. Manifold physical deformation processes were observed in the snow, among them elasticity, fracture and compaction mechanisms, and resintering. These processes can also occur in other rapid interaction processes involving snow. Thus, these processes offer an interesting field for further scientific studies.

3. Developed FEM Simulation of a Ski-Binding System in a Carved Turn

Applications

- The simulation tool developed in this thesis can be employed by ski and binding manufacturers to evaluate the design of new skiing equipment. It was designed to allow easy modifications of the ski and binding models. Thus offering the opportunity for equipment manufacturers to evaluate new designs before performing the expensive prototyping and testing cycles. To reach this goal, a more user-friendly program surface would be useful. Work towards this goal is in process.
- A major advantage of the simulation tool developed in this theses compared to previously developed tools is the incorporation of the binding, which allows detailed studies of the ski-binding interrelationship and may lead to better harmonised system solutions.
- A systematic investigation of the interrelationship between different turn parameters is possible with the presented numerical model. For example, the influence of the edging angle, the load on the system, or the snow properties on the ski radius can be studied in detail. Especially the interaction between a binding system and the ski has so far rarely been studied due to the lack of appropriate evaluation methods. The presented simulation tool can to some extent close this gap.
- Based on the former investigation guidelines for an adjustment of the skiing equipment to different snow conditions or different athletes can be derived. Thus, the simulation tool may help athletes and coaches to select skiing equipment, which is best suited to the athlete's body characteristics and skill. Especially for young athletes, whose skill and body weight change quickly, it is often a difficult task to select the most suitable ski.

Possible Extensions

- The model presented here is based on the assumption of an absence of vibrations of the ski-binding system during the turn. However, in actual turns vibrational effects are assumed to significantly alter the ski-snow interaction and thus the whole turning process. However, a dynamic simulation of the ski-binding system in a turn is a difficult task. As a first step towards a dynamic analysis, the damping properties of the ski-binding system on the snow surface could be investigated starting from the calculated quasi-static equilibrium state calculated by the simulation tool presented here.
- The finite element simulation program is only applicable for carved turns. An extension for skidded turns would significantly enlarge the field of applications.
- The forces and moments transferred by the athlete onto the binding have been determined experimentally for the purpose of this thesis. However, a biomechanical body model of a skier could also provide this input data. Coupling such model to the simulation tool presented here would allow further studies of the biomechanics of skiing and the interaction of the athlete with his equipment.

8. References

- [1] Lind D., Sanders S.P.: „*The Physics of Skiing – Skiing at the Triplepoint*“; Springer-Verlag, ISBN 1-56396-319-1, (1996).
- [2] International Skiing History Association: <http://www.skiinghistory.org>
- [3] International Ski Federation: <http://www.fis-ski.com>
- [4] International Society for Ski Safety (ISSS): <http://www.ski-injury.com/iss.htm>
- [5] International Sports Engineering Association (ISEA):
<http://www.sportsengineering.org>
- [6] Schultes H.: „*Principles of Modern Alpine Ski Design*“; Olin Ski Company, Middletown, USA. (1977).
- [7] Howe J.: „*Skiing Mechanics*“; Poudre Press, Laporte, CO, USA. (1983).
- [8] Howe J.: „*The New Skiing Mechanics*“; McIntire Publishing, Waterford, ME, USA. (2001).
- [9] Glenne B., VonAllmen B.: „*Biomechanics and Kinesiology of Alpine Skiing*“; Skiing Trauma and Safety: Third International Symposium, ASTM STP 1104, American Society for Testing and Materials, Philadelphia. (1982). p. 50-57.
- [10] Fetz F., Müller E.: „*Biomechanik des alpinen Skilaufs*“; Biomechanik der Sportarten, Band 2; Ferdinand Enke Verlag Stuttgart. ISBN 3-432-98681-5. (1991).
- [11] Schöllhorn W., Müller E., Lindinger S., Raschner C., Schwameder H., Benko U.: „*Individuality and Generality in Ski Turn Techniques*“; 2nd International Congress on Skiing and Science, January 9-15, 2000, St.Christoph am Arlberg, Austria, Verlag Dr. Kovac. (2000). p. 69-83.
- [12] Mössner M., Nachbauer W., Schindelwig K.: „*Einfluss der Skitailierung auf Schwungradradius und Belastung*“; Sportverletzung Sportschaden 11. (1997). p. 140-145.
- [13] Niessen W., Müller E.: „*Carving - biomechanische Aspekte bei der Verwendung stark taillierter Skier und erhöhter Standflächen im alpinen Skisport*“; Leistungssport 1. (1999).
- [14] Johnson J., Natri A., Shealy J., Ettliger C.: „*A Three Year Study of Shaped Skis*“; 2nd International Congress on Skiing and Science, January 9-15, 2000, St.Christoph am Arlberg, Austria. (2000). (abstract book) p. 52.
- [15] Raschner C., Schiefermüller C., Zallinger G. Hofer E., Müller E., Brunner F.: „*Carving Turns versus Traditional Parallel Turns - a Comparative Biomechanical Analysis*“; 2nd International Congress on Skiing and Science, January 9-15, 2000, St.Christoph am Arlberg, Austria, Verlag Dr. Kovac. (2001). p. 203-217.
- [16] Yoneyama T., Kagawa H., Okamoto A., Sawada M.: „*Measurement of the Joint Motion in the Carving Ski Turn in Comparison with the Normal Ski Turning Motion*“; 2nd International Congress on Skiing and Science, January 9-15, 2000, St.Christoph am Arlberg, Austria, Verlag Dr. Kovac. (2001). p. 218-231.

- [17] Burtscher M., Raschner C., Zallinger G., Schwameder H., Müller E.: „*Comparison of Cardiorespiratory and Metabolic Responses During Conventional and Carving Skiing*“; 2nd International Congress on Skiing and Science, January 9-15, 2000, St.Christoph am Arlberg, Austria, Verlag Dr. Kovac. (2000). p. 552-565.
- [18] Glenne B., Perla R. et.al.: „*Skiing*“; chapter 19 in "Handbook of Snow", edited by Gray D.M., Male D.H.; Pergamon Press, ISBN 0-08-025375-X. (1981). p. 709-740.
- [19] Glenne B.: „*Mechanics of Skis*“; chapter 20 in "Handbook of Snow", edited by Gray D.M., Male D.H.; Pergamon Press, ISBN 0-08-025375-X. (1981). p. 741-765.
- [20] Glenne B., DeRocco A., Vandergrift J.: „*The Modern Alpine Ski*“; Cold Regions Science and Technology 26. (1997). p. 35-38.
- [21] Gibson L. J., Ashby M.F.: „*Cellular Solids - Structure & Properties*“; Oxford Pergamon Press, ISBN 0-08-036607-4. (1988). p. 252-269.
- [22] Scherrer P., Bidaux J.-E., Kim A., Manson J.-A.E., Gotthardt R.: „*Passive Vibration Damping in an Alpine Ski by Integration of Shape Memory Alloys*“; Journal of Physics IV France 9. (1999). p. 389-393.
- [23] Casey H.: „*Materials in Ski Design & Development*“; Materials and Science in Sports, TMS (The Minerals, Metals & Materials Society). (2001). p. 12-17.
- [24] Nigg B., Schwameder H., Stefanyshyn D.: „*The Effect of Ski Binding Position on Performance and Comfort in Skiing*“; 2nd International Congress on Skiing and Science, January 9-15, 2000, St.Christoph am Arlberg, Austria, Verlag Dr. Kovac. (2000). p. 3-13.
- [25] Schwameder H., Nigg B., Tscherner V.v., Stefanyshyn D.: „*The Effect of Binding Position on Kinetic Variables in Alpine Skiing*“; 2nd International Congress on Skiing and Science, January 9-15, 2000, St.Christoph am Arlberg, Austria, Verlag Dr. Kovac. (2000). p. 43-54.
- [26] Neuwirth S., Biesse P., Peter G.: „*Die Auswirkungen von Fersenerhöhungen bei Bindungen von Alpinski*“; diploma thesis at the Institut für Bewegungs- und Sportwissenschaften, ETH Zürich, Switzerland. (2001).
- [27] Müller B.: „*Experimentelle Erfassung des Einflusses von unterschiedlichen Platten und Bindungen auf die Flächendruckverteilung eines Ski*“; diploma thesis at the Institut für Bewegungs- und Sportwissenschaften, ETH Zürich, Switzerland, (2003).
- [28] Mester J., Hartmann U., Hoffmann U., Seifriz F., Schwarzer J., Spitzenpfeil P.: „*Biological Response to Vibration Load: General Principles, Lab and Field Studies in Alpine Skiing*“; 2nd International Congress on Skiing and Science, January 9-15, 2000, St.Christoph am Arlberg, Austria, Verlag Dr. Kovac. (2000). p. 325-344.
- [29] Schwarzer J., Spitzenpfeil P., Mester J.: „*Physical Assessment and Quantification of Vibration Load- Analysis of Potential Risks: Vision as an Example*“; 2nd International Congress on Skiing and Science, January 9-15, 2000, St.Christoph am Arlberg, Austria, Verlag Dr. Kovac. (2000). p. 345-352.
- [30] Niessen W., Müller E., Raschner C., Schwameder H.: „*Structural Dynamic Analysis of Alpine Skis During Turns*“; First International Congress on Skiing and Science, St. Christoph am Arlberg, Austria, January 7-13, 1996; Chapman & Hall, Cambridge University Press. (1997). p. 216-225.

- [31] Schwameder H., Tscherner V.v.: „*Filtering of Force Variables in Skiing by Specific Wavelet Analysis*“; 2nd International Congress on Skiing and Science, January 9-15, 2000, St.Christoph am Arlberg, Austria. (2000). (abstract book)
- [32] Piziali R.L., Mote C.D.: „*The Snow Ski as a Dynamic System*“; Journal of Dynamic Systems, Measurement, and Control, June 1972. (1972). p. 133-138.
- [33] Glenne B., Jorgensen J.E., Chalupnik J.D.: „*Ski Vibrations and Damping*“; Experimental Techniques Vol. 18. (1994). p. 19-22.
- [34] Devaux P., Trompette P.: „*Modal Analysis of a Ski by the Finite Element Method*“; Journal of Sound and Vibration 73 (4). (1980). p. 597-600.
- [35] Ulrich C., Ferraris G., Lalanne M., Lacroix J.: „*Prediction of the Frequency and Time Responses of Composite Structures: Application to Skis*“; ASME, DE-Vol 64. (1993). p. 9-13.
- [36] Kitazawa S., Kazama T., Shimada T., Kobayashi M., Nagamatu A.: „*Construction of Ski Testing System by Using Computer Aided Engineering*“; 2nd International Congress on Skiing and Science, January 9-15, 2000, St.Christoph am Arlberg, Austria. (2000). (abstract book) p. 168.
- [37] Lieu D.K. : „*Mechanics of the Turning Snow – Ski*“; Dissertation at the Department of Mechanical Engineering, College of Engineering, University of California, Berkley. (1982).
- [38] Lieu D.K., Mote C.D. Jr.: „*Mechanics of the Turning Snow Ski*“; Ski Trauma and Safety: Fifth International Symposium, ASTM STP 860, R. J. Johnson and C.D. Mote, Jr., Eds., American Society for Testing and Materials, Philadelphia, USA. (1985). p. 117-140.
- [39] Lieu D.K., Mote C.D. Jr.: „*Experiments in the Machining of Ice at Negative Rake Angles*“; Journal of Glaciology, Vol. 30, No. 104. (1984). p. 77-81.
- [40] Clerc C., Gaertner R., Trompette P.: „*Computer Aided Design of Skis*“; Finite Elements in Analysis and Design 5. (1989). p. 1-14.
- [41] Renshaw A., Mote C.D. Jr.: „*A Model for the Turning Snow Ski*“; Skiing Trauma and Safety: Eighth International Symposium, ASTM STP 1104, C. D. Mote Jr. And Robert J. Johnson, Eds., American Society for Testing and Materials, Philadelphia, USA. (1991). p. 217-238.
- [42] Hirano Y., Tada N.: „*Mechanics of Turning Snow Ski*“; International Journal of Mechanical Science, Vol. 36, No. 5. (1994). p. 421-429.
- [43] Tada N., Hirano Y.: „*Simulation of a Turning Ski Using Ice Cutting Data*“; Sports Engineering 2. (1999). p. 55-64.
- [44] Tada N., Hirano Y.: „*In Search of the Mechanics of a Turning Alpine Ski Using Snow Cutting Force Measurements*“; Sports Engineering 5. (2002). p. 15-22.
- [45] Casolo F., Lorenzi V., Vallatta A., Zappa B.: „*Simulation Techniques Applied to Skiing Mechanics*“; First International Congress on Skiing and Science, St. Christoph a. Arlberg, Austria, January 7-13, 1996, Chapman & Hall, Cambridge University Press. (1997). p. 116-130.

- [46] Casolo F., Lorenzi V.: „*Relevance of Ski Mechanical and Geometrical Properties in Carving Technique: A Dynamic Simulation*“; 2nd International Congress on Skiing and Science, January 9-15, 2000, St.Christoph am Arlberg, Austria, Verlag Dr. Kovac. (2000). p. 165-179.
- [47] Nordt A.A., Springer G.S., Kollár L.P.: „*Simulation of a Turn on Alpine Skis*“; Sports Engineering 2. (1999). p.181-199.
- [48] Glitsch U.: „*Computer Simulation of Alpine Skiing*“; 2nd International Congress on Skiing and Science, January 9-15, 2000, St.Christoph am Arlberg, Austria, Verlag Dr. Kovac. (2000). p. 141-154.
- [49] Kaps P., Mössner M., Nachbauer W., Stenberg R.: „*Pressure Distribution under a Ski During Carved Turns*“; 2nd International Congress on Skiing and Science, January 9-15, 2000, St.Christoph am Arlberg, Austria, Verlag Dr. Kovac. (2000). p.180-202.
- [50] Terribilini M., Gadiant V., Schläppi R., Chevalier P., Hotz A., Pfefferlé P., Tarnutzer H.A.: „*Schneesport Schweiz - Speziallernlehrmittel Ski*“; Schweizerischer Interverband für Skilauf (SIVS), Eidg. Sportschule Magglingen (ESSM) am Bundesamt für Sport (BASPO) (Hrsg.), Unionsdruckerei Luzern AG, Switzerland. (2000).
- [51] Kneubühl F. K.: „*Repitorium der Physik*“; Teubner Stuttgart, ISBN 3-519-43012-6. (1990).
- [52] Beitz W., Grote K.-H. (eds.): „*Dubbel, Taschenbuch für den Maschinenbau*“; 20. edition, Springer-Verlag Berlin, ISBN 3-540-67777-1. (2001).
- [53] Sahashi T., Ichino S.: „*Method for Drawing Locus of a Sliding Ski as Observed from Direction Perpendicular to Snow Surface*“; Jpn. J. Appl. Phys. Vol 34. (1995). p. 674-679.
- [54] Sahashi T., Ichino S.: „*Carving-Turn and Edging Angle of Skis*“; Sports Engineering. (2001). p. 135-145.
- [55] Raschner C.: „*Kinematische und dynamische Technikanalyse im Slalom als Grundlage für die Entwicklung skispezifischer Krafttrainingsgeräte und Krafttrainingsmethoden*“; thesis, University of Salzburg. (1997).
- [56] Oberhofer K.: „*Experimentelle Bestimmung der Kraftübertragung vom Skifahrer auf den Ski und Berechnung des Aufkantwinkels während der Kurvenfahrt, Abschätzung der Messgenauigkeit verschiedener Messmethoden*“; Semesterarbeit Institut für Bewegungs- und Sportwissenschaften, ETH Zürich, Switzerland. (2003).
- [57] Raschner C., Müller E., Schwameder H.: „*Kinematic and Kinetic Analysis of Slalom Turns as a Basis for the Development of Specific Training Methods to Improve Strength and Endurance*“; Science and Skiing, E. Müller, et al. (Ed.), London. (1997). p. 251-261.
- [58] Eck C., Geering H.P., Bose S.C.: „*Model Based INS/GPS Navigation*“; Proceedings of the 7th Saint Peterburg International Conference on Integrated Navigation Systems, St. Petersburg, Russia. (2000). p. 95-102.
- [59] Bruton A.M., Glennie C.L., Schwarz K.P.: „*Differentiation for High Precision GPS Velocity and Acceleration Determination*“; GPS Solutions 2, (4). (1999). p. 7-22.
- [60] Skaloud J., Merminod B.: „*DGPS-Calibrated Accelerometric System for Dynamic Sports Events*“; ION GPS, Salt Lake City, Utah, USA. (2000).

- [61] Skaloud, J., Limpach, P.: „*Synergy of CP-DGPS, Accelerometry and Magnetic Sensors for Precise Trajectory in Ski Racing*“; ION GPS/GNNS 2003, Portland, Oregon, September 9-12. (2003).
- [62] Ducret S., Ribot P., Vargiolu R., Midol A., Mathia T.: „*Analysis of Downhill Ski Performance Using GPS and Ground Force Recording*“; Bacharach D., Seifert J. (Eds): 3rd International Congress on Science and Skiing, 28.March-3.April 2004, Aspen, Co, USA. (2004). (abstract book) p. 65-66.
- [63] Federolf P.: „*Skitest 13.3.02 - Zusammenfassung der Resultate*“; Internal Report, Team Snow Sports, Institut for Snow and Avalanche Research (SLF). (2002).
- [64] Federolf P.: „*Measurement of Turning Parameters and Snow Resistance in Alpine Skiing and their Implementation in FEM-Simulations of a Ski-Binding System*“; Interim Report, Institut for Snow and Avalanche Research, Davos, Switzerland. (2003).
- [65] Novel GmbH., Ismaninger Strasse 51, 81675 Munich, Germany: www.novel.de
- [66] Hull M.L., Mote C.D. Jr.: „*Analysis of Leg Loading in Snow Skiing*“; Journal of Dynamic Systems, Measurement and Control, Vol. 100, No. 3. (1978). p. 177-186.
- [67] Friedrichs E., Bergen F.v.: „*Sensor Plates Designed for Measuring Forces between Ski and Binding - a Developmental Summary*“; First International Congress on Skiing and Science, St. Christoph a. Arlberg, Austria, January 7-13, 1996; Chapman & Hall, Cambridge University Press. (1997). p. 180-188.
- [68] Bergen F.v.: „*Different Possibilities of Measuring Force Transition between Ski and Binding*“; First International Congress on Skiing and Science, St. Christoph a. Arlberg, Austria, January 7-13, 1996; Chapman & Hall, Cambridge University Press. (1997). p. 189-199.
- [69] Babel S., Hartmann U., Spitzenpfeil P., Mester J.: „*Ground-Reaction Forces in Alpine Skiing, Crosscountry Skiing and Ski Jumping*“; First International Congress on Skiing and Science, St. Christoph a. Arlberg, Austria, January 7-13, 1996; Chapman & Hall, Cambridge University Press. (1997). p. 200-207.
- [70] Wimmer A., Holzner R.: „*Constraint Forces May Influence the Measurement of Vertical Ground Reaction Forces During Slalom Skiing*“; First International Congress on Skiing and Science, St. Christoph a. Arlberg, Austria, January 7-13, 1996; Chapman & Hall, Cambridge University Press, (1997), p. 208-215.
- [71] Redlake, SanDiego, CA, USA: www.redlake.com
- [72] Mikromak Service K. Brinkmann, Berlin, Germany: <http://www.mikromak.com>
- [73] Tsai R. Y.: „*An Efficient and Accurate Camera Calibration Technique for 3D Machine Vision*“; IEEE Computer Society, Proceedings of the Conference on Computer Vision and Pattern Recognition. (1986). p. 364-374.
- [74] Mikromak: „*WINanalyse - Automatic Motion Analysis*“; Manual Version 1.4; mikromak Mikroelektronik für Messtechnik, Anlagen und Kamerasysteme GmbH. Am Wolfsmantel 18, 91058 Erlangen, Germany; p. 82-89.
- [75] Mikromak: „*WINanalyse - Body Model Module*“; Manual Version 1.0; mikromak Mikroelektronik für Messtechnik, Anlagen und Kamerasysteme GmbH. Am Wolfsmantel 18, 91058 Erlangen, Germany; p. 82-89.

- [76] Hanavan E.P.: „*A Mathematical Model of the Human Body*“; AMRL Technical Report (TR-64-102), Wright-Patterson Air Force Base, OH, USA. (1964).
- [77] Schaback R., Werner H.: „*Numerische Mathematik*“; Springer Verlag Berlin, Heidelberg, New York, ISBN 3-540-54738-X. (1993).
- [78] Lüthi A., Federolf P., Fauve M., Oberhofer K., Rhyner H.U., Ammann W., Stricker G., Schiefermüller C., Eitzlmair E., Schwameder H., Müller E.: „*Determination of Forces in Carving Using Three Independent Methods*“; 3rd International Congress on Science and Skiing, 28.March.-3.April 2004, Aspen, Co, USA. (2004). (abstract book) p. 3-4.
- [79] Kistler Instrumente AG, Winterthur, Switzerland: www.kistler.com
- [80] International Commission on Snow and Ice: „*UNESCO: Avalanche Atlas*“; ISBN 9230016969. (1981).
- [81] Colbeck S.C.: „*A review of the Metamorphism and Classification of Seasonal Snow Cover Crystals*“; Avalanche Formation, Movement and Effects. IAHS Publ. No. 162. (1987).
- [82] McClung D., Schaerer P.: „*The Avalanche Handbook*“; The Mountaineers, Seattle, WA, USA. ISBN 0-89886-364-3. (1993).
- [83] Ramseier R.: „*Sintering of Snow as a Function of Temperature*“; IAHS Publication No. 69. IAHS Press, Wallingford, UK. (1965). p.119-127.
- [84] Kry P.R.: „*Quantitative Stereological Analysis of Grain Bonds in Snow*“; Journal of Glaciology, Vol. 14, No. 72. (1975). p. 467-478.
- [85] Kry P.R.: „*The Relationship between the Visco-Plastic Structural Properties of Fine-Grained Snow*“; Journal of Glaciology, Vol. 14, No. 72, (1975), p. 479-500.
- [86] Bader H.: „*The Physics and Mechanics of Snow as a Material*“; Report of the Experimental Engineering Division, U.S. Army Cold Regions Research and Engineering Laboratory, Part II - Physical Science, Section B. (1962).
- [87] Mellor M.: „*Properties of Snow*“; Cold Regions Science and Engineering, U.S. Army Materiel Command, Part III: Engineering, Sect. A Snow Engineering, Cold Regions Research & Engineering Laboratory, Hanover, New Hampshire, USA. (1964).
- [88] Mellor M.: „*A Review of Basic Snow Mechanics*“; Ass. Int. Sciences of Hydrology. (1974). p. 251.
- [89] Salm B.: „*Mechanical Properties of Snow*“; Review of Geophysical and Space Physics, Vol 20, Nr. 1. (1982). p. 1-19.
- [90] Shapiro L.H., Johnson J.B., Sturm M., Blaisdell G.L.: „*Snow Mechanics: Review of the state of knowledge and Applications*“; Report of the Experimental Engineering Division, U.S. Army Cold Regions Research and Engineering Laboratory. (1993).
- [91] Johnson J.B., Schneebeli M.: „*Characterizing the Microstructural and Micromechanical Properties of Snow*“; Cold Regions Science and Technology, 30. (1999). p. 91-100.
- [92] Schneebeli M., Johnson J.B.: „*Measuring Snow Microstructure and Hardness Using a High Resolution Penetrometer*“; Cold Regions Science and Technology, 30. (1999). p. 101-114.

- [93] Fauve M.: „*Vorstudie zur Verbesserung von Wirtschaftlichkeit und Umweltverträglichkeit der Schneeproduktion mit einer neuen Schneeanlage*“; Schlussbericht vom KTI Projekt Nr. 4529.2 KTS, SLF Interner Bericht Nr. 737. (2000).
- [94] Fauve M., Rhyner H.U., Schneebeli M.: „*Pistenpräparation und Pistenpflege - das Handbuch für den Praktiker*“; Davos, Eidg. Institut für Schnee und Lawinenforschung, ISBN 3-905621-01-0. (2002).
- [95] Coldbeck S.C.: „*The Kinetic Friction of Snow*“; Journal of Glaciology 34 (116), 78. (1988).
- [96] Evans D.C.B.: „*The Kinetic Friction of Ice*“; Proc. R. Soc. Lond. 347, 493. (1976).
- [97] Tanner C., Frank T.: „*Infrarotaufnahmen von Skispuren*“; Eidgenössische Materialprüfungs- und Forschungsanstalt (EMPA), Prüfbericht 840 161.(1999).
- [98] Roberts C.C.: „*Analysis of Thermal Patterns on a Motorized Ski Deck*“; Proc. of the Intern. Soc. of Optical Engineering, Thermosense. (1987).
- [99] Fauve M., Bäuerle L., Lüthi A., Rhyner H.U., Tanner C.: „*Variation of Snow Surface Temperature during Alpine Skiing*“; Int. Cong. on Skiing and Science, Aspen, CO, USA. (2004). (abstract book) p. 90-91.
- [100] Coldbeck C.: „*A Review of the Processes that Control Snow Friction*“; Cold Regions Research and Engineering Laboratory (CRREL) Monograph 2. (1992).
- [101] Buhl D., Fauve M., Bruderer C., Rhyner H.U., Ammann W.: „*Schlussbericht KTI Projekt 3781.1: Zusammenwirken von Ski, Snowboard, Bindung, Belag, Wax und Schnee auf die Gleit- und Fahreigenschaften*“; Internal Report, Swiss Federal Institute of Snow and Avalanche Research, Davos, Switzerland. (1999).
- [102] Buhl D., Fauve M., Rhyner H.U.: „*The Kinetic Friction of Polyethylene on Snow: the Influence of the Snow Temperature and the Load*“; Cold Regions Science and Technology, Volume 33, Issues 2-3. (2001). p. 133-140.
- [103] Fauve M.: „*Influence of Snow and Weather Conditions on the Gliding Properties*“; Int. Cong. on Skiing and Science, Aspen, CO, USA. (2004). (abstract book) p. 88-89.
- [104] Nachbauer W., Schröcksnadel P., Lackinger B.: „*Effects of Snow and Air Conditions on the Ski Friction*“; Ski Trauma and Safety: Tenth Volume, ASTM STP 1266, C.D. Mote, et al. Eds., American Society for Testing and Materials. (1996). p. 178-185.
- [105] Moldestad D.A.: „*Some Aspects of Ski Base Sliding Friction and Ski Base Structure*“; Phd. Thesis, Departement of Structural Engineering, Norwegian University of Science and Technology, Norway. (1999).
- [106] Fauve M.: Personal Communications. (2004).
- [107] Ericksson R.: „*Friction of Runners on Snow and Ice*“; SIPRE Report TL 44, Meddelande 34/35. (1955). p. 1-63.
- [108] Brown C.A., Outwater J.O.: „*On the Skiability of Snow*“; Skiing Trauma and Safety: Seventh International Symposium, ASTM STP 1022, R. J. Johnson, C. D. Mote, Jr. and M.-H.Binet, Eds., American Society for Testing and Materials, Philadelphia, USA. (1989). p. 329-336.
- [109] Stephenson D.A., Agapiou J.S.: „*Metal Cutting Theory and Practice*“; Marcel Dekker Inc. ISBN 0-8247-9579-2. (1997).

- [110] Schumacher R.P.: „Einsatz numerischer Methoden zur Berechnung von Umformprozessen kompressibler Stoffe“; VDI Verlag Düsseldorf. ISBN 3-18-318920-8. (1996).
- [111] Mössner M., Nachbauer W., Innerhofer N., Schretter H.: „Mechanical Properties of Snow on Ski Slopes“; 15th International Congress on Ski Trauma and Skiing Safety (ICSS), St. Moritz / Pontresina, Switzerland, Abstract. (2003).
- [112] Fukue M.: „Mechanical Performance of Snow Under Loading“; Tokai University Press. (1979).
- [113] Johnson J.B., Solie D.J., Brown J.A., Gaffney E.S.: „Shock Response of Snow“; Journal of Applied Physics 73(10). (1993). p. 4852-4861.
- [114] Johnson J.B.: „A Preliminary Numerical Investigation of the Micromechanics of Snow Compaction“; Annals of Glaciology 26. (1998). p. 51-54.
- [115] Hawkes I., Mellor M.: „Deformation and Fracture of Ice under Uniaxial Stress“; Journal of Glaciology, Vol. 11, No 61. (1972). p. 103-131.
- [116] Abele G., Gow A.J.: „Compressibility Characteristics of Compacted Snow“; CRREL Report 76-21. (1976).
- [117] Abele G.: „Snow Roads and Runaways“; US Army Corps of Engineers, Cold Regions Research & Engineering Laboratory. (1990).
- [118] Bertschinger S., Heeb R.: „Agenvis RSM² - Skitester zur Optimierung der Kurvenfahrt“; diploma thesis, Interstaatliche Hochschule für Technik Buchs (NTB), Buchs, Switzerland. (2001).
- [119] Interstaatliche Hochschule für Technik Buchs, Buchs, Switzerland: www.ntb.ch
- [120] SCANCO Medical AG, Auenring 6-8, 8303 Bassersdorf, Switzerland: <http://www.scanco.ch>.
- [121] Kronholm, K.: „Spatial Variability of Snow Mechanical Properties with Regard to Avalanche Formation“; PhD. thesis, University Zürich, Switzerland. (2003).
- [122] Schoepf V.: „Three-dimensional Reconstruction of Snow Crystal Clusters - Report of an Internship at the Federal Institute for Snow and Avalanche Research SLF“; Federal Institute for Snow and Avalanche Research SLF. (1998).
- [123] Achammer T., Denoth A.: „Snow Dielectric Properties: from DC to Microwave X-band“; Annals of Glaciology 19. (1994). p. 92-96.
- [124] Brun E., Rey L.: „Field Study on Snow Mechanical Properties with Special Regard to Liquid Water Content“; Avalanche Formation, Movement and Effects (Proceedings of the Davos Symposium, September 1986. IAHS Pub. no. 162. (1987). p. 183-193.
- [125] JeanRichard F.: „Characterization of the Snow Properties under High Deformation Rates“; diploma thesis at the Institut des Matériaux, EPF Lausanne, Switzerland. (2003).
- [126] Montmollin V.de.: „Shear Tests on Snow Explained by fast Metamorphism“; Journal of Glaciology Vol 28 N. 98. (1982). p. 187-197.

- [127] Federolf P., Fauve M., Szabó D., Lüthi A., Rhyner H.U., Schneebeli M., Ammann W., Dual J.: „*Mechanical Properties of Snow During Rapid Impacts*“; Snow Engineering V, Bartelt, Adams, Christen, Sack & Sato (eds.), Taylor & Francis Group, London, UK. ISBN 90 5809 634 3. (2004). p. 209-214.
- [128] Numerical Modeling GmbH., Winterthur, Switzerland: <http://www.nmtec.ch>
- [129] Numerical Modeling GmbH.: „*NM-SESES, Finite Element Software for Computer Aided Engineering - User Manual, Version Februar 2003*“; Numerical Modeling GmbH., Winterthur, Switzerland. (2003).
- [130] Landau L., Lifschitz E.: „*Elastizitätstheorie; Lehrbuch der theoretischen Physik, Band 7*“; Verlag Harri Deutsch, ISBN 3-05-500580-5. (1991).
- [131] Bathe K.: „*Finite Element Procedures*“; Prentice Hall - International. (1996).
- [132] Timoshenko S., Woinowsky-Krieger S.: „*Theory of Plates and Shells*“; McGraw-Hill. (1959).
- [133] Graber C.: „*Nichtlineare Analyse von Schalen mit linearisierten elastoplastischen Schnittkraft-Verformungs-Beziehungen*“; Verlag der Fachvereine, Zürich, Switzerland. (1990).
- [134] Roos M. et al.: „*Membrane Modelling: Shell vs. Volumetric Elements*“; Proc. of the Micromechanics Europe Workshop. (1995).
- [135] Wäckerlin J.: „*Numerische Modellierung von Rennskis*“; diploma thesis at the Technikum Winterthur, Switzerland. (1997).
- [136] Sakata T., Kawai S., Kawada F.: „*Free Vibrations of a Snowboard*“; Int. J. Mech. Sci. Vol 38, No. 6. (1996). p. 579-588.
- [137] Roos M.: Personal communications. (2002).
- [138] Dual J.: Personal communications. (2002).
- [139] Gwinner J.-M.: „*SESES Parameterstudien*“; Praktikumsbericht, Swiss Federal Institute of Snow and Avalanche Research, Davos, Switzerland. (2003).
- [140] Fritschi AG. Swiss Bindings: „*Max Flex° System*“; http://www.fritschi.ch/e/rave_maxflex.asp.
- [141] Baumann A., Fischer R., Honegger D.: „*Messsystem zur Ermittlung der Verformung infolge von Biegung, Torsion und Schwingung von Alpinskis und Snowboards*“; diploma thesis at the Interstaatliche Ingenieurschule Neu-Technikum Buchs (NTB), Buchs, Switzerland. (1999).
- [142] Lüthi A., Federolf P., Fauve M., Rhyner H.U., Ammann W.: „*Schlussbericht KTI Projekt Nr. 5275.2: Erarbeiten einer wissenschaftlichen Simulationsmethode des Systems Ski/Bindung beim Kurvenfahren unter Berücksichtigung der Schneemechanik - Umsetzung in der Entwicklung eines integralen Systems Ski - Bindung*“; Internal Report, Swiss Federal Institute of Snow and Avalanche Research, Davos, Switzerland. (2005).
- [143] Zehnder René, Mugg Peter: „*Messsystem für Flächendruckverteilung am Alpinski*“; diploma thesis at the Interstaatliche Ingenieurschule Neu-Technikum Buchs (NTB), Buchs, Switzerland. (1997).

- [144] Gwinner J.-M.: „*Kurvensimulation (SESES)*“; Praktikumsbericht, Team Snowsports (Confidential). Swiss Federal Institute of Snow and Avalanche Research, Davos, Switzerland. (2003).
- [145] Hellberg F., Federolf P.: „*Parameterstudie Prototyp*“; Praktikumsbericht, Team Snowsports (Confidential). Swiss Federal Institute of Snow and Avalanche Research, Davos, Switzerland. (2003).
- [146] Rhyner H.U.: *Personal communications*. (2004).
- [147] Müller E., Schiefermüller C., Kröll J., Raschner C., Schwameder H.: „*Skiing with Carving Skis - What is New?*“; Bacharach D., Seifert J. (Eds): 3rd International Congress on Science and Skiing, 28.March-3.April 2004, Aspen, Co, USA. (2004). (abstract book) p. 1-2.

9. Glossary

active motion: motion caused by muscular action of the skier's body, e.g. →vertical motion, →inward shifting.

carving: turning motion in which the ski glides within its trace. The energy losses due to snow deformation are therefore minimised compared to other types of turning, e.g. →drifting, or →skidding.

change of the ski edges: the moment in between two turns in which the skis are flat on the snow surface. In this moment the →outer and →inner ski are exchanged. See also →turn phases.

crossing of the fall line: the moment in which the skis are parallel to the →fall line. This moment can often be considered to be the beginning of the →steering phase of a turn.

drifting: turning motion in which the skier glides more forward than turns. This motion is caused by reduction of the pressure on the ski, which is caused by a change in the motion of the skier's centre of mass. The reduction of the pressure leads to lesser bending of the ski. The skis still glide within their own trace, but the turn radius does not coincide with the radius of the lower ski edge (as in forward gliding on a flat ski).

edging: the motion by which the skis are set on their edge or their edging angle is increased.

fall line: the imaginary line parallel to the slope with the highest inclination angle. Usually the fall line is thought of as a downward orientated vector parallel to the slope.

impact speed: in this thesis this expression is used for the speed with which the stamp of the device Fast Snowdeformer hits the snow surface, whereas the →penetration speed refers to the actual speed of a device which penetrates the snow. During an impact test with the device Fast Snowdeformer the →penetration speed decreases from the impact speed down to a speed of zero.

initiation phase: the turn phase in which the skier →edges his skis by an →inward shifting of his centre of mass and thus initiates the turn. Often a →vertical motion is part of the turn initiation phase. The initiation phase is in a smooth transition followed by the →steering phase.

inner ski: the right ski in a right turn and the left ski in a left turn. The inner ski is usually less loaded and less edged than the →outer ski.

inward shifting: active motion of the skier in the →initiation phase of the turn by which he shifts his body towards the centre of the turn, and thus assumes the inclined position by which he generates the centripetal forces of the turn.

motion effects: in this thesis this term is used to describe two effects, which have to be taken into account when implementing the boundary condition for the ski-snow interface: the →hysteresis in the function describing the snow resistance pressure, and the →side cut effect.

outer ski: the left ski in a right turn and the right ski in a left turn. The outer ski is usually more loaded and more edged than the →inner ski.

penetration speed: actual speed with which a device (measurement device or ski) penetrates the snow surface.

resistance pressure: Pressure the snow exerts to the contact surface of a penetrating device. In this thesis the mean resistance pressure has been experimentally determined as a function of the penetration depth of the device into the snow. The simulation tool calculates an actual resistance pressure for each point of the contact surface between ski and snow.

side cut effect: The side cut of a ski causes a lateral displacement of the lower ski edge and thus of the trace, which is generated by the lower ski edge in the snow. This effect has to be taken into account when implementing the boundary condition describing the ski-snow interaction during a carved turn.

skidding: in a skidded turn there is a positive blade angle between the ski axis and the velocity vector of the ski (see Figure 4 in the introduction). Thus the ski cannot glide within its own trace, but has to machine the snow surface as it passes. The energy losses due to the ski-snow interaction are therefore significantly higher than in →carved turns.

snow hysteresis: The hysteresis in the function of the snow's →resistance pressure to a penetrating device, which is caused by the plastic deformation of the snow surface. This effect has to be taken into account when implementing the boundary condition describing the ski-snow interaction during a carved turn.

steering phase: the turn phase in which the skier has assumed the turning position and is mainly being turned by the external forces rather than by active body motions. In the steering phase the instantaneous turn radii are the smallest. The steering phase follows the →initiation phase in a smooth transition.

turn phases: see →change of the ski edges, →initiation phase, →crossing of the fall line, and →steering phase.

vertical motion: an active lifting or lowering of the skiers centre of mass. During a turn this motion is usually combined with the →inward shifting.

Curriculum Vitae

Peter Andreas Federolf

Promenade 78, 7270 Davos Platz, Switzerland

PERSONAL DATA:

Date of Birth: 18. January 1974

Place of Birth: Rottweil, Germany

Nationality: German

Marital Status: Single Male

EDUCATION

1980 - 1993 Elementary school and Gymnasium in D-Hechingen

1993 - 1994 Civilian Service in a school for disabled children in D-Mössingen

1994 - 2000 Course Studies for the degree of diploma physicist at the Swiss Federal Institute of Technology Zurich, CH

1997 - 1998 Course Studies for the degree of diploma physicist at the Brunel University, Uxbridge, UK-London

2000 - 2004 Doctoral research at the Swiss Federal Institute for Snow and Avalanche Research Davos, CH

DIPLOMA THESIS

„Characterization of Capacitive Chemical Microsensors“ at the Physical Electronics Laboratory, Institute for Quantum Electronics, Swiss Federal Institute of Technology Zurich, CH.

LANGUAGE SKILLS

German (mother tongue)

English